

DOTTORATO DI RICERCA

BIOINGEGNERIA

Ciclo XX

Settore scientifico disciplinare di afferenza: ING-IND/34

**Development of musculoskeletal models
for the design and the pre-clinical
validation of hip resurfacing prosthesis**

**Sviluppo di modelli muscolo-scheletrici
per la progettazione e valutazione pre-
clinica di protesi d'anca di rivestimento**

Presentata da: Ing. MARTELLI SAULO

Coordinatore Dottorato:

Chiar.mo Prof. ANGELO CAPPELLO

Relatore:

Chiar.mo Prof. LUCA CRISTOFOLINI

Co-relatori:

Ing. MARCO VICECONTI

Ing. FULVIA TADDEI

Alla mia famiglia e ad Angela.

CONTENT

INTRODUCTION.....	1
RIASSUNTO.....	5
CHAPTER 1	9
HIP RESURFACING ARTHROPLASTY: A NEW APPLICATION OF AN OLD CONCEPT	9
1.1 History of hip joint replacement.....	10
1.2 Comparison of hip resurfacing arthroplasty and traditional THR.....	13
1.3 Indications, risk factors, treatment and post operative care	14
1.3.1 Indications	14
1.3.2 Risk factors and treatment.....	15
1.3.3 Postoperative care	16
1.4 Types of failure observed in practice	16
1.5 Definition of failure mode.....	17
1.6 Mechanical implications on relevant biological processes	18
1.6.1 Bone: a living tissue	19
1.6.1.1 The bone matrix	19
1.6.1.2 Bone biology	20
1.6.2 Adverse biological processes for orthopaedic implants.....	24
1.6.2.1 The stress shielding effect.....	25
1.6.2.2 Osteolysis	26
1.6.2.3 Tissue differentiation at the bone-prosthesis interface.....	28
1.7 Prediction of failure.....	28
1.7.1 Predicting mechanically-related failure modes	29
1.7.1.1 Combined stress theory of failure	29
1.7.1.2 Fatigue.....	31
1.7.1.3 Fretting	33
1.7.1.4 Shock and impact	35
1.7.1.5 Wear	35
1.7.2 Predicting adverse biological processes.....	36

1.7.2.1 Adverse bone resorption and remodelling	36
1.7.2.2 Osteolysis	38
1.7.2.3 Adverse tissue differentiation at the prosthesis interface.....	39
1.8 Properties of materials composing the orthopaedic implants	39
1.8.1 Prosthesis and cement	40
1.8.2 Bone	42
1.8.2.1 Cortical bone	42
1.8.2.2 Cancellous bone	45
1.9 Development of a protocol of analysis	47
CHAPTER 2	57
EXPERIMENTAL VALIDATION OF THE OVERALL ACCURACY OF SUBJECT-SPECIFIC FINITE ELEMENT MODELS OF LONG BONES	57
2.1 Subject-specific finite element models of long bones: An in vitro evaluation of the overall accuracy	58
2.1.1 Materials and methods	60
2.1.1.1 Femur specimen	60
2.1.1.2 CT scanning	61
2.1.1.3 Experimental measurements	61
2.1.1.4 Subject-specific finite element model.....	63
2.1.1.5 Spatial registration between model and experiment	65
2.1.1.6 Determination of the model accuracy	66
2.1.2 Results	66
2.1.2.1 Experimental measurements	66
2.1.2.2 Comparison FEM vs experimental stresses	67
2.1.3 Discussions.....	68
2.2 Accuracy of subject-specific finite element model of an implanted femur: an in-vitro study	71
2.2.1 Materials and methods	71
Finite element model.....	72
2.2.2 Results	73
2.2.3 Discussion	74
2.3 Conclusions.....	75

CHAPTER 3	80
SENSITIVITY OF SUBJECT-SPECIFIC FE MODELLING TECHNIQUES TO UNCERTAINTIES ON PARAMETERS.....	80
3.1 Finite-Element modelling of bones from CT data: sensitivity to geometry and material uncertainties	81
3.1.1 Materials and methods	82
3.1.1.1 Finite-Element models generation	84
3.1.1.2 The loads	84
3.1.1.3 Estimation of the random input variables	85
3.1.1.4 Identification of the output variables	87
3.1.1.5 The probabilistic design	87
3.1.2 Results	88
3.1.3 Discussion	89
3.2 Conclusion.....	91
CHAPTER 4	94
IDENTIFICATION OF THE PROTOCOL FOR THE ANALYSIS OF THE RISK OF BIOMECHANICAL FAILURE OF RESURFACED FEMURS.....	94
4.1 The preclinical validation of hip resurfacing prostheses.....	95
4.1.1 A general protocol for pre-clinical validation	96
4.1.1.1 Know your enemy	96
4.1.1.2 Detailed design of the validation protocols.....	97
4.1.1.3 The role of numerical models in pre-clinical validation	97
4.1.1.4 A possible list of protocols.....	98
4.1.2 Discussions.....	100
4.2 In-vitro replication of spontaneous fractures of the proximal human femur	101
4.2.1 Identification of the most critical loading scenario: FE simulations.....	102
4.2.3 Results: Most critical loading scenario	103
4.2.4 Discussions.....	105
4.3 Conclusions	106
CHAPTER 5	110
TESTING OF THE PRE-CLINICAL VALIDATION PROTOCOL ON A SUCCESSFUL DESIGN OF HIP RESURFACING PROSTHESIS	110

5.1 Combined experimental-numerical method for the pre-clinical validation of epiphyseal prosthesis: exemplification of the method with an established design	111
5.1.1 Materials and methods	112
5.1.1.1 Bone specimens for the in-vitro study	112
5.1.1.2 The bone specimen for the numerical study	112
5.1.1.3 Failure modes associated to failure scenarios	113
5.1.1.4 Identification of predictive parameters	113
5.1.1.5 Experimental tests (intact and implanted specimen).....	115
5.1.1.6 FE models and boundary conditions	115
5.1.1.7 Loading conditions for numerical simulations.....	116
5.1.2 Results.....	117
5.1.2.1 Femoral neck fracture	117
5.1.2.2 Prosthesis fractures	117
5.1.2.3 Aseptic loosening caused by cement damage.....	117
5.1.2.4 Aseptic loosening caused by fretting debris of the cement.....	117
5.1.2.5 Aseptic loosening caused by lack in bone-prosthesis in-growth	118
5.1.2.6 Aseptic loosening caused by damage of cancellous bone.....	118
5.1.2.7 Aseptic loosening caused by bone re-modelling.....	118
5.1.3 Discussion	119
5.2 Conclusions.....	121
CHAPTER 6	126
DESIGN OPTIMISATION AND PRE-CLINICAL VALIDATION OF A NEW CONCEPTUAL DESIGN OF A RESURFACING PROSTHESIS	126
6.1 Preliminary finite element study of the first prosthesis prototype	127
6.1.1 Materials and methods	127
6.1.1.1 CT Dataset	127
6.1.1.2 The finite element model of the intact femur.....	127
6.1.2 Results.....	129
6.1.3 Discussion	131
6.2 Sensitivity of the risk of failure to some factors of influence.....	132
6.2.1 Roughness of the stem surface.....	133
6.2.1.1 Modelling data	133

6.2.1.2 Results	133
6.2.2 Interdigitation	134
6.2.2.1 Methods	134
6.2.2.2 Results	135
6.2.3 Osteoporosis	135
6.2.3.1 Methods	136
6.2.3.2 Results	136
6.2.4 Discussion	137
6.3 Results of experimental tests on the first prototype	138
6.4 First step of design revision: refinement of the first prototype geometry	138
6.4.1 Materials and methods	138
6.4.2 Results	139
6.4.3 Discussion	140
6.5 Sensitivity of the risk of failure to influencing co-factors	141
6.5.1 Surgical errors: prosthesis mispositioning	141
6.5.1.1 Material and methods	141
6.5.1.2 Results	142
6.5.2 Anatomical variability: femur size	143
6.5.2.1 Material and methods	144
6.5.2.2 Results	145
6.5.3 Roughness of the stem surface	146
6.5.3.1 Materials and methods	146
6.5.3.2 Results	147
6.5.4 Discussion	148
6.6 Second step of design revision: geometry optimisation of small sizes	149
6.6.1 Materials and methods	149
6.6.2 Results	149
6.6.3 Discussion	150
6.7 Results of experimental tests on the optimised device	151
6.8 Extended pre-clinical validation of the finalized design on a simulated population	151
6.8.1 Materials and methods	152

6.8.1.1 Analysis of the implanted femur	152
6.8.1.2 Comparative analysis of the implanted and the intact femur	155
6.8.2 Results	156
6.8.2.1 Analysis of the implanted femur	156
6.8.2.2 Comparative analysis of the implanted and the intact femur	158
6.8.3 Discussion	160
6.9 Conclusions	161
CHAPTER 7	165
MODELLING THE MUSCULOSKELETAL SYSTEM FOR PREDICTING IN-VIVO MUSCLE FORCES: THE NEW CHALLENGE	165
7.1 Biomechanical modelling of the musculoskeletal apparatus: status and key issues.....	166
7.1.1 Biomechanical modelling of the body	168
7.1.1.1 Modelling strategies	168
7.1.1.2 Possible uses of Whole-Body Models	170
7.1.1.3 Model identification	170
7.1.2 Biomechanical modelling of organs	172
7.1.2.1 Modelling strategies	172
7.1.2.2 Whole bones.....	172
7.1.2.3 Myotendinous units.....	173
7.1.2.4 Ligaments and cartilages.....	174
7.1.2.5 Joint models	174
7.1.3 Biomechanical modelling of tissues	175
7.1.3.1 Some examples of tissue biomechanics modelling.....	176
7.1.3.2 Models of tissue adaptation.....	176
7.1.4 Multiscale and probabilistic models	177
7.1.5 The living human project: current challenges.....	179
7.1.5.1 Community building and data repositories	179
7.1.5.2 Data fusion and data processing	180
7.1.5.3 A framework for numerical modelling	181
7.1.5.4 Information and scientific visualization.....	182
7.1.5.5 The road ahead.....	183

7.1.6 Discussion	184
7.2 Subject-specific musculoskeletal models from medical images	185
7.2.1 Material and Methods.....	185
7.2.2 Results and Discussion.....	187
7.3 Conclusions	189
CONCLUSIONS.....	199
ACKNOWLEDGMENTS	201
BIBLIOGRAPHY	202
APPENDIX A	205
A METHOD TO IMPROVE EXPERIMENTAL VALIDATION OF FINITE ELEMENT MODELS OF LONG BONES	205
APPENDIX B.....	217
IN VITRO REPLICATION OF SPONTANEOUS FRACTURES OF THE PROXIMAL HUMAN FEMUR.....	217
APPENDIX C	230
ADDITIONAL RESULT PLOTS FOR CHAPTER 6.....	230
APPENDIX D	242
MUSCULOSKELETAL MODELS FOR PREDICTING SKELETAL LOADINGS	242

Introduction

The present thesis describes the results of the researches performed throughout my Ph. D. in Bioengineering. The work presented in this thesis was entirely carried out at the Laboratorio di Tecnologia Medica (LTM) of Istituti Ortopedici Rizzoli (Bologna).

The field of interest of the presented research thesis is the surgical treatment of dysfunctional hips such in case of arthritis, avascular necrosis, and other debilitating pathologies which are very severe and costly conditions for the public health. In spite of the clinical success of total hip replacement (THR) characterised by a survivorship typically higher than 90% after ten year from surgery, still THR surgeries produce strong limitations to the quality of life on operated individuals. As people live and remains active longer than in the past, the needs of more appropriate techniques in the treatment of dysfunctional joints quickly increased in the last years and it is expected to increase further. Such need pushed the industry and the research in developing new methods for the treatment of dysfunctional hips with particular attention to young and active patients.

Hip resurfacing techniques have been recently reintroduced as a mini-invasive techniques that preserve the original architecture of the hip and, mostly because of this, they seem to hold the promise of various advantages over traditional THR. The concept behind hip resurfacing is not new, it was first introduced in the 60's and immediately abandoned because of a high failure rate, later attributed to technological limits of the medical alloys available at that time. Since late 90's, the new CrCo medical alloys overcome the original limits giving a new spin to hip resurfacing techniques; preliminary follow-up studies are very promising.

Although many innovative designs claim to radically improve the functional outcome of traditional techniques, no hard evidences can be produced with the assessment methods currently available; thus, revision is the only reliable, although very gross, end point for assessment.

This delayed assessment of the quality of orthopaedic devices is a consistent obstacle to the development of more effective designs. In fact, the lesson provided in the past by many branches of engineering is that success in designing competitive products while averting premature failure can be achieved only by evaluating all potential failure modes. To be effective in averting failure, it is essential for designer to have a good working knowledge of analytical and/or empirical techniques in predicting failure. The work developed during the three years of Ph.D. studies aimed to develop a protocol for predicting failure of hip resurfacing prosthesis. This aim was pursued by modelling the musculoskeletal system so as to provide a tool for the design and the pre-clinical validation of new devices.

The work can be divided in three principal activities: a first preliminary study in which the technique for the generation of subject specific finite element (FE) models, previously developed at the LTM, was validated either in case of intact or resurfaced femurs. The second activity,

which combines a formal analysis of failure, numerical modelling and in-vitro experiments to provide the best possible validation of a new device. The third and last part is the starting of a new research activity that holds as its primary objective the direct computing of boundary conditions through modelling the muscular actions at the hip. It should be noted that, as it is well specified in the thesis title, the author conducted the numerical part of the work while the experimental testing activity was entirely carried out by the experimental group of LTM, and then briefly reported so as to strengthen the validity of conclusions.

After **Chapter 1**, which describes failure scenarios for hip replacements, biomechanical parameters to be used in predicting failure and engineering techniques for predicting the relevant parameters, **Chapter 2** describes the validation against experimental measurements of model predictions of the bone stresses and the contact mechanics at the bone-prosthesis interface. The FE meshes of an intact and of the same femur implanted were generated by a well established procedure developed in the past years at LTM, by using a set of medical images. All needed data were derived from the computerised tomography of an intact femur of a male donor of middle age which was made available from the “Banca dell’Osso” of the Istituti Ortopedici Rizzoli. After the validation of the intact model the same femur was implanted with a resurfacing prosthesis and it underwent the same validation protocol. The results of the FE simulations were compared with the measurements recorded by 13 rosette strain-gauges applied on the bone surface of the femur for five different loading conditions. The average error of predictions on bone stresses never exceeded the 10% of the measured maximum absolute value. The maximum error on prosthesis micromovement was within a micron. This results were satisfactory for the adoption of these models as a reliable tool in studying the resurfaced femur biomechanics and aligned with the current state of the art in this field.

A possible source of errors that affect the validation process are differences in boundary condition realised by the experimental set-up and the boundary conditions simulated by the model. To control these differences, a loading cell was studied to measure the location on the femoral head where the force is effectively applied so as to better model the experimental boundary conditions. As it is not of direct interest for this Ph.D. thesis, a more detailed description of the work is reported in **Appendix A**.

Whatever the method adopted for the generation of the FE mesh from medical imaging data and for the material properties mapping, unavoidable errors occurs in the creation of the model that influence, in an unpredictable manner, the results of the FE analysis. To understand the effects that the errors affecting the various steps of the model generation have on the FE prediction, a sensitivity FE analysis was performed. The results of the study, which are presented in **Chapter 3**, indicated that the uncertainty on the FE prediction is always lower than 10% of the predicted value for the method adopted for the generation of finite element models from CT data.

The next step, described in **Chapter 4**, aimed to identify the protocol of analysis for evaluating all relevant failure mode for hip resurfacing prosthesis. To this scope, the definition of the protocol was carried out by the formal analysis of possible failure modes coherent with the resurfaced femur bio-mechanics and by the subsequent association of each failure mode with the more appropriated techniques of investigation.

The resulting protocol included the prediction of femoral neck fractures, which met the limit of the modelling techniques in predicting the bone mechanics in the post-elastic phase. Hence, the competence of evaluating the ultimate load to failure of implanted femurs was left to the experimental group of LTM, opening the question on which experimental set-up is the best trade off between the need to replicate physiological conditions and the need of simplicity of the set-up itself. This problem was numerically approached.

Simulations were run to identify the loading scenario which more likely produce head-neck fractures, and to determine where it is possible to simplify the experimental set-up when the head-neck region is of interest. The experimental set-up was consequently designed and clinically relevant fractures were obtained on 10 cadaveric femurs. Details of the tests conducted by the experimental group of LTM are reported in Appendix B.

So after, the protocol was ready for the analysis of resurfaced femurs. **Chapter 5** describe the first application of the method to a successful design of resurfacing prosthesis developed over years. A model of an implanted femur of average size, with normal bone stock, and simulating an ideal positioning of the prosthesis during surgery was generated. Muscle forces acting on the proximal femur were modelled deriving all needed information from the literature and simulations were run for a broad range of activities of daily living. Destructive tests were conducted (by the LTM experimental group) on three pairs of cadaver specimens to measure the influence of the prosthesis implantation on the risk of neck fractures. Results of numerical simulations and of experimental test were all in a good agreement with known clinical outcomes for this class of devices. This was encouraging for its further use in studying a new prototype of prosthesis.

Chapter 6 describe the geometry optimisation process of a prototype of a new resurfacing prosthesis. The first deterministic simulations underlined some weak aspects of the prototype geometry. These initial concerns were confirmed by destructive tests conducted by the experimental group. The subsequent optimisation loop reviewed, in two steps, both the prosthesis and the rasp geometry leading to an optimised design which didn't rise any concern for any of the investigated risks, over a large set of operative condition the implant may face during its service life. Additional destructive tests on cadaver specimens underlined a strength increase (+15% with respect to the intact controlateral femur, +25% with respect to the first prototype of the resurfacing prosthesis) of the femoral neck implanted with the optimised design over the strength of femoral neck implanted with the first prototype.

Although this seemed to significantly improve the resurfacing prosthesis biomechanics, a full pre-clinical validation method should consider the whole population of patients the device is indicated to. To this aim, a statistical study of the risk of implant failure was carried out to extend the deterministic analysis over a larger set of conditions and taking into consideration the mutual interaction between the various input variables. Statistical input were anatomical, surgical and activity related variables. Results confirmed the overall quality of the new design although a small set of conditions were found at high risk of neck fractures. Those cases were characterised by critical combination of body weigh, bone mineral content (i.e. high osteoporosis) and activity level. A second statistical analysis compared the risk of neck fractures of the implanted and of

the intact femur, leading to the conclusion that the prosthesis insertion do not alter the “natural” risk of neck fractures of the patient.

The achieved low risk of failure associated to the biomechanical behaviour of the optimised design highlighted that either the quality of the conceptual design or the effectiveness of the adopted optimisation protocol. The optimised design was then considered appropriate for its intended function so as the resurfacing prosthesis recently started clinical trials. Nevertheless, the statistical analysis provided some critical combinations of the input parameters (i.e. related to the individual anatomy, activity and the surgery accuracy) which were found critical. These scenarios might constitute an indicative information to be used during the patient selection phase before surgery.

On the author opinion, the most important limitation of the present study is about loading conditions at the proximal femur. The analysis conducted in the present study based the loading scheme applied to the proximal femur on published data for few subjects during few activities of daily living. These boundary conditions, even significant, can hardly be considered representative of the entire range conditions the implant might face over the population the resurfacing prosthesis is indicated to.

Since experimental techniques to non-invasively measure in-vivo muscle forces are not yet available, the only feasible method to study the muscle contribution to a specific motion task is through modelling the musculoskeletal system. To this aim a new research activity was started with a literature review on musculoskeletal models of the lower limb which is the topic of the last chapter.

Chapter 7 describe the result of the initial literature review and current challenges the LTM is dealing with. After a first training period at the Bio-mechanical Engineering Laboratory of the Delft Technical University (Delft, The Nederland) working on a sophisticated musculoskeletal model of the shoulder, a new activity was started to develop subject-specific musculoskeletal models from medical images. In **Appendix D** are collected a series of activities that were object of international congresses on this topic.

RIASSUNTO

La presente tesi descrive i risultati della ricerca effettuata nell'arco del Dottorato in Bioingegneria. Il titolo della ricerca è: "Sviluppo di modelli muscolo-scheletrici per la progettazione e valutazione pre-clinica di protesi d'anca di rivestimento". Il lavoro, condotto presso il Laboratorio di Tecnologia Medica (LTM) degli Istituti Ortopedici Rizzoli (Bologna), è brevemente presentato nel seguito di questo capitolo.

L'ambito in cui questa tesi si inserisce riguarda il trattamento di patologie debilitanti dell'anca come è il caso di artriti, artriti reumatoidi, necrosi avascolari, dislocazioni congenite, traumi e altre che insieme costituiscono indicazione per la ricostruzione chirurgica del giunto articolare. Tali condizioni risultano ancor oggi, e in modo crescente, un fattore di grande impatto per la salute pubblica, rappresentandone una voce di costo significativa.

Sebbene l'artroplastica d'anca, condotta con le tecniche tradizionali, abbia raggiunto percentuali di successo tipicamente superiori al 90% dopo dieci anni dall'intervento, ancora oggi i trattamenti chirurgici indicati per il trattamento delle patologie sopra elencate, comportano limitazioni importanti dello stile di vita dei pazienti operati. Tali osservazioni assumono, giorno dopo giorno, maggiore rilevanza se si considerano il continuo innalzamento dell'età media della popolazione unito con il protrarsi di stili di vita particolarmente attivi fino ad età avanzata. Questi scenari particolarmente longevi, poco realistici fino a pochi anni fa, hanno prodotto una richiesta crescente di tecniche efficienti, richiesta attesa in ulteriore crescita nei prossimi anni.

Le tecniche di rivestimento d'anca come tecniche mini-invasive sembrarono, fin dai primi anni 60, promettere una migliore efficacia nel ripristino funzionale dell'articolazione quando invece, scontarono alte percentuali di fallimento a causa della mobilizzazione di entrambi gli inserti (acetabolare e femorale). Il loro successivo abbandono venne attribuito a limiti tecnologici dell'epoca ritenuti responsabili delle numerose e premature mobilizzazioni dell'impianto. Recentemente, le leghe in CrCo sviluppate per uso medico, sembrano aver superato i limiti originali così che le tecniche di rivestimento d'anca sono nuovamente una via percorribile e probabilmente capace di mantenere le attese iniziali. Da pochi anni reintrodotte, mostrano risultati clinici preliminari molto promettenti e in linea con le attese.

Mentre molti nuovi disegni protesici dichiarano radicali miglioramenti dell'esito funzionale rispetto ai disegni protesici tradizionali, non è oggi possibile produrne l'evidenza con i metodi di valutazione disponibili, se non attraverso studi retrospettivi. La revisione quindi continua ad essere l'unico strumento affidabile, pur se tardivo, per la valutazione della qualità dell'impianto. In aggiunta, questo approccio rudimentale ostacola lo sviluppo di impianti più efficaci attraverso l'identificazione preventiva di possibili scenari ad alto rischio di fallimento.

Lo sviluppo di prodotti ad alte prestazioni attraverso la previsione, durante la fase di progetto, di probabili scenari di fallimento in opera non è un problema nuovo. La lezione fornita in passato

da molteplici campi applicativi insegna che il successo nella progettazione di prodotti competitivi, evitando fallimenti prematuri, può essere raggiunto soltanto attraverso la valutazione di tutti i potenziali meccanismi che possono alterare le condizioni desiderate di buon funzionamento. Per essere efficace nella previsione del fallimento, è essenziale per il progettista avere una buona conoscenza delle tecniche di analisi e/o empiriche per la previsione del fallimento.

L'obiettivo del lavoro sviluppato nel corso dei tre anni di dottorato è stato sviluppare modelli muscolo-scheletrici per la progettazione e la validazione pre-clinica di protesi di rivestimento d'anca. Il lavoro può essere diviso in tre principali attività: studi preliminari, in cui la tecnica modellistica per l'analisi biomeccanica di segmenti scheletrici (precedentemente sviluppata presso il LTM) è stata validata attraverso il confronto diretto delle predizioni modellistiche con misure sperimentali. La seconda parte contiene l'attività principale, che combina l'analisi formale del fallimento per impianti di rivestimento d'anca, identifica un protocollo di analisi per finire con l'ottimizzazione geometrica e la validazione pre-clinica del comportamento biomeccanico di un nuovo disegno protesico. La terza e ultima parte rappresenta l'inizio di una nuova attività di ricerca che contiene come obiettivo primario il calcolo diretto delle condizioni al contorno all'anca attraverso la modellazione numerica del sistema muscolo-scheletrico.

Nel suo complesso l'analisi delle protesi di rivestimento ha richiesto una combinazione di analisi numeriche e prove sperimentali, spesso le une al servizio delle altre. L'autore ha condotto la parte numerica del lavoro mentre le prove sperimentali sono state condotte dal gruppo sperimentale del LTM e qui sono brevemente riportati i risultati per supportare la validità delle conclusioni.

Nel seguito è descritto il contenuto dei diversi capitoli della tesi che ne svolgono il titolo, mentre sono riportate in appendice le attività svolte al contorno.

Il **Capitolo 1** è un capitolo introduttivo che descrive gli aspetti storici delle tecniche di rivestimento d'anca, gli scenari di fallimento possibili, i parametri biomeccanici rilevanti per lo studio di detti scenari e le tecniche ingegneristiche usate per discriminare situazioni potenzialmente ad alto rischio di fallimento in un contesto multifunzionale.

I successivi capitoli riguardano il lavoro svolto durante il dottorato. La parte iniziale ha visto la messa a punto degli strumenti da impiegare nelle analisi successive, iniziando dalla validazione dei modelli per confronto diretto: le condizioni di prova sono state simulate definendo l'accuratezza del modello attraverso il confronto dei risultati predetti con le misure sperimentali.

Poter controllare i parametri che definiscono il set-up sperimentale è un fattore chiave per un corretto confronto tra i valori modellati e quelli misurati. Con questo scopo è stata sviluppata una apposita cella di carico in grado di misurare la posizione del carico applicato rispetto al femore durante le prove sperimentali. Una descrizione meglio dettagliata dello studio è riportata in **Appendice A**.

Il **Capitolo 2** descrive gli studi di validazione delle capacità dei modelli nella predizione dello stato di sollecitazione dell'osso in campo elastico e della biomeccanica di interazione osso-protesi. I modelli ad elementi finiti (FE) del femore intatto e dello stesso femore operato sono stati validati attraverso il confronto diretto tra i valori di tensione predetti dai modelli e le misure

sperimentali. Il confronto è stato condotto con le misure di 13 rosette estensimetriche applicate sulla superficie dell'epifisi femorale, acquisite durante l'applicazione di diverse condizioni di carico scelte. L'errore medio sul campo di tensione è risultato minore del 10% della massima tensione dell'osso mentre, l'errore commesso sulla predizione dei movimenti osso-protesi è risultato nell'ordine del micrometro.

L'accuratezza ottenuta è stata considerata adatta per le analisi successive, molte delle quali richiederanno la nova generazione del modello per simulare condizioni differenti. Per limitare a quello presentato gli studi di validazione necessari, sono state analizzate le incertezze introdotte nei risultati dalle incertezze sui parametri di modellazione. Infatti, qualunque sia il metodo adottato per la generazione di modelli ad elementi finiti da immagini medicali e per la definizione delle proprietà dei materiali del tessuto osseo, gli inevitabili errori influenzano, in modo imprevedibile, i risultati delle analisi. Per studiare la relazione che intercorre tra le incertezze di modellazione e i risultati è stato condotto uno studio di sensitività; i risultati, presentati nel **Capitolo 3**, indicano che le incertezze sui parametri di modellazione producono un'incertezza nell'ordine del 10%.

Il **Capitolo 4** descrive l'identificazione del protocollo di analisi di protesi di rivestimento d'anca per lo studio del rischio di fallimento associato al comportamento biomeccanico dell'impianto. Il confronto degli scenari di fallimento noti con i meccanismi che potenzialmente possono condurre agli scenari riportati ha permesso di compilare una lista di analisi possibili. Tale lista comprende l'analisi dell'effetto dell'impianto sul rischio di frattura del collo del femore, evento conclusivo della fase post-elastica dell'osso. Essendo i modelli validati solo in campo elastico, la valutazione del carico a rottura del collo del femore è stata prodotta dal gruppo sperimentale del LTM attraverso schemi di carico prodotti numericamente. Le simulazioni sono state in grado di identificare la condizione fisiologica critica e di semplificare il set-up sperimentale al fine di riprodurre in laboratorio fratture clinicamente rilevanti. Lo studio riportato in **Appendice B** descrive l'applicazione delle condizioni di carico identificate numericamente su 10 femori di cadavere. Le fratture ottenute sono risultate essere del tipo voluto e coerenti con il tipo di fratture che si osservano nella clinica.

Il **Capitolo 5** descrive la prima analisi biomeccanica di una protesi di rivestimento di successo e da anni utilizzata nella clinica. I risultati del metodo combinato numerico/sperimentale hanno evidenziato un ottimo accordo con i risultati clinici a corto e medio termine noti per questa categoria di dispositivi. Tali risultati sono stati incoraggianti e hanno costituito la base per la successiva analisi di disegno protesico.

Il **Capitolo 6** descrive l'analisi, il processo di ottimizzazione della geometria e la validazione pre-clinica di un prototipo di protesi epifisaria. Dopo l'identificazione di alcuni aspetti critici del disegno iniziale i seguenti due cicli di revisione della geometria dell'impianto, supportati passo a passo dall'analisi numerica, hanno condotto ad un disegno ottimizzato. Il disegno finale non ha evidenziato rischi rilevanti per nessuno degli scenari di fallimento investigati e una seconda serie di prove distruttive ha confermato gli effetti positivi dell'ottimizzazione condotta. I test distruttivi su femori di cadavere condotti dal gruppo sperimentale del LTM hanno

evidenziato un incremento del 25% del carico ultimo a rottura degli impianti effettuati con protesi ottimizzate rispetto ad impianti realizzati con il prototipo iniziale.

La validazione pre-clinica del nuovo disegno è stata estesa per via statistica, simulando condizioni rappresentative dell'intera popolazione cui l'impianto è potenzialmente destinato. I risultati hanno confermato la qualità del nuovo disegno (che nel frattempo ha iniziato la sperimentazione clinica), sottolineando sia qualità del disegno concettuale di partenza sia l'efficacia del protocollo di ottimizzazione adottato.

Un parametro risultato particolarmente significativo nella la definizione del rischio di frattura del collo di femore è il livello di attività del paziente, analizzato in questo studio utilizzando i pochi dati pubblicati, raccolti in-vivo attraverso protesi strumentate con dispositivi telemetrici. Tali condizioni, anche se significative, non possono essere considerate rappresentative di tutta la gamma di condizioni in cui la protesi può trovarsi ad operare. Ciò ha costituito lo stimolo per l'apertura di una nuova linea di ricerca nel campo della modellazione muscolo-scheletrica dell'intero arto inferiore per la previsione delle forze muscolari, iniziata con una revisione approfondita della letteratura. Il **Capitolo 7** contiene l'analisi dello stato dell'arte nell'ambito della modellazione del sistema muscolo-scheletrico e le sfide attuali che il LTM si trova ad affrontare. In **Appendice D** sono raccolte alcune attività svolte in questo tema e che sono state oggetto di congressi internazionali.

Chapter 1

Hip resurfacing arthroplasty: a new application of an old concept

Arthroplasty (literally "formation of joint") is an operative procedure of orthopaedic surgery performed, in which the arthritic or dysfunctional joint surface is replaced, re-modelled or re-aligned by osteotomy or other procedures. The first popular attempts in the treatment of dysfunctional joints was interpositional arthroplasty with interposition of some other tissue like skin, muscle or tendon to keep inflammatory surfaces apart or excisional arthroplasty in which the joint surface and bone was removed leaving scar tissue to fill in the gap. Other forms of arthroplasty include re-sectional arthroplasty, resurfacing arthroplasty, mold arthroplasty, cup arthroplasty, silicone replacement arthroplasty, etc. Osteotomy to restore or modify joint congruity is also an arthroplasty.

For the last 45 years the most successful and common form of arthroplasty is the surgical replacement of arthritic or destructive or necrotic joint or joint surface with prosthesis.

Hip replacement arthroplasty is the surgical replacement of all or part of the hip joint with an artificial device. Replacement of joint surfaces may be performed on both the pelvis and the femur side or only on the femur head. The first procedure is called total hip replacement (THR) while the second is called hemiarthroplasty in which only the head of femur head is replaced while the acetabular cartilage remains intact.

The purpose of this procedure is to relieve pain, to restore range of motion and to improve walking ability, thus leading to the improvement of muscle strength. A number of pathologies constitute indication for joint replacement, among others:

- osteoarthritis
- rheumatoid arthritis
- avascular necrosis or osteonecrosis
- congenital dislocation of the hip joint
- acetabular dysplasia
- traumatized and malaligned joint
- joint stiffness

Particularly relevant is failure of orthopaedic implants for which failure is a catastrophic event that may cause very high risks for the patient in relation to the complexity of the reconstructive surgery therapy. Nevertheless it constitutes a relevant part of costs of public health.

Processes that may cause failure of orthopaedics implants present particular conditions in which mechanical aspects interact with biological processes so as activated biological processes might lead to failure rather than safe conditions.

Last years have seen the resurgence of mini-invasive techniques for the complete replacement of the articular surfaces of the hip (hip resurfacing arthroplasty). On one side, the reduced impact on the hip architecture of these new devices seems to hold the promise of a substantial improvement of the quality of life of operated individuals. On the other side, the introduction of radically new designs would lead to new scenarios of failure hard to be predicted a priori.

It is clear that the understanding of the risk level of a specific application would help designers in producing new devices with a lowered risk. The present chapter addresses a method for the systematic analysis of failure of hip resurfacing devices which may be used by designers in order to achieve low risk designs of new implants.

1.1 History of hip joint replacement

Research for arthritis treatment has been trying for more than a century to successfully treat this debilitating disease. It was clear that many people required surgery to relieve pain and keep their joints mobile. Initial attempts to treat arthritic hips included arthrodesis (fusion), osteotomy, nerve division [1], and joint debridements. The goal of these early debridements was to remove arthritic spurs, calcium deposits, and irregular cartilage in an attempt to smooth the surfaces of the joint.

Indeed, there was a great search for some material which could be utilized to resurface or even replace the hip. Several proposals and trials were made including the use of muscles, fat, chromatized pig bladder, gold, magnesium and zinc. All met with failure. Surgeons and scientists were unable to find a material which was biocompatible with the body, and yet strong enough to sustain the high forces placed on the hip joint.

In 1925, a surgeon in Boston, Massachusetts, M.N. Smith-Petersen, M.D., molded a piece of glass into the shape of a hollow hemisphere which could fit over the ball of the hip joint and provide a new smooth surface for movement. The glass could not sustain the stress of walking and quickly failed. Afterward he pursued other materials including plastic and stainless steel. The use of stainless steel for surgery, where it might well resist corrosion by bodily fluids, seemed natural. During the 1940's, mold arthroplasty was "state of the art."

A dramatic improvement was made in 1936 when scientists manufactured a cobalt-chromium alloy which was almost immediately applied to orthopaedics. This new alloy was both very strong and resistant to corrosion, and has continued to be employed in various prostheses since that time. While this new metal proved to be a great success, the actual resurfacing technique was found to be less than adequate. It became clear that pain relief was not as predictable as

hoped, and hip movement remained limited for many patients. Mold arthroplasty also did not allow surgeons to treat the numerous and varied arthritic deformities of the hip.

Frederick R. Thompson of New York and Austin T. Moore of South Carolina, separately developed replacements for the entire ball of the hip. These could be used to treat hip fractures and also certain arthritis cases. This type of hip replacement, called hemiarthroplasty, only addressed the problem of the arthritic femoral head. The prosthesis consisted of a metal stem which was placed into the marrow cavity of the femur, connected in one piece with a metal ball which fit into the hip socket. While very popular in the 1950's, results remained unpredictable and arthritic destruction of the socket persisted. In addition, there was no truly effective method of securing the component to the bone. Large numbers of patients developed pain because of this loosening of the implant.

In 1938, Dr. Jean Judet and his brother, Dr. Robert Judet, of Paris, attempted to use an acrylic material to replace arthritic hip surfaces. This acrylic provided a smooth surface, but unfortunately tended to come loose. The idea did lead Dr. Edward J. Haboush from the Hospital for Joint Diseases in New York City to utilize a "fast setting dental acrylic" to effectively join the prosthesis to the bone starting a new era in fixation techniques.

In England, a very innovative surgeon, John Charnley, was also attempting to solve these ongoing problems. He pursued effective methods of replacing both the femoral head and acetabulum of the hip. In 1958, he addressed the eroded arthritic socket by replacing it with a polymeric implant. In order to obtain fixation to the bone he used polymethylmethacrylate from the dentists. These was the starting of a new era which is still the more common method in the treatment of dysfunctional hips; by 1961, Charnley was performing the surgery regularly with good results and the long term outcomes became very predictable.

In spite of the great improvement of clinical outcomes with the new techniques, since that time many attempts were done to reduce the amount of bone resection which is typical for traditional endomedullary stems (Fig. 1). Resurfacing arthroplasty of the hip has always been attractive conservative option in the treatment of end-stage arthritis of the hip in young and active patients. Bone conservation and non-violation of the femoral shaft make it a less invasive option. Normal load transmission and normal biomechanics hold the promise of a better preservation of the conserved bone. The life expectancy of a young patient is very likely to be more than the longevity of any artificial device, when the implant needs to be revised, resurfacing offers better revision options.

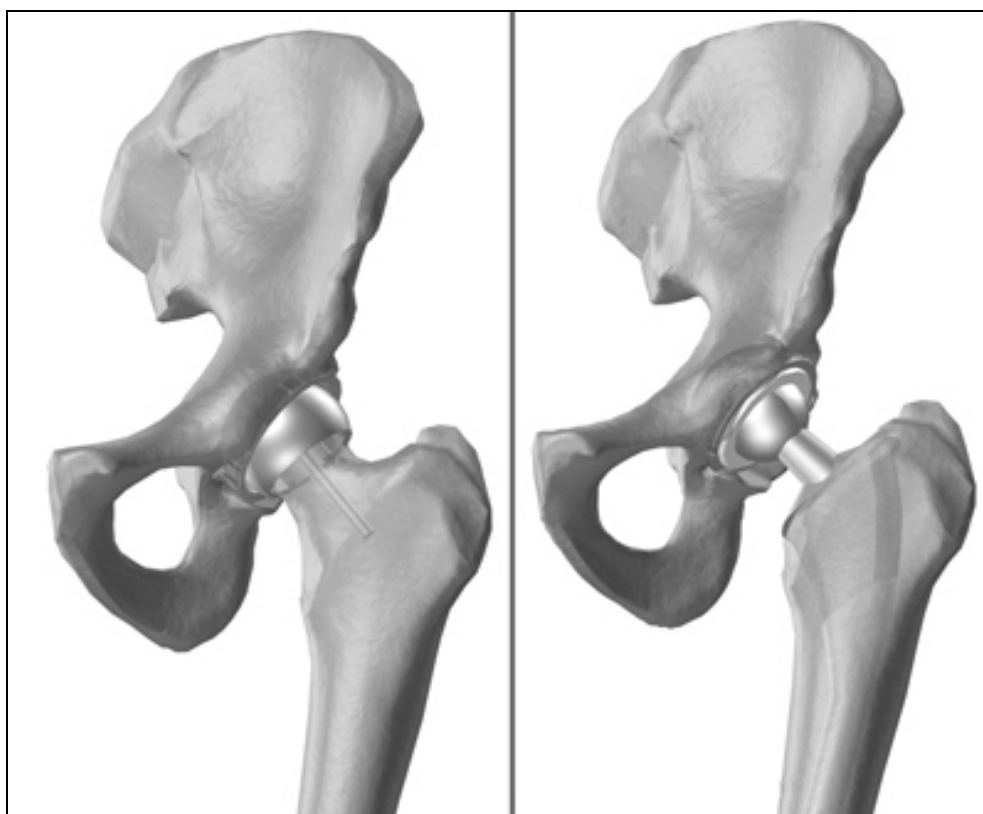


Figure 1 - On the left: a resurfaced hip. On the right: a traditional endomedullary stem.

Many different designs and material combinations were used in the past. Sir John Charnley [2] used an uncemented PTFE/PTFE arthroplasty device which had a high early failure rate. He attributed the failure to the resurfacing procedure and went on to perform metal/PTFE total hip replacement. When they also failed with osteolysis he found that PTFE wear was the problem. He also realised that a large diameter hard-on-soft bearing would give rise to excessive wear and warned against resurfacing.

In 1960s Müller used a press-fit metal-on-metal resurfacing device [3]. England [4], Japan [5, 6], the USA [7], and Germany [8]. Freeman and Furuya [4, 5] initially used PE components against metal cups but, later, they all used metal head on PE cups. Wagner tried a ceramic femoral component, which also failed to improve the result significantly. In France a metal-on-metal double cup device was developed [9] that permitted movement between the metal bearing surface and also between the outer cup and the reamed socket. The results of all these different devices appear promising in the early years, but the medium and long-term results were uniformly unsatisfactory.

It was presumed that many of these failures occurred as a result of femoral head osteonecrosis [10, 11] or stress-shielding [11, 12]. In the early period after surgery the disruption of the natural vascularisation of the femoral head was indicated as a possible source of necrosis in that region. If they survived osteonecrosis, the modification after surgery of the stress distribution under load (stress-shielding) might lead to bone resorption and consequently, to a probable mid or long term prosthesis loosening. It was predicted that high frictional torque forces from the large diameter head would be responsible of the high production of wear debris and of the subsequent

osteolysis. Cement disease was presumed in other cases responsible of stimulating osteolysis by cement debris produced by cement fretting and cementless devices were introduced. Even these did not make a marked improvement in survival. Resurfacing was thus written off as a bad concept altogether [13]. With hindsight, it is now known that many of these failures were a result of accelerate polyethylene wear from a large diameter bearing leading to osteolysis [14, 15].

In Birmingham there was 50% failure rate at 6-7 years with Wagner resurfacing. Retrieval studies on the failure showed the presence of granulomas filled with polyethylene wear particle-laden macrophages in the region of osteolysis. The femoral head outside the osteolytic regions showed a well vascularised viable trabecular bone extending right up the cement margin.

The introduction of metal-on-metal bearings was first abandoned arguing that large diameters would give rise to high frictional torque and lead to early failure [16] However in many patients with metal-on-metal endomedullary stems there was no evidence of osteolysis in spite of an extensive open bone-implant interface.

Work started towards large-diameter metal-metal resurfacings and the earlier notion that resurfacing inevitably lead to femoral head osteonecrosis was dispelled [17, 18].

Advanced in manufacturing made precision finish in terms of surface roughness and out-of-roundness possible and guaranteed a polar bearing configuration. It is now clear that such design might lead to an extremely low wear rate and advancement in tribology now lead to the understanding that large diameter have the potential to function as metal-fluid-metal joints with negligible wear [19]. Thus, it is believed that smooth surfaces and a small clearance might produce satisfactorily a low wear.

The advantage of metal-on-metal bearings must be balanced against the possible adverse effects of particulate metal debris. Some studies [20, 21] have shown increased level of metallic ions in body fluids and adjacent tissue after joint arthroplasties with metal-on-metal bearings. No studies reports evidences for linking metal-on-metal bearing with adverse biological effects even if it is known that metal ions may cause allergic hypersensitivity.

1.2 Comparison of hip resurfacing arthroplasty and traditional THR

Resurfacing of arthritic joint surfaces with prosthetic components is accepted and widely used standard in total hip replacement. Simple resurfacing of the worn joint surfaces has less frequently been used as means of total hip arthroplasty however resurfacing has several theoretical advantages (Fig 1, left).

One obvious advantages of resurfacing is that it preserves bone on the femoral side. It is preferable to retain the femoral head and avoid using the intramedullary device that is implanted in standard hip replacements. However, resurfacing requires a more difficult surgical exposure to prepare the acetabulum without excising the femoral head and neck. For resurfacing to be truly conservative, the surgeon should not remove anymore bone from the acetabulum than would be required for THR, a goal that has been only recently addressed by companies manufacturing thinner acetabular shells.

An additional advantage is a better stress transfer to the proximal femur. This may avoid long term problems caused by stress-shielding of the proximal femur, which can occur with intramedullary fixation of traditional stems [22].

A large femoral head diameter (36 to 54 mm) is associated with lower dislocation rate than conventional prosthesis, which have smaller diameter head (22 to 32 mm in diameter). In two large recent series, no dislocations of the hip were found [23, 24]. Kinematically resurfacing implants more closely resembles the original anatomy and may have better proprioception than conventional THR.

Another theoretic advantage is that revision of the femoral component, when necessary, may be easier than revision of intramedullary stem as more bone is preserved [23-26].

For balance, hip resurfacing has some disadvantages [20]. Although the reduced bone resection at the femoral side should allow maintaining unchanged the original joint centre, when it's the case the lack of modularity of these device reduce the ability to adjust the leg length. Resurfacing is not appropriated in hips with loss of femoral head and neck bone stock or in hips with femoral cysts.

However, the second generation prosthesis has very promising outcomes, even though only preliminary. The femoral neck fracture has an incidence ranging from 0% to 4% [27].

Fracture is usually found early in series, with declining rates as the surgeon overcomes the learning curve. The cause of fracture appears to be both patient and technique related. Patient related factors include obesity, decreased bone mass and inflammatory arthritis. Intra-operative characteristic that may lead to fracture include femoral neck cysts and exposed bone found during preparation. Surgical errors include notching of the femoral neck, tilting of the prosthesis into excess varus and improper prosthetic seating. In the Australian national study (Bueyry 2007) it has been shown that technical problems occurred in 85% of neck fractures.

Aseptic loosening has been found in some series [24]. Most were observed in the first group of the series and were attributed to intra-operative errors. Demographic factors that influenced loosening included an average femoral stem shaft angle of 128.3°, which differed from the rest of the patients that was in average 136°.

1.3 Indications, risk factors, treatment and post operative care

1.3.1 Indications

Total hip replacement is most commonly used to treat joint failure caused by osteoarthritis. Other indications include posttraumatic osteoarthritis, secondary osteoarthritis, and avascular necrosis of the femoral head if remaining bone stock is adequate, inflammatory arthritis if bone quality is adequate, patients with a deformity of the femur and/or internal fixation device that would make insertion of a stemmed femoral component difficult, patients with a high risk of dislocation.

Local protocols should be drawn up for criteria for referral when the symptoms impair quality of life. Referral should be based on an explicit scoring system that should be developed locally, and should take into account the extent to which the condition is causing pain, disability, sleeplessness, loss of independence, inability to undertake normal activities, reduced functional capacity or psychiatric illness.

1.3.2 Risk factors and treatment

The high majority of people who received a THR experience a better joint mobility and loss of pain. Revision is much more substantial than the primary operation and it is always a long and demanding procedure.

In the short term post-operatively, infection is a major concern. Deep infection will often require one or two stage revision surgery with an extended hospital stay and antibiotics. Recurrent dislocation is another indication for revision that might be faced either in the short or in the long term although it is more common in the early period after surgery.

In the long term, many problems relate to loosening. Inflammatory process leading osteolysis as well as the modified bone mechanics may cause bone re-sorption and the subsequent loosening or fracture.

Drawing a personalised risk indicator is not an easy task as many factors concur to the success or the failure. Anatomy, biology and the level of activity are all relevant in defining the individual risk of failure as they define condition at the bonding of the prosthesis. It is however possible to list a number of factors known to influence the implant outcomes. It is interesting to observe that managing the load carried by the prosthesis is a key factor either for the success or the success of the treatment. Known risk factor are:

1. Previous operation of the joint, in general the revision of a resurfaced femur is carried out by the insertion of a traditional endomedullary stem.
2. Surgery accuracy. Studies demonstrated that the rate of loosening is higher in hospitals that perform only small amounts of total joint operations
3. The design of the artificial joint as some models loosen more often than others.
4. The quality of bone: the more of the bone stock, the stronger the interlock will be and the longer the prosthesis will last.
5. Physical activity. Young active patients have higher rates of aseptic loosening.
6. Excessive weight. The higher is the load, the more rapid is the loosening of the implant.

As revision is much more substantial than the first surgery, particular care should be taken if an incipient failure is expected. If the patients experience discomfort or even pain from their artificial joints and the diagnosis revealed an incipient aseptic loosening, the first step is usually a restricted weight bearing regime.

The loose prosthesis may find a new stable position, the discomfort and pain disappears. If the pain and other discomfort from the artificial joint increases then a revision operation becomes necessary.

The more challenging aspect of treatment is the early diagnosis of the incipient loosening. Current research in this field would find methods for the early diagnosis of the incoming failure.

1.3.3 Postoperative care

The modern trend for discharge between 3 and 5 days means that a considerable amount of care that was formerly in hospital is now in the community. Rehabilitation before operation and in hospital is also important. Post-operative rehabilitation includes exercises for stimulating the joint mobility and muscle strength. Among others strengthening exercises (seated leg extension, lying hip abduction, standing hip extension and abduction, knee bends and bridging), stretching exercises, progression of walking distance etcetera.

There is a belief that with hip resurfacing the patient can return to full participation in recreational or professional sports. Long-term results have not been studied to support this idea. Most surgeons agree that joint resurfacing allows patients to be more active than is acceptable for a standard total hip replacement (www.eorthopod.com).

1.4 Types of failure observed in practice

Hip resurfacing arthroplasty has been only recently reintroduced in the market after their first introduction in the 60s failed. Although the very high failure rate of the first generation (15-40%, Australian Orthopaedic Registry) of resurfacing devices discouraged its further use, their attractive potentialities over traditional THR sustained the development of a second generation for which recent outcomes seem very promising.

Hip resurfacing become day by day more common especially for young and active patients so as some retrospective studies are now available reporting up to six year follow-up statistics [23-25, 28-36]

Harlan reported a 94.4% survivorship (95% confidence interval, 91% to 98%) within a group of 400 patients of an average age of 48 years. He also underlined the more common complications, indicating aseptic loosening and femur neck fractures as the most important causes for failure.

RIPO (Registro Italiano Protesi Ortopediche, <http://ripo.cineca.it/>) reported 621 cases during a follow-up of five years of a large group of different devices from different manufacturers (Table 1). Despite the high different failure rate shown by different design, the overall survivorship was (97% confidence interval, 95.1% to 98.8%) higher than what reported by Harlan. No indications are provided here about the type of dysfunctional condition that leads to revision.

Prosthesis model and brand	N.	%	N. of failures	%
BHR (Midland Medical Technologies)	326	52.5	5	1.5
BHR (Smith and Nephew)	144	23.2	1	0.7
ASR (DePuy)	30	4.8	-	-
MRS (Lima)	34	5.5	3	8.8
ADEPT (Finsbury)	19	3.1	1	5.3
RECAP (Biomet)	18	2.9	2	11
CONSERVE PLUS (Wright)	17	2.7	-	-
ICON (International Orthopaedics)	15	2.4	-	-
MITCH TRH (Finsbury)	11	1.8	-	-
DURON Hip Resurfacing (Zimmer)	7	1.1	-	-
Total	621	100	12	1.9

Table 2 - Type and statistics of resurfacing devices in EmiliaRomagna(IT) in 2006 [36].

Clinical outcomes of this new type of hip replacement have been compared to traditional THR underlining that the failure rate is still slightly higher [27] for resurfacing surgeries and the type of observed failure is significantly different.

Many other authors [23-25, 28-35] studied the clinical outcomes. Although luxation, which is the major risk of complication for traditional THR [36], is not a major concern for resurfaced hips, the two main causes of failure are loosening and fractures of the femoral neck.

1.5 Definition of failure mode

Success in designing competitive products while averting premature mechanical failure can be consistently achieved only by recognizing and evaluating all potential failure modes [37].

To be effective in averting failure, it is essential for designer to have a good working knowledge of analytical and/or empirical techniques of predicting failure.

Engineering design is an iterative decision-making process that has as its objective the creation and optimisation of a new or improved engineering device for the fulfilment of a human need or desire. Whether a designer is creating a new device or improving an existing design, it is essential to provide the “best”, or optimum, design consistent with constraints, as time or technological limits.

The needs of improving the performance of actual design force designer to study the behaviour of materials more carefully, to better assess the nature of actual service conditions and the many modes of failure.

Failure may be defined as a change in a mechanical system that renders it incapable of satisfactorily performing its intended function.

Following the idea suggested, one might define “failure mode” as the physical process (or processes) that take place (or combine their effect) to produce failure.

It has been suggested that a systematic classification might be devised by which all possible failure modes can be predicted. Such a classification is based on defining three categories; each specific failure is then identified as a combination of one or more manifestation of failure together with one or more failure-inducing agents and failure locations.

1. Manifestation of failure

- a. Elastic deformation
 - b. Plastic deformation
 - c. Rupture or fracture
 - d. Material change (structural, chemical, nuclear and biological)
2. Failure-inducing agents
 - a. Force (steady, transient, cyclic and random)
 - b. Time (very short, short, long)
 - c. Temperature (low, room, elevated, etcetera...)
 - d. Active environment (chemical, nuclear, biological)
 3. Location of failure
 - a. Body type
 - b. Surface type

This general classification would lead to precisely describe any specific failure mode selecting appropriate category without omitting any of the three major categories. For example one might select plastic deformation from the first category, steady force and room temperature from the second category and body type from the third category. Thus, the failure mode selected could be properly described as body-type plastic deformation under steady force at room temperature. This mode is commonly called yielding.

Thanks to the specific operative condition of orthopaedic implants not all combination of categories listed above are of interest for orthopaedic implants. For example, temperature is not relevant as the body temperature is constant at 37 °C.

A further restriction of the field of analysis can be achieved when experimental trials are available for the prototype of the device under analysis or on similar designs. Thus, the analysis can be focused on a restricted set of failure modes including only those that are able to produce dysfunctional conditions coherent with what observed in practice.

1.6 Mechanical implications on relevant biological processes

The insertion of the prosthesis in the hosting bone during surgery produce an alteration of biochemical and biomechanical environments producing a number of reactions within living tissues that are not always predictable. However, before to be used in clinics materials undergo a broad and severe series of bio-compatibility tests which are not the focus of the present work. What is interesting here is to point out a group of mechano-biological implications that might promote loosening and the subsequent failure of the implant. The study of mechanical implication in biological processes is named mechanobiology.

The modification of the bone mechanics produced by THR surgery is more relevant in those bone regions close to the prosthesis and the amplitude of this variation depend mainly upon the type of prosthesis and the hosting bone characteristics, if the individual activity remains constant.

Cited modifications might be big enough to stimulate precise biological processes that in different manner might produce failure. Of this class of physical phenomenon are the adverse bone re-modelling, osteolysis and the formation of a fibrotic interface at the bonding of the prosthesis.

1.6.1 Bone: a living tissue

The bone tissue is the structural material in charge of sustaining physiological loads against external and muscular forces in order to produce the desired body motion. It must change its dimensions during the life of the individual following the juvenile body growth and it is able to adapt himself optimising its structure to the particular level of activity. To this final goal, bone tissue is an extremely complicated system that serve to biological and structural functions in which some of the biological processes serve to maintaining the mechanical competences of the structure.

Following chapters evidences the complexity of the structural part in which desired mechanical properties are achieved by an appropriate mixture of a stiff mineral (hydroxyapatite) and tough organic material (collagen).

In the next two paragraphs it is described more in detail the structure of the bone matrix and the biological processes in charge of maintaining the structure efficiency over time.

1.6.1.1 The bone matrix

The two major components of mineralised bone are organic and inorganic materials. Inorganic salts makes up 76% of cortical bone, while the remaining 24% is made of organic matrix.

The fluid phase of the organic matrix is defined as the extra- cellular organic phase. It is primarily composed of protein, glycoprotein, and polysaccharide, which is secreted by osteogenic cells and surrounds them. The organic matrix consists mainly of collagen fibres (90%) embedded in an amorphous ground substance.

The amorphous ground substance is a non-collageneous cementing substance in which collagen fibres and crystals of various minerals are embedded. Although not fully characterized yet, bone ground substance is known to contain phosphoproteins, glycoproteins, and small amounts of proteoglycans, lipids and peptides. All these components play a role in the mineralization.

Bone collagen, like the collagen of tendons is composed exclusively of type I collagen. But, while collagen in bone calcifies, the type I collagen found in skin tendons does not. This difference may be due rather than to specific properties of the collagen alone to the interaction of collagen fibrils with macromolecules within the extracellular matrix. Recently, phosphoproteins have been proposed as possible regulators of mineral deposition.

Several biomechanical differences exist between the collagen of bone and that of tendons. These differences involve the post-translational modifications of the collagen and the distribution of intermolecular cross-link. Bone collagen is less soluble, more densely packed and less hydrated. Bone collagen does not swell when exposed to dilute acids. However, how these differing properties contribute to the capacity to mineralise remains unknown.

Mineral constitutes 75% of bone weight. Around 50% of bone mineral content is in a form similar to hydroxyapatite $[\text{Ca}_{10}(\text{PO}_4)_6(\text{OH})_2]$. In mature bone, the hydroxyapatite is present as needles, thin plates or leaves 15 to 30 Å long.

Crystals are minute and impure, containing many ions other than calcium, phosphate and the hydroxyl ions found in pure synthetic hydroxyapatite. Furthermore, there are substantial quantities of carbonate, citrate sodium, and magnesium in bone mineral. The quantity of fluoride is variable. Trace amounts of iron, zinc, copper, lead, manganese, tin, aluminium, strontium, boron and silicon have also been reported.

The hydroxyapatite crystals are regularly distributed at intervals of 600 to 700 Å along the length of the collagen fibres. Ground substance surrounds and stabilizes these crystals. This interaction between hydroxyapatite and collageneous proteins brings about the hardness and the rigidity of bone.

During growth, the amount of organic material per unit volume remains relatively constant, while the amount of water decreases and the proportion of bone mineral increases, attaining a maximum of about 65% of the fat-free dry weight of the tissue in adults. The reduction of water content results in a stiffer bone in adult with respect to the child, thus in bone structure that is less resistant to fracture loads.

1.6.1.2 Bone biology

Five kinds of bone cells can usually be recognized in the growing and adult skeleton [38]: osteoprogenitor cells, osteoblasts, osteocytes, osteoclasts, bone lining cells.

Osteoprogenitor cells have the capacity of mitosis and further differentiation and specialization into mature bone cells. There are two types of osteoprogenitor cells, one giving rise to bone-forming osteoblasts, and the other giving rise to bone re-sorption osteoclasts. Both types are commonly found near the bone surface [38].

Osteoblasts are roughly cubical mononuclear cells about 15-30 microns across. Osteoblasts are bone-forming cells. They are responsible for the synthesis and deposition of non mineralised bone matrix, the osteoid [39, 40]. Osteoblasts also appear to participate in the calcification of bone, and they seem to regulate the flow of calcium and phosphate in and out of bone. The life cycle of an osteoblast involves:

- the birth from a progenitor cell;
- the differentiation and participation in elaborating matrix and calcifying units;
- either returning to the pre-osteoblast pool, transform into bone-lining cell and burial as osteocytes, or death.

Osteocytes are the principal cells of fully formed bones. They are hosted in lacunae (only one cell is ever found in a lacuna) and derive from osteoblasts that have secreted bone around them. Mature and relatively inactive osteocytes possess a cell body that has the shape of an ellipsoid, the longest axis (about 25 microns) parallel to the surrounding bony lamellae and its shortest is perpendicular to the plane of the lamellae.

Osteocytes have many cell processes that can extend from considerable distances (on the order of micron) in canaliculi. These cell processes can contact other osteocytes and bone surface cells thank to extensive microfilaments and gap junctions at the contact points. This explains how

cells can survive in such an isolated environment: ions, nutrients, waste products, and small molecules can pass through the gap junctions of adjoining cell processes; fluids can percolate through both the space between the cell and their processes and through lacunar and canalicular walls [41].

The exact functions of osteocytes are not yet clear. However, it is widely assumed that they must have an essential role in the maintenance of bone and in signalling the requirement to resorb micro-damaged bone. They may act as local sensors of the mechanical and chemical state of the bone. The average life cycle of an osteocyte varies with the metabolic activity of the bone and the likelihood that it will be remodelled, but has been estimated to be about 25 years [42, 43].

Osteoclasts are multinucleated giant cells (20-100 μ m or more) that are responsible for the bone re-sorption process. Active re-sorption osteoclasts are usually found in or near cavities on bone surfaces (re-sorption pits or Howship's lacunae) [44].

In the light microscope, the surface of the osteoclast adjacent to the bone has a striated appearance corresponding to an area of extensive membrane infoldings, termed the ruffled border [45]. This is a unique surface modification, which facilitates bone re-sorption. The structure and the substances concentrated at this border help the transport of materials through the membrane, while bone can be seen to dissolve beneath it. Osteoclasts lacking ruffled border are not capable of bone re-sorption.

Around the ruffled border there is a zone (clear or filamentous zone) devoid of organelles, containing actin filaments: this zone seems to be the site for the adhesion of the cell to the bone surface.

There is little information concerning the life cycle of osteoclasts in vivo. The life cycle of an osteoclast is believed to be about 10 days. Cessation of bone re-sorption is associated with migration of osteoclasts from endosteal surfaces into adjacent marrow space, where they are believed to degenerate and disintegrate.

Very flat, elongated cells with spindle-shaped nuclei, the bone-lining cells, cover most resting bone surfaces in adult skeleton. Their name is suitable to describe the cells that are apposed to inactive bone surfaces, even if it has been incorrectly used to describe any cell apposed to the bone surface [46].

Bone-lining cells serve as a barrier separating fluids percolating through the osteocyte and lacunar canalicular system from the interstitial fluids. This membrane barrier around bone may have a role in mineral homeostasis, by regulating the calcium and phosphate flows in and out the bone fluids, as well as in controlling the bone growth by maintaining a suitable environment [41].

There are now increasing evidences that the bone lining-cells are transducers for bone re-sorption and that they prepare the surface for osteoclastic re-sorption [39]. It is also clearer that the bone-lining cells can contribute to sense the shape of bone and its reactions to stress and strain stimuli, and to transmit these sensations as signals to the bone surface, where new bone formation or re-sorption is possible.

Bone-lining cells seem to be derived from osteoblasts and/or osteoblast precursors that have ceased their activity or differentiation and that they have flattened out on bone surface. The fate of bone-lining cells is still an enigma. They can return to the stem cell or pre-osteoblast pool and/or meet their death [41].

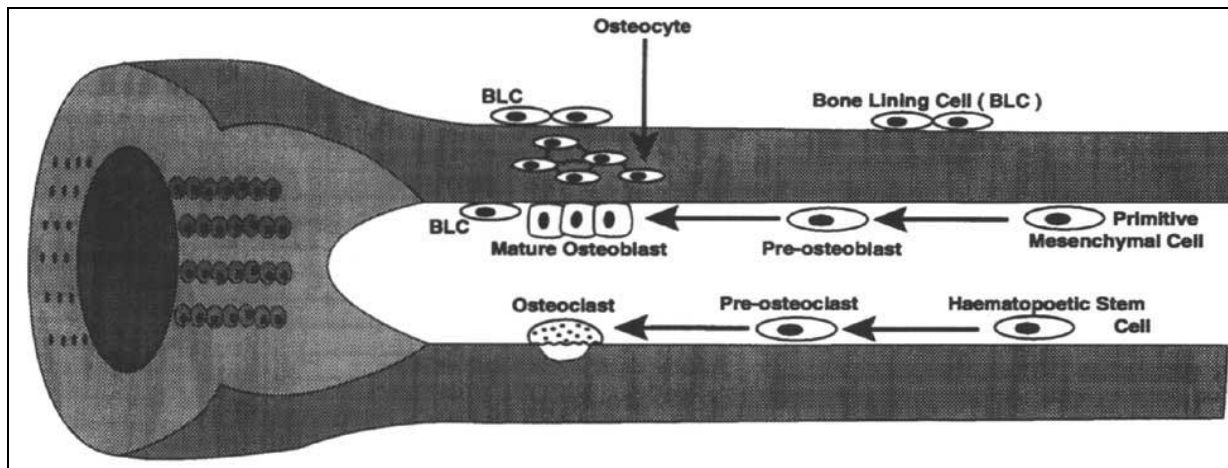


Figure 2 – Schematic diagram of a developing long bone illustrating the cells of bone

This complicated system of cells is responsible to maintain the efficiency of the bone structure by adapting its shape and toughness to its mechanical competences and activities.

When a third body replace a part of a bone segment such in case of joint replacement surgeries (see stress-shielding, paragraph 1.6.2.1) the local mechanical competence of bone might be substantially modified. This may alter the previous equilibrium of the bone biology stimulating the bone adaptation to the new conditions by modifying the bone shape and the local amount of its mineral content. Between others, the two processes of bone re-sorption and re-modelling, which are responsible of the cited process of bone adaptation, are particularly relevant for orthopaedic implants.

Bone re-sorption

The resorption of bone involves [47-50]:

- the initial release of calcium and phosphate ions into the extracellular fluid;
- the removal of the organic matrix.

These events occur simultaneously or in rapid succession on the bone surface adjacent to osteoclasts. The actual mechanism of osteoclastic bone resorption is still unclear. Most agents that induce resorption produce biochemical changes, which create the ideal environment conditions for resorbing cells. There is now growing evidence that the cells of the osteoblast lineage have a role in the regulation of bone resorption. The two main hypotheses for osteoclastic bone resorption are:

- 1) osteoclasts may be active throughout the total resorptive period;
- 2) bone resorption may be a two-period process initiated by osteoclasts dissolving bone mineral matrix, followed by the digestion of the organic matrix by action of mononuclear cells.

Many studies have been performed to analyse the effect of organic and inorganic substances as activators or inhibitors of bone resorption. In some cases, such substances have been experimented as localized treatment associated to surgical therapies [51-55].

Bone re-modelling

At infancy bone mass is quantitatively inferior, while the quality of bone tends to decrease in time in the adult (where with “quality”, it is meant the bone mineral content). Therefore, like many other tissues, bone must replace or renew itself. This replacement of immature and old bone occurs by a sequence of re-sorption and production of new lamellar bone. The result is the remodelling process, necessary to produce and maintain bio-mechanically and metabolically competent bone. For this reason, the remodelling process is not limited to growth, but it characterizes the whole life of bones.

Remodelling is a composed process, which occurs at the foci. On each focus there are specialized groups of cells that accomplish a single quantum of turnover. This quantum consists in the erosion and recreation of one quantum of bone: new bone replaces approximately the same quantity of old bone.

The group of cells is called bone remodelling unit. Bone remodelling units travel through the cortex or across the trabecular surface. This mobility allows the units to concentrate in the regions where remodelling takes place. Following signalling mechanisms that are still under study, the remodelling unit reaches the target focus. Then, the unit undergoes a series of cellular events [38, 41] (Figure 3).

1. Firstly, a group of osteoclasts proliferate from progenitor cells.
2. Then, osteoclasts begin to excavate a volume of old bone.
3. Once their task is completed, they disappear.
4. A reversal zone is then produced, so that new cement line smoothes off the irregular surface of the re-sorption.
5. A group of osteoblasts appear in order to produce new bone.

The entire process is controlled and governed by stimuli that are still unknown. What is clear, is that biomechanical stimuli are converted into messages that are understandable by the cells (chemical, hormonal). The complicate network and sequence with which these stimuli act on the cells regulate the remodelling process: the time scale, the volume of bone resorbed, the volume of bone generated. The new bone structure is this way adjusted according to the characteristics of the biomechanical stimulus at the origin of the remodelling process.

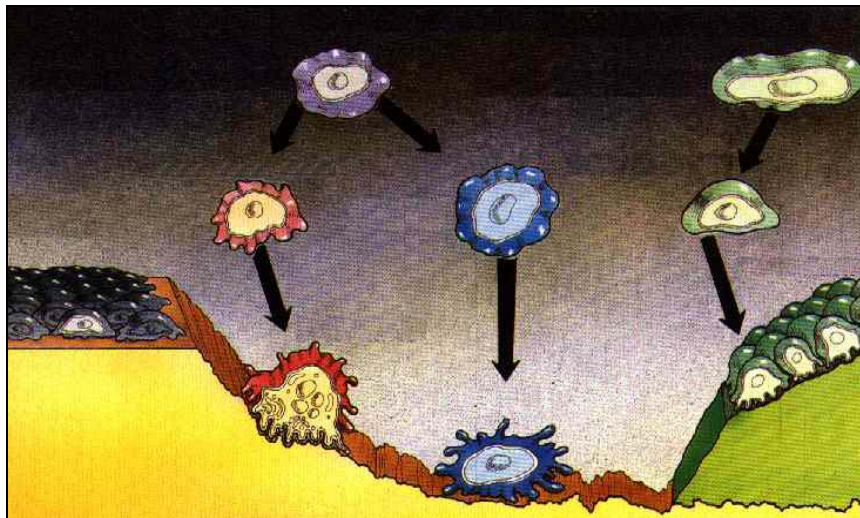


Figure 3 - Diagram of the bone remodelling process.

Haversian and cortical remodelling. Cortical remodelling is the destruction of compact bone followed by the generation of new Haversian system. The osteoclasts of the bone remodelling unit form a re-sorption tunnel within the bone, which is refilled by the osteoclastic apposition of concentric lamellae, so as to form a secondary Haversian system (osteon).

Trabecular bone remodelling. Unlike cortical remodelling, trabecular remodelling occurs on a bone surface, the trabecular-endosteal surface. Apart from this aspect, the remodelling process is quite similar in trabecular and cortical bone (Table 3).

Factor	Cortical	Trabecular	Whole skeleton
Mineral apposition rate* ($\mu\text{m}/\text{d}$)	0.8	0.6	0.7
Duration of BRU re-sorption (days)	24	21	21
Duration of BRU formation (days)	124	91	101
Duration of remodelling period (days)	147	112	122
Total birth rate (per activation of new BRU)	180	720	900
Bone turnover rate (%/yr.)	3	26	8
Total turnover (mg Ca/day)	70	158	220

Table 3 - Comparison of bone dynamics and turnover in cortical, trabecular and whole skeleton. (*): corrected for orientation. BRU: Bone remodelling unit.

1.6.2 Adverse biological processes for orthopaedic implants

It has been common belief in the last decades that the bone turnover processes were mostly governed by homeostasis, ignoring or underestimating the role of mechanical functions.

Frost [56] re-proposed that bone turnover processes serve the needs of bone mechanics. According to this vision, bone turnover mechanisms respond directly to mechanical usage, thank to the Minimum Effective Strain mechanism. Depending on the mechanical usage of bone, signals are transmitted to the ultimate responding modelling and remodelling systems, which actively alter bone mass and shape.

In normal conditions bone is always characterized by a balanced coexistence of resorptive and appositional processes which have been classified in processes of bone formation, modelling, repair, re-modelling and re-sorption.

The bone formation occurs by a first formation of a non-mineralised matrix and its subsequent mineralization. This complex process is regulated by hormones, synthetic growth, and local factors. Modelling is defined as the alteration of the bone size and shape, it serves primarily both to alter the amount of the present bone and to determine its shape. An example of bone modelling is given in Figure 4. Bone repair is the “heal and protection” mechanism of bone. The classic example of bone repair is fracture healing in which the bone repair process restore the segment functionality trough a number of different phases from the first haemorrhage to the last compaction and remodelling (Figure 4).

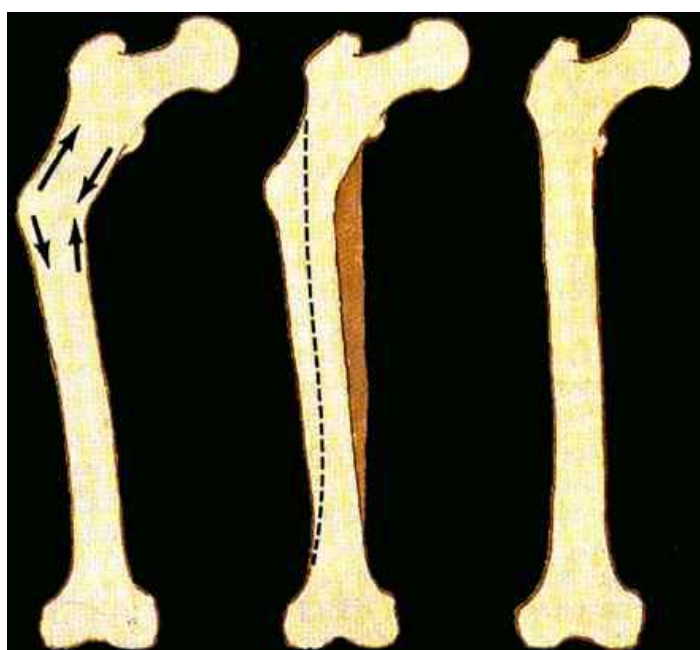


Figure 4 - An example of bone modelling. Here the bone modelling is induced in the femur by a traumatic event. The post-traumatic defective healing has deformed the femur, which gradually models towards a shape that is similar to the original one.

1.6.2.1 The stress shielding effect

When a surgery replace a part of the skeleton with an artificial device differences introduced by variations in stiffness and shape affect the original flow of stresses in bone producing the effect named “stress shielding”.

The skeleton in our bodies is normally loaded by the body weight and muscles forces, where the load increase the skeleton grows more bone tissue in the loaded area. On the contrary, in areas with diminished load the skeleton retains only so much bone tissue that is necessary to sustain the diminished load leading to a weaker region.

A simple mechanical rule says that in every system composed of two materials loaded in parallel, the stiffer component will sustain the greater part of the load.

In case of THR, the shaft component is much stiffer than the skeleton and it sustains the greater part of the femoral load in the proximal region leading to the consequent risk of bone re-sorption. Contrarily, the stress rising around the tip of the femoral shaft induce a bone thickening which is often painful for the patient.

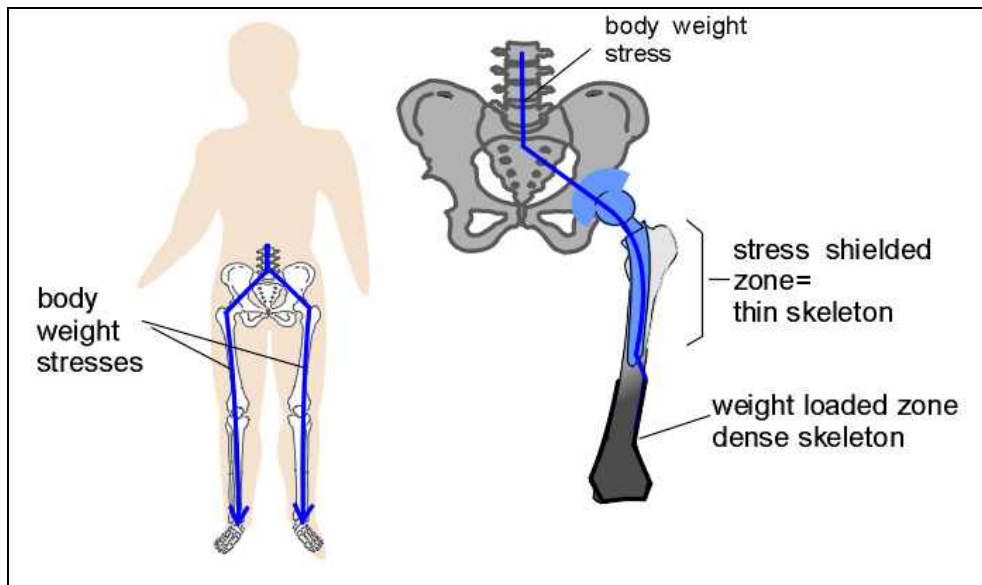


Figure 5 – Stress flow trough an healthy skeleton (left) and modified stress flow after THR (right)

In summary, consequences of the changed mechanics are two:

1. The upper part of the femur is more susceptible to fracture.
2. Thickening of the skeleton at distal stem is often painful as many patients with cementless shafts often claim about the pain, especially during the first years after the surgery.

These modifications in the bony structure are the result of processes of re-sorption and re-modelling, the same process that play also a fundamental role in maintaining the integrity of normal bones. Bone re-sorption and re-modelling are better detailed in the following.

1.6.2.2 Osteolysis

There are many causes why the once stable total joint becomes loose. Among others, the deep infection is a well known cause of loosening of artificial joints.

The reaction of the peri-prosthetic tissue to the implanted device is the result of a complex network of cellular functions. The interaction mechanics between bone and prosthesis might stimulate an inflammatory response, the alterations of the immunitary system and changes in blood components.

The gliding surfaces of the artificial joints generate continuously an enormous number of submicroscopic wear particles which spread into the tissues around the artificial joint and provoke an inflammation reaction. The inflammation reaction triggers osteolysis, as mechanism is called, which dissolves the skeleton around the bone-prosthesis contact surfaces.

Ooparaugo reviewed the literature and linked the revision for excessive osteolysis of the peri-prosthetic bone with the volumetric wear rate [57]. The incidence of osteolysis was low in case of wear rate lower than 80 mm³/year.

The analysis of the particles size (from 0.3 micrometers to few micrometers) of the debris is not easy to measure as their very small size require sophisticated techniques to be detected. Nevertheless studies[58] of the retrieved periprosthetic bone revealed billions of these tiny particles in the tissue (average, 1.65 x 10¹¹ particles per gram of tissue)

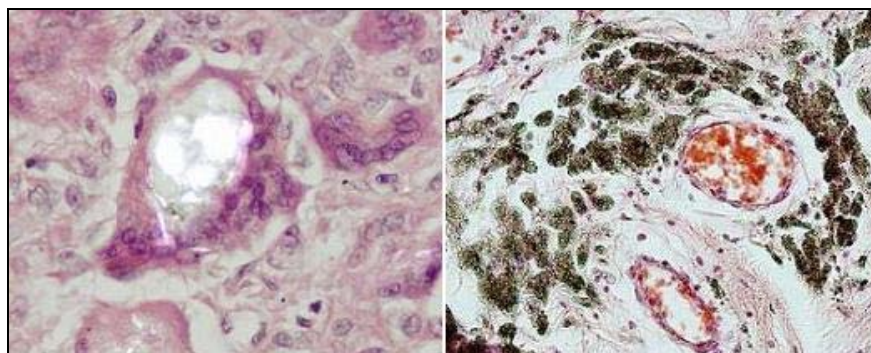


Figure 6 - Histology images of peri-prosthetic tissue on two different hip implants. On the left, wear polyethylene particles produced by a metal-polyethylene friction. On the right, wear ceramic particles produced by a ceramic-ceramic friction.

The prevailing theory that explains how the osteolysis dissolves the skeleton consider responsible of the process to start very small particles produced by wear of gliding surfaces. Rhythmic movements of the total joint pressurize the joint fluid containing these particles in the tissues around the total joint. The natural function to clean out tissues from all rests of dead cells and other undesired particles is ahead of macrophages cells.

When macrophages digest the fine particles, transported with the joint fluid, they change their benign nature and begin to digest the healthy bone tissue producing osteolysis.

In some patients this "dissolving" of the bone stock may be so widespread that large parts of the skeleton are being completely destructed. But certainly there are special biological factors, that predestine one person to develop osteolysis easier than other patients. This is a large research field for the "molecular biology" in the future [59].

Scientist [57, 58]also discussed other factors that might be involved in the development of osteolysis around an artificial joint. One such factor is the alleged hypersensitivity of some patients to the materials from which the artificial joint is fabricated.

The rates of aseptic loosening in published [57, 58] studies depends on:

1. The selection of patients, their age, their hip diseases
2. The type of the prosthesis, cemented, cementless, etc.

There is also much "hidden pain" in many reports. Many patients (according to some studies about 25 % of all patients) have had pain in their total joint although they were not operated on second time. These patients do not appear in statistics.

1.6.2.3 Tissue differentiation at the bone-prosthesis interface

Some retrieved stems showed a fibrous layer at the bone-prosthesis interface which is characterised by low mechanical properties, likely responsible of loosening [60-64].

The bone layer adjacent to the bone-prosthesis interface keeps the implant stable and is of extreme importance as loosening is responsible of the two-third of hip replacement failures. When the layer of bone tissue that once adhered close to the artificial joint is replaced by a layer of loose connective tissue that now separates the artificial joint from the bone the stability of the implant may be compromised.

Differentiation of the tissue in this region may happen in various different manner not yet fully understood. Major evidences underlines two principal processes that might induce the local transformation of bone, both process seems completely driven by the bonding interface mechanics.

The first process involve in a local bone re-sorption that follows, very locally, the same process that has been discussed in case of stress-shielding. It has been hypothesised the microstimulation at the bone-implant interface upregulates osteoclast activation pathways [61] so that osteoclast differentiation factor (RANKL/OPG) have been monitored during experiments. Results underlined that micromotion at the bone-implant interface induce a rapid response of the bone re-sorption process.

The second process that has been hypothesised involve differentiation of mesenchymal cells (MSCs). Although no clear mechano-biological explanation has yet been given, models have been developed that hypothesise a relation between mechanical environment and tissue differentiation [65-67] into fibroblast rather than chondrocytes. A number of experiments suggested that local mechanical environments of MSCs influences cellular proliferation, and the subsequent remodelling or degradation of the repair tissue, while cartilage formation and ossification only occur after the soft tissue have provided sufficient stability.

Again, bone-prosthesis micromovement would be considered the mechanical stimuli and a safe threshold below which more likely occur the MSCs differentiation into osteogenic pathways.

1.7 Prediction of failure

Succeeding in the development of a new prosthesis design that adequately accomplish its desired functions with a minimum number of failures is of major importance in any branch of engineering, particularly when designing orthopaedic devices. When failure analysis and prevention are coupled with product design from its conception, potentially shorter design times and fewer redesigns are necessary to arrive to a final product design.

Engineering focused the need of addressing potential failure modes at the conceptual design phase with different methods such as Function-Failure Design Method (FFDM) [68], Failure Mode and Effect Analysis (FMEA) [69, 70] and others. Each of them has been introduced to enable failure-based decision-making during the early stages of conceptual design and have it is pro and cons.

Predicting failure of orthopaedic devices have its specific problems associated to its operating conditions. They support very complex loading systems that are not yet fully understood, implant parts have complex geometries, material properties of bone are very different through its volume and mechanical conditions might influence biological processes as to increase the risk of failure.

When engineers face problems of this complexity their inclination is always to develop a theory that relates behaviour in the complex situation to behaviour in a simple easily evaluated test. Specifically, predicting failure under a complex conditions involve in using a theory that relates failure in the complex situation to failure by the same mode in a simple condition test through a well chosen “modulus”. To be useful such modulus must be calculable in the complex condition and measurable in the simple test.

In the following paragraphs are reported the proposed methods to discriminate critical failure conditions of hip resurfacing devices for each failure mode considered critical for this class of prosthesis.

1.7.1 Predicting mechanically-related failure modes

The choice of the various failure mode to be investigated for THR is carried out by matching the different categories exposed in paragraph 1.5 with observed failure conditions reported in paragraph 1.4.

Possible failure, purely related to the joint mechanics, is the component fracture (of bones, prosthesis and cement), fatigue of the prosthesis and the cement, cement fretting, shock or impact of bone cement and prosthesis and wear of the bearing surfaces.

Adverse biological processes for the implant success are bone resorption and remodelling, osteolysis and tissue differentiation at the bone-prosthesis interface.

1.7.1.1 Combined stress theory of failure

Predicting failure is a relatively simple matter in case of uniaxial state of stresses of isotropic materials. Once the stress-strain curve, obtained from few simple tension and compression experiments, is available the prediction of failure involves in comparison of the predicted stress with the stress threshold for failure.

Unfortunately that is not the case of orthopaedic implants for which geometry and loading conditions are very complex either for the prosthesis, the cement or the bone. The material properties of the prosthesis are generally well known and uniform within its volume. Materials properties of the cement are known with a higher level of uncertainties as they depend by a large number of parameters of the adopted surgical technique. Materials properties of the bone are variable location by location, direction depended, strictly related to its local mineral content and they change over time on the base of a variety of mechanical and biological factors not all yet fully understood.

The basic assumption that constitutes the framework for all combined stress failure theories is that failure is predicted to occur when the maximum value of the selected mechanical modulus in the multi-axial state of stress becomes equal or to exceeds the value of the same modulus that produce failure in a simple uniaxial stress test using the same material.

Experimentation with a variety of materials would show that the theory works well for certain materials but not very well for others. Such attempts to devise failure theories and experimentally verify them as led to many failure theory proposal.

A very large number of failure criterion has been proposed in engineering for predicting failure under a tri-axial state of stresses. Bone behaves as brittle materials [71, 72] which produce failure in a manner well described by the Saint Venant's theory. Bone cement which also behave as a brittle material, produce failures well described by the Rankine's theory [73]. Metal alloys used in manufacturing prosthesis are ductile materials for which failure is well described by the Von Mises's theory.

Rankine's theory

The maximum normal stress proposed by Rankine may be expressed as follow:

“Failure is predicted to occur in the multi-axial state of stress when the maximum principal normal stress becomes equal or to exceeds the maximum normal stress at the time of failure in a simple uniaxial stress test using a specimen of the same material”

Thus, failure is predicted by the maximum normal stress theory to occur if:

$$\sigma_1 \geq \sigma_t$$
$$|\sigma_3| \geq \sigma_c$$

where $\sigma_1, \sigma_2, \sigma_3$ are the principal normal stresses; σ_t is the uni-axial failure strength in tension; and σ_c is the uni-axial strength in compression.

Evaluation of the proposed maximum normal stress theory leads to the observation that the prediction of failure is based solely on the magnitude of the maximum normal component of stress, regardless of the magnitude or direction of the other two principal stresses.

The ability of the Rankine's theory in predicting failure of ductile materials is generally poor, on the other hand, for brittle materials the maximum normal stress theory is probably the best available failure theory, though it may yield conservative results for some state of stress.

St. Venant's theory

In words, the maximum normal strain theory, proposed by St. Venant, may be expressed as follow:

“Failure is predicted to occur in the individual state of stress when the maximum principal normal strain becomes equal or to exceed the maximum normal strain at the time of failure in a simple uniaxial stress test using a specimen of the same material”

Thus, failure is predicted by the maximum normal strain theory to occur if:

$$\begin{aligned} \varepsilon_1 &\geq \varepsilon_t \\ |\varepsilon_3| &\geq \varepsilon_c \end{aligned}$$

where ε_1 , ε_2 , ε_3 are the principal normal stresses; ε_t is the uni-axial failure strain in tension; and ε_c is the uni-axial strain in compression.

Von Mises's theory

“Failure is predicted to occur in the multi-axial state of stress when the distortion energy per unit volume at the time of failure becomes equal to or exceed the distortion energy per unit volume at the time of failure in a simple uni-axial test using a specimen of the same material”

The total strain energy can be divided in two parts: the energy associated solely with change in volume (dilatation energy) and the energy associated solely with change in shape (distortion energy). It was postulated that failure, particularly under conditions of ductile behaviour, is related only to the distortion energy with no contribution from the dilatation energy.

The mathematical expression that describes the proposed concepts is:

$$(\sigma_1 - \sigma_2)^2 + (\sigma_2 - \sigma_3)^2 + (\sigma_3 - \sigma_1)^2 \geq 2\sigma_f^2$$

where σ_1 , σ_2 , σ_3 are the principal normal stresses; σ_f is the uni-axial failure strength.

1.7.1.2 Fatigue

Orthopaedic implants sustain highly fluctuating loads that induce a respective fluctuating stress that might produce failure by fatigue. It is impossible to distinguish changes in the material and failure may happen with little or no warning at all. A resting period, with fatigue stress removed, lead to some recovery from the effect of the prior cyclic stressing only in living tissues.

Thus, in general, the damage done during the fatigue process is cumulative and generally unrecoverable. The given definition is surely true for most of engineering materials, as prosthesis and cement, while it is not true for bone. In fact, the large number of microcracks produced in bone by the daily activity is contrasted by the osteoblast activity which tend to restore the bone integrity.

Fatigue failure investigations over years have led to the observation that the fatigue process embrace two different domains of cyclic stressing or straining that are significantly different in character, and in each of which failure is probably produced by different physical mechanism. One domain of cyclic load is that for which significant plastic strain occurs during each cycle. The domain is associated with high load and low number of cycles to produce fatigue failure, and is commonly referred to as low-cycle fatigue. The other domain of cyclic loading is that for which the strain cycles are largely confined to the elastic range. This domain is associated with lower loads and long lives or high number of cycles to produce fatigue failure. It is commonly referred to as high-cycle fatigue. Low-cycle fatigue is typically associated with cycle lives from one up to 10⁴ or 10⁵ cycles and high fatigue cycles for lives greater than about 10⁵.

Biological processes responsible of maintaining the bone structure efficient are more detailed discussed in dedicated paragraph where the bone cells activity is briefly presented. What is relevant in fatigue of bone is that biological processes in charge of repair structural damages needs time and fatigue failure in bone is also possible, although in case of a vigorous activity [74-78].

Orthopaedics implants have to guarantee a reasonable life of the implant which commonly considered within 10 and 20 year with about a million cycle per year (severt 1990, eskelinen 2006, puolakka 2001). Thus, prosthesis and the cement would be subjected to high fatigue cycles. In bone it is a different story, the ability of the bone to repair itself tends to balance the accumulation of the damage so as failure for high-fatigue cycles become possible only for high frequency cycles or in case of low-fatigue cycle. This two last scenarios are typical for very active individuals, in contrast with clinical recommendation for operated patients and not that common among this category of individuals. Thus in the following only high-fatigue cycle is presented as the risk of fatigue failure will be addressed, in following chapters, only for the prosthesis and the cement .

High-cycle fatigue

Historically, most attention has been focused on high-cycle fatigue that require more than 10⁵ cycles to failure where stress is low and deformation primarily elastic.

In high-cycle fatigue material performances is commonly characterised by the Wöhler curve (Figure 7) which is a graph of the magnitude of a cyclical stress (S) against the logarithmic scale of cycles to failure (N).

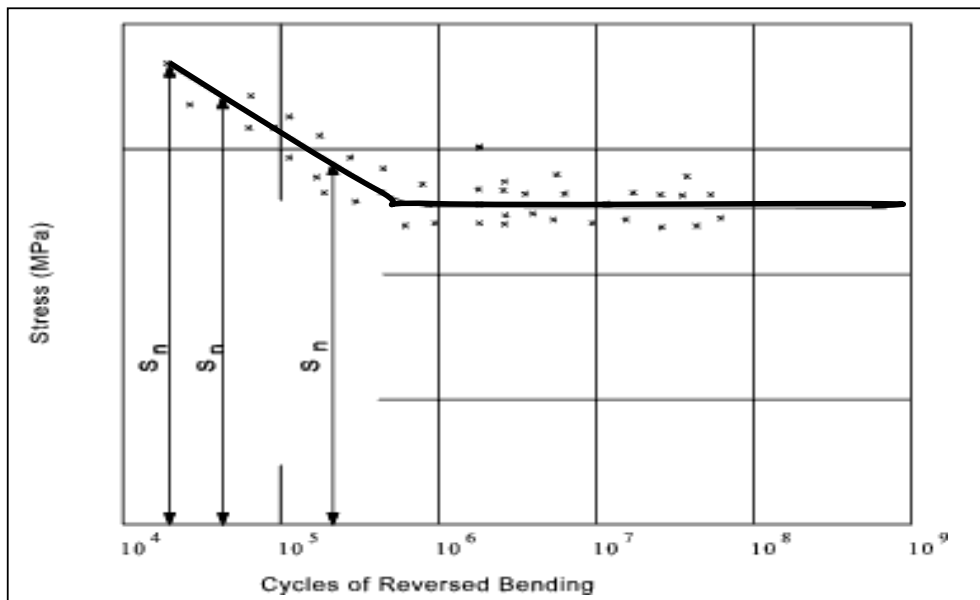


Figure 7 – A typical Wöhler curve for a ferrous alloy

The S-N curves are only derived from experimental tests on specimens of the material to be characterised applying a regular sinusoidal stress through the testing machine. As tests from a homogeneous group of specimens in general manifest high variation in their number of cycles to

failure; the S-N curve should more properly be an S-N-P curve capturing the probability of failure after a given number of cycles of a certain stress.

Material response to cyclic loading might be distinguished in two different types. The ferrous alloys and titanium exhibit a step branch in the relatively short life range, levelling off to approach a stress asymptote at longer lives. This asymptotic stress is called fatigue limit (or endurance limit) and is the stress level below which an infinite number of cycles can be sustained without failure. Other material as non ferrous alloy or polymeric materials do not exhibit an asymptote as the curve of stresses versus life continue to drop off infinitely. For such alloys there is no fatigue limit, and failure as a result of cyclic load is only a matter of applying enough cycles. All materials, however, exhibit a relatively flat curve in the long life range. To characterise the failure response of these materials the term fatigue strength (which is the stress level that produce failure at a specified life) is commonly used.

In practice real loads are complex, often random, sequences and assessing the life of a component is not possible simply by comparing the real stress history with which measured by tests. This case, a phenomenological description of fatigue (Miner or Paris's relationship) may help to describe the damage accumulation at any cycle and predicting the component life.

1.7.1.3 Fretting

Basically, fretting action has, for many years, been defined as combined mechanical and chemical action in which the contacting surface of two solid bodies are pressed together by a normal force and are cause to execute oscillatory sliding relative motion, wherein the magnitude of the normal force is great enough and the amplitude of the of the oscillatory sliding motion is small enough to significantly restrict the flow of fretting debris away from the originating site. More recent definitions of fretting action have been proposed to include cases in which contact surfaces periodically separate as well as cases in which the fluctuating friction-induced surface traction produce stress fields that may ultimately result in failure.

The complexity of the physical phenomena is high, it involves in plastic deformation caused by surface asperities plowing through each other, welding and tearing of contacting asperities, shear and rupture of asperities, friction generated subsurface shearing stress, dislodging of particles and corrosion products at the surface, chemical reactions, debris accumulation and entrapment, abrasive action, microcrack initiation, surface delamination, and others.

Service failure of mechanical components due to fretting fatigue has gradually come to be recognised as a failure mode of major importance, both in terms of frequency of occurrence and seriousness of the failure consequences. Fretting wear has also presented major problems in certain applications. Both fretting fatigue and fretting wear as well as fretting corrosion are directing attributable to fretting action.

Damage of components due to fretting action may be manifested as corrosive surface damage due to fretting corrosion, loss of proper fit or change in dimensions due to fretting wear , or accelerated fatigue failure due to fretting fatigue.

Fretting wear is a change in dimension through wear directly attributable to the fretting process between two maintaining surfaces. It is thought that the abrasive pit-digging mechanism, the asperity contact microcrack initiation mechanism, and the wear-sheet delamination mechanism may be all important in the most fretting wear failures. Although some studies [79] described the weight loss during fretting, for designers the wear depth is of more interest. Some investigators have suggested that estimates of fretting wear depth may be based on the classical adhesive or abrasive wear equations, in which wear depth is proportional to load and total distance slid, where the total distance slid is calculated by multiplying relative motion per cycle times number of cycles. Although there are some supporting data for such a procedure [80], more investigation is required before it could be recommended as an acceptable approach for general application.

Particularly important for orthopaedic implants is fretting wear of non-metallic materials such as polymers and ceramic, investigations have been reported for these type of materials by Krichen [81].

Fretting fatigue is a fatigue damage directly attributable to the fretting process between two maintaining surfaces. It is thought that the abrasive pit-digging mechanism, the asperity contact microcrack initiation [82], friction-generated cyclic stress that may lead to the formation of microcracks, or subsurface cyclic shear stresses that lead to surface delamination in the fretting region may be all important in the most fretting fatigue failures. Supporting evidence has been generated to indicate that under various circumstances each of the four mechanism is active and significant in producing fretting damage.

Effort to apply the tools of fracture mechanics to the problem of life prediction under fretting fatigue conditions have produced encouraging preliminary results that may provide designers with a viable quantitative approach [83]. These studies emphasise that principal effect of fretting in the fatigue failure process is to accelerate crack initialisation and the early stages of crack growth. They suggested that when cracks have reached a sufficient length, the fretting no longer has a significant influence on crack propagation. At this point the fracture mechanics description of crack propagation becomes valid. It is further suggested that in many cases the fretting fatigue lives are primarily determined by crack propagation, with crack initiation occurring so early in life as to be a factor of second order importance [84]. Based on preliminary results it would appear that fretting fatigue design procedures based on the fracture mechanics approach to crack growth may become a viable tool in the future.

Although fretting phenomena is a potential failure mode in a wide variety of mechanical systems and much research effort has been devoted to the understanding of the fretting process no generally applicable design procedure has been established for predicting failure under fretting conditions.

A method to ensure that fretting wear damage would not occur is to ensure the relative movements of the two maintaining surfaces under than the so-called stick-slip limit below which no relative displacement of the surfaces asperities is expected. This limit has been studied for the bone cement (polymethylmethacrylate, PMMA) by Zhou [85] assigning the limit to 50 microns.

Less simple is the identification of the crack dimension in the cement after implantation for the application of the fracture mechanics criterions. Although, fretting fatigue remains a possible relevant phenomenon that concur to the cement fracture no methods are currently known to accurately predict it without a precise knowledge of the status of the defects after implantation. Thus, the only reliable method to evaluate the life endurance of a certain application is to experimentally simulate its operating conditions [86, 87] [88]. This aspect won't be numerically addressed in the present study.

1.7.1.4 Shock and impact

When a load is rapidly applied to a structure or a member it is often found that the stress level and deformations reaches very much larger values than those reached applying the same load gradually as exchanged forces increase to absorb the kinetic energy of the impact. Such rapidly applied loads or displacements are usually called shock or impact loads. Whether the loading on a structure should be considered as quasi-static or impact loading is often judged by comparing the time of application of the load with the longest natural period of the structure. If the rise time is less than about one-half of the longest natural period it is necessary to consider the load as impact load. It should be noted that, in case of impact, also the materials properties may be significantly influenced by rapidly applied loads or displacements.

For simple parts or members the maximum stress or deflection under impact conditions may be approximated by utilising the concept of conservation of energy, wherein the external work done on a structure must be equal to the potential energy of strain stored in the structure, if losses are assumed to be negligible.

This type of failure is of interest when studying failure of hip implants such in case of side fall, stumbling, crashes and in general when sudden and unexpected events occur. Unfortunately hip implants can hardly considered as “simple parts” and much research work is needed to study the implant to failure in case of very high dynamic loads. Only after it is possible to integrate this knowledge in predictive models of failure of orthopaedic implants under shock conditions.

1.7.1.5 Wear

Wear is the undesired cumulative change in dimensions brought about by the gradual removal of discrete particles from contacting surface in motion, due predominantly to mechanical action. Wear is not a single process but a number of different processes that may take place independently or in combination. It is generally accepted that there are at least five major subcategories of wear, including adhesive wear, abrasive wear, corrosive wear, surface fatigue wear and deformation wear.

The complexity of the wear process may be better appreciated by recognising that many variables are involved including hardness, toughness, ductility, modulus of elasticity, yield strength, fatigue properties, and structure and composition of the mating surfaces, as well as geometry, contact pressure, temperature, state of stress, stress distribution, friction and others. Although its complexity, progress has been made in recent years toward development of

quantitative empirical relationship for the various subcategories of wear under specified operating conditions. Much experimental work remains to be completed before these relationships are widely accepted.

For what concerns wear of orthopaedic devices, it is known that the UHMWPE (or PE in general) debris trigger osteolysis. Hirakawa et. al. [58] studied the relationship between characteristics of the implant and clinical variables and the concentration of particles isolated from peri-articular tissues founding a very high number of tiny particles (up to 5.7×10^{11}). Oparaugo et. al. [57] related the amount of wear with excessive osteolysis highlighting a low risk of failure for a wear rate below 80 mm³/year.

However the most of resurfacing implants consist in metal-on-metal bearing surfaces, producing much less wear than PMMA-on metal assemblies. Less is known on biological implication of metallic ions. Although there is no evidence of osteolysis, it is known that the metallic debris might cause hypersensitivity and it is suspected to promote cancer.

1.7.2 Predicting adverse biological processes

The following paragraphs do not presume to give indication in fully quantitatively predict the contribute of each biological process to the implant stability or loosening, as this is still a current challenge for researchers.

The present knowledge in bone biology allows to state that mechanical environments play a fundamental role in balancing adverse and positive actions to the implant stability. There are evidences that bone remodelling, osteolysis and tissue differentiation at bone-prosthesis interface might be addressed by some functions of a single parameter leading to a relatively safe implants if the parameter of interest remains below a safe threshold.

In the following lines are presented biomechanical parameters and criterions that can be used in predicting critical conditions of orthopaedic implants as they are proposed in the recent literature.

1.7.2.1 Adverse bone resorption and remodelling

Bone remodelling is the result of changes in bone load carrying mechanics induced by the insertion of the prosthesis stem, stiffer than the hosting bone, during surgeries.

This mechanical phenomenon would be of academic interest only, were it not for its assumed role as a stimulus for bone resorption. In accordance with Wolff's Law, the reduction of stresses relative to the natural situation would cause bone to adapt itself by reducing its mass, either by becoming more porous (internal re-modelling) or by getting thinner (external re-modelling) [56, 89-94].

The relationship between implant flexibility and the extent of bone loss, frequently established in clinical series and animal experiments, does suggest that the changes in bone morphology are an effect of stress shielding and a subsequent adaptive re-modelling process [92, 95].

This relationship has been investigated by many authors using strain-adaptive bone-remodelling theory in combination with finite element models to simulate the bone remodelling process which have sustained the hypothesis that the resorptive processes are an effect of bone adaptation to stress shielding. It has also been established that individual differences in bone reactivity and mechanical bone quality (density and stiffness) may account for the individual variations found in patients and animal experiments [96-98].

The simulation process is based on a conservative (or site-specific) formulation of strain-adaptive bone-remodelling theory, which assumes that bone reacts to a local difference between actual strain values in the bone with prosthesis and the strain values at the same location in the intact bone [99]. This procedure requires the definition of a remodelling signal, which represents the stimulus for strain-adaptive net bone remodelling, and of a remodelling rule, which is the mathematical description of the remodelling process. The remodelling signal is based on the assumption that bone strives to normalize the average elastic energy per unit of mass for a particular loading history. The signal, average elastic energy per unit of mass, can then be expressed as

$$S = \frac{1}{n} \sum_{i=1}^n \frac{U_i}{\rho}; \quad (1)$$

where U_i is the strain-energy density (SED) in the bone for loading case i , n is the number of loading cases considered, and ρ is the apparent density. A similar signal was proposed by Carter [100, 101]. The objective of the net bone-remodelling process can then be described as

$$S - S_{ref} = 0; \quad (2)$$

where S_{ref} is the signal value in the intact bone, S is measured in the bone with prosthesis, at the same location and for the same loading history. Although equation (2) can already be considered a remodelling rule, two more refinements are added. As suggested by Frost [56, 102] and experimentally confirmed by Maloney [103], true normalization of bone strains, in the sense of equation (3), does not occur. Hence, a minimum effective strain signal (MES [56]) is necessary to stimulate remodelling. This can be seen as a dead zone in the remodelling process, measuring $(1-s) S_{ref}$, [95, 104]. As suggested by Martin [105], the remodelling rate depends on the relative amount of pore surface available in the bone. This amount, a (mm^2/mm^3), can be expressed as a function of apparent density ($a = a(\rho)$), using a geometric model for the pore shape [104, 106]. The remodelling rule can then be expressed as the net remodelling rate $d\rho/dt$, according to

$$\begin{aligned} \frac{d\rho}{dt} &= a(\rho) \{ S - (1-s)S_{ref} \}, & \text{if } S &\leq (1-s)S_{ref} \\ \frac{d\rho}{dt} &= 0, & \text{if } (1-s)S_{ref} &\leq S \leq (1+s)S_{ref} \\ \frac{d\rho}{dt} &= a(\rho) \{ S - (1+s)S_{ref} \}, & \text{if } S &\geq (1+s)S_{ref} \end{aligned}$$

If the bone resorption significantly affect the initial bone structure different type of failure such as bone fractures or loosening might be faced after surgery. Many models have been proposed in the last years to describe the remodelling process and to predict the remodelled bone structure

with good qualitative results [107-112]. The high complexity of the remodelling process, as explained in the paragraphs above, make difficult the development of accurate and validated models for the quantitative prediction of the amount of bone remodelling. Therefore, the only way to ensure that an excessive bone resorption do not occur is to maintain the original bone stock, which is controlled by clinicians at the time of surgery, over time postoperatively. This condition is achieved if the distortion on bone stresses produced by the prosthesis insertion produce an activation signal below the activation threshold.

1.7.2.2 Osteolysis

Wear-generated debris of the UHMWPE parts of the implant[57, 58] is the main cause of initiating this destructive process that activates pro-inflammatory signalling, which leads to increased osteoclast recruitment and activation contributing to increased bone re-sorption and osteolysis.

A quantitative relation between the wear rate of UHMWPE components and excessive osteolysis was defined by Oparaugo [57]. He found a low incidence of osteolysis in case of wear rate lower than 80 mm³/year.

Although UHMWPE-on-metal bearing surfaces are a possible solution for hip resurfacing implants (i.e. using a UHMWPE acetabular cup coupled with a CrCo femoral component), more frequent is the adoption of a metal-on-metal solution.

A number of experiments have shown a very large variability in wear test of most commercial metal-on-metal hip prosthesis, wear rate ranges from 0.09 to 61 cubic millimetres per million cycles [113-119]. However, the biological effect on the peri-prosthetic bone of the metallic debris do not stimulate osteolysis, although it is suspected to trigger hypersensitivity or cancer.

In conclusion, even if the risk of excessive osteolysis is still a concern for hip resurfacing prosthesis when the UHMWPE-on-metal solution is adopted, the wear rate is not accurately predictable by models. Due to the complexity of the wear process it is possible to predict the amount of wear only through controlled experiments, in which the operating conditions of the prosthesis are accurately simulated.

1.7.2.3 Adverse tissue differentiation at the prosthesis interface

The desired condition at the bone-prosthesis interface after surgery is a full osteointegration of the two counter-faced surfaces in which the bone tissue completely adhere to the stem surface.

Control of micromotion at the bone-implant interface is probably one of the most significant biological requirements for a load-bearing implants. This requirement is of utmost importance for early- and immediately loaded implants.

It is believed that the amount of micromotion between the implant and the bone tissue is an important factor for successful osseointegration [60, 62, 120]. The literature suggests that there is a critical threshold of micromotion above which fibrous encapsulation prevails over

osseointegration. The tolerated micromotion threshold was found to lie somewhere between 50 and 150 microns [120]. Studies of Kenwright and Goodship [98, 121] have shown that a controlled axial displacement (1.0 mm at 0.5 Hz for 20–30 min per day) promotes fracture healing.

Artificial application of controlled micromotion may be considered as a future treatment option to promote early bone-implant interface maturation. Nevertheless, it should be taken into consideration that approximately 30 microns of micromotion allows bone ingrowth into rough implant surfaces and increasing the motion (150 microns and higher) causes fibrous tissue formation [120].

Although simply controlling bone-prosthesis micromovements is considered a valid method to discriminate loosening [120] other factors play a role for a successful osteointegration. An high roughness of the prosthesis surface increase the contact surface so as to increase the area where a full osteointegration may occur and, at the same time, it tend to limit the bone-prosthesis micromovements promoting a mechanical interlock when the surface roughness is over 10 microns [122]. The design of the implant surface controls stress concentrations at the interface and affects bone response. If the surface is rough, the area that forces are transferred to the bone increases [123].

The prosthesis osteointegration might be stimulated by a calcium phosphate coating (i.e. $\text{Ca}_{10}(\text{PO}_4)_6(\text{OH})_2$) which, thanks to its biocompatibility, promote an efficient osteoconduction process.

1.8 Properties of materials composing the orthopaedic implants

Predicting failure at the conceptual design stage mean to be able to predict the mechanical conditions of the implant. To this aim, it is necessary to know all the variables that univocally define the state of stress and strain of all parts of the system: geometry, loads and material properties. Only after it is possible to compare the estimated mechanical conditions with chosen failure criterion for predicting the risk level of the analysed design.

1.8.1 Prosthesis and cement

The prosthesis fracture is a rare failure type [36] which may occur because of fractures or, more likely, fatigue. Most common materials used in manufacturing prosthesis are stainless steel alloys and titanium plus ceramic or polymers usually used in manufacturing bearing components.

Despite the high variability of mechanical properties between different choices in composition, micro structure or treatment, the identification of a safe threshold to be used in failure prediction is usually easy for this part. When the desired properties is not directly available on-line (<http://www.matweb.com>) it is definition can be evaluated experimentally trough well established protocols. See ASTM (www.astm.org) or ISO (www.iso.org) standards.

More difficult is a precise identification of material properties of the cement that depends on the techniques to prepare it and on conditions met during surgery. The table below resume the

tensile properties of the most popular bone cement and their dependence on the techniques used to prepare it.

Formulations	Mixing Details	Curing, Aging, and Test Environment Conditions	Tensile Properties		
			UTS (MPa)	E_t (MPa)	$\epsilon_{\max t}$ (%)
Simplex P	Manual	Stored in water for at least 24 h	36.7	1583	
	Manual, followed by mixing by ultrasonic vibration for 60 s	Stored in water for at least 24 h	41.9	1889	
	Manual; 1 Hz for 60 s	NS	31.4		
	Vacuum; 33 kPa (absolute); 60 s; Stryker High Vacuum Cement Injection System	NS	36.7		
	CC stored at 23 ± 2 °C prior to manual mixing; 1 Hz for 60 s	Placed in 37 °C saline for at least 24 h; tested in 37 °C saline	44.4	3080	0.86
	Manual; according to manufacturer's instructions; Hz for 90 s	Cured in 37 °C water for 15 min; aged in 37 °C water for at least 7 days; tested at 37 °C	36.2	2530	1.62
	LM stored at 0 °C prior to centrifugation mixing at 3000 rpm for 30 s	Cured in 37 °C water for 15 min; aged in 37 °C water for at least 7 days; tested at 37 °C	44.7	2430	2.49
	Manual	Aged in saline at 37 °C for			
		1 day	27.1		
		7 days	30.0		
		35 days	30.2		
		CC stored at 5 °C prior to manual mixing; 1 Hz	Cured in 37 °C water for at least 24 h; tested in 37 °C water	27.0	2140
	CC stored at 5 °C prior to vacuum mixing; 20 kPa (absolute)	Cured in 37 °C water for at least 24 h; tested in 37 °C water	46.0	2410	
Zimmer Regular®	CC stored at 23 ± 2 °C prior to manual mixing; 1 Hz for 60 s	Placed in 37 °C saline for at least 24 h; tested in 37 °C	44.4	2700	0.99
	Manual	NS	23.6	1900	
	Manual; according to manufacturer's instructions; 1 Hz for 45 s	Cured in 37 °C water for 15 min; aged in 37 °C for at least 7 days; tested at 37 °C	32.3	2810	1.41
	LM stored at 0 °C prior to centrifugation mixing at 3000 rpm for 30 s	Cured in 37 °C water for 15 min; aged in 37 °C water for at least 7 days; tested at 37 °C	46.0	2840	1.99
Zimmer LVC®	CC stored at 23 ± 2 °C prior to manual mixing; 1 Hz for 60 s	Placed in 37 °C saline for at least 24 h; tested in 37 °C saline	44.8	4120	0.86
	Manual	Aged in saline at 37 °C for			
		1 day	28.6		
		7 days	30.4		
		35 days	30.7		
		Manual; according to manufacturer's instructions; 1 Hz for 75 s	Cured in 37 °C water for 15 min; aged in 37 °C water for at least 7 days; tested at 37 °C	39.8	3070
	LM stored at RT prior to centrifugation mixing at 3000 rpm for 30 s	Cured in 37 °C water for 15 min; aged in 37 °C water for at least 7 days; tested at 37 °C	49.2	2950	2.05
	CC stored at 5 °C prior to manual mixing; 1 Hz	Cured in 37 °C water for at least 24 h; tested in 37 °C water	27.0		
	CC stored at 5 °C prior to vacuum mixing; 20 kPa (absolute)	Cured in 37 °C water for at least 24 h; tested in 37 °C water	44.0		
Palacos® R	CC stored at 5 °C prior to manual mixing; 1 Hz	Cured in 37 °C water for at least 24 h; tested in 37 °C water	33.0		
	CC stored at 5 °C prior to vacuum mixing; 20 kPa (absolute)	Cured in 37 °C water for at least 24 h; tested in 37 °C water	40.0		
CMW™-1	CC stored at 5 °C prior to manual mixing; 1 Hz	Cured in 37 °C water for at least 24 h; tested in 37 °C water	25.0		
	CC stored at 5 °C prior to vacuum mixing; 20 kPa (absolute)	Cured in 37 °C water for at least 24 h; tested in 37 °C water	47.0		

NS, conditions not stated in the report; CC, cement constituents; LC, liquid monomer constituents; RT, room temperature.

Table 4 - Mean values of uniaxial static tensile properties of 5 commercial formulations of bone cement from Lewis [73]

Nevertheless, a large number of studies have been carried out that define all physical and mechanical properties of acrylic bone cement which are considered to be relevant to its performances (Lewis, 1997).

1.8.2 Bone

Predicting the mechanical behaviour of bone is a challenging task for the current research as experimental tests on fresh human bones are often limited by the difficulty in obtaining specimens and the complexity of testing protocols.

Although the local properties of bone changes continuously location by location two main different type of tissue may be distinguished. The outer layer limited by the periosteum is characterised by dense and compact bone which have the highest mechanical properties, it is the cortical bone. The inner part, or cancellous bone, is characterised by a higher level of porosity, lower mechanical properties, higher vascularisation and an higher ability to absorb energy before fracture, it is the cancellous (or trabecular) bone.

1.8.2.1 Cortical bone

Mechanical properties of cortical bone have been well documented. Traditional mechanical testing techniques such as uniaxial tensile or compressive testing and three-points or four-points bending have been used for measuring these properties [124] as well as ultrasonic techniques, by subjecting the bone to ultrasound and measuring the velocity of the sound [125]. A typical tensile stress-strain diagram for the cortical bone under a compression load is shown in Figure 8

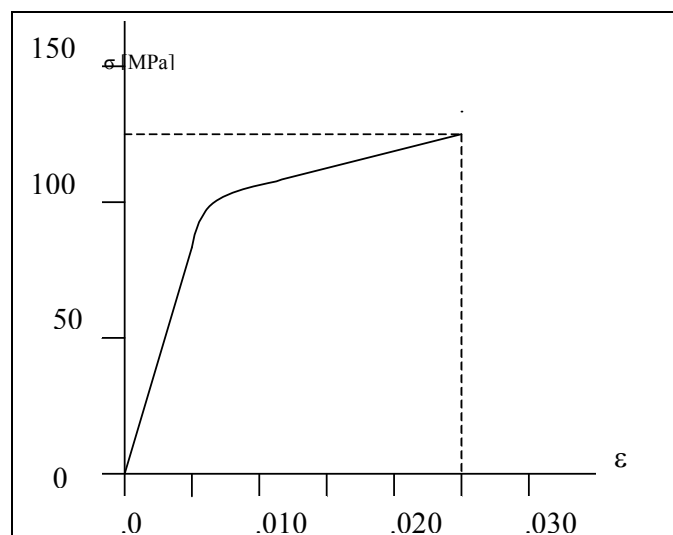


Figure 8 - Compressive stress-strain diagram for human cortical bone loaded in the longitudinal direction (strain rate $\dot{\epsilon} = 0.05 \text{ s}^{-1}$)

This \square - \square curve was drawn using the averages of the elastic modulus, strain hardening modulus, ultimate strain and ultimate stress values determined for the human femoral cortical bone by Reilly [124]. He tested specimen of bone tissues (human and bovine) under compressive loads

applied in the longitudinal direction at a moderate strain rate ($\dot{\varepsilon}=0.05 \text{ s}^{-1}$). The diagram (Figure 8) that can be considered representative of the behaviour of cortical bone under compression shows three distinct regions. In the initial region the behaviour is linear-elastic and the slope of the straight line is equal to the elastic Young modulus (E) of the bone, which in the example is almost 17 GPa. In the intermediate region the bone exhibits a non-linear elasto-plastic behaviour. Material yielding also occurs in this region. In the final region, the bone exhibits a linearly plastic material behaviour and the \square - \square diagram is another straight line. The slope of this line represents the strain hardening modulus of bone tissue, which was about 0.9 GPa in the example.

A different behaviour of the cortical bone is observed when loaded by a tensile stress. The yielding region disappear and the material behave elastically up to failure with an elastic modulus approximately equivalent to the compression elastic modulus.

The elastic modulus and the strength value are dependent on the rate at which the loads are applied [126]. This viscoelastic nature of bone can be described with the qualitative diagram plotted in Figure 9

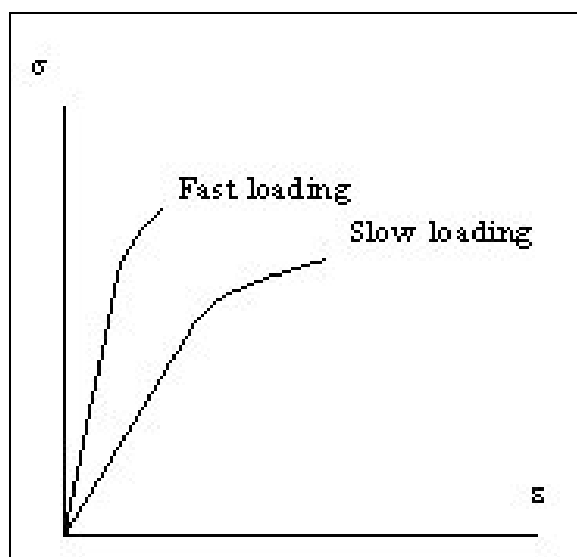


Figure 9 - The strain rate dependent stress-strain curve for cortical bone tissue

The specimen of bone tissue subjected to a rapid loading generally shows an increase in bone fragility and a parallel increase in the elastic modulus. With respect to a specimen loaded more slowly, there is a reduction in the post-elastic phase (it can even lack) and in the strain to failure as well as an increase in the ultimate stress. The absorbed energy, which is the area under the σ - ε curve, generally decreases with increased strain rate.

Bone will bear a higher stress if it is loaded at a higher strain rate. Carter and Caler [127] found an empirical relationship between failure stress and strain, or stress, rate:

$$\sigma_f = 87 \dot{\sigma}^{0.053}$$

$$\sigma_f = 87 \dot{\varepsilon}^{0.055}$$

The stress-strain behaviour of bone is also dependent upon the orientation of bone with respect to the loading direction. This anisotropic material behaviour can be qualitatively described by the diagram plotted in Figure 10.

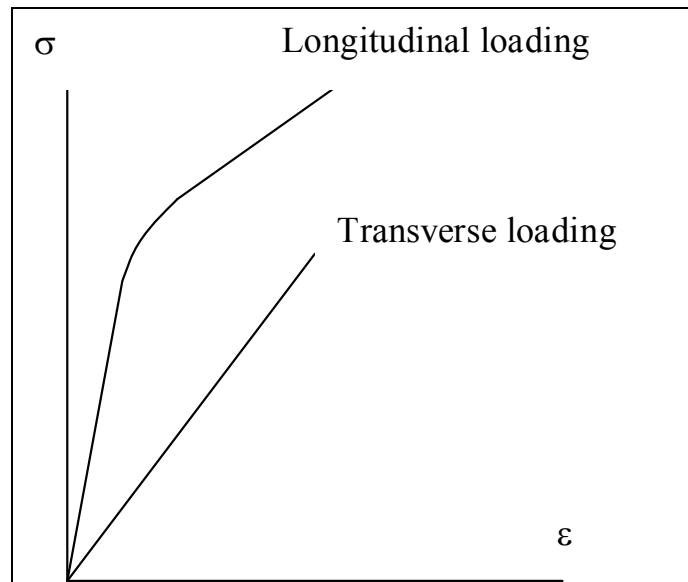


Figure 10 - The direction dependent stress-strain curve for bone tissue.

The cortical bone shows a larger ultimate strength and a larger elastic modulus in the longitudinal direction than in the transverse direction. Moreover, bone specimens loaded in the transverse direction fail in a more brittle manner, without showing a considerable yielding, as compared to bone specimens loaded in the longitudinal direction.

Although the qualitative behaviour of cortical bone described previously is commonly accepted, still a great range for the values of the mechanical characteristics can be found in the literature for many reasons. First of all, differences in the measured values can be due to the different treatment of specimens. It has been shown that drying bone and re-wetting it can produce differences in the results [128] as formalin fixation does [129]. Testing dry bone produces results quite different from those in wet bone: dry bone is stiffer, stronger and considerably more brittle. The dimension of the specimen influences the results as well. Very small specimens produce lower values for stiffness and strength than larger specimens [130]. In addition the age and health of the donor is a fundamental variable. Age may affect intrinsic properties. Osteoporotic bone may differ from 'normal' bones in ways other than the fact that is more porous: there is evidence that the collagen is different from that in similar-aged non-osteoporotic subjects [131]. Finally there are differences between bones and among different sites in the same bone. Long bones differ along their length and around their circumference. Lotz et al. [130], for example, showed that the longitudinal Young's modulus varied from 12.5 GPa to 9.6 GPa considering diaphysis specimens or metaphysis ones. In the following paragraphs values are reported that should be considered to be valid for a well-performed test on bone obtained from a middle-aged person with no disease [132].

Stiffness

The values reported in Table 5 are taken from [124, 125]. In the orthotropic formulation reported, the indices 1, 2, 3 to the moduli values indicate respectively the radial, circumferential and longitudinal direction, where the longitudinal direction is the one parallel to the main axis of the femur.

	Femur Tension	Femur Compression
Elastic Moduli (GPa):		
E₁	12.0	11.7
E₂	13.4	11.7
E₃	20.0	18.2
Shear Moduli (GPa):		
G₁₂	4.5	-
G₁₃	5.6	-
G₂₃	6.2	-
Poisson's ratios:		
v₁₂	0.38	0.63
v₁₃	0.22	-
v₂₃	0.24	-
v₂₁	0.42	0.63
v₃₁	0.37	0.38
v₃₂	0.35	0.38

Table 5 - Mechanical properties of cortical bone of human femur (Source [132])

Reilly at al[124] tested femoral specimen to determine whether the value of Young's modulus was different in tension and compression. A paired Student's 't' test showed no significant difference between the compressive and the tensile moduli at the 95% confidence level. The load-deformation traces showed no change of slope going from compression into tension and vice versa.

Calculations [127] predict that Young's modulus is modestly dependent upon strain rate:

$$E = 21402 (\text{strain rate (s}^{-1}\text{)})^{0.050} \text{ MPa}$$

Strength

The values reported in Table 6 are taken from Keller [133].

<i>Mode</i>	<i>Orientation</i>	<i>Breaking</i>	<i>Yield Stress</i>	<i>Ultimate strain</i>
Tension	Longitudinal	133	114	0.031
	Tangential	52	-	-
	Longitudinal	205	-	-
Compression	Tangential	130	-	-
	Shear	67	-	-

Table 6 - Strength of cortical bone (Source [132])

As already reported, a slight dependence on strain rate has been demonstrated, which becomes significant for strain rate variation of some order of magnitude.

1.8.2.2 Cancellous bone

The chemical compositions as well as the base structure of cortical and cancellous bone tissue are similar. The distinguishing characteristic of the cancellous bone is its porosity. Trabecular bone consists primarily of lamellar bone, arranged in packets that make up an interconnected

irregular array of plates and rods, called trabeculae. Most mechanical properties of trabecular bone depend to a large degree on the apparent density, which is defined as the mass of bone tissue present in a unit volume of bone[134]. Volume fraction typically ranges from 0.6 for dense trabecular bone to 0.05 for porous trabecular bone [135, 136]. The (wet) tissue density for human trabecular bone is fairly constant and is in the approximate range 1.6-2.0 g/ cm³. By contrast, the (wet) apparent density varies substantially and is typically in the range 0.05-1.0 g/cm.

<i>Tissue source</i>	<i>Cadavers</i>		<i>Specimens</i>	<i>Wet Apparent Density (g/cm³)</i>	
	<i>Nr.</i>	<i>Ages</i>	<i>Nr.</i>	<i>Mean (SD)</i>	<i>Range</i>
Proximal Tibia	9	59-82	121	0.29 (0.10)	0.09-0.66
Femur	10	58-83	299	0.50 (0.16)	0.14-1.00
Lumbar Spine	42	15-87	40	0.24 (0.07)	0.11-0.47
Lumbar Spine	3	71-84	231	0.19 (0.08)	0.06-0.40

Table 7 - Typical wet apparent densities for human trabecular bone (Source [134])

Individual trabeculae have relatively uniform compositions that are similar to cortical bone tissue, but are slightly less mineralised and slightly more hydrated than cortical tissue. The percent volume of water, inorganic and organic component have been reported at 27%, 38% and 35%, respectively , [137] although the precise values depend on anatomical site, age and health.

The cancellous bone tissue mechanical behaviour can be qualitatively represented as in Figure 11.

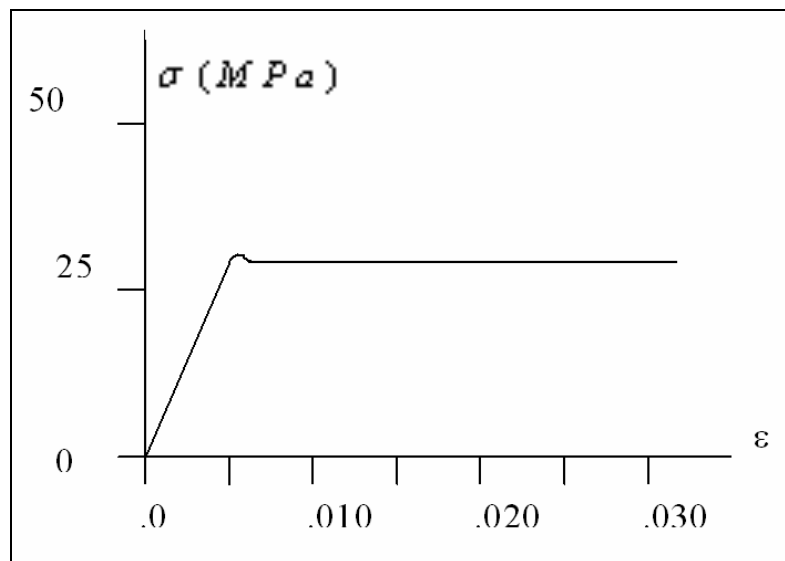


Figure 11 - Compressive stress-strain curve for cancellous bone tissue

The compressive stress-strain curves of cancellous bone show an initial linear elastic region up to a strain of about 0.05. The material yielding occurs as the trabeculae begin to fracture. A plateau region of almost constant stress follows this initial elastic region until fracture, exhibiting a ductile material behaviour. After yielding, it can sustain large deformations (up to 50% strain) while still maintaining its load-carrying capacity. Thus, trabecular bone can absorb substantial energy before mechanical failure. By contrast, cancellous bone fractures abruptly under tensile forces, showing a brittle material behaviour. The energy absorption capacity is considerably higher under compressive loads than under tensile loads.

Being a heterogeneous open cell porous solid, trabecular bone has anisotropic mechanical properties that depend on the porosity of the specimen as well as the architectural arrangement of the individual trabeculae. In order to specify its mechanical properties, one must therefore specify factors such as the anatomical site, loading direction with respect to the principal orientation of the trabeculae, age and health of the donor. Young's module can vary 100-fold within a single epiphysis [138] and can vary on average by factor of three depending on loading direction [139, 140]. Pathologies such as osteoporosis, osteoarthritis and bone cancer are known to affect mechanical properties [141, 142]. Typically the modulus of human trabecular bone is in the range 0.010-2 GPa depending on the above factors. Strength, which is linearly and strongly correlated with modulus [138], is typically in the range 0.1-30 MPa [134].

1.9 Development of a protocol of analysis

In the previous paragraphs it is described the hip resurfacing technique, its desired function, the types of failure related to the operated hip biomechanics, the possible phenomenon behind the observed failure, the biomechanical parameters that should be monitored to predict failure and the type and the mechanical characteristics of materials involved in resurfaced hips.

It emerged that for some type of failure processes, such as impact, the current knowledge doesn't allow an exhaustive description of the implant biomechanics. For other failure processes, such as polyethylene wear, it is only possible to evaluate the behaviour of a specific device by experimental tests to simulate the in-vivo environments of the prosthesis.

Thus, the development of models to predict the entire set of possible scenarios on the base of information preliminarily collected is far to be feasible yet. When it is not possible to pre-clinically evaluate the incidence of a certain scenario of failure either by experimental test (e.g. in case of excessive wear) or numerical methods (e.g. in case of a poor primary stability of the prosthesis leading to loosening), it is only possible to assess the implant quality after retrospective studies, which might be available only after years on clinical practice. If a specific type of failure is suspected relevant, clinicians might end up with indications to limit the life style of the operated individual (e.g. to reduce the patient activity).

Thus complete understanding of the biomechanical behaviour of an orthopaedic implant can be achieved by a combination of numerical simulations, experimental test and a final, strictly controlled, clinical validation study.

Thanks to the experience gathered over years it is now possible, at the beginning of the design phase, to predict by numerical techniques the amount of a large set of biomechanical phenomenon that might be responsible, or combine their effect, in producing failure. Once a protocol for such an analysis is available, it might become a powerful tool in estimating or improving the design quality. This is the base idea behind the presented research thesis: "Development of musculoskeletal models for the design and the pre-clinical validation of hip resurfacing prosthesis".

The modelling method adopted in the present research thesis is the finite element (FE) method. The needed geometry and local mechanical properties of bone segments are derived from CT data with a well established procedure developed at LTM [143, 144].

The very high flexibility of the method is the main reason of the choice. The possibility to model very complex bodies, in terms of geometry and material characteristic with no specific restrictions on the anatomical district, make this method a very appealing techniques for biomechanical researchers.

Since the biomechanical behaviour of the implant is of interest, it is necessary to have available models with a known accuracy, high enough to discriminate possibly critical conditions. In fact, a basic concept behind modelling is that model predictions are false till when proven true. In other words, the models need to go for a complex validation process to study its ability in predicting the real phenomenon. As soon as the model is validated it can be adopted for further studies.

Once accurate techniques in predicting the biomechanical parameter of interest, the list of analysis composing the protocol should be achieved linking by a cause-effect relation the mechanical function of the joint assembly with observed scenarios of failure.

The work described in the next chapters discuss the following aspects:

- 1) The validation studies through the comparison of model predictions to experimental measurements (Chapter 2).
- 2) The sensitivity study of the model prediction to the uncertainties on modelling parameters (Chapter 3).
- 3) The definition of the protocol by identifying a list of methods so as to study any biomechanical parameter of interest (Chapter 4).
- 4) The first application of the protocol by analysing a successful design on the market so as to test its ability in predicting known clinical outcomes (Chapter 5)
- 5) The first prototype of a new device is analysed by means of the developed protocol and the geometry optimised to reduce the risk of failure associated with the biomechanical behaviour of the implant. After a low-risk design was achieved, a statistical study was carried out for an extended pre-clinical validation of the optimised design over a population of interest (Chapter 6).
- 6) The research focus was moved to musculoskeletal model of the lower limb for the prediction of the muscle contribute to the body movement. The Chapter 7 contains a literature review of the current state of the art.

REFERENCES

1. Fabre, T., et al., *Complete femoral nerve division at total hip arthroplasty*. J Bone Joint Surg Br, 1996. **78**(1): p. 148-9.
2. Charnley, J., *Surgery of the hip-joint: present and future developments*. Br Med J, 1960. **1**(5176): p. 821-6.
3. Paltrinieri, M. and C. Trentani, [*Modification of hip arthroprosthesis*]. Chir Organi Mov, 1971. **60**(2): p. 85-95.
4. Freeman, M.A., H.U. Cameron, and G.C. Brown, *Cemented double cup arthroplasty of the hip: a 5 year experience with the ICLH prosthesis*. Clin Orthop Relat Res, 1978(134): p. 45-52.
5. Furuya, K., M. Tsuchiya, and S. Kawachi, *Socket-cup arthroplasty*. Clin Orthop Relat Res, 1978(134): p. 41-4.
6. Tanaka, S., *Surface replacement of the hip joint*. Clin Orthop Relat Res, 1978(134): p. 75-9.
7. Amstutz, H.C., et al., *Total hip articular replacement by internal eccentric shells: the "tharies" approach to total surface replacement arthroplasty*. Clin Orthop Relat Res, 1977(128): p. 261-84.
8. Wagner, H., *Surface replacement arthroplasty of the hip*. Clin Orthop Relat Res, 1978(134): p. 102-30.
9. Gerard, Y., *Hip arthroplasty by matching cups*. Clin Orthop Relat Res, 1978(134): p. 25-35.
10. Bogoch, E.R., V.L. Fornasier, and W.N. Capello, *The femoral head remnant in resurfacing arthroplasty*. Clin Orthop Relat Res, 1982(167): p. 92-105.
11. Head, W.C., *Wagner surface replacement arthroplasty of the hip. Analysis of fourteen failures in forty-one hips*. J Bone Joint Surg Am, 1981. **63**(3): p. 420-7.
12. de Waal Malefijt, M.C. and R. Huiskes, *A clinical, radiological and biomechanical study of the TARA hip prosthesis*. Arch Orthop Trauma Surg, 1993. **112**(5): p. 220-5.
13. Bell, R.S., et al., *A study of implant failure in the Wagner resurfacing arthroplasty*. J Bone Joint Surg Am, 1985. **67**(8): p. 1165-75.
14. Howie, D.W., B.L. Cornish, and B. Vernon-Roberts, *Resurfacing hip arthroplasty. Classification of loosening and the role of prosthesis wear particles*. Clin Orthop Relat Res, 1990(255): p. 144-59.
15. Kabo, J.M., et al., *In vivo wear of polyethylene acetabular components*. J Bone Joint Surg Br, 1993. **75**(2): p. 254-8.
16. Charnley, J., *Low Friction Arthroplasty of the Hip: Theory and Practice*. 1979, New York: Springer-Verlag.
17. Amstutz, H.C., F. Dorey, and P.F. O'Carroll, *THARIES resurfacing arthroplasty. Evolution and long-term results*. Clin Orthop Relat Res, 1986(213): p. 92-114.
18. Bradley, G.W., M.A. Freeman, and P.A. Revell, *Resurfacing arthroplasty. Femoral head viability*. Clin Orthop Relat Res, 1987(220): p. 137-41.

19. Jin, Z.M., D. Dowson, and J. Fisher, *Analysis of fluid film lubrication in artificial hip joint replacements with surfaces of high elastic modulus*. Proc Inst Mech Eng [H], 1997. **211**(3): p. 247-56.
20. MacDonald, S.J., *Metal-on-metal total hip arthroplasty: the concerns*. Clin Orthop Relat Res, 2004(429): p. 86-93.
21. Vendittoli, P.A., et al., *Chromium and cobalt ion release following the Durom high carbon content, forged metal-on-metal surface replacement of the hip*. J Bone Joint Surg Br, 2007. **89**(4): p. 441-8.
22. Kishida, Y., et al., *Preservation of the bone mineral density of the femur after surface replacement of the hip*. J Bone Joint Surg Br, 2004. **86**(2): p. 185-9.
23. Daniel, J., P.B. Pynsent, and D.J. McMinn, *Metal-on-metal resurfacing of the hip in patients under the age of 55 years with osteoarthritis*. J Bone Joint Surg Br, 2004. **86**(2): p. 177-84.
24. Amstutz, H.C., et al., *Metal-on-metal hybrid surface arthroplasty: two to six-year follow-up study*. J Bone Joint Surg Am, 2004. **86-A**(1): p. 28-39.
25. Mont, M.A., et al., *Use of metal-on-metal total hip resurfacing for the treatment of osteonecrosis of the femoral head*. J Bone Joint Surg Am, 2006. **88 Suppl 3**: p. 90-7.
26. Silva, M., et al., *The biomechanical results of total hip resurfacing arthroplasty*. J Bone Joint Surg Am, 2004. **86-A**(1): p. 40-6.
27. TEC, A. *Metal-on-Metal Total Hip Resurfacing*. 2007 [cited; Available from: www.bcbs.com/betterknowledge/tec/vols/22/metal-on-metal-total-hip.html]
28. Back, D.L., et al., *Early results of primary Birmingham hip resurfacings. An independent prospective study of the first 230 hips*. J Bone Joint Surg Br, 2005. **87**(3): p. 324-9.
29. De Smet, K.A., *Belgium experience with metal-on-metal surface arthroplasty*. Orthop Clin North Am, 2005. **36**(2): p. 203-13, ix.
30. Treacy, R.B., C.W. McBryde, and P.B. Pynsent, *Birmingham hip resurfacing arthroplasty. A minimum follow-up of five years*. J Bone Joint Surg Br, 2005. **87**(2): p. 167-70.
31. Schmalzried, T.P., et al., *Optimizing patient selection and outcomes with total hip resurfacing*. Clin Orthop Relat Res, 2005. **441**: p. 200-4.
32. Beaulé, P.E., et al., *Risk factors affecting outcome of metal-on-metal surface arthroplasty of the hip*. Clin Orthop Relat Res, 2004(418): p. 87-93.
33. Revell, M.P., et al., *Metal-on-metal hip resurfacing in osteonecrosis of the femoral head*. J Bone Joint Surg Am, 2006. **88 Suppl 3**: p. 98-103.
34. Lilikakis, A.K., S.L. Vowler, and R.N. Villar, *Hydroxyapatite-coated femoral implant in metal-on-metal resurfacing hip arthroplasty: minimum of two years follow-up*. Orthop Clin North Am, 2005. **36**(2): p. 215-22, ix.
35. Siebel, T., S. Maubach, and M.M. Morlock, *Lessons learned from early clinical experience and results of 300 ASR hip resurfacing implantations*. Proc Inst Mech Eng [H], 2006. **220**(2): p. 345-53.
36. Registro dell'Implantologia Protetica (R.I.P.O.), Report 2006, <https://ripo.cineca.it>.

37. Kutz, M., *Mechanical engineer's handbook, materials and mechanical design*, ed. r. Edition. 2005: Jhon Wiley & Sons.
38. Weiss, L., *Cell and Tissue Biology*. 6th ed. ed. 1990, Baltimore: Urban & Schwarzenberg.
39. Chambers, T.J., J.A. Darby, and K. Fuller, *Mammalian collagenase predisposes bone surfaces to osteoclastic resorption*. Cell Tissue Res, 1985. **241**(3): p. 671-5.
40. Rodan, G.A. and T.J. Martin, *Role of osteoblasts in hormonal control of bone resorption-a hypothesis*. Calcif Tissue Int, 1981. **33**(4): p. 349-51.
41. Hancox, N.M., *The biology of bone*. 1972, Cambridge: Cambridge University Press.
42. Shimizu, H., M. Sakamoto, and S. Sakamoto, *Bone resorption by isolated osteoclasts in living versus devitalized bone: differences in mode and extent and the effects of human recombinant tissue inhibitor of metalloproteinases*. J Bone Miner Res, 1990. **5**(4): p. 411-8.
43. Skerry, T.M., et al., *Early strain-related changes in enzyme activity in osteocytes following bone loading in vivo*. J Bone Miner Res, 1989. **4**(5): p. 783-8.
44. Baron, R., *Molecular mechanisms of bone resorption by the osteoclast*. Anat Rec, 1989. **224**(2): p. 317-24.
45. Vaananen, H.K. and M. Horton, *The osteoclast clear zone is a specialized cell-extracellular matrix adhesion structure*. J Cell Sci, 1995. **108 (Pt 8)**: p. 2729-32.
46. Jones, S.J. and A. Boyde, *Experimental study of changes in osteoblastic shape induced by calcitonin and parathyroid extract in an organ culture system*. Cell Tissue Res, 1976. **169**(4): p. 499-65.
47. Lakkakorpi, P.T. and H.K. Vaananen, *Cytoskeletal changes in osteoclasts during the resorption cycle*. Microsc Res Tech, 1996. **33**(2): p. 171-81.
48. Lakkakorpi, P.T. and H.K. Vaananen, *Kinetics of the osteoclast cytoskeleton during the resorption cycle in vitro*. J Bone Miner Res, 1991. **6**(8): p. 817-26.
49. Lakkakorpi, P., et al., *Organization of osteoclast microfilaments during the attachment to bone surface in vitro*. J Bone Miner Res, 1989. **4**(6): p. 817-25.
50. Laitala-Leinonen, T., et al., *Resorption-cycle-dependent polarization of mRNAs for different subunits of V-ATPase in bone-resorbing osteoclasts*. Mol Biol Cell, 1996. **7**(1): p. 129-42.
51. Perreault, S., et al., *Validation of a decision model for preventive pharmacological strategies in postmenopausal women*. Eur J Epidemiol, 2005. **20**(1): p. 89-101.
52. Morony, S., et al., *The inhibition of RANKL causes greater suppression of bone resorption and hypercalcemia compared with bisphosphonates in two models of humoral hypercalcemia of malignancy*. Endocrinology, 2005. **146**(8): p. 3235-43.
53. Martin, T.J., E.H. Allan, and S. Fukumoto, *The plasminogen activator and inhibitor system in bone remodelling*. Growth Regul, 1993. **3**(4): p. 209-14.
54. Marshall, L.J., et al., *Plasminogen activator inhibitor-1 supports IL-8-mediated neutrophil transendothelial migration by inhibition of the constitutive shedding of endothelial IL-8/heparan sulfate/syndecan-1 complexes*. J Immunol, 2003. **171**(4): p. 2057-65.

55. Daci, E., et al., *Bone resorption induced by 1 alpha,25 dihydroxyvitamin D(3) in vivo is not altered by inactivation of the plasminogen activator inhibitor 1*. Bone, 2000. **27**(1): p. 97-102.
56. Frost, H.M., *The mechanostat: a proposed pathogenic mechanism of osteoporoses and the bone mass effects of mechanical and nonmechanical agents*. Bone Miner, 1987. **2**(2): p. 73-85.
57. Oparaugo, P.C., et al., *Correlation of wear debris-induced osteolysis and revision with volumetric wear-rates of polyethylene: a survey of 8 reports in the literature*. Acta Orthop Scand, 2001. **72**(1): p. 22-8.
58. Hirakawa, K., et al., *Characterization and comparison of wear debris from failed total hip implants of different types*. J Bone Joint Surg Am, 1996. **78**(8): p. 1235-43.
59. Puzas, J.E., R.J. O'Keefe, and J.R. Lieberman, *The orthopaedic genome: what does the future hold and are we ready?* J Bone Joint Surg Am, 2002. **84-A**(1): p. 133-41.
60. Andreykiv, A., et al., *Bone ingrowth simulation for a concept glenoid component design*. J Biomech, 2005. **38**(5): p. 1023-33.
61. Stadelmann, V.A., A. Terrier, and D.P. Pioletti, *Microstimulation at the bone-implant interface upregulates osteoclast activation pathways*. Bone, 2008. **42**(2): p. 358-64.
62. Vandamme, K., et al., *The effect of micro-motion on the tissue response around immediately loaded roughened titanium implants in the rabbit*. Eur J Oral Sci, 2007. **115**(1): p. 21-9.
63. Vandamme, K., et al., *Influence of controlled immediate loading and implant design on peri-implant bone formation*. J Clin Periodontol, 2007. **34**(2): p. 172-81.
64. Yang, S.Y., et al., *Murine model of prosthesis failure for the long-term study of aseptic loosening*. J Orthop Res, 2007. **25**(5): p. 603-11.
65. Kelly, D.J. and P.J. Prendergast, *Mechano-regulation of stem cell differentiation and tissue regeneration in osteochondral defects*. J Biomech, 2005. **38**(7): p. 1413-22.
66. Lacroix, D. and P.J. Prendergast, *A mechano-regulation model for tissue differentiation during fracture healing: analysis of gap size and loading*. J Biomech, 2002. **35**(9): p. 1163-71.
67. Pauwels, F., *[A new theory on the influence of mechanical stimuli on the differentiation of supporting tissue. The tenth contribution to the functional anatomy and causal morphology of the supporting structure.]*. Z Anat Entwicklungsgesch, 1960. **121**: p. 478-515.
68. Stone, R.B., I.Y. Tumer, and M. Van Wie, *The Function-Failure design method*. Journal of Mechanical Design, 2004. **127**: p. 397-407.
69. Choen, M.R., J. Senders, and N.M. Davis, *Failure mode and effect analysis: a novel approach to avoiding dangerous medication errors and accident*. Hosp Pharm, 1994. **29**: p. 319-324, 326-328, 330.
70. Leveson, N., *Software safety: What, Why and How*. ACM computing surveys, 1986. **18**(2).

71. Schileo, E., et al., *Subject-specific finite element models implementing a maximum principal strain criterion are able to estimate failure risk and fracture location on human femurs tested in vitro*. J Biomech, 2008. **41**(2): p. 356-67.
72. Schileo, E., et al., *Subject-specific finite element models can accurately predict strain levels in long bones*. J Biomech, 2007. **40**(13): p. 2982-9.
73. Lewis, G., *Properties of acrylic bone cement: state of the art review*. J Biomed Mater Res, 1997. **38**(2): p. 155-82.
74. Zioupos, P., *In vivo fatigue microcracks in human bone: material properties of the surrounding bone matrix*. Eur J Morphol, 2005. **42**(1-2): p. 31-41.
75. Taylor, D., J.G. Hazenberg, and T.C. Lee, *Living with cracks: damage and repair in human bone*. Nat Mater, 2007. **6**(4): p. 263-8.
76. Taylor, D. and P.J. Prendergast, *A model for fatigue crack propagation and remodelling in compact bone*. Proc Inst Mech Eng [H], 1997. **211**(5): p. 369-75.
77. Fyhrie, D.P., et al., *Effect of fatiguing exercise on longitudinal bone strain as related to stress fracture in humans*. Ann Biomed Eng, 1998. **26**(4): p. 660-5.
78. Burr, D.B., et al., *In vivo measurement of human tibial strains during vigorous activity*. Bone, 1996. **18**(5): p. 405-10.
79. Uhlig, H.H., *Mechanism of fretting corrosion*. Journal of Applied Mechanics, 1954. **76**: p. 401-407.
80. Lyons, H., *An investigation of the phenomenon of fretting-wear and attendant parametric effect towards development of failure prediction criteria*, in Ohio State University 1978: Columbus.
81. Krichen, A., et al., *Surface damage of poly(methylmethacrylate) under fretting loading*. Wear, 1999. **230**(2): p. 146-155.
82. Collins, J.A., *Fretting-fatigue damage-factor determination*. Journal of engineering for industry, 1965. **87**(8): p. 298-302.
83. Alic, J.A. and A.L. Hawley, *On the early growth of fretting fatigue cracks*. Wear, 1979. **56**(2): p. 377-389.
84. Liaw, P.K., et al., *Fatigue crack growth behavior of D6AC space shuttle steel*. Engineering Fracture Mechanics, 1992. **43**(3): p. 379-400.
85. Zhou, Z.R., V. Pellerin, and L. Vincent, *Fretting - Wear of aluminium and titanium alloys*, in *Titanium & aluminium*, P.A. Coulon, Editor. 1989, I.I.T.T. Internationa. p. 145-153.
86. Cristofolini, L., et al., *Preclinical assessment of the long-term endurance of cemented hip stems. Part 1: effect of daily activities--a comparison of two load histories*. Proc Inst Mech Eng [H], 2007. **221**(6): p. 569-84.
87. Cristofolini, L., et al., *Preclinical assessment of the long-term endurance of cemented hip stems. Part 2: in-vitro and ex-vivo fatigue damage of the cement mantle*. Proc Inst Mech Eng [H], 2007. **221**(6): p. 585-99.
88. Brown, L., et al., *Reproduction of fretting wear at the stem-cement interface in total hip replacement*. Proc Inst Mech Eng [H], 2007. **221**(8): p. 963-71.

89. Currey, J.D., *What should bones be designed to do?* Calcif Tissue Int, 1984. **36 Suppl 1**: p. S7-10.
90. Currey, J.D., *Can strains give adequate information for adaptive bone remodeling?* Calcif Tissue Int, 1984. **36 Suppl 1**: p. S118-22.
91. Engh, C.A., J.D. Bobyn, and A.H. Glassman, *Porous-coated hip replacement. The factors governing bone ingrowth, stress shielding, and clinical results.* J Bone Joint Surg Br, 1987. **69**(1): p. 45-55.
92. Frost, H.M., *Skeletal structural adaptations to mechanical usage (SATMU): 2. Redefining Wolff's law: the remodeling problem.* Anat Rec, 1990. **226**(4): p. 414-22.
93. Frost, H.M., *Skeletal structural adaptations to mechanical usage (SATMU): 4. Mechanical influences on intact fibrous tissues.* Anat Rec, 1990. **226**(4): p. 433-9.
94. Ramtani, S. and M. Zidi, *A theoretical model of the effect of continuum damage on a bone adaptation model.* J Biomech, 2001. **34**(4): p. 471-9.
95. Huiskes, R., et al., *Adaptive bone-remodeling theory applied to prosthetic-design analysis.* J Biomech, 1987. **20**(11-12): p. 1135-50.
96. Goodship, A.E., L.E. Lanyon, and H. McFie, *Functional adaptation of bone to increased stress. An experimental study.* J Bone Joint Surg Am, 1979. **61**(4): p. 539-46.
97. Goodship, A.E. and J. Kenwright, *The influence of induced micromovement upon the healing of experimental tibial fractures.* J Bone Joint Surg Br, 1985. **67**(4): p. 650-5.
98. Goodship, A.E., et al., *The role of fixator frame stiffness in the control of fracture healing. An experimental study.* J Biomech, 1993. **26**(9): p. 1027-35.
99. Huiskes, R., *Stress shielding and bone resorption in THA: clinical versus computer-simulation studies.* Acta Orthop Belg, 1993. **59 Suppl 1**: p. 118-29.
100. Carter, D.R., D.P. Fyhrie, and R.T. Whalen, *Trabecular bone density and loading history: regulation of connective tissue biology by mechanical energy.* J Biomech, 1987. **20**(8): p. 785-94.
101. Carter, D.R., T.E. Orr, and D.P. Fyhrie, *Relationships between loading history and femoral cancellous bone architecture.* J Biomech, 1989. **22**(3): p. 231-44.
102. Frost, H.M., *A determinant of bone architecture. The minimum effective strain.* Clin Orthop Relat Res, 1983(175): p. 286-92.
103. Maloney, W.J., et al., *Biomechanical and histologic investigation of cemented total hip arthroplasties. A study of autopsy-retrieved femurs after in vivo cycling.* Clin Orthop Relat Res, 1989(249): p. 129-40.
104. Beaupre, G.S., T.E. Orr, and D.R. Carter, *An approach for time-dependent bone modeling and remodeling-application: a preliminary remodeling simulation.* J Orthop Res, 1990. **8**(5): p. 662-70.
105. Martin, R.B., *The effects of geometric feedback in the development of osteoporosis.* J Biomech, 1972. **5**(5): p. 447-55.
106. Martin, R.B., *Porosity and specific surface of bone.* Crit Rev Biomed Eng, 1984. **10**(3): p. 179-222.
107. Cowin, S.C., *Tissue growth and remodeling.* Annu Rev Biomed Eng, 2004. **6**: p. 77-107.

108. Cowin, S.C., *Bone stress adaptation models*. J Biomech Eng, 1993. **115**(4B): p. 528-33.
109. Cowin, S.C., A.M. Sadegh, and G.M. Luo, *An evolutionary Wolff's law for trabecular architecture*. J Biomech Eng, 1992. **114**(1): p. 129-36.
110. Doblare, M. and J.M. Garcia, *On the modelling bone tissue fracture and healing of the bone tissue*. Acta Cient Venez, 2003. **54**(1): p. 58-75.
111. Doblare, M. and J.M. Garcia, *Anisotropic bone remodelling model based on a continuum damage-repair theory*. J Biomech, 2002. **35**(1): p. 1-17.
112. Huiskes, R., *If bone is the answer, then what is the question?* J Anat, 2000. **197 (Pt 2)**: p. 145-56.
113. Firkins, P.J., et al., *Quantitative analysis of wear and wear debris from metal-on-metal hip prostheses tested in a physiological hip joint simulator*. Biomed Mater Eng, 2001. **11**(2): p. 143-57.
114. McKellop, H.A., T. Rostlund, and G. Bradley, *Evaluation of wear in an all-polymer total knee replacement. Part 1: laboratory testing of polyethylene on polyacetal bearing surfaces*. Clin Mater, 1993. **14**(2): p. 117-26.
115. McKellop, H.A., et al., *In vivo wear of titanium-alloy hip prostheses*. J Bone Joint Surg Am, 1990. **72**(4): p. 512-7.
116. Medley, J.B., et al., *Kinematics of the MATCO hip simulator and issues related to wear testing of metal-metal implants*. Proc Inst Mech Eng [H], 1997. **211**(1): p. 89-99.
117. Semlitsch, M., R.M. Streicher, and H. Weber, *[The wear behavior of capsules and heads of CoCrMo casts in long-term implanted all-metal hip prostheses]*. Orthopade, 1989. **18**(5): p. 377-81.
118. Semlitsch, M. and H.G. Willert, *Clinical wear behaviour of ultra-high molecular weight polyethylene cups paired with metal and ceramic ball heads in comparison to metal-on-metal pairings of hip joint replacements*. Proc Inst Mech Eng [H], 1997. **211**(1): p. 73-88.
119. Willert, H.G., G.H. Buchhorn, and T. Hess, *[The significance of wear and material fatigue in loosening of hip prostheses]*. Orthopade, 1989. **18**(5): p. 350-69.
120. Viceconti, M., et al., *Even a thin layer of soft tissue may compromise the primary stability of cementless hip stems*. Clin Biomech (Bristol, Avon), 2001. **16**(9): p. 765-75.
121. Kenwright, J., et al., *Axial movement and tibial fractures. A controlled randomised trial of treatment*. J Bone Joint Surg Br, 1991. **73**(4): p. 654-9.
122. Cehreli, M., S. Sahin, and K. Akca, *Role of mechanical environment and implant design on bone tissue differentiation: current knowledge and future contexts*. J Dent, 2004. **32**(2): p. 123-32.
123. Beksac, B., et al., *Surface finish mechanics explain different clinical survivorship of cemented femoral stems for total hip arthroplasty*. J Long Term Eff Med Implants, 2006. **16**(6): p. 407-22.
124. Reilly, D.T. and A.H. Burstein, *The elastic and ultimate properties of compact bone tissue*. J Biomech, 1975. **8**(6): p. 393-405.
125. Ashman, R.B., et al., *A continuous wave technique for the measurement of the elastic properties of cortical bone*. J Biomech, 1984. **17**(5): p. 349-61.

126. Lakes, R.S. and J.L. Katz, *Viscoelastic properties of wet cortical bone--III. A non-linear constitutive equation*. J Biomech, 1979. **12**(9): p. 689-98.
127. Carter, D.R. and W.E. Caler, *Cycle-dependent and time-dependent bone fracture with repeated loading*. J Biomech Eng, 1983. **105**(2): p. 166-70.
128. Currey, J.D., *The effects of drying and re-wetting on some mechanical properties of cortical bone*. J Biomech, 1988. **21**(5): p. 439-41.
129. Sedlin, E.D., *A rheologic model for cortical bone. A study of the physical properties of human femoral samples*. Acta Orthop Scand, 1965. **:Suppl**(83): p. 1-77.
130. Lotz, J.C., T.N. Gerhart, and W.C. Hayes, *Mechanical properties of metaphyseal bone in the proximal femur*. J Biomech, 1991. **24**(5): p. 317-29.
131. Bailey, A.J., et al., *Biochemical changes in the collagen of human osteoporotic bone matrix*. Connect Tissue Res, 1993. **29**(2): p. 119-32.
132. Currey, J.D., *Cortical bone*, in *Handbook of Biomaterial Properties*, J. Black and G. Hastings, Editors. 1998, Chapman&Hall: London (UK). p. 3-14.
133. Keller, T.S., *Predicting the compressive mechanical behavior of bone*. J Biomech, 1994. **27**(9): p. 1159-68.
134. Keaveny, T.M., *Cancellous Bone*, in *Handbook of Biomaterial Properties*, J. Black and G. Hastings, Editors. 1998, Chapman&Hall: London, UK. p. 15-23.
135. Kuhn, J.L., et al., *Evaluation of a microcomputed tomography system to study trabecular bone structure*. J Orthop Res, 1990. **8**(6): p. 833-42.
136. Mosekilde, L., et al., *The predictive value of quantitative computed tomography for vertebral body compressive strength and ash density*. Bone, 1989. **10**(6): p. 465-70.
137. Gong, J.K., J.S. Arnold, and S.H. Cohn, *Composition of Trabecular and Cortical Bone*. Anat Rec, 1964. **149**: p. 325-31.
138. Goldstein, S.A., et al., *The mechanical properties of human tibial trabecular bone as a function of metaphyseal location*. J Biomech, 1983. **16**(12): p. 965-9.
139. Linde, F., et al., *Three-axial strain controlled testing applied to bone specimens from the proximal tibial epiphysis*. J Biomech, 1990. **23**(11): p. 1167-72.
140. Townsend, P.R., et al., *The distribution and anisotropy of the stiffness of cancellous bone in the human patella*. J Biomech, 1975. **8**(6): p. 363-7.
141. Hipp, J.A., A.E. Rosenberg, and W.C. Hayes, *Mechanical properties of trabecular bone within and adjacent to osseous metastases*. J Bone Miner Res, 1992. **7**(10): p. 1165-71.
142. Pugh, J.W., E.L. Radin, and R.M. Rose, *Quantitative studies of human subchondral cancellous bone. Its relationship to the state of its overlying cartilage*. J Bone Joint Surg Am, 1974. **56**(2): p. 313-21.
143. Taddei, F., A. Pancanti, and M. Viceconti, *An improved method for the automatic mapping of computed tomography numbers onto finite element models*. Med Eng Phys, 2004. **26**(1): p. 61-9.
144. Viceconti, M. and F. Taddei, *Automatic generation of finite element meshes from computed tomography data*. Crit Rev Biomed Eng, 2003. **31**(1-2): p. 27-72.

Chapter 2

Experimental validation of the overall accuracy of subject-specific finite element models of long bones

Simulation models are increasingly being used in problem solving and in decision making. The concern with whether a model and its results are “correct” is of great importance for developers and users of these models as well as for people affected by decisions based on such models. This concern is addressed through model validation.

Model validation is usually defined to mean “substantiation that a computerized model within its domain of applicability possesses a satisfactory range of accuracy consistent with the intended application of the model” [1].

The substantiation that a model is valid is generally considered to be a process and is usually part of the model development process. Tests and evaluations are conducted until sufficient confidence is obtained that a model can be considered valid for its intended application [2, 3].

In biomechanics, the determination of the biomechanical behaviour of parts of the human skeleton and its interaction with orthopaedic devices during physiological activities would have a number of implications in various branch of orthopaedic research. In particular, having available valid models in predicting the biomechanical behaviour of the femur, intact and when implanted with a resurfacing device, is a key factor for the success of the here presented research activity.

In this chapter it is described the validation study of the model of an intact femur generated by adopting a modelling procedure developed in the past years at the LTM[4, 5] on the base of a cadaver specimen. After the validation of the intact model, carried out simulating the boundary conditions realised by the experimental set-up, the cadaver femur was implanted with a resurfacing device. A second model of the implanted femur was afterward generated and it underwent a second validation process. The experimental tests were conducted by the experimental group of the LTM. Validation was carried out by comparing predicted and measured values on the stress field and, only for the implanted model, on the contact mechanics at the bone-prosthesis interface.

For validation purposes, it is fundamental to precisely simulate the boundary achieved by the experimental set-up. To more precisely use experimental data during model validation, a second study was carried out to measure the location of the resultant of the applied load during tests as a

moving target. As this study is not directly of interest in the present thesis, it is more extensively described in Appendix A.

2.1 Subject-specific finite element models of long bones: An in vitro evaluation of the overall accuracy²

The determination of the mechanical stresses that physiological activities induce in human bones is of great importance in both research and clinical practice. For example, in research it is essential to investigate any mechano-biological phenomenon [6]; while in the clinical practice it could be extremely useful to plan the individual rehabilitation after subject-specific limb-salvage procedures [7]. Unfortunately, the mechanical stress in bones cannot be measured in living subjects without the use of an invasive surgical procedure [8], which, in general, is not ethically permissible. The only way to estimate bone stresses non invasively in vivo is “subject-specific” finite element modelling. This procedure allows the creation of a numerical model of the bone segment from Computed Tomography (CT) images of that segment [4]; at present this represents the best source of information on bone morphology and mechanical properties applicable in vivo. As for any other mathematical model, subject-specific finite element models predict physical reality with an accuracy that is undetermined a priori.

Many methods have been proposed in the literature that are characterised by different level of automation. The adoption of an automatic mesh generator is a forced choice when the finite element method is to be compatible with the times of the clinical practice or when it should be used to perform the analysis on a large population, since the manual generation of a mapped finite element model requires an intensive effort and is a time consuming procedure. One fully automatic approach allows the direct generation of Cartesian meshes (also known as voxel meshes) from the CT data [9-11]. While this method is widely used to investigate small volumes of trabecular bones as imagined by micro CT scanners [12, 13], its application to whole bones has been criticised [14], and it is currently avoided in favour of a two steps process. This procedure requires the extraction of the bone geometry, that can be defined from CT images with good accuracy [15], followed by its automatic meshing with various well-established algorithms that are also implemented in commercial finite element programs [4]. Although some of these methods were found to provide enough automation, intrinsic accuracy, robustness and generality to be used in clinical applications [16], still the overall accuracy of these subject-specific finite element models is unclear. This is especially true for those anatomical regions, such as the epiphysis of long bones, where the morphological complexity increases. Those regions, that are often of great interest (e.g. in the studies of resurfacing prosthesis, to estimate the calcar stresses in total hip replacements or to investigate intramedullary and gamma nails, etc.), are usually characterized by a bulk of spongy bone surrounded by a thin layer of cortical tissue, which represents a very fine feature that is almost impossible to capture with an automatic mesh generation strategy. In addition, those regions present higher curvatures, e.g. in the femoral neck, that give rise to lower image quality due to the increase of partial volume artefacts in the CT

² Fulvia Taddei, Luca Cristofolinia, Saulo Martelli, H.S. Gill, Marco Viceconti. “Subject-specific finite element models of long bones: An in vitro evaluation of the overall accuracy”. *J. Biomech.*, 2006,39(13), p:2457–2467

images [15]. The full validation of this modelling technique is a necessary step before its adoption for routine use in clinical practice.

Experimental validation is without doubt the best tool to assess the overall accuracy of finite element model predictions. Unfortunately this validation has not been carried out extensively in the past, mostly due to the difficulty and tediousness of the procedure, and only a limited number of studies are available in the literature. The majority of these studies also lack the necessary generality to be applied to other models. One historic group of studies addressed the accuracy of “voxel-meshes” for predicting strain in long bones [17, 18]. This meshing strategy, although fully automatic, generates jagged edges on the bone surface that are known to lower the accuracy of the predicted stresses, especially on the bone surface [11]. This is the main reason for the reported very poor agreement between predicted and measured strains in the cited works. Considering other meshing strategies, the most recent and complete validation study reports the accuracy obtained with a CT-derived three-dimensional model of a human scapula [19]. Although this work provides acceptably good results, the peculiarity of the bone segment studied led the authors to adopt an innovative but extremely specific meshing strategy. This meshing strategy is not applicable to other bony segments and thus limits the generality of the reported agreement. This lack of generality is common to other works where very specialized and non-automatic meshing strategies were adopted [20] or where the material properties of the bone tissue were tailored to meet the experimental results [21] or derived from literature with no correlation to the CT numbers [22]. To the authors’ knowledge only one paper has been published that investigates the accuracy of an automatically generated finite element model of a human femur, particularly addressing the extreme epiphyseal region of the bone [23]. In that paper, however, the authors reported a really low accuracy that was probably due to the meshing strategy adopted and may be significantly improved.

Not only is the morphology of long bone epiphysis and metaphysis difficult to model correctly, but also in these regions the definition of the distribution of material properties presents a critical issue in the automatic generation of these models. The most recently published studies consider bone as an inhomogeneous material and derive its mechanical properties from the CT dataset, averaging the CT scalar field over each element volume using various algorithms [7, 24-26]. Until quite recently the majority of studies described bone as a homogenous two phase material, deriving the mechanical properties of cortical and spongy bone from the literature [27-29], a simplistic approach that has not been still completely abandoned [30]. It is true that the adoption of an inhomogeneous model, often characterised by dozens, if not hundreds, of different material properties, may induce a large computational effort, particularly when performing non-linear simulations. However, it should be verified that the adoption of a two-material model does not compromise the accuracy of a simulation to a non acceptable level. Other authors have addressed this question, but either lacked the experimental validation [31] or limited their comparison to the maximum stress predicted on the surface of the bone without investigating the differences in the stress field distribution in the whole bone [20]. In both cases the authors came to the conclusion that adopting a two-material model does change the stress field distribution, however the point is to quantitatively evaluate how much it lowers the accuracy of the predicted results.

The aim of the present study was to implement a general procedure to automatically generate subject-specific finite element models of bones from CT data and estimate the accuracy of this general procedure by applying it to one real femur. This femur was tested in vitro under different loading scenarios. The results from these tests were used to verify how the adoption of a simplified two-materials model would change the obtained accuracy with respect to the density-based inhomogeneous model. Special attention was paid to the epiphyseal and metaphyseal proximal regions of the bone.

2.1.1 Materials and methods

2.1.1.1 Femur specimen

The right femur of a 51 years old male donor, weight 75 kg, height 175 cm, deceased because of cerebral haemorrhage, was used for this study (Figure 1). The donor had no reported history of muscle-skeletal disease. The anatomical appearance of the femur was normal, with no signs of osteoarthritis at the cartilages and no deformities. In a radiographic examination the bone showed a normal trabecular density. The specimen was preserved wrapped in a cloth soaked with physiological saline solution and frozen at -25°C , a preservation procedure known not to alter the mechanical properties of the bone tissues [32].

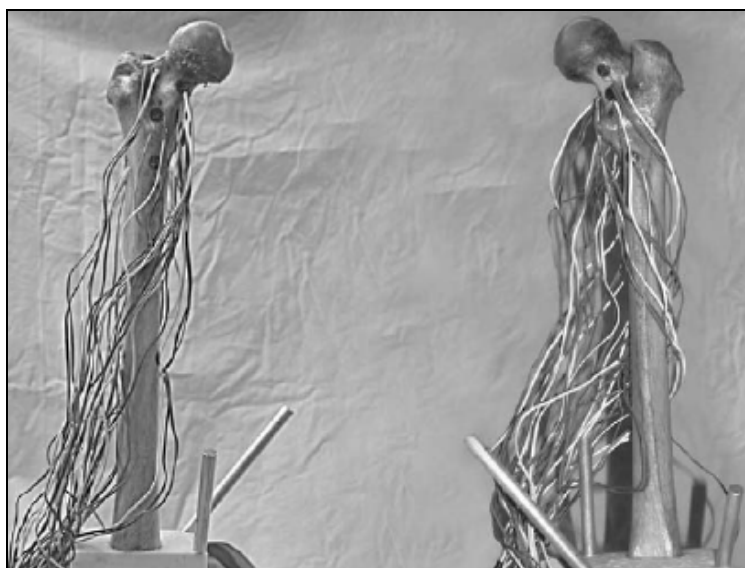


Figure 1 - An anterior (left) and posterior (right) view of the specimen, instrumented with the 13 strain gauges. The three aluminium rods embedded in the cement base used for the spatial registration are visible.

After dissection the femur was distally potted in PMMA together with three reference aluminium bars, each with a diameter of 10mm. The rods were not co-planar, to allow spatial registration (see below). Aluminium was chosen due to the low artefacts it produces when CT-scanned.

2.1.1.2 CT scanning

Prior to strain gauges application, the femur was CT-scanned, after being thawed and immersed in water to prevent beam-hardening artefacts (Brooks and Di Chiro, 1976). An axial scan protocol was adopted. The slice thickness was 1 mm and the spacing was 2mm in the proximal region, from the top of the femoral head down to the small trochanter, and 4mm in the rest of the femur. The slice spacing was also kept at 4mm in the condylar region, since an accurate description of the distal femur was not necessary as this region was embedded in cement, and to prevent the heating of the scanner. The pixel value was 0.46mm and the scanner physical parameters were: 180mA for the tube current and 120kVP, which are typical values for clinical examinations.

2.1.1.3 Experimental measurements

Strain gauges were located at the four anatomical aspects (medial, lateral, anterior, posterior), at four anatomical portions (femoral head, neck, metaphysis, diaphysis). To limit the number of acquisition channels, the anterior and posterior diaphysis gauges were omitted. Also the lateral neck gauge was omitted, as in this region the surface was too uneven. Thirteen locations were selected for strain measurement (Figure 2) and marked on the femur:

- Four around the neck, close to the edge of the articular cartilage of the head, on the Anterior, Lateral, Posterior and Medial sides;
- Three around the neck, distal to the previous ones, on the Anterior, Posterior and Medial sides;
- Four around the proximal diaphysis, just below the lesser trochanter, on the Anterior, Lateral, Posterior and Medial sides;
- Two at mid-diaphysis, on the Lateral, and Medial sides.

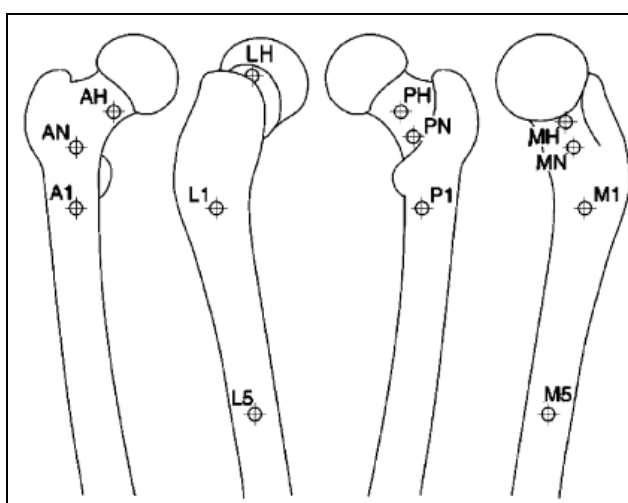


Figure 2 - Sketch of the femur specimen with an indication of the position of the strain gauges: anterior, lateral, posterior and medial views.

The area for strain measurement was prepared using a validated procedure [33], which has been shown to be adequate for testing of wet cadaveric specimens. This included:

- Completely cleaning the surface from soft tissues first with a scalpel, and finally with sandpaper (#100)
- Careful cleaning and degreasing first with ethanol, then with a cocktail of acetone and 2-propanol (RMS1, HBM, Darmstadt, Germany)
- Filling the pores and waterproofing of the surface with two layers of polyurethane protective (PU 120, HBM, Darmstadt, Germany)
- Smoothing and removing the excess of polyurethane with fine sandpaper (#400)
- Bonding the strain gauges with cyanoacrylate glue (CC-33A, Kyowa, Tokyo, Japan)
- Protecting and waterproofing the gauge with three layers of polyurethane protective (PU 120, HBM, Darmstadt, Germany)

Pre-wired stacked rosette strain gauges (Mod. KFG-3-120-D17-11L3M2S, Kyowa, Tokyo, Japan, with a grid length of 3 mm) were used. Resistance and insulation of each grid was tested with the strain gauge tester. A grid excitation of 0.5V was selected to avoid heating. Strains were sampled at a frequency of 10Hz, with a low-pass filter cut-off frequency of 1Hz.

The specimen was mounted on the load cell of the material-testing machine, which was equipped with a 5kN load cell (Mod. 8502, Instron, canton, MA, USA) on top of a platform that allowed tilting of the specimen at different angles (measured with a goniometry within $\pm 0.5^\circ$). The load was transmitted from the actuator by means of crossrails so as to avoid application of undesired horizontal force components (Figure 3).

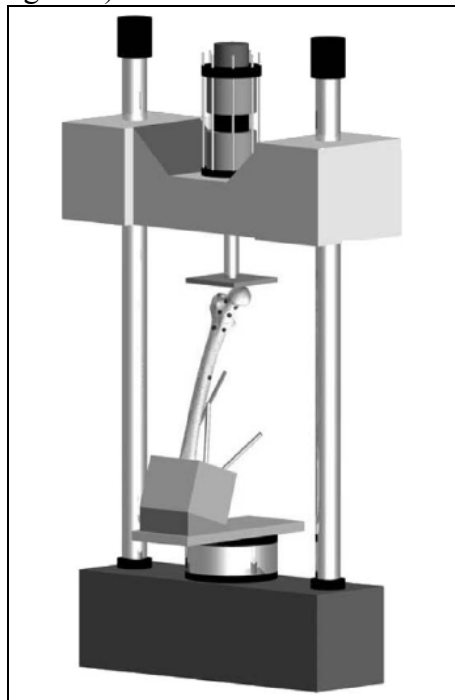


Figure 3 - Sketch of the testing machine with the femur in the 181 flexion load case (load case #4).

The following configurations were tested to cover the physiological range of maximum hip-reaction angles recorded in hip patients [34] during a wide range of activities (including level walking at different speeds, single leg stance, stair climbing and descending, standing up from seated position), and to generate bending in different planes, together with axial loading, and torsion:

1. Neutral: femoral axis vertical (0° adduction, 0° flexion)
2. Maximum adduction: femoral axis strongly adducted (24° adduction, 0° flexion)
3. Maximum abduction: in this case the femur is still slightly adducted (3° adduction, 0° flexion)
4. Maximum flexion: femoral axis flexed (0° adduction, 18° flexion)
5. Maximum extension: femoral axis slightly extended (0° adduction, 3° extension)

The specimen was first pre-loaded with the testing machine in position control up to a vertical load of 100N. The machine was then switched to load control (thus allowing for the specimen to creep when the load was held). The load was increased up to 800N in 100N increments at 30s intervals. Strains were recorded during the whole loading time and for at least 90s after load removal for each repetition. Five loading repetitions were performed for each loading configuration, with the specimen being allowed to recover at least 10 minutes between replicates.

This procedure allowed measuring strains at different strain levels, checking material linearity, quantifying viscoelastic phenomena and irreversible strains.

The room temperature was in the range 29.5 to 31.0°C , with a relative humidity of 40%. The specimen was constantly moistened by means of cloths wrapped around the entire specimen and soaked with physiological saline solution.

The data from the individual grids were processed to obtain principal directions and strains. Data were preliminarily screened with the Chauvenet's criterion for outliers, with no data needing to be discarded. Linearity was checked and finally data were processed statistically.

The maximum and minimum principal strain values collected from the 13 rosettes for each loading scenario for the highest load (800N) and 30s after load application were used for determining the principal stresses for the comparison with the finite element results. Overall, a total of 130 measurements were used for the validation of the numerical models.

2.1.1.4 Subject-specific finite element model

The finite element model was generated, starting from the CT dataset, using a procedure that can be summarized in the following steps: (i) extraction of the 3D bone surface, (ii) generation of the finite element mesh and (iii) mapping of the inhomogeneous bone tissue mechanical properties onto the mesh.

For the first step, the external contours of the bone were extracted from the CT slices with a semi-automatic software, based on a border-tracing algorithm [15]. The contours were then

interpolated to obtain the external surface of the femur using a Delaunay triangulation algorithm [35].

This tiled surface (Figure 8) model was converted into a NURBS model using the reverseengineering software Geomagic Studio (v. 6, Raindrop Geomagic, Inc., USA).



Figure 4 - The solid model of the femur.

For the second step, a 10-noded tetrahedral finite element mesh of the femur was automatically generated using the HyperMesh software package (Altair Engineering, Inc., USA) that implements an advancing-front algorithm. Care was taken that a regular layer of tetrahedra was generated on the femoral surface in order to limit, as much as possible, the unavoidable partial volume effects that would lower the model density in the neck surface region (Fig. 5). The condylar region of the femur was not modelled. The femur model was trimmed under the level of the cement block. The condylar region was of no interest since it was embedded in the cement block. The resulting mesh consisted of 76,026 elements and 118,970 nodes.

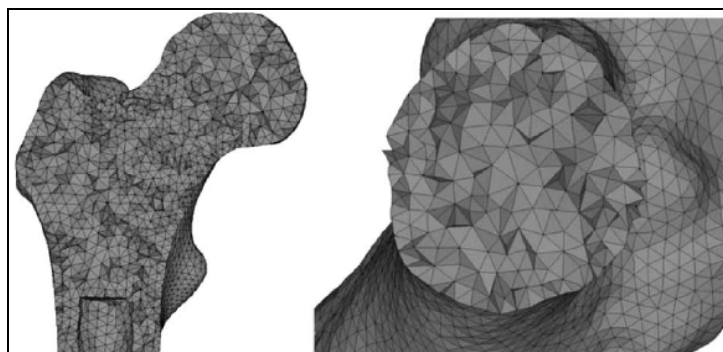


Figure 5 - Two section of the finite element model: on the left a coronal section and on the right a transversal neck section. The regular layer of tetrahedra along the boundary is visible.

For the third step, each element of the mesh was given a different Young's modulus computed on the basis of the density information derived from the CT dataset. An average Hounsfield Unit (HU) value was computed for each element performing a numerical integration of the HU field

over the element's volume using the in-house developed software Bonemat_V2 [5] (publicly available at <http://www.tecno.ior.it/back2net/>). A linear relationship between the HU numbers and the bone ash density was assumed [36]. The CT dataset was calibrated using a calibration phantom with bone-equivalent (solution of hydroxyapatite) insertions of different densities embedded in a water-equivalent resin-based plastic (The European Spine Phantom [37]). The following power relationship between ash density and Young's modulus was assumed [38]:

$$E = 10.5 \cdot \rho_{ash}^{2.29}$$

This relationship yields E in GPa when ρ_{ash} (ash density) is provided in g cm⁻³. A Poisson ratio of 0.3 was assumed.

The resulting values of the Young's modulus for cortical bone were up to 19.8GPa, with an average value of 12.9GPa, which is in excellent agreement with the values reported in the literature [39]. The density-based inhomogeneous model was characterized by 381 different materials.

The two-material model was generated assigning a Young's modulus of 19.3GPa for the cortical bone and of 590MPa for the spongy bone calculated from the calibrated CT dataset with relationship (1) for two averaged cortical and spongy HU values. The values are within the range reported in the literature [39]. The threshold to separate cortical from spongy bone was calculated on the basis of a visual inspection of the CT dataset.

The model was then fully constrained in the distal region corresponding to the cement block, hence assuming that no relative displacements could occur between the two, and neglecting the eventual elastic deformation of the cement during the experimental tests.

2.1.1.5 Spatial registration between model and experiment

In order to establish the relative position of the laboratory reference system and the CT reference system, the three aluminium cylindrical rods embedded, together with the femur, in the cement base (see above, Fig. 1) were used.

The positions of the 13 strain-gauges centres, the positions of several points on the surface of the femur and of the three aluminium rods were acquired using a Micro Scribe digitiser (Mod. 3DX, Immersion Corporation, U.S.A.). The resolution of the Digitiser was 0.2 mm; three repeated measurements were performed for each point.

An Iterative Closest Point (ICP) algorithm, as proposed for the express purpose of solving rigid registration problems [40], was used to perform the registration of the acquired points cloud on the tiled surface extracted from the CT exam, and also to find the transformation between the experimental laboratory reference system and the model one. When used to solve similar problems our implementation showed an average accuracy of 0.11 degrees on the rotations and 0.19mm on the translations [41]The maximum registration error in the present case was 1.3mm.

2.1.1.6 Determination of the model accuracy

The rosette strain gauges used in the experimental set-up provided the values of two principal strains and the principal directions averaged over the sensing area of the gauge. Under a given stress field, in a non-homogeneous material, the measured value of the surface strains is strongly affected by the module of elasticity of the material immediately underneath the strain gauge. In the epiphyseal regions, where a thin superficial shell of dense bone wraps the cancellous bone core, the strain measurements may be strongly affected by this extremely localised non-homogeneity. Thus it is more correct to determine the tissue properties immediately below each strain gauge from the CT data, and use this modulus of elasticity to convert the two measured principal strains into the two principal stresses, in analogy to what done by other authors [20, 22]. During the preparation of the mesh, care was taken to make sure that a node was coincident with each rosette centre. However, since the majority of the strain gauges were placed in region of high stress gradient, to correctly compare the predicted and measured stresses, the averages of the principal stresses predicted at the nodes corresponding to the sensing gauge's area were considered and compared with the ones obtained by converting the strain gauge measurements.

No effect of the load case was observed on the difference between measured and predicted principal stresses (factorial ANOVA, $p=0.93$). Thus, all 130 measurements were pooled together. The principal stresses predicted by each model were compared to the measured values in two ways. Firstly, a linear regression between the measured and the predicted values was performed. The goodness of the prediction was expressed by the coefficient of linear regression R^2 , and by the slope and intercept of the regression curve. Ideally, we should find a perfectly linear relationship between measurements and predictions ($R^2 = 1$) with unitary slope and zero intercept. While these metrics provide a global indication on the goodness of the predictions, for many conditions it is also important to know what is the local error one may expect from each single prediction. Thus, for each model we also computed the peak error, and the average error (computed as the quadratic norm error, also known as Root Mean Square (RMS) error).

Although the reference measurements available refer to surface stresses, the biggest differences between a homogeneous model and a non-homogeneous model are inside the bone volume. In order to make these differences evident, the distributions of Von Mises stress and Von Mises strain fields in the proximal region predicted by the two 5 material models were compared for all loading conditions.

2.1.2 Results

2.1.2.1 Experimental measurements

All strain measurements were successfully performed. Linearity was checked for each individual grid, each load replication, and each loading configuration. Linearity was excellent:

- $R^2 = 0.99$ for 88% of the cases where strains reached a value of 50 micro strain or larger. Only in 6 cases a value of R^2 lower than 0.90 was found. This confirmed that the bone could reasonably be assumed to behave linearly.

- In no case was R^2 lower than 0.70. Additionally, no grid had a consistently nonlinear behaviour under changed loading conditions. This confirmed the good quality of strain gauge bonding.

Strain measurements at the beginning and at the end of each loading level (load was held for 30s at each step) were compared. Strain magnitude tended to increase over time by typically 0.1-1.0% of the current value (maximum, in one case: 2.3%). This confirmed the presence of viscoelastic behaviour, and the need to define a time when strains are to be measured after load application. However, these detectable creep effects did not significantly alter the strain pattern.

After unloading strains returned rapidly to near-zero, with residual strains of a few percent of the peak value being found ten minutes after load removal. The largest residual strains were found along the diaphysis.

Repeatability was satisfactory but not excellent: the variability between replicates under the same conditions was generally of the order of few percents of the measured magnitude. Larger coefficients of variation (standard deviation expressed as % of the readout) were found along the diaphysis for some load cases. At a detailed inspection it was found that this scatter was mainly due to a conditioning effect: strain magnitudes tended to slightly decrease between replicates, despite the 10 minutes recovery time allowed between repetitions.

2.1.2.2 Comparison FEM vs experimental stresses

Predicted principal stresses correlated very well with experimental values for both the two-material 5 homogeneous and the density-based inhomogeneous model. The linear regressions are reported in Figure 8. In both cases the slope of the regression line and its intercept were not significantly different from one and zero respectively (Covariance Analysis, $p > 0.05$) [42].

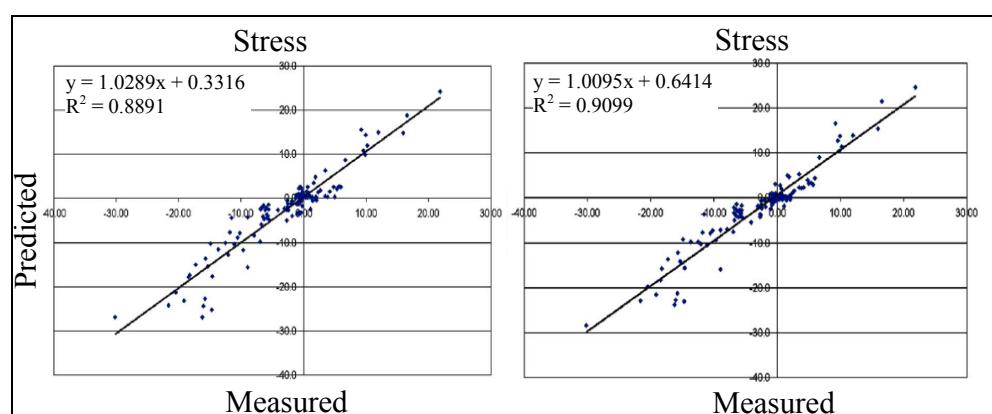


Figure 6 - On the left: Predicted vs. measured stresses (MPa) in the two-material homogeneous model. On the right: Predicted vs. measured stresses (MPa) in the density-based inhomogeneous model.

The average error (Root Mean Square Error) was 2.6MPa in the density-based inhomogeneous model and 2.9MPa for the two-material homogenous one, resulting, respectively, in an error of 8.6% and 9.6% of the maximum measured stress. The maximum error was of 10.6MPa in the

two-material homogeneous model, which represents the 35% of the maximum measured stress, while it was 8.3MPa for the density-based inhomogeneous model, which was 27% of the maximum stress. The results are summarised in Table 1.

	Two-material model	Density-based model
RMSE (MPa)	2.9	2.6
RMSE (%)	9.6%	8.6%
Max. error (MPa)	10.6	8.3
Max. error (%)	35%	27%

Table 1 - The average and maximum errors, both absolute and as a percentage of the maximum measured stress, in the two models

The distribution of the Von Mises stresses (Figure 7) and strains in the proximal femur, excluding the regions in the proximity of the boundary condition application points, were not normally distributed (Kolmogorov-Smirnov, Lilliefors Significance Correction, $p < 0.001$) and were found to be significantly different (Wilcoxon test, Tied PValue < 0.001) for all load cases. The maximum registered difference between the two models was of 35.9MPa that represents the 164% of the maximum measured value. The two-material homogeneous model on average, merging the results relative to all load cases, predicted slightly lower stress values than the density-based inhomogeneous one and the global average difference was the 4% of the maximum measured stress.

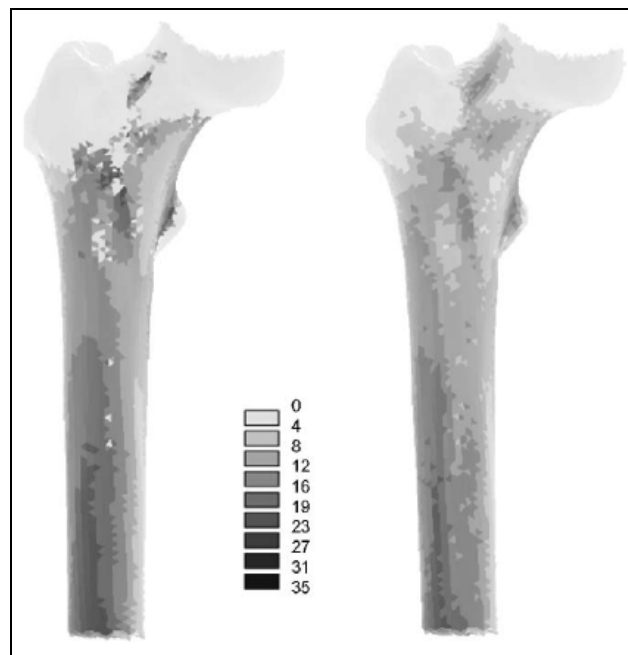


Figure 7 - The Von Mises equivalent stress (MPa) in the ROI in the proximal femur in the case of 181 flexion (load case #4) in the twomaterial homogeneous model (left) and in the density-based inhomogeneous one (right).

2.1.3 Discussions

In the past few years several methods have been proposed for the generation of subject-specific finite element models of bones from CT data. These new techniques usually rely on automatic

mesh generators to reduce the time necessary to build the model, making it possible to apply the finite element modelling to study real clinical cases or large populations. Before bringing this method in the clinical practice, however, it is necessary to assess the accuracy of these finite element models in the predictions of the bone stresses paying particular attention to those regions, such as the epiphyseal and metaphyseal parts of long bones, where the automatic methods are typically give reduced accuracy but that are of great interest and clinical relevance. The aim of the present study was to implement a general procedure to automatically generate subjectspecific finite element models of bones from CT data, estimate the accuracy of this general procedure by applying it to one real femur, which was in parallel tested in vitro under different loading scenarios, and verify how the adoption of a simplified two material homogeneous model would change the obtained accuracy with respect to the density-based inhomogeneous one. Particular attention was paid to the epiphyseal and metaphyseal proximal regions of the bone.

The results showed that the density-based inhomogeneous model predicts with a very good accuracy the measured stress field, while the homogeneous two-material model results were less accurate, although not dramatically. The numerically predicted stresses were highly correlated with the measured ones for both models: in both cases the R^2 was very high. In addition the gradient coefficients of the regression line were not significantly different from one and the intercepts were not significantly different from zero for both models. The global accuracy was good for the density-based inhomogeneous model since the average error was lower than 9% and the peak error was lower than 30% of the maximum measured stress. Lower accuracy was found for the two-materials homogenous model, where the average error was slightly higher, almost 10%, but the peak error reached 35% of the maximum measured stress. In addition the stress field distributions predicted by the two models were significantly different, and the average difference was the 4% of the maximum measured stress. The maximum predicted difference was 35.9MPa, which represented 164% of the maximum measured stress value. This result shows that the strategy of material properties mapping has a significant effect on the stress prediction, specifically when the stress field in the bulk of the bone is of interest as for example when studying the interaction between bone and a prosthetic implant.

The accuracy obtained in the present study with the density-based inhomogeneous model improves previously published results relative to human femoral models. In the only, to the authors' knowledge, previous work that addressed the very proximal part of the femur [23], a very low correlation between experimental and predicted strains ($R^2 = 0.66$) was found and, although not explicitly reported, a very high peak error, near 100% of the maximum measured strain, can be derived from the plot. This low accuracy may be due to the inadequacy of the mesh used since it was made of linear 4-noded tetrahedra, that, being stress-constant elements, are known to produce bad results unless the refinement of the mesh is really high [43]. Their model was probably too coarse to correctly represent the highly varying stress and strain fields that characterise the neck region. In her validation work, Keyak and coworkers reported a very low correlation between experimental and predicted strains ($R^2 = 0.59$) [18]. However, as already stated, this result was relative to a voxel-based mesh. Lengsfeld and co-workers obtained a far better correlation ($R^2 = 0.84$) [22] with a mapped hexahedral model; but, although it was not

explicitly reported in the study, it seems from the plotted results that the maximum error they obtained was higher than 50% of the maximum measured stress. This high error value may be due to the material model adopted, a two-material homogenous one, in fact their results are in a better agreement with what we found with our two-material homogenous model. Similarly, if we compare our results with the those more recently published by Gupta and co-workers [19], we find that our correlation is slightly better, although not dramatically, than the one reported ($R^2 = 0.898$). What is dramatically improved is the maximum error, which in the cited article exceeded 200% of 30 the maximum measured strain.

The different behaviour we found for the two-material homogeneous and density-based inhomogeneous models confirms the results obtained by other authors [20, 31]. In addition to their findings, where only superficial stresses were compared, we assert that the stress distributions inside the bone are significantly different as well.

The major limitation of the present work is that a single normal femur was used to perform the experiment. In the authors' opinion, however, this limit does not reduce the importance and generality of the obtained results for two basic reasons. Firstly a large number of strain gauges were used, more than in most previous studies, and five different loading scenarios were considered, hence a large amount of multi-dimensional numerical data were available from this single sample. Secondly, we concentrated the strain gauges in the most proximal part of the femur, which represents a valid example of an extremely difficult anatomical region to mesh with an automatic strategy, for the reasons explained above. Hence, the obtained high accuracy which is obtained with a general and automated approach applied on a randomly selected specimen, can have a general validity, at least for the finite element modelling of long bones from CT data. However, if the bone is affected by a severe pathology that dramatically changes its mechanical characteristics, the results may be no longer valid. But, in such a case, the relationships between density and bone Young modulus should also be verified and may need revision. This would require far more work and such studies are beyond the scope of the present work.

Another limitation of the present work is relative to the CT scan protocol adopted. If only a confined region of bone is to be considered, then the protocol adopted for this study may be applied also *in vivo*, but if an extensive region needs to be examined for clinical reasons, then the protocol may need to be changed to limit the dose the patient is exposed to. This may lower the accuracy of the proposed method, as well as of any other method, in an unpredictable way, hence the adoption of special scan protocol specifically designed for the optimisation of the image quality without increasing the radiation dose, such as that recently proposed by Lattanzi et al. [44], is recommended.

Finally, the presented model did not take into account the known local anisotropic behaviour of the bone tissue, assigning an average Young's modulus to each element, even in the density-based inhomogeneous model. It is true that the global anisotropic behaviour of the bone, as a structure, is captured by the inhomogeneity of the model, but it is possible that the introduction of a local anisotropy may further improve the predictive capabilities of the model. However, deriving the subject-specific anisotropic properties of the bone tissue from CT data may not be

trivial, and the introduction of an a priori knowledge in the model could be necessary. Further studies are to be done to understand how this process could become automatic and how it can improve the accuracy of the finite element model.

In summary, the good results obtained in the present study show that it is possible to automatically generate accurate finite element models of long bones from CT data for the prediction of the bone stress fields under various loading conditions. The material mapping strategy proved to positively influence the accuracy of the numerical prediction, hence it is important to correctly consider the inhomogeneity of the bone mechanical properties in the generation of finite element models when the stress levels inside the bone are of importance in the study.

2.2 Accuracy of subject-specific finite element model of an implanted femur: an in-vitro study³

Resurfacing as a solution to osteoarthritis of the hip is logical and intuitive, offering many theoretical advantages. There is a recent resurgence of interest in resurfacing, due mainly to the latest generation of resurfacing designs. Resurfacing has received considerable attention, and has been the subject of clinical and mechanical [45-50].

While several stemmed hip prostheses have been thoroughly investigated pre-clinically, and a paradigm exists for the validation of such devices (e.g.: [51]), to the Authors' knowledge no similar extensive validation has ever been carried out for any resurfacing prosthesis.

The goal of this work was to design and carry out a validation of a femur implanted with this type of devices to allow its use in further studies to elucidate possible failure scenarios.

2.2.1 Materials and methods

The femur specimen used for the validation study reported in paragraph 2.1 has been used in present work. In this paragraph only the additional information, necessary to complete the description of the resurfaced femur analysis are reported. Refer to paragraph 2.1.1 for additional information not reported here.

Following the testing of the intact specimen a surgeon with significant clinical experience with resurfacing prostheses implanted the cadaver femur with a partially cemented epiphyseal stem (Conserve Plus, Wright Medical, USA). The size was chosen to match the femoral head diameter as closely as possible. After implantation all the strain gauges were tested once again, to confirm that they suffered no damage during implantation.

³ This paragraph is extracted from: S. Martelli, et. al. "Accuracy of subject-specific finite element models of long bones from CT data: an *in-vitro* study". Proceeding of II ICCB, H. Rodrigues *et al.* (Eds.), Lisbon, Portugal, September 14-16, 2005

The femur was instrumented with two high precision waterproof spring-preloaded LVDT to measure stem-prosthesis micromotion. Position and alignment were defined based the maximum gap and maximum sliding predicted by a finite element study. The actual position and alignment of the LVDTs were very close to the intended ones: small changes were due to the complex bone geometry. One transducer was oriented to measure the detachment of the stem form the bone (GAP), while the other was oriented to measure the relative tangential micromotion (SHEAR). The final position and direction was measured for comparison against FE results.

FE results indicated that the maximum flexion load case (0° adduction, 18° flexion) was the one producing the highest stresses and inducible micro-movements. This load case was chosen for the experimental validation, and applied to the implanted specimen in the very same way it was applied to the intact specimen. The maximum magnitude of the applied load was 800N to avoid any irreversible strain.

All strain recording were collected and processed as already described for the intact femur, and recorded together with the micromotion measurements from the LVDT transducers.

The maximum and minimum principal strain values under peak load measured by the 13 rosettes were used to determine the principal stresses for the comparison with the finite element results.

Finite element model

The model of the implanted femur was built using the intact femur model, of the prosthetic stem and of the rasp. To generate the finite element model of the implanted femur we had to replicate in the model the relative position with respect to the femur in which the surgeon placed the prosthesis. Using the digitizer we collected many points on both the prosthesis and the femur surfaces and registered with the computer models using an ICP (iterative closest point) algorithm. The geometry of the implanted femur was found as Boolean difference between the femur and the rasp. The empty space between the prosthesis and the rimmed femur was considered as cement volume.

The bone, cement and prosthesis volumes were automatically meshed with the same procedure used for the intact femur and described above. The bone mesh was then considered a non-homogeneous body and the materials map was derived from the CT data and defined by the software Bonemat_V2.

Tree contact interfaces were defined: bone to cement, cement to prosthesis and prosthesis to cement. The bone to cement contact interface was assumed bonded while for the cement to prosthesis and for bone to prosthesis interfaces was defined as a friction contact.

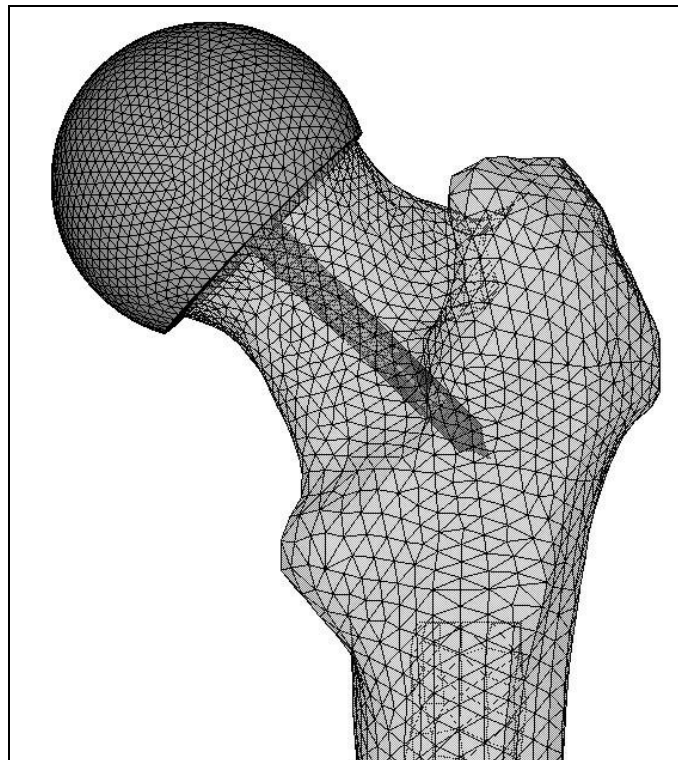


Figure 8 - The finite element model of the intact femur

Consistently with previous works [20] the tissue properties were determined from CT data immediately underneath each strain gauge, and the measured principal strains were converted into the equivalent principal stress.

To compare the predicted and measured stresses, the averages of the principal stresses predicted at the nodes surrounding the strain gauges area were compared with the ones derived from the strain gauges reading.

The principal stresses predicted by each model were compared to the measured values in two ways:

- Linear regression between the measured and the predicted values. Slope, intercept and coefficient of linear regression R^2 were compared.
- Peak error and average error as a Root Mean Square (RMS).

2.2.2 Results

All strain measurements were found to increase linearly with the applied load for all test set-ups. A moderate visco-elastic behaviour was observed immediately after the load application, and thus the measurements were taken after 30 seconds of load application.

In the implanted femur, the displacement readouts from the LVDTs were quite low and found to increase linearly with the applied load. Both recoverable and residual micro-movements were

always larger in the GAP opening mode than in the SHEAR direction. GAP and SHEAR micromotion are reported in Table 2.

Also the implanted femur model showed a good accuracy, although lower than that of the intact femur. Predicted principal stresses correlated very well with experimental values even if only one load case was investigated, especially considering that the model involved a major contact non-linearity. The slope of the regression line and its intercept were not significantly different from one and zero respectively.

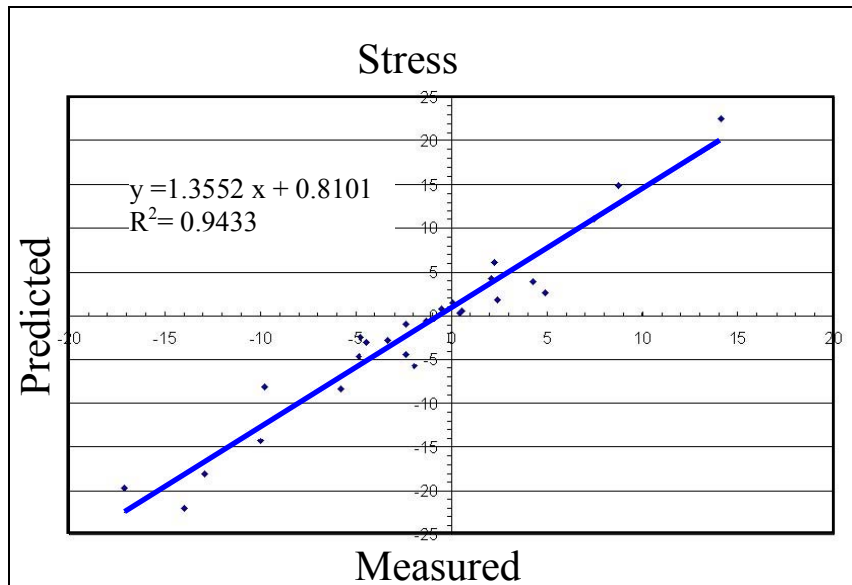


Figure 9 - Predicted vs. measured principal stresses in the implanted femur

The computed mean error (RMSE) between the predicted and the measured stresses was found to be 1.5 MPa, or 8.9% of the peak measured stress. The maximum error was found to be 8.5 MPa.

Also the predicted micro-movements matched very closely the measured values, confirming that also the local non-linear contact between the stem and the cement was accurately modelled.

	Measured	Predicted
GAP opening (mm)	0.030 ± 0.006	0.025
SHEAR motion (mm)	0.014 ± 0.004	0.012

Table 2 - Predicted vs. measured head micromotion

2.2.3 Discussion

Metal-on-metal hip resurfacing is becoming increasingly popular, and a number of new devices have been introduced recently. The two major goals of the current study were to experimentally validate model predictions of the resurfaced femur biomechanics to examine the mechanical effects of surface replacement.

For the femoral bone, both the experimentally measured principal strains and the FE-predicted principal stresses were reduced by less than 20% when the prosthesis was implanted; thus the likelihood of extensive remodelling of the neck and proximal femur is low. For the load cases

applied, the stress levels in the region of the femoral neck were low, well below the ultimate strength of the bone, indicating that the risk of mechanically induced neck fracture is low after resurfacing. For the implanted device (Conserve Plus) no relevant stress concentration was predicted near the tip of the metaphyseal stem. The experimental and the FE-predicted implant micro-motions were extremely small, particularly when compared to other cemented prostheses [52, 53].

The model predictions of cement mantle tensile stresses were below 6MPa for all loading conditions. This is less than a third of the failure stress for PMMA bone cement (21 MPa [54]) but two thirds of the cement fatigue limit of 9MPa [54].

Despite the presence of the strain gauges at mid-diaphysis and the use of additional measurements, it was difficult to accurately replicate point of load application in intact versus implanted FEM. Further studies are in progress to develop a method to monitor more accurately the point of application of the load (Appendix A).

These models can now be used to examine physiological load cases, and look at effects of design and implantation technique variation.

2.3 Conclusions

The aim of the validation studies presented in this chapter was to assess the accuracy of two finite element models generated from medical images [4, 5].

Although the implanted femur was validated only for a single loading configuration so as to avoid the noise introduced by possibly local plasticization, the accuracy achieved on bone stresses and prosthesis micromoments were satisfactorily. A parallel study [55] confirmed the validity of the adopted methodology by applying the method, with slight changes, to various cadaver femurs and confirming the same confidence also for the predictions of the bone strain field.

If compared to the common threshold for failure of strains and prosthesis micromovement (i.e. about 7000 microstrain for bone fractures [56], 50 microns for loosening [57]) with the achieved confidence level of 10% on the stress/strain field and one micron on the bone-prosthesis micromovement, these models appear valid for predicting failure of resurfaced femurs.

However, when it is of interest the biomechanical behaviour of the prosthesis when implanted on the population the device is indicated to, several models are needed to span the variability of the human anatomy. The long and demanding validation process here described is not practically feasible for a large number of models.

Hence, to extend the validity of the presented validation studies to other models generated by the same protocol, a second sensitivity analysis should follow to understand what are the effects of the uncertainties on modelling parameters on model predictions. This problem is addressed in the next chapter.

REFERENCES

1. Schlesinger, *Terminology for model credibility*. Simulation, 1979. **32**(3): p. 103-104.
2. Sargent, R.G. *Verification and validation of simulation models*. in *Simulation conference proceedings*. 1998. Washington,DC,USA.
3. Shannon, R.E., *System simulation: the art and the science*. 1975, Englewood Cliff, New Jersey: Prentice-Hall.
4. Viceconti, M. and F. Taddei, *Automatic generation of finite element meshes from computed tomography data*. Crit Rev Biomed Eng, 2003. **31**(1-2): p. 27-72.
5. Taddei, F., A. Pancanti, and M. Viceconti, *An improved method for the automatic mapping of computed tomography numbers onto finite element models*. Med Eng Phys, 2004. **26**(1): p. 61-9.
6. Ruimerman, R., et al., *A theoretical framework for strain-related trabecular bone maintenance and adaptation*. J Biomech, 2005. **38**(4): p. 931-41.
7. Taddei, F., et al., *Mechanical strength of a femoral reconstruction in paediatric oncology: a finite element study*. Proceedings of the Institution of Mechanical Engineers. Part H, Journal of engineering in medicine., 2003. **217**(2): p. 111-9.
8. Aamodt, A., et al., *In vivo measurements show tensile axial strain in the proximal lateral aspect of the human femur*. Journal of Orthopaedic Research, 1997. **15**(6): p. 927-31.
9. Keyak, J.H. and H.B. Skinner, *Three-dimensional finite element modelling of bone: effects of element size*. Journal of Biomedical Engineering, 1992. **14**(6): p. 483-9.
10. Keyak, J.H., et al., *Prediction of femoral fracture load using automated finite element modeling*. Journal of Biomechanics, 1998. **31**(2): p. 125-33.
11. Keyak, J.H., et al., *Automated three-dimensional finite element modelling of bone: a new method*. Journal of Biomedical Engineering, 1990. **12**(5): p. 389-97.
12. Jacobs, C.R., et al., *NACOB presentation to ASB Young Scientist Award: Postdoctoral. The impact of boundary conditions and mesh size on the accuracy of cancellous bone tissue modulus determination using large-scale finite- element modeling*. North American Congress on Biomechanics. Journal of Biomechanics, 1999. **32**(11): p. 1159-64.
13. Hollister, S.J. and B.A. Riemer, *Digital image based finite element analysis for bone microstructure using conjugate gradient and Gaussian filter techniques*, in *Mathematical Methods in Medical Imaging II*, J.N. Wilson and D.C. Wilson, Editors. 1993, SPIE. p. 95-106.
14. Viceconti, M., et al., *A comparative study on different methods of automatic mesh generation of human femurs*. Medical Engineering and Physics, 1998. **20**(1): p. 1-10.
15. Testi, D., et al., *Border-tracing algorithm implementation for the femoral geometry reconstruction*. Computer Methods and Programs in Biomedicine, 2001. **65**(3): p. 175-82.
16. Viceconti, M., et al., *Automatic generation of accurate subject-specific bone finite element models to be used in clinical studies*. J Biomech, 2004. **37**(10): p. 1597-605.

17. Les, C.M., et al., *Development and validation of a series of three-dimensional finite element models of the equine metacarpus*. Journal of biomechanics, 1997. **30**(7): p. 737-42.
18. Keyak, J.H., et al., *Validation of an automated method of three-dimensional finite element modelling of bone*. Journal of biomedical engineering, 1993. **15**(6): p. 505-9.
19. Gupta, S., et al., *Development and experimental validation of a three-dimensional finite element model of the human scapula*. Proceedings of the Institution of Mechanical Engineers. Part H, Journal of engineering in medicine., 2004. **218**(2): p. 127-42.
20. Dalstra, M., R. Huiskes, and L. van Erning, *Development and validation of a three-dimensional finite element model of the pelvic bone*. Journal of biomechanical engineering, 1995. **117**(3): p. 272-8.
21. Couteau, B., et al., *Finite element analysis of the mechanical behavior of a scapula implanted with a glenoid prosthesis*. Clinical biomechanics (Bristol, Avon), 2001. **16**(7): p. 566-75.
22. Lengsfeld, M., et al., *Comparison of geometry-based and CT voxel-based finite element modelling and experimental validation*. Medical engineering & physics, 1998. **20**(7): p. 515-22.
23. Ota, T., I. Yamamoto, and R. Morita, *Fracture simulation of the femoral bone using the finite-element method: how a fracture initiates and proceeds*. J Bone Miner Metab, 1999. **17**(2): p. 108-12.
24. Perillo-Marcone, A., A. Alonso-Vazquez, and M. Taylor, *Assessment of the effect of mesh density on the material property discretisation within QCT based FE models: a practical example using the implanted proximal tibia*. Comput Methods Biomech Biomed Engin, 2003. **6**(1): p. 17-26.
25. Keaveny, T.M. and D.L. Bartel, *Effects of porous coating and collar support on early load transfer for a cementless hip prosthesis*. J Biomech, 1993. **26**(10): p. 1205-16.
26. Huiskes, R., N. Verdonschot, and B. Nivbrant, *Migration, stem shape, and surface finish in cemented total hip arthroplasty*. Clin Orthop Relat Res, 1998(355): p. 103-12.
27. Villarraga, M.L., et al., *Contact analysis of a posterior cervical spine plate using a three-dimensional canine finite element model*. J Biomech Eng, 1999. **121**(2): p. 206-14.
28. Verdonschot, N.J., R. Huiskes, and M.A. Freeman, *Pre-clinical testing of hip prosthetic designs: a comparison of finite element calculations and laboratory tests*. Proc Inst Mech Eng [H], 1993. **207**(3): p. 149-54.
29. Spears, I.R., et al., *The effect of interfacial parameters on cup-bone relative micromotions. A finite element investigation*. J Biomech, 2001. **34**(1): p. 113-20.
30. Cegonino, J., et al., *A comparative analysis of different treatments for distal femur fractures using the finite element method*. Comput Methods Biomech Biomed Engin, 2004. **7**(5): p. 245-56.
31. Cattaneo, P.M., M. Dalstra, and L.H. Frich, *A three-dimensional finite element model from computed tomography data: a semi-automated method*. Proceedings of the Institution of Mechanical Engineers. Part H, Journal of engineering in medicine., 2001. **215**(2): p. 203-13.

32. Evans, F.G., *Mechanical properties of Bone*. 1973, Springfield, Illinois, USA: Charles C. Thomas Publishers.
33. Viceconti, M., A. Toni, and A. Giunti, *Strain gauge analysis of hard tissues: factors influencing measurements*, in *Experimental Mechanics. Technology transfer between high tech engineering and biomechanics.*, L.E. G., Editor. 1992, Elsevier Science: Amsterdam. p. 177-184.
34. Bergmann, D., *Hip98, loading of the hip joint*. 2001, Freie Universität: Berlin.
35. Boissonnat, J.-D. and B. Geiger, *Three dimensional reconstruction of complex shapes based on the Delaunay triangulation*, in *Biomedical Image Processing and Biomedical Visualisation*, R.S. Acharya and D.B. Goldgof, Editors. 1993, SPIE. p. 964-975.
36. Les, C.M., et al., *Estimation of material properties in the equine metacarpus with use of quantitative computed tomography*. Journal of Orthopaedic Research, 1994. **12**(6): p. 822-33.
37. Kalender, W.A., *A phantom for standardization and quality control in spinal bone mineral measurements by QCT and DXA: Design considerations and specifications*. Medical Physics, 1992. **19**(3): p. 583-586.
38. Keller, T.S., *Predicting the compressive mechanical behavior of bone*. Journal of Biomechanics, 1994. **27**(9): p. 1159-1168.
39. Wirtz, D.C., et al., *Critical evaluation of known bone material properties to realize anisotropic FE-simulation of the proximal femur*. Journal of biomechanics, 2000. **33**(10): p. 1325-30.
40. Besl, P. and N. McKay, *A method for registration of 3-D shapes*. IEEE Transactions on Pattern Analysis and Machine Intelligence, 1992. **14**(2): p. 239-256.
41. Popescu, F., et al., *A new method to compare planned and achieved position of an orthopaedic implant*. Comput Methods Programs Biomed, 2003. **71**(2): p. 117-27.
42. Armitage, P. and G. Berry, *Statistical Methods in Medical Research*. 1994, Blackwell Scientific Publications: Oxford. p. 397-99.
43. Polgar, K., M. Viceconti, and J.J. O'Connor, *A comparison between automatically generated linear and parabolic tetrahedra when used to mesh a human femur*. Proc Inst Mech Eng [H], 2001. **215**(1): p. 85-94.
44. Lattanzi, R., et al., *Specialised CT scan protocols for 3-D pre-operative planning of total hip replacement*. Med Eng Phys, 2004. **26**(3): p. 237-45.
45. Kishida, Y., et al., *Preservation of the bone mineral density of the femur after surface replacement of the hip*. J Bone Joint Surg Br, 2004. **86**(2): p. 185-9.
46. Little, J.P., et al., *Changes in femur stress after hip resurfacing arthroplasty: response to physiological loads*. Clin Biomech (Bristol, Avon), 2007. **22**(4): p. 440-8.
47. Long, J.P. and D.L. Bartel, *Surgical variables affect the mechanics of a hip resurfacing system*. Clin Orthop Relat Res, 2006. **453**: p. 115-22.
48. Mont, M.A., et al., *Hip resurfacing arthroplasty*. J Am Acad Orthop Surg, 2006. **14**(8): p. 454-63.
49. Ong, K.L., et al., *Biomechanics of the Birmingham hip resurfacing arthroplasty*. J Bone Joint Surg Br, 2006. **88**(8): p. 1110-5.

50. Taylor, M., *Finite element analysis of the resurfaced femoral head*. Proc Inst Mech Eng [H], 2006. **220**(2): p. 289-97.
51. Viceconti, M., et al., *Pre-clinical validation of a new partially cemented femoral prosthesis by synergetic use of numerical and experimental methods*. J Biomech, 2001. **34**(6): p. 723-31.
52. Cristofolini, L., E. Varini, and M. Viceconti, *In-vitro method for assessing femoral implant-bone micromotions in resurfacing hip implants under different loading conditions*. Proc Inst Mech Eng [H], 2007. **221**(8): p. 943-50.
53. Monti, L., L. Cristofolini, and M. Viceconti, *Methods for quantitative analysis of the primary stability in uncemented hip prostheses*. Artif Organs, 1999. **23**(9): p. 851-9.
54. Lewis, G., *Properties of acrylic bone cement: state of the art review*. J Biomed Mater Res, 1997. **38**(2): p. 155-82.
55. Schileo, E., et al., *Subject-specific finite element models can accurately predict strain levels in long bones*. J Biomech, 2007. **40**(13): p. 2982-9.
56. Bayraktar, H.H., et al., *Comparison of the elastic and yield properties of human femoral trabecular and cortical bone tissue*. J Biomech, 2004. **37**(1): p. 27-35.
57. Zhou, Z.R., V. Pellerin, and L. Vincent, *Fretting - Wear of aluminium and titanium alloys*, in *Titanium & aluminium*, P.A. Coulon, Editor. 1989, I.I.T.T. International. p. 145-153.

Chapter 3

Sensitivity of subject-specific FE modelling techniques to uncertainties on parameters

As described in the previous chapters, using the modelling techniques developed in the past few years [1, 2] it is possible to generate finite element models that take into account the morphology of the bone segment and the distribution of the bone tissue mechanical properties of a specific subject.

However, the data processing techniques used to extract this information from the CT data are frequently affected by non-negligible errors that propagate in an unknown way through the various steps of the model generation, affecting in an unpredictable way the accuracy of the model predictions.

The first source of geometric error and distortion are the resolution and the image quality of the dataset used that depend on the scan parameters setting as well as on the characteristics of the CT scanner.

The second one is the segmentation of the region of interest. Whatever the segmentation algorithm chosen, an uncertainty on the boundary definition is always present. In the majority of cases data segmentation is carried out using a threshold-based algorithm. The result of a threshold-based segmentation, however, may vary strongly, depending on the threshold chosen [3, 4]. This geometric error then propagates through the various passages of data elaboration up to the mesh generation process.

In many studies the density information provided by the CT dataset is used to derive an inhomogeneous distribution of the bone tissues mechanical properties. This procedure involves two steps. At first the CT data are calibrated to correlate the Hounsfield Unit values to the apparent or to the ash density of the bone tissue. This step is sometimes performed using a calibration phantom [5-9], or assuming conventional values derived from literature for selected regions [10]. In both cases the obtained density values cannot be considered to be error-free. Then the density of the bone tissue is related to its Young's modulus, or to its strength, using empirical equations based on experimental measurements. The coefficients of these equations are affected by an uncertainty due to the significant scattering of these experimental measurements [11-14].

The uncertainties unavoidably related to the various steps of the model generation surely affect the accuracy of its predictions while a direct validation of models is not always feasible or convenient. The technique for the generation of finite element models of long bones was originally developed for the structural analysis of the femur on living subjects. As non-invasive techniques for the *in-vivo* measurements of the bone strains are not yet available, a direct validation of the model is not feasible in this case. Different is the case presented in this Ph.D. thesis as it is of interest the biomechanical behaviour of hip resurfacing devices in the entire range of operative conditions the implant might face over a population of interest. Hence several models are needed to span the variability of the human anatomy for which the long and demanding process for the model validation (see chapter 2) is not practically possible for all models generated.

The assessment of the models' accuracy should then be carried out into two separate steps: at first the intrinsic accuracy of the developed methods should be verified against experimental results of *in-vitro* tests (chapter 2), then a sensitivity analysis should follow to understand what is the effects of the uncertainties on the prediction of the model.

Aim of the present study was to provide a reliable statistical assessment of the effects that the uncertainties in geometric modelling and material properties assignment have on the prediction of a subject-specific finite element model derived from Computed Tomography data. The study has been carried out on three different femurs spanning a large range of sizes and of patient ages.

3.1 Finite-Element modelling of bones from CT data: sensitivity to geometry and material uncertainties²

The finite-element method is increasingly used to analyze the mechanical behaviour of bone segments. Using the modelling techniques developed in the past few years it is now possible to generate finite-element models that take into account the morphology of the bone segment and the distribution of the bone tissue mechanical properties of the specific subject. Whatever the methods adopted, these models derive the necessary information to build the bone model from medical imaging data. Computed tomography (CT) represents, at present, the method of choice for the generation of these subject-specific finite-element models, since from CT data it is possible to define the geometry and the local tissue properties of the bone segment to be modelled. However, the data processing techniques used to extract this information from the CT data may frequently be affected by non-negligible errors that propagate in an unknown way through the various steps of the model generation, affecting in an unpredictable way the accuracy of the model predictions.

The first source of geometric error and distortion is the resolution of the dataset that depends on the scan parameters setting. The second one is related to the segmentation process of the region of interest. Several segmentation algorithms have been proposed, with various level of

² F. Taddei, S. Martelli, B. Reggiani, L. Cristofolini, and M. Viceconti. "Finite-Element modelling of bones from CT data: sensitivity to geometry and material uncertainties". *IEEE Transaction Biomed. Eng.*, 53(11), 2006, p: 2194-2199

automation, starting from complete manual contours extraction, to complex fully automatic algorithms. Whatever the algorithm chosen, an uncertainty on the boundary definition is always present. In the majority of cases data segmentation is carried out using a threshold-based algorithm. The result of a threshold-based segmentation, however, may vary strongly, depending on the threshold chosen [3, 4]. This geometric error then propagates through the various steps of data treatment up to the mesh generation process.

In many studies the density information provided by the CT dataset is used to derive an inhomogeneous, although locally isotropic, distribution of the bone tissues mechanical properties. This procedure involves two steps. At first the CT data are calibrated to correlate the Hounsfield units to the apparent or to the ash density of the bone tissue. This step is sometimes performed using a calibration phantom [5-9], or assuming conventional values derived from literature for selected regions [10]. In both cases the obtained density values cannot be assumed to be error-free. Then the density of the bone tissue is related to its Young's modulus, or to its strength, using empirical equations based on experimental measurements. The coefficients of these equations are affected by an uncertainty due to the significant scattering of these experimental measurements [11-14].

The uncertainties that are unavoidably related to the various steps of the model's generation surely affect the accuracy of its predictions. Unfortunately these subject-specific models cannot be directly validated, since it is not possible, at present, to non-invasively measure stress or strain levels in vivo. The assessment of the model accuracy should then be carried out into two separate steps: at first the intrinsic accuracy of the developed methods should be verified against experimental results of in vitro tests, and then a sensitivity analysis should follow to understand what is the effect of the uncertainties of the in vivo measurements on the prediction of the model. While the in vitro validation of the finite-element models of bone segments has been performed by several authors [15-18], is still unknown what influence the errors associated to the measures taken in vivo may have on the results produced by a subject-specific finite-element model.

The aim of this paper is to provide a reliable statistical assessment of the effects that the uncertainties in geometric modelling and material properties assignment have on the predictions of a subject-specific finite-element model derived from CT data.

<i>Subject</i>	<i>KvP</i>	<i>Tube Current (mA)</i>	<i>Pixel dimensions (mm)</i>
1	120	200	0.74
2	120	180	0.55
3	120	200	0.70

Table 1 - the CT scanner settings for the three exams

3.1.1 Materials and methods

Three CT datasets of human femurs, taken in vivo for clinical purposes, were used for this paper. The three subjects ranged from a child to a pathological adult to explore different situations. Subject 1 was a 40-year-old woman, affected by a hip arthritis due to a mono-lateral

developmental dysplastic hip, and presented no visible pathology at the contralateral femur chosen for this paper. Subject 2 was a 7-year-old child operated for a Ewing's sarcoma at one femur, and similarly to Subject 1 presented no visible pathology at the contralateral selected femur. Subject 3, was a 42-year-old woman affected by a severe hip arthritis due to a developmental dysplastic hip at the femur considered for the study. A scanning protocol specifically designed to optimise the three-dimensional (3-D) reconstruction and to maintain the same radiation level of conventional protocols [19], was used in all cases. The CT exams were taken in the helical mode; the slice thickness was set to 3 mm in the epiphyseal regions and 5-mm in the diaphyseal regions with a pitch of 1.5. The CT dataset were reconstructed with spacing of 2 mm in the epiphyseal regions and of 4mm in diaphyseal ones. The scanner (mod. HiSpeed, General Electric Co. Fairfield, CT) settings for the three exams are reported in Table 1.

The finite-element models of the three femurs were generated from the CT datasets using a previously validated procedure [1, 18, 20] that will be described in the following for clarity. The three femurs models were tested under two simplified loading conditions: compression-bending load and torque load.

A statistical sensitivity analysis was performed considering as random input variab

les the geometry, the density and the mechanical properties of the bone tissue (the Young's modulus, E , and the compressive strength, S). These random input variables were statistically characterized, in terms of their distributions, analysing the uncertainties related to the most important steps of the model generation procedure. The most used biomechanical FEM indicators, relevant for the orthopaedic field of application, were considered as statistical output variables and analyzed. A Monte Carlo Simulation was performed and the sensitivity analysis was based on the correlation coefficient between all random input variables and all output variables. The input variables that showed a significant correlation with the output ones were ranked in a descending order of importance. The details of the study are reported in the following paragraphs.

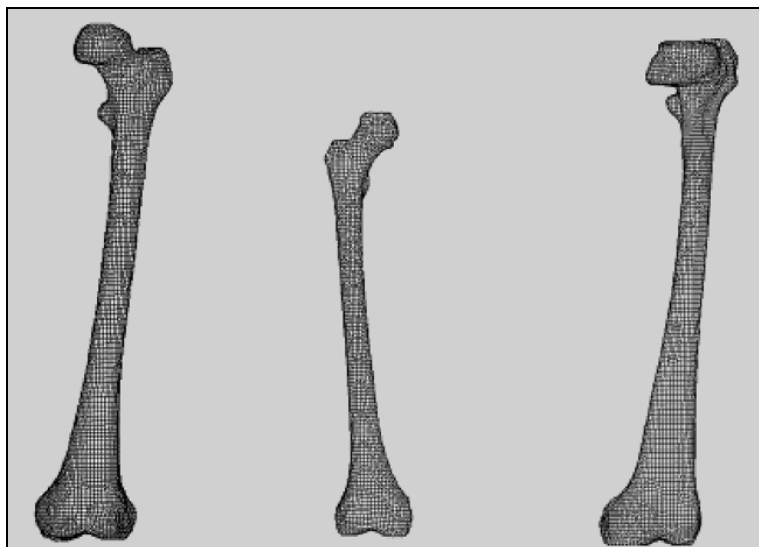


Figure 1 - The three femur models. From left to right: Subject 1 (102255 DOF), Subject 2 (66723 DOF) and Subject 3 (128826 DOF).

3.1.1.1 Finite-Element models generation

The adopted procedure can be summarized in three steps: extraction of the 3-D bone surface, generation of the finite-element mesh and mapping of the inhomogeneous bone tissue mechanical properties onto the mesh.

For the first step, the external contours of the bone were extracted from the CT slices with a semi-automatic software, based on a border-tracing algorithm [3]. The contours were then interpolated to obtain the external surface of the femurs using a Delaunay triangulation algorithm [21]. Then, the solids defined by the resulting tiled external surfaces were meshed using the HEXAR (Cray Research, Seattle, WA) automatic mesh generator. This software implements a grid-based algorithm [22] that generates 8-noded iso-parametric linear elements.

A convergence test on eight meshes with increasing refinement levels was performed. The meshes used for the simulation are represented in Fig. 1 with the relative number of degrees of freedom (DOF).

A different Hounsfield Unit (HU) value was computed for each element of the mesh performing a numerical integration over the element's volume of the HU field, as derived from the CT dataset. This was done using a modified version of the in-house developed software BONEMAT_V2 (freely available at <http://www.cineca.it/hosted/LTM-IOR/back2net/SW/index.html>) [22].

3.1.1.2 The loads

The human femur, in physiological conditions is subjected to an instantaneous loading pattern that can be quite complex, due to the many muscles that insert in the femur and develop contractile forces. This loading pattern may change considerably with time and with the type of movement being performed. However, the overall structural effect of these loading conditions can always be seen as the superposition of an off-axis compression and torque moment around the long axis of the femur.

Two simplified loading conditions were used that will be referred to as Compression and Torsion. The first one consisted of a single force directed along the femur longitudinal axis applied on the femoral head, whose direction passed through the femoral head centre. The magnitude of the load was calculated imposing that a unitary bending moment (1 N m) should be generated at mid-diaphysis. The second one consisted of force couple, applied to the trochanteric region, lying on a tomographic plane, that generate a unitary torque (1 N m) (Fig. 2).

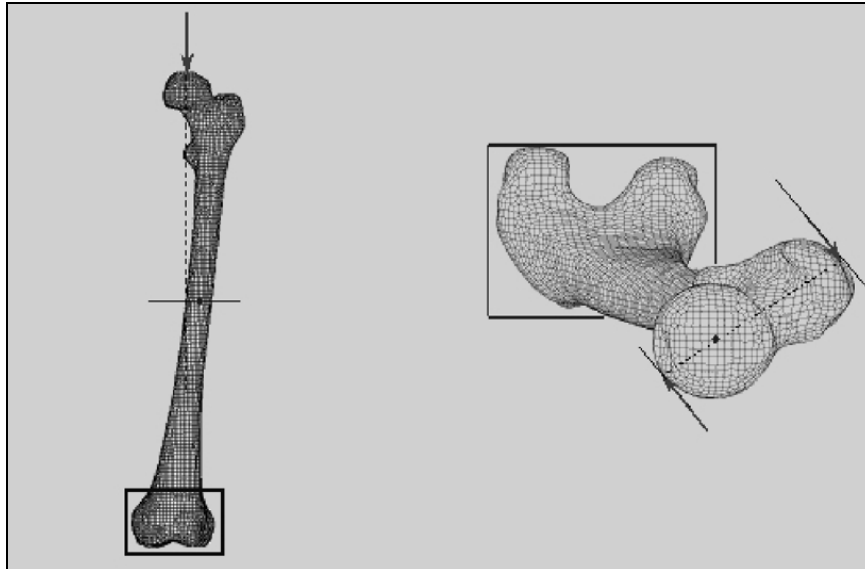


Figure 2 - The two loading conditions.

3.1.1.3 Estimation of the random input variables

The uncertainties relative to the three basic steps of the model's generation procedure (geometry definition, calibration of the CT dataset, and bone material properties assignment) were estimated as follows.

Geometry definition

The average repeatability error in the extraction, with the border-tracing algorithm, of a femoral geometry from a CT dataset taken in vivo was estimated in a previous study [3]. The average error was found to be higher in the trochanteric region, where it was almost of six pixels, while it was lower than two pixels in the whole diaphyseal region. This difference between the epiphyseal and diaphyseal regions can be explained with the presence, in the former, of higher partial volume effects. The maximum error occurred in the epiphyseal region and it was almost of 13 pixels.

The different average error in the segmentation of the various femoral regions was reproduced in the statistical analysis adopting, for each model, a uniform random scaling coefficient in the direction of the tomographic planes.

In fact, due to the higher linear dimensions of the trochanteric region in the tomographic planes, with respect to the diaphyseal region, a uniform scaling ratio on the whole femoral model results in a higher deviation, from the nominal model, in the former region than in the latter (Fig. 3). It was assumed that the scaling coefficient followed a Normal distribution with a unity average value, corresponding to the nominal model. The standard deviation (SD) of the scaling coefficient was calculated, for each model, imposing that the maximum error in the trochanteric region, identified with six SD, was 13 pixels. The resulting distributions are reported in Table II.

CT dataset calibration and material properties assignment

A linear relationship between the HU numbers and the bone ash density was assumed [11]. The CT dataset was calibrated using a calibration phantom with three bone-equivalents (solution of hydroxyapatite) insertions of different densities embedded in a water-equivalent resin-based plastic (The European Spine Phantom [23]).

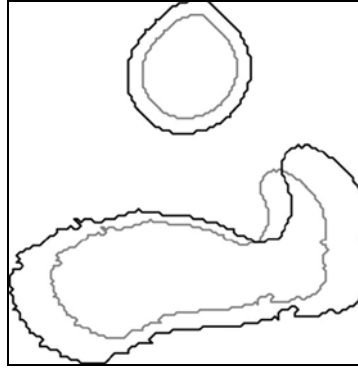


Figure 3 - The uniform scaling effect, intentionally enlarged to make it clearly visible, applied to the contours extracted in the diaphyseal region (top) and in the trochanteric region (bottom).

Scaling coefficients		
Subject	Mean	Std
1	1	0.019
2	1	0.0176
3	1	0.016

Table 2 - the scaling coefficients

The CT slices comprising the three bone equivalent insertions were analyzed with the OSIRIS software [24]. The certified nominal mineral density was assigned to each insertion and a linear regression was performed to identify the linear relationship between the HU numbers and the mineral density rash. The standard errors of the intercept values and slope coefficient were calculated using StatView (v. 5.0.1, SAS Institute, Cary, NC) and a Normal distribution assumed for both coefficients. The values for the calibration equations are reported in Table III.

An average HU number was assigned to each finite element of the meshes using the Bonemat_V2 software [2]. The Young's modulus and the compressive strength of each element of the mesh were computed using the following power relationship proposed by Keller [12]:

$$E = c \cdot \rho^d \quad (c = 10.5, d = 2.57 \pm 0.02, R^2 = 0.965) \quad (1)$$

$$S = e \cdot \rho^f \quad (e = 117, f = 1.93 \pm 0.02, R^2 = 0.969) \quad (2)$$

that yields E expressed in GPa and S in MPa if the density is expressed in gr/cm^3 . The exponents of the (1) and (2) were assumed to follow a Normal distribution.

Calibration equation: $\rho_{ash} = \alpha * HU + \beta$				
	α_{mean}	α_{SDV}	β_{mean}	β_{SDV}
KVP=120, Current=200	0.656	0.001	-656.070	1.404
KVP=120, Current=180	0.644	0.001	-640.432	1.463

Table 3 - The calibration equations used for the simulations

3.1.1.4 Identification of the output variables

The most used biomechanical indicators were chosen as control output variables and were as follows.

- Max displacement of the femoral head centre (Displ HC).
- Max tensile principal stress .
- Max compressive principal stress .
- Max Von Mises stress .
- Max tensile principal strain .
- Max compressive principal strain.
- Max Von Mises strain.
- Max Strain Energy Density (Max SED).
- Min Safety Factor (Min SF).

The Safety Factor SF was defined as:

$$SF = \sigma_{ultimate} / \sigma_{EQV}; \quad (2)$$

and was calculated for each element of the model. The ultimate strength of the bone tissue was calculated taking into account the different behaviour of bone to tension or compression. Following a method already proposed in the literature [10] we determined the primary mode of stress in each element of the model, comparing the absolute value of the maximum (tensile) and minimum (compressive) principal stress for each element. For elements where the tensile principal stress was the largest, ultimate tensile strengths were assigned by multiplying the ultimate compressive strength by 0.8.

In order to avoid local effects, the comparisons were limited to a control region defined excluding the portions of mesh too close to the regions where the boundaries conditions were applied.

The statistical distribution of the output variables was determined using a Kolmogorov-Smirnov test. The linear Pearson's coefficient was used to perform the sensitivity analysis to evaluate the correlation between the output and input variables.

3.1.1.5 The probabilistic design

For each model a Latin Hypercube Sampling technique (LHS), which is a more efficient form of a Monte Carlo Simulation method, was applied using ANSYS v7.0 (ANSYS Inc., Canonsburg, PA). The convergence of the analysis was assessed checking that the mean value and the standard deviation of all output variables reached an asymptotic plateau with respect to the number of iterations. Due to the low number of input random parameters involved in the simulation and to the linearity of the problem, 200 runs were sufficient in all cases to reach convergence. The variation between two subsequent values was less than 0.5% for the standard deviation and 0.05% for the mean value of all variables. A typical behaviour of the mean value is plotted in Fig. 4. In synthesis the random input variables were as follows:

- a) Scaling factor S describing the uncertainties associated with the segmentation procedure.

- b) Intercept value and slope coefficients of the calibration equation (calA and calB).
- c) Exponent coefficient of the equation for the definition of the Young's modulus and compressive strength of the bone tissue (ExpE and ExpS) that describe the uncertainties related with material properties assignment.

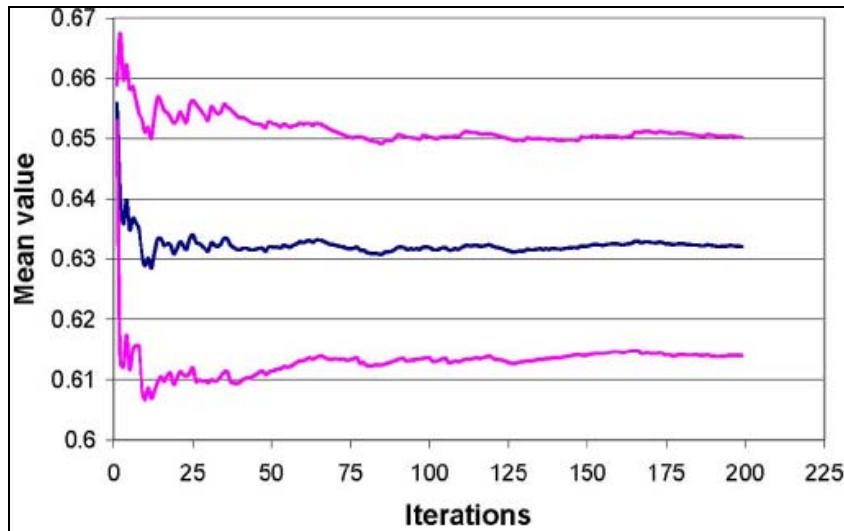


Figure 4 - Mean value of Max $\sigma 1$ (dark), with the confidence interval, in the control region versus the number of iterations for Subject 3.

3.1.2 Results

All output variables did follow a Normal distribution (Kolmogorov-Smirnov Test, $\alpha < 0.05$).

The scaling factor was always significantly correlated (linear Pearson's coefficient $\alpha < 0.05$) with all output variables and was always the dominant variable for the stresses. However, no input variables have a dominant effect on the output in all cases. The presence of a significant correlation between a certain output variable and the input variables depends on the load case and is different between subjects (Table 4).

The coefficients of variation (percentage) are reported in Table 5 for all output variables. For the Torsion load case the displacement of the femoral head centre was close to null (min = 0.0002, max = 0.003) and the variation coefficient becomes not significant.

The maximum tensile principal stress (Max $\sigma 1$), for Subject 1 for Compression load case, is the output indicator, among those whose variability can be explained in terms of one single input variable, that shows the highest coefficient of variation. The linear regression between Max $\sigma 1$ in this case and the input variable scaling was calculated. The regression equation was

$$Y = 3.013 - 2.037 * X, R^2 = 0.994 \quad (3)$$

This means that an error of 13 pixels in the segmentation of the epiphyseal region, (which represent the maximum error reported in the literature [3]), corresponds to a variation in the predicted maximum tensile principle stress of 10%.

Subject 1											
Load 1						Load 2					
	scaling	A	B	D	F		scaling	A	B	D	F
Displ HC	0.850	0.257	0.379	-0.303	-	Displ HC	0.244	0.50	0.536	-0.681	-
Max σ_1	-0.997	-	-	-	-0.148	Max σ_1	-0.942	-	-0.159	0.289	-
Max σ_3	0.963	-	0.152	-0.191	-	Max σ_3	0.970	-	-	-0.192	-
Max σ_{EQV}	-0.963	-	-0.153	0.188	-	Max σ_{EQV}	-0.997	0.170	-	-	-
Max ϵ_1	-0.366	-0.630	-0.561	0.445	-	Max ϵ_1	0.523	0.362	0.448	-0.638	-
Max ϵ_3	0.797	0.267	0.337	-0.430	-	Max ϵ_3	-0.404	-0.522	-0.544	0.538	-
Max ϵ_{EQV}	-0.339	-0.621	-0.559	0.473	-	Max ϵ_{EQV}	-0.421	-0.523	-0.544	0.516	-
Max SED	-0.931	-0.154	-0.265	0.217	-	Max SED	-0.881	-	-0.263	0.369	-
Min SF	0.699	0.319	0.396	-0.180	-0.399	Min SF	0.539	0.181	0.202	-	-0.715
Subject 2											
Load 1						Load 2					
	scaling	A	B	D	F		scaling	A	B	D	F
Displ HC	0.875	0.286	0.221	-0.351	-	Displ HC	0.55	0.405	0.372	-0.662	-
Max σ_1	-0.994	-	-	-	-	Max σ_1	-0.996	-	-0.151	-	-
Max σ_3	0.996	-	-	-	-	Max σ_3	0.998	-	0.148	-	-
Max σ_{EQV}	-0.997	-	-	-	-	Max σ_{EQV}	-0.996	-	-0.15	-	-
Max ϵ_1	-0.704	-0.385	-0.272	0.593	-	Max ϵ_1	-0.750	-0.361	-0.431	0.442	-
Max ϵ_3	0.736	0.364	0.260	-0.566	-	Max ϵ_3	0.639	0.422	0.462	-0.530	-
Max ϵ_{EQV}	-0.70	-0.388	-0.274	0.596	-	Max ϵ_{EQV}	-0.719	-0.384	-0.439	0.467	-
Max SED	-0.919	-0.226	-	0.325	-	Max SED	-0.922	-0.215	-0.323	0.220	-
Min SF	0.795	0.268	0.193	-0.144	-0.422	Min SF	0.802	0.213	0.354	-	-0.504
Subject 3											
Load 1						Load 2					
	scaling	A	B	D	F		scaling	A	B	D	F
Displ HC	0.827	0.283	0.281	-0.297	-	Displ HC	-0.196	0.532	0.413	-0.735	-
Max σ_1	-0.999	-	-	-	-	Max σ_1	0.864	-0.164	-0.303	0.377	-
Max σ_3	0.974	-	-	-	-	Max σ_3	-0.991	-	-0.175	-	-
Max σ_{EQV}	-0.975	-	-	-	-	Max σ_{EQV}	0.984	-	0.183	-	-
Max ϵ_1	-0.228	-0.605	-0.456	0.611	-	Max ϵ_1	-0.512	-0.447	-0.501	0.559	-
Max ϵ_3	0.491	0.461	0.362	-0.60	-	Max ϵ_3	0.652	0.294	0.445	-0.561	-
Max ϵ_{EQV}	-0.502	-0.457	-0.359	0.594	-	Max ϵ_{EQV}	-0.559	-0.414	-0.489	0.549	-
Max SED	-0.897	-0.197	-0.166	0.253	-	Max SED	-0.843	-0.193	-0.373	0.367	-
Min SF	0.862	0.241	0.213	-	-0.358	Min SF	0.729	0.313	0.355	-	-0.498

Table 4 - The correlation matrices between input variables (S , $calA$, $calB$, $ExpE$, $ExpS$) and output variables (rows) for the three subjects and two load cases. The correlation coefficient between two variables, when omitted, was not significant ($\alpha = 0.05$)

3.1.3 Discussion

Aim of the present study was to estimate the sensitivity of the results of a subject-specific finite-element model to the errors in the geometric definition and in the material properties assignment of the model. The study focused on the finite-element model of a human femur generated starting from CT data. Three CT datasets taken for clinical purposes were used to build the models of three different femurs that ranged from a child femur to a pathological adult one to explore different situations. A statistical finite-element analysis was conducted to establish the sensitivity of the most common biomechanical indicators to the known errors associated with the generation of the finite-element models.

	<i>Subject 1</i>		<i>Subject 2</i>		<i>Subject 3</i>	
	<i>Load 1</i>	<i>Load 2</i>	<i>Load 1</i>	<i>Load 2</i>	<i>Load 1</i>	<i>Load 2</i>
<i>Displ HC</i>	3.7	n.s.	3.5	n.s.	3.3	n.s.
<i>Max σ1</i>	4.0	3.0	3.5	3.0	3.4	2.9
<i>Min σ3</i>	3.2	3.5	3.6	3.2	2.7	3.0
<i>Max σ_{EQV}</i>	3.2	3.8	3.5	3.4	2.8	3.2
<i>Max ϵ1</i>	8.3	7.1	4.6	5.8	5.4	6.5
<i>Min ϵ3</i>	6.9	6.5	4.3	6.4	4.2	4.6
<i>Max ϵ_{EQV}</i>	7.1	7.4	4.6	6.5	4.3	6.2
<i>Max SED</i>	6.3	8.7	6.8	6.9	6.5	7.0
<i>Min SF</i>	4.2	6.1	3.9	4.8	3.5	4.2

Table 5 - The coefficients of variation (%) for all the output variables: the maximum value is highlighted

The results show that it is not possible to define a priori the influence of the errors related to the geometry definition process and to the material assignment process on the finite-element analysis results. Only very general patterns could be found. The errors in the geometric representation of the bone are always the dominant variables for the stresses, as was expected. However, for all the variables, the results seemed to be dependent on the loading condition and to vary from subject to subject. This suggests that whenever it is necessary to know the effect of an error in the generation process of a finite-element model on a specific output parameter, a statistical approach is mandatory.

The most interesting result is, however, that using the proposed method to build a finite-element model of a femur from a CT dataset, of a quality usually achievable in the clinical practice, the variation coefficients of the output variables never exceed 9%. This uncertainty on the results seems admissible since these models are commonly used in the orthopaedics research to discriminate between conditions involving much larger differences. Furthermore, the uncertainties related to the boundary conditions definition in the generation of a subject-specific finite- element model of a bone segment are definitely far higher.

The major limit of the presented work is actually the fact that the uncertainties in the definition of the boundary conditions were not considered. The prediction of the stresses induced in a human bone by a physiological activity can be seen as two separate problems: the prediction of the structural behaviour of the bone under any force system, and the actual force system induced by that activity. To establish the global sensitivity of these models, we need to investigate both aspects. While the errors associated to the generation of a structural model of a human bone from CT data have been extensively defined, those related to the prediction of the muscle and joint forces during a given activity have been only partially investigated [5]. Because of this we decided to focus this study on the first part of the problem. However, it is possible that the variation due to boundary conditions uncertainties might be much bigger than those due to geometry and materials' definition. Future studies will have to address this aspect.

The inclusion of the seven-years old child bone among the cases here analyzed may also be questionable. The empirical laws that correlate CT data with the mechanical properties of human bones were obtained for mature tissues. However, the correlation between ash density and Young's modulus of bone used in this study seems very general, as it was found valid for the

bone tissue of different species [25] and at very different stages of maturity (5 months to adult bone of 20 years in the horse) [11].

A direct comparison of the results obtained against the literature is not possible, since to the authors' knowledge, no work has been published specifically addressing this subject. However, the importance of a statistical approach in managing finite element simulation of biological structures has been stressed recently [26]. Some authors have recently adopted the probabilistic finite-element method to investigate the effect of the intra-subject variability in the definition of the bone material properties and boundary conditions onto the results of the finite-element analysis [27-29], especially in the field of prosthetic implants, confirming that the modelling techniques and the computational resources are now available to bring this powerful investigation method into biomechanics.

3.2 Conclusion

Aim of the present study was to provide a reliable statistical assessment of the effects that the uncertainties in geometric modelling and material properties assignment have on the prediction of a subject-specific finite element model derived from Computed Tomography data.

The uncertainty was found up to 4% on stresses and up to 8.3% on the strain predictions. This values are slightly lower than the intrinsic accuracy of the models found in the previous chapter confirming the validity of the adopted techniques for the generation of finite element models of the human femur.

Hence the methodology can be a valid support for the biomechanical analysis of hip resurfacing devices. The next chapter describe the identification of the protocol of analysis by means of finite element models.

REFERENCES

1. Viceconti, M., et al., *A new method for the automatic mesh generation of bone segments from CT data*. Journal of Medical Engineering and Technology, 1999. **23**(2): p. 77-81.
2. Taddei, F., A. Pancanti, and M. Viceconti, *An improved method for the automatic mapping of computed tomography numbers onto finite element models*. Medical engineering & physics, 2004. **26**(1): p. 61-9.
3. Testi, D., et al., *Border-tracing algorithm implementation for the femoral geometry reconstruction*. Computer Methods and Programs in Biomedicine, 2001. **65**(3): p. 175-82.
4. Schneider, J., R. Decker, and W. Kalender, *Accuracy in medical modelling*. Phidias Newsletter, 2002. **9**: p. 5-14.
5. Silva, M.J., T.M. Keaveny, and W.C. Hayes, *Computed tomography-based finite element analysis predicts failure loads and fracture patterns for vertebral sections*. Journal of Orthopaedic Research, 1998. **16**(3): p. 300-8.
6. Oden, Z.M., D.M. Selvitelli, and M.L. Bouxsein, *Effect of local density changes on the failure load of the proximal femur*. Journal of Orthopaedic Research, 1999. **17**(5): p. 661-7.
7. Keyak, J.H., et al., *Prediction of femoral fracture load using automated finite element modeling*. Journal of Biomechanics, 1998. **31**(2): p. 125-33.
8. Cody, D.D., et al., *Femoral structure and stiffness in patients with femoral neck fracture*. Journal of Orthopaedic Research, 2000. **18**(3): p. 443-8.
9. Cattaneo, P.M., M. Dalstra, and L.H. Frich, *A three-dimensional finite element model from computed tomography data: a semi-automated method*. Proceedings of the Institution of Mechanical Engineers. Part H, Journal of engineering in medicine., 2001. **215**(2): p. 203-13.
10. Ford, C.M., T.M. Keaveny, and W.C. Hayes, *The effect of impact direction on the structural capacity of the proximal femur during falls*. Journal of bone and mineral research, 1996. **11**(3): p. 377-83.
11. Les, C.M., et al., *Estimation of material properties in the equine metacarpus with use of quantitative computed tomography*. Journal of Orthopaedic Research, 1994. **12**(6): p. 822-33.
12. Keller, T.S., *Predicting the compressive mechanical behavior of bone*. Journal of Biomechanics, 1994. **27**(9): p. 1159-1168.
13. Ciarelli, M.J., et al., *Evaluation of orthogonal mechanical properties and density of human trabecular bone from the major metaphyseal regions with materials testing and computed tomography*. Journal of Orthopaedic Research, 1991. **9**(5): p. 674-82.
14. Carter, D.R. and W.C. Hayes, *The compressive behavior of bone as a two-phase porous structure*. The Journal of bone and joint surgery. American volume., 1977. **59**(7): p. 954-62.
15. Dalstra, M., R. Huiskes, and L. van Erning, *Development and validation of a three-dimensional finite element model of the pelvic bone*. Journal of biomechanical engineering, 1995. **117**(3): p. 272-8.
16. Gupta, S., et al., *Development and experimental validation of a three-dimensional finite element model of the human scapula*. Proceedings of the Institution of Mechanical Engineers. Part H, Journal of engineering in medicine, 2004. **218**(2): p. 127-42.
17. Keyak, J.H., et al., *Validation of an automated method of three-dimensional finite element modelling of bone*. Journal of biomedical engineering, 1993. **15**(6): p. 505-9.

18. Viceconti, M., et al., *A comparative study on different methods of automatic mesh generation of human femurs*. Medical engineering & physics, 1998. **20**(1): p. 1-10.
19. Lattanzi, R., et al., *Specialised CT scan protocols for 3-D pre-operative planning of total hip replacement*. Medical engineering & physics, 2004. **26**(3): p. 237-45.
20. Zannoni, C., R. Mantovani, and M. Viceconti, *Material properties assignment to finite element models of bone structures: a new method*. Medical engineering & physics, 1998. **20**(10): p. 735-40.
21. Boissonnat, J.-D. and B. Geiger, *Three dimensional reconstruction of complex shapes based on the Delaunay triangulation*, in *Biomedical Image Processing and Biomedical Visualisation*, R.S. Acharya and D.B. Goldgof, Editors. 1993, SPIE. p. 964-975.
22. Taghavi, R., *Automatic, parallel and fault tolerant mesh generation from CAD*. Engineering with Computers, 1996. **12**: p. 178-185.
23. Kalender, W.A., *A phantom for standardization and quality control in spinal bone mineral measurements by QCT and DXA: Design considerations and specifications*. Medical Physics, 1992. **19**(3): p. 583-586.
24. Ligier, Y., et al., *Osiris: a medical image-manipulation system*. M.D. computing : computers in medical practice, 1994. **11**(4): p. 212-8.
25. Currey, J.D., *The effect of porosity and mineral content on the Young's modulus of elasticity of compact bone*. Journal of Biomechanics, 1988. **21**(2): p. 131-9.
26. Dar, F.H., J.R. Meakin, and R.M. Aspden, *Statistical methods in finite element analysis*. Journal of Biomechanics, 2002. **35**(9): p. 1155-61.
27. Perez, M.A., et al. *Probabilistic damage model for life prediction of cemented total hip arthroplasty*. in *International Congress on Computational Bioengineering*. 2003. Zaragoza, Spain.
28. Nicoletta, D.P., B.H. Thacker, and H. Katoozian, *Probabilistic risk analysis of a cemented hip implant*. Journal of Mathematical Modeling and Scientific Computing, 2001. **13**(1-2): p. 98-108.
29. Bah, M.T. and M. Browne. *Probabilistic analysis of a cemented hip implant*. in *International Congress on Computational Bioengineering*. 2003. Zaragoza, Spain.

Chapter 4

Identification of the protocol for the analysis of the risk of biomechanical failure of resurfaced femurs

In the Chapter 1 are described the scenarios that commonly constitute an indication for revision of resurfaced hip and biomechanical conditions that potentially promote failure. It has been described how the biomechanical behaviour of the prosthesis might stimulate many different processes that potentially produce a loss of functionality and the subsequent revision of the implant. Hence, one might define “failure mode” as the physical process (or processes) that take place (or combine their effect) to produce failure.

Other branches of engineering are pioneer in the systematic analysis of failure of mechanical systems. The experience accumulated over years lead to the conclusion that success in designing competitive products while averting premature mechanical failure can be consistently achieved only by recognizing and evaluating all potential failure modes [1].

Since the final aim of the present thesis is to develop musculoskeletal models for the design and the pre-clinical validation of hip resurfacing device, it is essential to identify an adequate protocol to discriminate adverse biomechanical conditions after surgery.

The scope pursued in this chapter is to identify a possible list of analysis, for all relevant failure modes, to be conducted which would constitute the protocol for the systematic analysis of failure and the consequent definition of a quality index of the implant.

The formal analysis of all failure modes, described in the first paragraph, highlighted that fractures of the femoral neck after implantation are a relevant scenario of failure. Thus, assessing the influence of the prosthesis implantation on the strength of the hosting femoral neck is a key action for a predictive protocol. Unfortunately this met the limit of finite element models described in chapter 2 and 3, as they are validated only in the elastic field. The possibility to accurately model the ultimate load to failure is, at this stage, not clear [2] so it was not considered as a possible option.

This lead to a combined protocol composed by numerical simulations plus the experimental assessment of the ultimate load to failure of implanted femurs by destructive tests on cadaver specimens. The experimental work, entirely carried out by the experimental group of LTM, is briefly reported in this thesis so as to strengthen the validity of conclusions.

What was afterward not clear was which experimental set-up should be adopted in order to produce fractures of the femoral neck, in a coherent way with spontaneous fractures observed by clinicians.

This problem was numerically approached and successfully solved. The description of the numerical part is reported in the second paragraph of this chapter while the complete description of the work, which contains also the description of destructive tests, is reported in Appendix B.

4.1 The preclinical validation of hip resurfacing prostheses²

In spite of the clinical success of total hip replacement (or probably because of it), the medical industry is trying to innovate the design of total hip replacements (THR) more radically than in the past. Sometime we face situations similar to those observed in the late '60s, when everything was allowed and possible. However, today the environment is totally different: medical devices are heavily regulated both in USA and in Europe, and in Europe THR will be moved to risk class 3 this year. Typical success rate for THR is around 90% at 10-15 years [3], and any outcome significantly lower than this is considered not acceptable. On the other hand, the clinical assessment of the surgery outcome is still rudimental at least to say. While many innovative designs claim to radically improve the functional outcome of THR, no hard evidences can be produced with the assessment methods currently available; thus, revision is the only reliable, although very gross, end point for assessment.

The physical/biological reality is infinitely complex, and thus cannot be studied directly. We need to create a representation of the reality, which retains only those features that we believe are more relevant to explain a specific manifestation of the reality, the one under investigation. We can build this representation using an inductive approach or a deductive approach; in the latter we create a special type of representation called model. A model can be experimental or numerical; it can be based on *ex vivo* materials, animal preparations, or *in vivo* experiments. The only thing in common is that we should be able in all cases to control the variables of the system under investigation. In this sense, a clinical trial is not a model, while an experiment where during tenotomy surgery with measure the muscle force when we electrically stimulate the muscle [4] is a model.

A fundamental limitation of any model is that it is designed and validated to predict with given accuracy a certain manifestation of the reality. The fact that your model is "realistic" does not change this fact; the only experiment that can reproduce all manifestations is that based on the observation of the reality in its entirety; unfortunately, on such experiment we lack control and thus no deductive reasoning can be used.

One implication of these general considerations, relevant here, is that no pre-clinical validation model (experimental or numerical) can predict a manifestation of the reality that we do not know already. In other words, pre-clinical validation can help us to make sure we do not do again the

² S. Martelli, F. Taddei, L. Cristofolini, and M. Viceconti, "Preclinical validation of epiphyseal prostheses", Proceeding of the conference "Engineers and Surgeons: Joined at the Hip", IMechE, April 19th-21st, 2007, London, UK

same mistakes observed in the past, but cannot prevent us to make totally new mistakes; this is why pre-clinical validation will never replace entirely the clinical trials.

This is why radically innovative prostheses pose a major challenge to pre-clinical validation; highly innovative designs can produce failure scenarios that we never imagined in advance, and thus that we couldn't capture during the pre-clinical validation. A related problem is when new designs reproduce failure scenarios that were not observed in the clinical practice since many years. There are failure scenarios described in the past, but considered today unusual, that are not thoroughly investigated. Of course in an ideal world where the budgets and the time are unlimited, one should test all known failure scenarios for each new design. But this is unrealistic.

The aim of this paragraph is to describe a process that we have developed over the years, that combines a formal analysis, numerical modelling and in vitro experiments to provide the best possible validation for a given budget/time frames.

4.1.1 A general protocol for pre-clinical validation

4.1.1.1 Know your enemy

Any new design entering the pre-clinical validation process should be initially subjected to a consensus process, involving all clinicians and all marketing experts working on this design, aimed to produce two lists: the first is the list of commercial claims, e.g. the aspects of the new design that we expect would perform better than the competition. These claims can be of course limited to a certain indication (e.g. our stem gives better survivorship in young patients with necrosis of the femoral head). These aspects must be spelt out clearly before the validation process begins. The second list contains all possible failure scenarios that one could reasonably expect to face with such a device. This list is then processed by the product manager and translated into a full risk analysis, where for each failure scenario we estimate, on the basis of the available information, the probability that this adverse event occurs, and the severity of the outcome it would produce. In the meanwhile, the pre-clinical validation group should devise a protocol to assess the concrete probability that each failure scenario can occur, or the limit condition (of load, of number of cycles, etc.) below which the failure will deterministically not occur. This list should include a brief description of the protocols to be conducted, and a gross estimate of the cost and duration for each of them. The product manager would cross its risk analysis with this list, and decide which failure scenarios should be tested.

It is worth to note that this risk analysis is mandatory for the CE marking, but it is usually done only once the design is finalised, and the pre-clinical validation have been completed. On the contrary, we advocate that this work should be done at the very beginning of the development process, to be truly useful.

4.1.1.2 Detailed design of the validation protocols

In some cases, the experience makes possible to define without any further investigation the experimental protocol required to answer a certain question. In our lab we have a lot of experience with anatomical cementless stems; if we need to assess the inducible micro-movements (primary stability, associated to a failure scenario of aseptic loosening) in such devices, we already know where to place the sensors in order to make significant measurements. On the contrary, when an epiphyseal stem is involved, is much more difficult to imagine where are the zones of the largest bone-implant micromotion. Epiphyseal stems interact in complex ways with a highly anisotropic volume of cancellous bone; in addition, most designs rely on complex fixations where a part of the interface is cemented and a part is not. In these cases, guessing a location can be dangerous, and find it experimentally can be long and costly. In these cases we prefer to rely on a fully validated finite element model.

4.1.1.3 The role of numerical models in pre-clinical validation

There are many reasons why one would use a numerical model during a pre-clinical validation study: he does not have the facilities to test a failure scenario experimentally; he faces severe budget limitations that can be met only by a quick finite element (FE) model; he receives pressure from the clinical experts, that consider the numerical model more “realistic” and thus more reliable. Useless to say, all these are the wrong reasons to resort to a numerical model.

First of all, a numerical model is the incarnation of a hypothesis. Until it is not proven true, by comparing the predictions with the measurements made during controlled experiments, a numerical model is only an unverified hypothesis, e.g. an opinion. Thus, in a non-speculative exercise like pre-clinical validation, any numerical model should be fully validated. Different is the story when the numerical models are used in the design phase; here the risk that our model is wrong is balanced by the impossibility to make controlled experiments on every single draft design. A fully validated numerical model is by no means a shortcut; it is expensive, it requires the entire array of skills and facilities, and if left in the hand of inexperienced modellers might require a lot of time and effort. But once available, it can be an incredibly powerful instrument. If we look back at the example made before, once I have a fully validated model of the bone-implant interaction in my epiphyseal implant in can explore what are the loading directions that are most critical, and spot the locations where I have the peak micromotion.

Another advantage of working with validated models is that we do not fall in the temptation to bend the model to the technological limitations of our computer or of our software. A typical example is contact. In 90% of the cases the interaction between the stem and the bone or between the stem and the cement cannot be reliably modelled without including in the model a large-sliding frictional contact. If you assume the interfaces fully bonded you model remains linear, it solves very quickly, and the results frequently seem reasonable. It is only when you try to compare your predictions with controlled experiment results that you realise that gross errors are being committed. The addition of contact is difficult because the model becomes non-linear, its solution computationally demanding, and not all commercially available FE solvers ensure a

good convergence when large-sliding frictional contact is involved. Also the experience of the modeller needs to be much greater if a contact non-linearity is included in the model. Also the validation experiments need to be carefully designed. While the structural behaviour of an intact bone can be univocally described by a certain number of surface strain measurements induced by a controlled load, the contact interaction requires ad hoc validation experiments. In our experience, the validation of the FE model against the tangential sliding and/or the gap opening measured at accurately defined location while the bone-implant complex is loaded in a known way provide a good validation indication, much more reliable than indirect validation.

4.1.1.4 A possible list of protocols

If we consider a cemented epiphyseal stem, the clinical scenarios reported in the clinical literature are:

1. Aseptic loosening
 - a. Lack of primary stability
 - b. Production of fretting debris
 - c. Damage of cancellous bone
 - d. Adverse bone remodelling
2. Mechanical failure
 - a. Wear, corrosion, fretting
 - b. Femoral neck fracture
3. Subcapital dislocation
 - a. Biomechanical ischemia
 - b. Damage of cancellous bone
 - c. Adverse bone remodelling

A full contact model can be used to predict the bone-implant and cement-implant inducible micro-movements under a variety of loading conditions. Such model should be validated with measurements of tangential sliding and gap opening (detachment) at the bone-implant or at the cement-implant interfaces. The model validation should be conducted under multiple loading conditions, to ensure the contact interface works reliably in all cases. Average accuracy in the order to 10 microns should be expected, if the predictions need to be used to identify micromotion-induced tissue differentiation or cement-metal fretting abrasion. The contact model can also predict contact pressure between the bone and the prosthesis; however, this value cannot be directly validated, and thus should be used with caution. It might more convenient to use the 3D stresses predicted in the periprosthetic cancellous bone. Bone remodelling algorithms based on the deviation of stress field from that in the intact femur can also be used in this context; however, in most cases it is enough to make sure that the strain energy density does not change a lot with respect to the intact, without trying to predict the remodelling.

Mechanical failure of epiphysieal stems is unusual, and the use of hard bearing surfaces minimise wear problems. Crevice and/or fretting corrosion may occur in modular solutions, especially when two different metals are coupled. Beside the usual electrochemical tests, it is recommend to perform fretting analyses [5], eventually in artificial solutions mimicking the worse conditions that can be observed in crevice conditions [6].

The cement poses different issues. The relative micromotion of the metallic stem with respect to the cement may produce debris of cements and of metal, if the motion amplitude is larger than the so-called stick slip limit [7], which for bone cement is around 50 microns. The failure mode is frequently neglected, but many retrieved stems show massive abrasions at the cement interface. In addition, in the cement itself is frequently the weak link of the chain. The fatigue limit of PMMA is quite low, and if the thickness of the cement mantle is small, significant stresses can be induced during physiological loading. Some regions typically produce stress concentrations, e.g. the stem tip, and in those locations the cement mantles should be kept thicker. Thus, it is of vital importance to know the cement stresses under load. Although embedded strain gauges may give some information at a few locations, in general it is more convenient to use this information to validate a model, and then use the model to predict the entire stress field in the cement. PMMA fails in tension as brittle material, and tend to crack in mode I (opening); thus a principal tensile stress/strain failure criterion should be used to assess the risk of cement fracture; if significant compression is present a Von Mises criterion should be used instead. In some cases a small portion of the cement is exposed to very high stresses, but once it cracks/yields, the stress is relieved and no further damage is produced. To investigate this condition, a simple elasto-plastic constitutive law can be used for the PMMA if the failure region is under compression; if the failure is under tension, then the elements with principal tensile stress higher than the fatigue limit can simply be removed, and the analysis run again. If the localised failure of the cement simply transfers the same level of stress to the neighbour elements, this suggests that the failure would propagate and the design needs to be revised. Interdigitation can be a mitigating factor, but since the level of bone-cement interdigitation is highly variable depending on the bone quality, the cement viscosity, the surgical technique, etc., it is a safer assumption to neglect the interdigitation, if possible. Alternatively, a simple way to model an interdigitated layer is to assume that it has the same mechanical properties of the cement. In reality interdigitated cancellous bone has properties that are intermediate between those of the dense bone, and those of the cement. Since the latter are lower than the former, assuming the properties of the cement is thus conservative. This holds true only if we achieved the so-called “white-out” interdigitation, where all marrow space is replaced by cement.

The last failure scenario, subcapital dislocation, is probably the most difficult to investigate, probably because the true aetiology of this clinical failure is still strongly debated [8]. We suggest to verify that the contact pressures or the principal strains induced by the stem into the cancellous bone do not exceed the yield limits (strain-based failure criteria should be preferred, as they seems to be less sensitive to the bone density). Also, in order to exclude severe stress shielding effects, the strain energy density should not be too different from that predicted in the intact femur. All these predictions are liable only once the model have been fully validated by an experimental stress analysis on the cadaver bone, involving also strain gauges located on the neck and in the subcapital region, so as to ensure that the finite element model can reliably predict strains also in the epiphysis. The last possible explanation for subcapital dislocation is bone ischemia; in authors' knowledge this failure scenario cannot be currently assessed in a pre-clinical study, because we cannot currently model the spatial organisation of the small blood

vessels in the femoral epiphysis; significant research effort is required in this direction in the next few years.

4.1.2 Discussions

The aim of the presented analysis of failure of hip resurfacing devices was to identify a list of actions, which constitute the protocol of analysis, to be taken to assess the risk of failure of resurfacing devices of the hip.

The protocol was identified by matching any failure mode, coherent with failure scenarios observed in the clinic, with an adequate method of investigation.

The analysis highlighted both the potentiality and the limits of current techniques in predicting failure. The possible failure scenarios associated to the biomechanical behaviour of resurfaced femurs here analyses were the aseptic loosening of the prosthesis, the mechanical failure of the prosthesis, the cement and the femoral neck and, last, the subcapital dislocation of the femoral head.

Although there is a sufficient knowledge of the various mechanism that might concur in producing loosening of the prosthesis and in producing fractures of the various parts of the implant (prosthesis, bone and cement), it is less clear which mechanism concur in producing the subcapital dislocation of the femoral head. Even though a general indication was provided so as to prevent the subcapital dislocation, an extensive research activity is still necessary to improve the understanding of this phenomenon and subsequently to predict the subcapital dislocation. .

Fortunately, the major concerns for the resurfacing devices are not for subcapital dislocations. As it is discussed in chapter 1, almost the totality of observed failures are associated with the prosthesis mobilisation and the fracture of the femoral neck [9-13]. Thus the analysis of only these modes of failure might be effective in averting failure.

Another aspect that clearly emerges is that it is necessary to combine numerical and experimental techniques to address all resting failure modes. When available, numerical simulations are a powerful tool in terms of time cost and quantity of information but current modelling techniques are not adequate in predicting excessive wear and femoral neck fractures.

To date, the wear of metal-on-metal bearing of hip resurfacing devices can accurately be estimated only by experimental tests[14].

For what regard the predictions of femoral neck fractures, models described in chapter 2 and 3 are validated only in the bone elastic field, so their ability in predicting the ultimate load to fracture is unclear. To close this gap studies aimed to validate finite element predictions of bone fractures [2]are in progress at the time of writing. Waiting for more powerful models, the choice done was to measure the influence of the prosthesis on the femoral neck strength by destructive tests on cadaver femurs.

However, the experimental set-up had to be designed so as to produce *in-vitro* fractures of the femoral neck coherently with what observed in the clinic. This problem was numerically addressed.

The following paragraph describes the numerical definition of the experimental set-up. The study involved in the identification of the physiological loading condition that, among others, produce the highest risk of fracture in the femoral neck, and in the simplification of the loading scheme when the head-neck region is of interest.

The complete numerical/experimental paper, which also contains the description of the destructive tests of 10 cadaver femurs, is reported in Appendix B.

4.2 In-vitro replication of spontaneous fractures of the proximal human femur³

Spontaneous fractures of the hip can be defined as those fractures deriving from physiological or sudden loading, but not from a traumatic event (they may eventually result in secondary trauma, but they are not caused by trauma) [15, 16]. They most frequently occur in elderly (osteoporotic) subjects. Yang [17] developed two in vitro simulations (later replicated numerically by Gomez-Benito [18]) to determine the biomechanical background for spontaneous hip fractures. They suggested that abnormal muscle contraction of the rotator muscles could induce hip fracture. In addition, bone fractures may occur as a consequence of excessive cyclic loading [15, 16]. However, cyclic fractures typically occur because of excessive load/activity, and usually do not involve the proximal femur. As the focus of this paper is on fractures of the proximal femur occurring in elderly subjects, cyclic fractures will not be considered hereafter. There are mainly two reasons to investigate the biomechanics of spontaneous fractures of the proximal femoral metaphysis:

- (1) A significant fraction (though not the majority) of fractures of the untreated hip in the elderly are not associated with a primary traumatic event [15]. While the actual estimate of such fraction is difficult (elderly patients are often unable to report whether they fell before or after the fracture), it must account for 10-60% of the hip fractures [19-22] suggested that buckling of the thin cortical shell could be one failure-initiating event if the underlying trabeculae are weakened by osteoporosis.
- (2) With the recent return to resurfacing prostheses, concerns exist about risk of neck fractures due to physiological loading [23-26]. This event is clinically undesirable. It also has serious legal implications (especially in the case of spontaneous fractures).

In most cases, patients cannot recall what motor task was performed at the time of fracture, or report having been stumbling or tripping on an obstacle [19, 21]. In the first case the motor task is unknown, but even in the second case the direction of the applied loads is hard to determine. Therefore, there is no clear indication as to which is the relevant loading mode when

³ This paragraph contains the numerical study extracted from (see Appendix B): Luca Cristofolini, Mateusz Juszczak, Saulo Martelli, Fulvia Taddei, Marco Viceconti. “*In-vitro* replication of spontaneous fractures of the proximal human femur”. *J Biomech.*, 2007, 40(13), p:2837–45

spontaneous fractures occur. Additionally, the type of fracture that will develop and the required load cannot be easily predicted a priori [27].

Traumatic femoral fractures due to impact on the greater trochanter as a consequence of sideways fall have been extensively investigated in vitro [20, 28-30]. Traumatic and spontaneous fractures exhibit different cracking modes and regions [15, 28, 31-34].

Several numerical and in vitro studies have been carried out attempting to simulate spontaneous fractures. However, there is no consensus concerning the relevant loading scenario to be simulated. The direction of the force applied on the femoral head ranges between 0° [30, 35-37], 11° [38], 20° [29, 32, 39], 24° [40], and 25° [41, 42] in the frontal plane, or even perpendicular to the shaft [43]. In other cases (e.g. Alho [44]; [45]; Patel and Murphy[46]) the loading direction is not specified (with limitations discussed elsewhere[47]. This lack of agreement concerning the loading scenario undermines comparison between tests, as the direction of the load severely affects the stress distribution [48-50], hence failure. Keyak et al. [33, 34] addressed the issue of the loading direction and tried to assess the relevance of the muscle force on simulated failure [51]. Their conclusions were that it should not be necessary to simulate the muscles, and single-leg stance (resultant force at 10° in the frontal plane) and stair-climbing (30° in the sagittal plane) are the most relevant loading conditions. However, their indications cannot be considered conclusive, as they never tested experimentally the single-leg stance loading condition they identified (in all experiments they applied a resultant force at 20° in the frontal plane [29, 33, 34, 51]). In addition in the cited work [33, 34], they did not provide any indications on the femoral region subjected to the highest stress-strain levels in the one-leg stance configuration, thus providing no numerical evidence that this configuration may result in clinically relevant neck fractures. Therefore, there is a need for more extensive work based on state-of-the-art FE models, to confirm which is the most relevant loading scenario for replicating in vitro spontaneous neck fractures.

The goals of the numerical part of this work were to:

- develop a rationale and identify the most relevant loading scenario to recreate in vitro spontaneous hip fractures;
- develop the simplest possible testing protocol so as to increase repeatability and reproducibility (including assessment of the need to apply the muscle forces in the in vitro setup);

4.2.1 Identification of the most critical loading scenario: FE simulations

A highly detailed finite element (FE) model of a human femur, which was previously validated against experimental measurements [52, 53] was used to complement this study. A relevant donor for the FE study was selected (male, died 51 of intracerebral hemorrhage, free of musculoskeletal disease, smoker, osteoporotic, 175 cm tall, weighing 75 kg). The FE model included a dedicated material mapping strategy to assign suitable material properties to each element [52, 53]. It was used to perform a preliminary sensitivity analysis to address the following two questions:

- (1) Does the application of the muscle forces (below the intertrochanteric region) affect the strain distribution in the head-neck region, or is it sufficient to apply the joint load with the right direction and intensity? This question was addressed by simulating inclusion and exclusion of the muscle forces, when the same resultant joint force was simulated under simulated single-leg stance during gait [54].
- (2) Which is the direction of the hip joint resultant force that can cause the highest risk of failure in the head-neck region with respect to the diaphyseal one, to obtain clinically relevant failure scenario for the proximal femur. In fact, a preliminary study indicated that when unsuitable scenarios are applied, diaphyseal fractures might occur before the head-neck region fails. Once the first question was answered, the second one was addressed by exploring the five most frequent loading scenarios (level walking, stair climbing and descending, one-leg stance, standing up), as reported in [54].

The model consisted of 76,026 10-node tetrahedral elements. The inhomogeneous material properties were derived from the calibrated computed tomography (CT) dataset of the same femur [55] and resulted in 381 different materials. More details are reported in Taddei et al. [52, 53].

4.2.3 Results: Most critical loading scenario

In the FE model, the inclusion/exclusion of the abductor muscles affected the strain distribution in the superior aspect of the head-neck region. However, this effect was quite moderate. Moreover, higher peak tensile strains were found when the muscles were not simulated. Therefore, exclusion of the muscles tends to slightly overestimate the risk of fracture (when the same joint resultant force is applied).

The FE models indicated that, among the directions recorded by Bergmann [54], the loading scenario that generates the highest risk of failure of the neck region is the one-leg stance configuration, when the force lies in the frontal plane at 81° from the diaphysis. In fact, while other scenarios have a larger stress below the trochanteric region or in the diaphysis, this is the condition with the highest risk in the neck (i.e. one-leg stance is the loading scenario that, if incrementally scaled, may lead to a fracture in the head-neck region first).

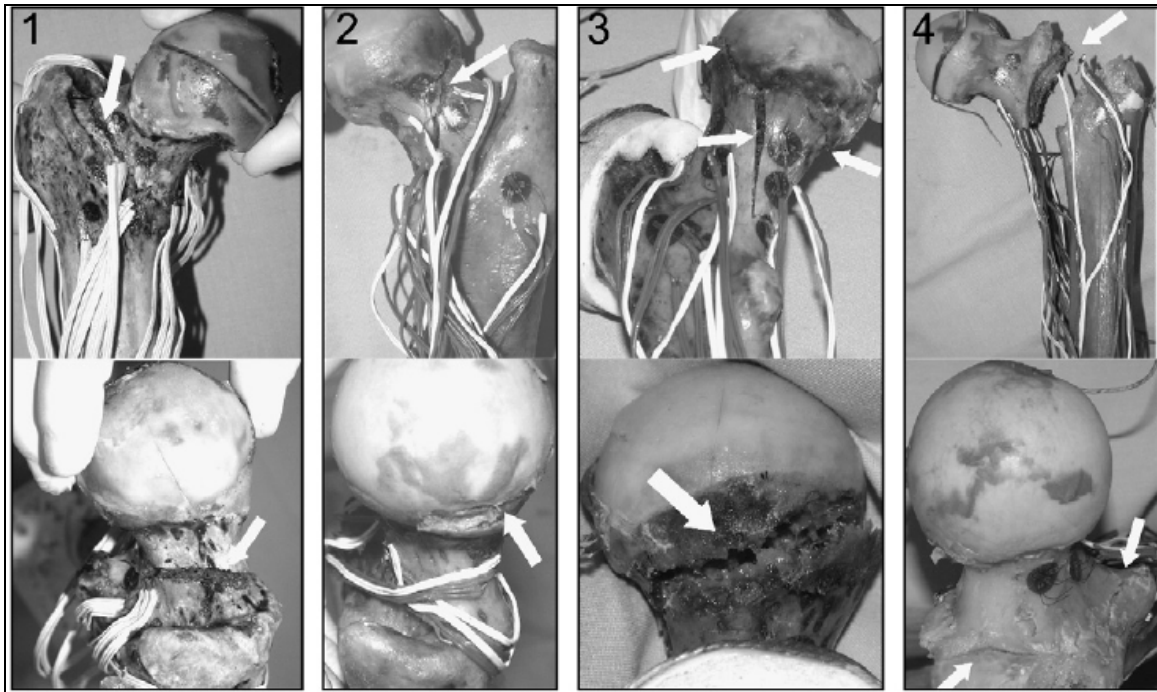


Figure 1 - Typical fractures found in the in vitro fractured specimens (highlighted by the white pointers). (1) Base-of-the-neck fracture, close to the greater trochanter (top: frontal view; bottom: detail from the lateral-superior side of the neck). (2) Cervical fracture, showing two crack initiation sites laterally, which indicate uniform fracture risk area (top: posterior view on top; bottom: detail from the lateral-superior side of the neck). (3) Cervical fracture, propagating parallel to the neck, and including a secondary subcapital crack on the medial side (top: posterior view; bottom: lateral view of the head).

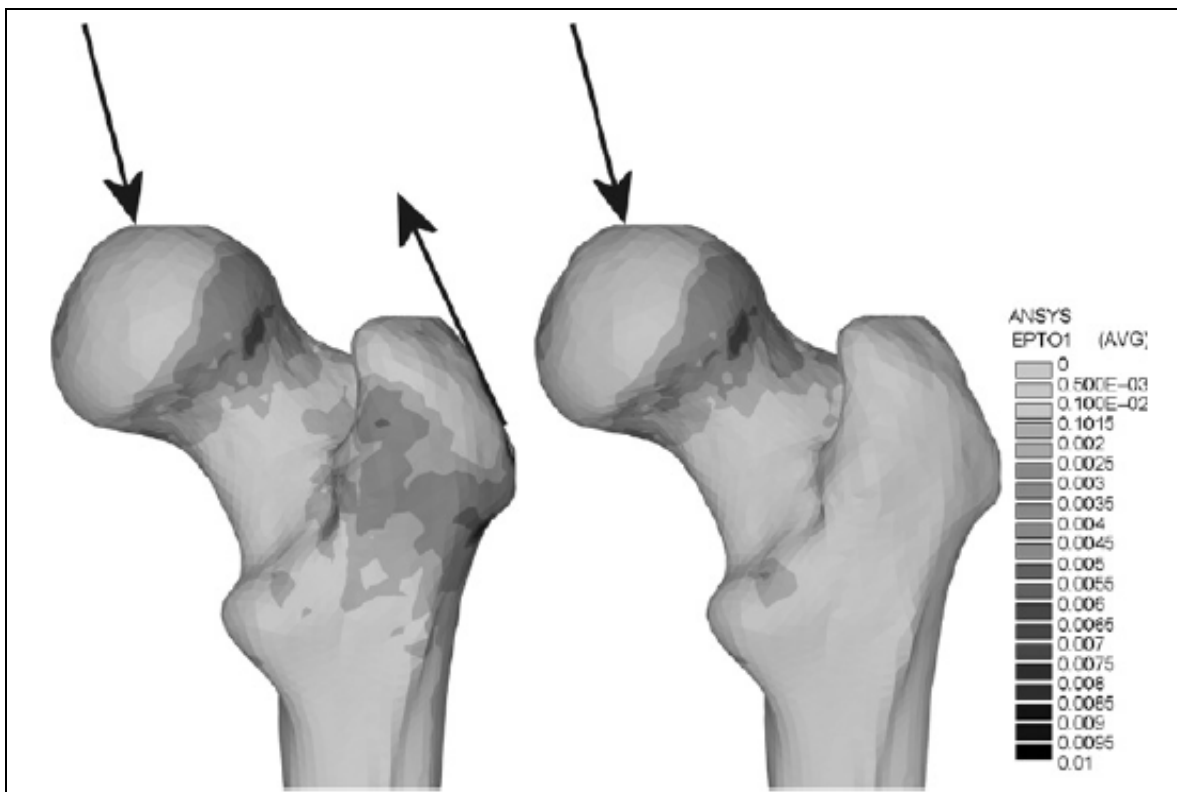


Figure 2 - Principal tensile strain in the proximal femur when the abductor muscles are simulated (left) and when these muscles are not simulated, while the same resultant force is applied to the femoral head (right). The plots show that minimal strain alterations are induced in the head-neck region by the inclusion/exclusion of the abducting muscles.

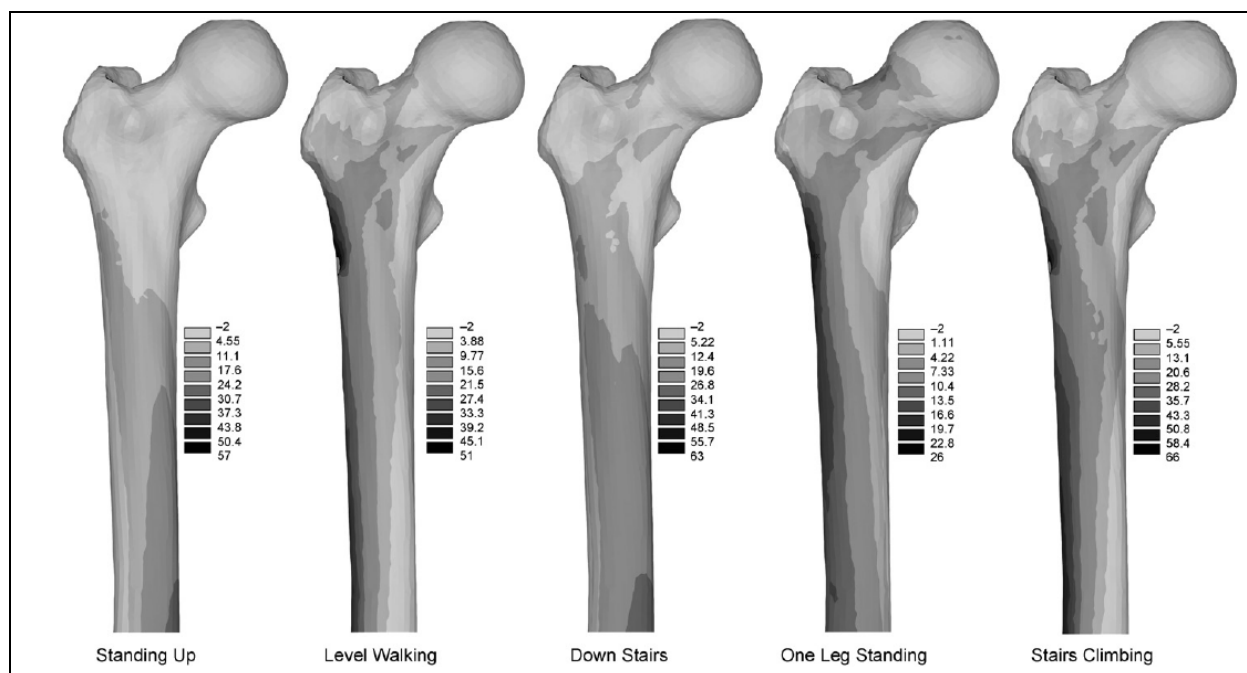


Figure 3 - Principal tensile stress distribution as predicted by finite element analysis for five different loading scenarios. Different scales are used for the five loading scenarios, to allow comparison between the head-neck and diaphyseal region within the same case. These plots were explored to determine for which loading scenario the stress in the head-neck region is higher, in comparison with the diaphysis (i.e. proximal fractures are more likely than diaphyseal ones).

4.2.4 Discussions

Spontaneous fractures of the hip are caused by occasional overloads during daily activities, and are associated with hip resurfacing implants [15, 16]. They are associated with poor bone quality due to age and osteoporosis. In fact, a decrease of bone tissue toughness is associated with age [56].

Despite some preliminary study [33, 34, 51], there is no strong indication concerning the most relevant loading scenario for replicating spontaneous neck fractures in vitro. The final scope was to design a knowledge-based test setup to simulate in vitro spontaneous fractures of the proximal femur. The original goals of the numerical part of the presented study were successfully met:

- Based on a validated FE model, the most critical loading scenario (among the possible motor tasks that a subject typically performs when spontaneous fractures occur) was identified, which should be simulated in vitro.
- Based on past experience and on the current FE simulations, the simplest possible testing protocol was designed and implemented. It was demonstrated that it is not necessary to simulate the action of the muscles to investigate fractures in the head-neck region. This enables simplification and better reproducibility both of experimental simulations and of in vitro test setups.

The loading scenario identified as most critical here is compatible with numerical studies [33, 34], and is quite similar to the one used by Link et al. [38] (11° in the frontal plane). Also, this

study indicated that it is not necessary to simulate the muscle forces to create a suitable stress state in the head-neck region in accordance with previously published works [41, 51].

It must be stressed that the scope of this study was to recreate in vitro the conditions for spontaneous fractures of the proximal caused by a single sudden loading event (typically in elderly subjects), as opposed to fatigue fractures, which are caused by cyclic loading (usually associated with active subjects, and involving other regions than the proximal femur [15, 16]. Consistently with most of similar works, the authors recommend simulation of a single-loading ramp, as this seems to best represent the occasional overloading leading to non-traumatic fractures) [16, 19, 21, 22]. Others [30, 35, 36] have chosen to apply loading cycles of increasing magnitude.

The most common fracture initiation site was the subcapital region (80% of the specimens). This is the most common type of spontaneous fractures [15]. Indeed, a similar fraction of subcapital fractures was obtained in vitro by others (69%, Cody et al. [41] and 94%, Keyak et al. [33, 34]).

The test protocol developed and validated herein can thus be applied to investigate spontaneous fractures of the natural femur. It could also be extended to address neck fractures in the presence of epiphyseal prostheses.

4.3 Conclusions

The aim of the work discussed in this chapter was to identify a possible protocol of analysis to address the risk of failure associated to the biomechanical behaviour of the resurfaced femur.

The protocol presented here intends to provide a method to keep the designer(s) of a new hip resurfacing prosthesis cognizant of failure modes at the early stage of the design phase.

In spite of the impossibility of addressing all failure scenarios (e.g. the biomechanical implications in producing subcapital dislocations of the femoral head is not yet clear enough to allow an effective prediction of this type of events), the presented protocol addressed the large majority of possible failure modes for hip resurfacing implants. This would provide an effective method in averting failure by a combination of numerical and experimental methods although it cannot substitute the necessary retrospective studies to confirm the validity of prediction.

The first attempt to test the protocol ability in predicting the biomechanical behaviour of resurfaced femurs is reported in the following chapter. The protocol was applied to a successful device on the market with about ten years of clinical experience. Hence, the availability of published retrospective studies allows the comparison of the known performances of the prosthesis with predictions of the proposed protocol.

REFERENCES

1. Kutz, M., *Mechanical engineer's handbook, materials and mechanical design*, ed. r. Edition. 2005: Jhon Wiley & Sons.
2. Schileo, E., et al., *Subject-specific finite element models implementing a maximum principal strain criterion are able to estimate failure risk and fracture location on human femurs tested in vitro*. J Biomech, 2008. **41**(2): p. 356-67.
3. Stea, S., et al., *Registration of hip prostheses at the Rizzoli Institute. 11 years' experience*. Acta Orthop Scand Suppl, 2002. **73**(305): p. 40-4.
4. Maganaris, C.N. and J.P. Paul, *In vivo human tendon mechanical properties*. J Physiol, 1999. **521 Pt 1**: p. 307-13.
5. Viceconti, M., et al., *Fretting wear in a modular neck hip prosthesis*. J Biomed Mater Res, 1997. **35**(2): p. 207-16.
6. Viceconti, M., et al., *Design-related fretting wear in modular neck hip prosthesis*. J Biomed Mater Res, 1996. **30**(2): p. 181-6.
7. Zhou, Z.R., V. Pellerin, and L. Vincent, *Fretting - Wear of aluminium and titanium alloys*, in *Titanium & aluminium*, P.A. Coulon, Editor. 1989, I.I.T.T. Internationa. p. 145-153.
8. Sorbie, C., *Arthroplasty in the treatment of subcapital hip fracture*. Orthopedics, 2003. **26**(3): p. 337-41; quiz 342-3.
9. Morlock, M.M., et al., *Biomechanical, morphological, and histological analysis of early failures in hip resurfacing arthroplasty*. Proc Inst Mech Eng [H], 2006. **220**(2): p. 333-44.
10. Mont, M.A., et al., *Hip resurfacing arthroplasty*. J Am Acad Orthop Surg, 2006. **14**(8): p. 454-63.
11. Kishida, Y., et al., *Preservation of the bone mineral density of the femur after surface replacement of the hip*. J Bone Joint Surg Br, 2004. **86**(2): p. 185-9.
12. Itayem, R., et al., *Stability of the Birmingham hip resurfacing arthroplasty at two years. A radiostereophotogrammetric analysis study*. J Bone Joint Surg Br, 2005. **87**(2): p. 158-62.
13. Glyn-Jones, S., et al., *Roentgen stereophotogrammetric analysis of the Birmingham hip resurfacing arthroplasty*. J Bone Joint Surg Br., 2004. **86-B**(2): p. 172-176.
14. Affatato, S., et al., *Larger diameter bearings reduce wear in metal-on-metal hip implants*. Clin Orthop Relat Res, 2007. **456**: p. 153-8.
15. Cotton, D.W., et al., *Are hip fractures caused by falling and breaking or breaking and falling? Photoelastic stress analysis*. Forensic Sci Int, 1994. **65**(2): p. 105-12.
16. Jeffery, C.C., *Spontaneous fractures of the femoral neck*. Orthop Clin North Am, 1974. **5**(4): p. 713-27.
17. Yang, K.H., et al., *The relationship between loading conditions and fracture patterns of the proximal femur*. J Biomech Eng, 1996. **118**(4): p. 575-8.
18. Gomez-Benito, M.J., J.M. Garcia-Aznar, and M. Doblare, *Finite element prediction of proximal femoral fracture patterns under different loads*. J Biomech Eng, 2005. **127**(1): p. 9-14.
19. Grisso, J.A., et al., *Risk factors for falls as a cause of hip fracture in women. The Northeast Hip Fracture Study Group*. N Engl J Med, 1991. **324**(19): p. 1326-31.
20. Mayhew, P.M., et al., *Relation between age, femoral neck cortical stability, and hip fracture risk*. Lancet, 2005. **366**(9480): p. 129-35.

21. Michelson, J.D., et al., *Epidemiology of hip fractures among the elderly. Risk factors for fracture type*. Clin Orthop Relat Res, 1995(311): p. 129-35.
22. Muckle, D.S., *Iatrogenic factors in femoral neck fractures*. Injury, 1976. **8**(2): p. 98-101.
23. Amstutz, H.C., P.A. Campbell, and M.J. Le Duff, *Fracture of the neck of the femur after surface arthroplasty of the hip*. J Bone Joint Surg Am, 2004. **86-A**(9): p. 1874-7.
24. Shimmin, A.J. and D. Back, *Femoral neck fractures following Birmingham hip resurfacing: a national review of 50 cases*. J Bone Joint Surg Br, 2005. **87**(4): p. 463-4.
25. Shimmin, A.J., J. Bare, and D.L. Back, *Complications associated with hip resurfacing arthroplasty*. Orthop Clin North Am, 2005. **36**(2): p. 187-93, ix.
26. Siebel, T., S. Maubach, and M.M. Morlock, *Lessons learned from early clinical experience and results of 300 ASR hip resurfacing implantations*. Proc Inst Mech Eng [H], 2006. **220**(2): p. 345-53.
27. Jarvinen, T.L., et al., *Revival of bone strength: the bottom line*. J Bone Miner Res, 2005. **20**(5): p. 717-20.
28. Eckstein, F., et al., *Reproducibility and side differences of mechanical tests for determining the structural strength of the proximal femur*. J Bone Miner Res, 2004. **19**(3): p. 379-85.
29. Keyak, J.H., et al., *Prediction of femoral fracture load using automated finite element modeling*. J Biomech, 1998. **31**(2): p. 125-33.
30. Lochmuller, E.M., et al., *Correlation of femoral and lumbar DXA and calcaneal ultrasound, measured in situ with intact soft tissues, with the in vitro failure loads of the proximal femur*. Osteoporos Int, 1998. **8**(6): p. 591-8.
31. Backman, S., *The proximal end of the femur: investigations with special reference to the etiology of femoral neck fractures; anatomical studies; roentgen projections; theoretical stress calculations; experimental production of fractures*. Acta Radiol Suppl, 1957(146): p. 1-166.
32. Keyak, J.H., *Relationships between femoral fracture loads for two load configurations*. J Biomech, 2000. **33**(4): p. 499-502.
33. Keyak, J.H., et al., *Prediction of fracture location in the proximal femur using finite element models*. Med Eng Phys, 2001. **23**(9): p. 657-64.
34. Keyak, J.H., H.B. Skinner, and J.A. Fleming, *Effect of force direction on femoral fracture load for two types of loading conditions*. J Orthop Res, 2001. **19**(4): p. 539-44.
35. Lochmuller, E.M., et al., *Mechanical strength of the proximal femur as predicted from geometric and densitometric bone properties at the lower limb versus the distal radius*. Bone, 2002. **30**(1): p. 207-16.
36. Lochmuller, E.M., et al., *In situ femoral dual-energy X-ray absorptiometry related to ash weight, bone size and density, and its relationship with mechanical failure loads of the proximal femur*. Osteoporos Int, 2000. **11**(4): p. 361-7.
37. Lotz, J.C., E.J. Cheal, and W.C. Hayes, *Fracture prediction for the proximal femur using finite element models: Part I--Linear analysis*. J Biomech Eng, 1991. **113**(4): p. 353-60.
38. Link, T.M., et al., *Structure analysis of high resolution magnetic resonance imaging of the proximal femur: in vitro correlation with biomechanical strength and BMD*. Calcif Tissue Int, 2003. **72**(2): p. 156-65.
39. Lang, T.F., et al., *Volumetric quantitative computed tomography of the proximal femur: precision and relation to bone strength*. Bone, 1997. **21**(1): p. 101-8.
40. Smith, M.D., et al., *Proximal femoral bone density and its correlation to fracture load and hip-screw penetration load*. Clin Orthop Relat Res, 1992(283): p. 244-51.

41. Cody, D.D., et al., *Femoral strength is better predicted by finite element models than QCT and DXA*. J Biomech, 1999. **32**(10): p. 1013-20.
42. Delaere, O., A. Dhem, and R. Bourgois, *Cancellous bone and mechanical strength of the femoral neck*. Arch Orthop Trauma Surg, 1989. **108**(2): p. 72-5.
43. Dalen, N., L.G. Hellstrom, and B. Jacobson, *Bone mineral content and mechanical strength of the femoral neck*. Acta Orthop Scand, 1976. **47**(5): p. 503-8.
44. Alho, A., T. Husby, and A. Hoiseth, *Bone mineral content and mechanical strength. An ex vivo study on human femora at autopsy*. Clin Orthop Relat Res, 1988. **227**: p. 292-7.
45. Ota, T., I. Yamamoto, and R. Morita, *Fracture simulation of the femoral bone using the finite-element method: how a fracture initiates and proceeds*. J Bone Miner Metab, 1999. **17**(2): p. 108-12.
46. Patel, S.H. and K.P. Murphy, *Fractures of the proximal femur: correlates of radiological evidence of osteoporosis*. Skeletal Radiol, 2006. **35**(4): p. 202-11.
47. Cristofolini, L. and M. Viceconti, *Comments on "Stair climbing is more critical than walking in pre-clinical assessment of primary stability in cementless THA in vitro" by Jean-Pierre Kassi, Markus O. Heller, Ulrich Stoeckle, Carsten Perka, Georg N. Duda, Published on J. Biomechanics 2005; 38: 1143-1154*. J Biomech, 2006. **39**(16): p. 3085-7; author reply 3087-40.
48. Cristofolini, L., *A critical analysis of stress shielding evaluation of hip prostheses*. Crit Rev Biomed Eng, 1997. **25**(4-5): p. 409-83.
49. Cristofolini, L. and M. Viceconti, *Towards the standardization of in-vitro load transfer investigations of hip prostheses*. J. Strain Anal. Eng. Des., 1999. **34**: p. 1-15.
50. Voide, R., G.H. Van Lenthe, and R. Muller. *Femoral neck stiffness critically depends on loading direction*. in *Fifth World Congress of Biomechanics Book of Abstracts*. 2006. Munich
51. Keyak, J.H., et al., *Predicting proximal femoral strength using structural engineering models*. Clin Orthop Relat Res, 2005(437): p. 219-28.
52. Taddei, F., et al., *Subject-specific finite element models of long bones: An in vitro evaluation of the overall accuracy*. J Biomech, 2006. **39**(13): p. 2457-67.
53. Taddei, F., et al., *The material mapping strategy influences the accuracy of CT-based finite element models of bones: an evaluation against experimental measurements*. Med Eng Phys, 2007. **29**(9): p. 973-9.
54. Bergmann, G., et al., *Hip contact forces and gait patterns from routine activities*. J Biomech, 2001. **34**(7): p. 859-71.
55. Taddei, F., A. Pancanti, and M. Viceconti, *An improved method for the automatic mapping of computed tomography numbers onto finite element models*. Med Eng Phys, 2004. **26**(1): p. 61-9.
56. Wang, X. and S. Puram, *The toughness of cortical bone and its relationship with age*. Ann Biomed Eng, 2004. **32**(1): p. 123-35.

Chapter 5

Testing of the pre-clinical validation protocol on a successful design of hip resurfacing prosthesis

Hip resurfacing arthroplasty was always an attractive solution especially for the treatment of arthritic hips on young and active patients. Their first introduction in the 60s failed with an high failure rate, later attributed to the poor material properties of the medical alloys available at that time [1, 2]. The more recent development of performing CrCo medical alloys gave a new spin to resurfacing techniques. The second generation of hip resurfacing devices, recently re-introduced, is currently a potential alternative to traditional THR for a large sub-group of patients, although some complications are still suspected.

Short and mid term follow-up [3-7] are today available on the literature showing very promising results so as its adoption is expected to quickly increase. However, probably due to the failure met by the first generation of devices together with its expected advantages over traditional endomedullary stems, today the attention of the scientific community on hip resurfacing performances is very high. Many authors suspected that this device may have an high risk of failure related to its biomechanical behaviour [8-12] opening a debate on biomechanical implications on its early failures.

This debated scenario highlighted the need of an analysis protocol able to pre-clinically address possible complication in the clinics when this or other types of devices are adopted. This scenario was chosen for the first application of the protocol described in chapter 4. The availability of short- and mid-term published results allowed a first test of the protocol contemporary contributing to the current debate open in the literature.

The complete protocol, more extensively described in the previous chapter, consist of a numerical study, carried out by the author, and of destructive tests carried out by the experimental group of LTM. The numerical analysis was performed on a single femur, of average size, normal anatomy which was implanted with a well established resurfacing device on the market, placed in the ideal position with respect to the femur.

The joint reaction and the muscular forces acting on hip were derived from the literature [13-16]. The biomechanical failure of the bone, the cement, the prosthesis and of the prosthesis-bone and prosthesis-cement interaction mechanics were studied under a large set of activities of daily living.

The results of the numerical analysis indicated, in general terms, a very low risk of failure for any of the investigated failure modes and, for each of them, the type of activity which produce the higher risk.

Once the results of the numerical and of the experimental study were merged together, the overall set of results showed an excellent agreement with the known clinical performances of the device encouraging the authors to a further use of the presented protocol.

5.1 Combined experimental-numerical method for the pre-clinical validation of epiphyseal prosthesis: exemplification of the method with an established designⁱⁱ

The first adoption of hip resurfacing arthroplasty (HRA) showed high failure rate mainly due to polyethylene wear and the subsequent osteolysis [1, 2]. The recent development of advanced metal-on-metal bearing gave a new impulse to resurfacing techniques which are supposed to have various advantages over traditional endomedullary stems [1, 2, 7]. HRA are supposed to lead to a better preservation of the femoral bone stock [17], a very low rate of dislocations [2, 7], a better proprioception and there are no indication for a reduced activity after surgery. Hence, HRA is today largely indicated for young and active patients. Short and mid-term clinical outcomes are very promising [4, 7] but long-term follow-up are not yet available so some authors suggest to consider their use with caution [7]. Nevertheless their adoption is increasing year by year and it is expected to increase further.

Although preliminary results are promising, some early complications are reported by recent retrospective studies [3, 4, 6, 18, 19]. While biomechanics of traditional endomedullary stems has been studied by many authors still relatively few studies have been proposed to investigate the HRA biomechanical behaviour and the debate on its early failures is still open. On one hand, some numerical studies warned about loosening [8-10, 12, 20] and neck fractures [8, 9, 12, 20]. On the other hand, some *in-vivo* studies that investigated the implant stability two years after surgery found no evidence of prosthesis mobilisation [4, 21]. Other authors [7, 22] attribute most of failures to the surgeon's learning curve [7, 22] where the higher surgery uncertainties might compromise the prosthesis biomechanics [9, 23]. The analysis of retrieved implants lead to other contradictory conclusions, while Little hypostatized that the HRA reaming procedure, which disrupt the natural vascularisation, lead to osteonecrosis Morlock [22] found no evidence of correlation between osteonecrosis and the surgery methodology.

To date, the biomechanical analysis performed to understand the implant behaviour has been carried out analysing only the stress-shielding and the peak of stress/strain under a limited range of boundary conditions. For example Taylor [10] loaded the resurfaced femur with a simplified loading scheme, Gupta analysed the implant during walking and stair climbing while other

ⁱⁱ Saulo Martelli, Luca Cristofolini, Fulvia Taddei, Marco Viceconti. "Combined experimental-numerical method for the pre-clinical validation of epiphyseal prosthesis: exemplification of the method with an established design". To be submitted to J Biomech.

authors investigated a single activity [9, 12, 20]. However, the process leading to the failure event is probably complex and different physical mechanisms may interact and concur in producing failure. Together with those cited above, other failure mechanism have been observed in producing failure of orthopaedic implants [24-26]. For example, aseptic loosening has been studied by many authors [8-12] as a result of bone re-sorption produced by stress\strain shielding while micromovements at the bone-prosthesis interface have been hypothesised to influence both tissue differentiation and bone re-sorption at the bonding interface [24]. Fretting of the cement might also produce loosening by removing cement debris and stimulating osteolysis [27].

To the authors opinion, a systematic approach to failure analysis may help in a better understanding of the biomechanical implications on observed HRA failure scenarios. Aim of the present study is to propose a combined numerical\experimental method to analyse the biomechanics of the of resurfaced femurs. The proposed protocol aims to evaluate the risk associated to each failure scenario trough a systematic analysis of failure modes associated to each failure scenario by a cause-effect relation. To this aim an experimental test was conducted on three pairs of cadaver femurs to analyse the risk of femoral neck fracture, while all the other failure modes were numerically analysed by means of validated FE model in order to predict the relative risk of failure. Tests were conducted simulating a large set of physiologically relevant loading conditions [13-16] on a representative design for a broad category of HRA devices.

5.1.1 Materials and methods

5.1.1.1 Bone specimens for the in-vitro study

Three pairs of cadaveric human femurs (*Table 1*) were obtained through the International Institute for the Advancement of Medicine (IIAM, Jessup, PA, USA). One femur, for each pair, was implanted using the Birmingham Hip Resurfacing (BHR, Smith & Nephew, UK). Implantation was performed following the protocol recommended by the Manufacturer.

Subject ID	Sex	Age at death	Height (cm)	Weight (kg)	DEXA (%) (left – right)
1	male	70	175	90	79.6 - 85.7
2	male	51	175	164	99.4 - 107.7
3	male	80	178	88	76.4 - 69.4

Table 1 - Details for all the tested specimens

5.1.1.2 The bone specimen for the numerical study

Materials of the numerical study have been already discussed by Taddei [28], most important aspects are briefly reported:

- Right femur from a 51-year-old male, weight 75 kg
- CT scan (HiSpeed, General Electric Co., USA) performed using physical parameters of clinical practice (tube current: 180mA, 120xVP)

- Virtual implantation (Conserve Plus, Wright Medical Technology, USA) using the Hip-Op[®] software [29]

5.1.1.3 Failure modes associated to failure scenarios

The recent clinical outcomes for HRA were derived from literature [3, 4, 7] to identify relevant bio-mechanical implications. Possible failure modes related with observed failure scenarios by a cause-effect relation are listed in the following table:

Investigated failure scenarios	Bio-mechanical process	Bio-mechanical parameter
<i>Implant fractures</i>	<i>Femoral neck fracture</i>	<i>Principal tensile strain [30]</i>
	<i>Cement fracture</i>	<i>Principal tensile stress [31]</i>
	<i>Prosthesis fracture</i>	<i>Von Mises stress</i>
<i>Aseptic loosening</i>	<i>Fretting debris</i>	<i>Micromovement and contact pressure [32]</i>
	<i>Lack of bone in-growth</i>	<i>Micromovement [33, 34]</i>
	<i>Biomechanical damage of cancellous bone</i>	<i>Principal tensile strain [30]</i>
	<i>Adverse bone re-modeling</i>	<i>Changes in strain energy density (SED) [35, 36]</i>

Table 2 - List of investigated parameters related to observed clinical failure

5.1.1.4 Identification of predictive parameters

Predictive parameters for each failure mode were derived from the literature and further discussed in the following paragraphs.

Femoral neck fracture

The prosthesis implantation influence on the femoral neck strength was defined by experimental tests. The ultimate load was measured on both the implanted femur and the intact controlateral one. After normalization in terms of body weight (BW), the implantation influence on the femoral neck strength was defined as the ratio between the ultimate load of the implanted and of the intact femur.

Prosthesis fractures

Prosthesis fractures produced by yielding or fatigue were considered. Overload was considered to produce a Von Mises stress over the yield strength. The CrCo alloy used to manufacture hip implants shows very different fatigue and yield strength properties depending on chemical components and on the adopted manufacturing process. High risks of overloading and fatigue fractures were defined considering the weakest alloy of this category of materials [37, 38] (Fatigue strength: 200 MPa. Yield strength: 450MPa)

Aseptic loosening caused by cement damage

Cement fractures might occur by overloading and fatigue. The cement behaves as a brittle material and shows a different strength to tensile and compressive loads. Overloading of the cement (Simplex P, Stryker Orthopaedics, USA) was assumed over the threshold limit for tensile loads (27MPa) and for compressive loads (83.9 MPa) [31]. High risk of fatigue fractures was assumed over the threshold limit of 11 MPa found by Krause [39].

Aseptic loosening caused by fretting debris of cement

At the cement-implant interface the implant loosening may occur because of fretting abrasion. In this case, relative micromotions occurring in those locations where the surfaces separate under load are not relevant. When surfaces are pressed one against the other fretting may occur if the relative micromotion is bigger than the so-called stick-slip limit assigned to 50 microns [32].

Aseptic loosening caused by lack in bone-prosthesis in-growth

At the bone-implant interface it is relevant to determine the absolute relative micromotion between the two counter-faced surfaces, which above certain levels might disrupt the natural bone in-growth process (absolute micromotion) [25, 26, 40, 41]. The choice of the absolute micromotion level below which the bone in-growth process is allowed has been discussed in earlier studies [33, 34]. The risk of lacking of bone in-growth was computed comparing the predicted relative micro movement pattern with the threshold limit of 150 microns.

Aseptic loosening caused by damage of cancellous bone

Aseptic loosening caused by cancellous bone damage may occur in the bone layer encircling the bone-implant contact surface. The risk of bone damage was checked comparing the strain pattern to threshold limits found by [30] below which bone damage would not occur (principal tensile strain threshold: 0.62%; principal compressive threshold: 1.04%).

Aseptic loosening caused by bone re-modelling

Changes in strain energy density (SED) in bone is commonly considered as biomechanical stimulus for bone remodelling [35] [36]. Positive changes in SED produce an increment in bone mineral content while negative changes make the bone re-sorption process to start. Element solutions were compared with the threshold limit ± 0.008 J/gr [35, 36], which is commonly considered the boundary of the so-called 'lazy zone' within which no significant bone re-modelling events are expected.

5.1.1.5 Experimental tests (intact and implanted specimen)

The specimen was mounted on the load cell of the testing machine (Instron 8502, Canton, MA, USA) on top of a platform that allowed tilting it at different angles ($\pm 0.5^\circ$), so as to apply the resultant hip joint force mimicking the hip reaction force during the one leg stance. Destructive tests on the intact and implanted specimens were carried out with a displacement rate of 2mm/sec [42, 43]. Failure load was scaled by the donor's BW to reduce inter-specimen scatter [42, 43].

5.1.1.6 FE models and boundary conditions

The implanted femur model

The implanted model here used has been based on a cadaver femur during a previous validation study [44] where a more extensive description of the model generation process can be found. Main models characteristics were:

1. Geometry: extracted from the CT scan
2. Mesh type: 10-noded tetrahedral unstructured mesh automatically generated
3. Material properties:
 - a. Non-homogeneous material properties on bone (Bonemat_V3, B3C, Italy) [45]
 - b. Prosthesis was given the material properties of the CrCo alloy ($E = 210$ GPa, $\nu = 0.3$)
 - c. Cement (Simplex P, Stryker Orthopaedics, USA) was given a Young modulus $E = 2700$ MPa and a Poisson coefficient $\nu = 0.3$ [46]
4. Frictional unilateral contact was assumed on bone-prosthesis and cement-prosthesis contact surfaces (friction coefficient: 0.3 [47, 48])
5. The resulting mesh consisted of 74,288 elements and 108,477 nodes
6. Accuracy on the stress/strain field showed a root mean square error (RMSE) lower than 10%. Accuracy on prosthesis micromotions was within a micron [28]

The intact femur model

The intact femur model was generated to allow an element-by-element result comparison with the implanted model. The femur volume removed during surgery underwent the same modelling process described in the paragraph above for completing the implanted femur mesh. Nodes at the interface of the two meshes were merged to ensure the element connectivity.

The resulting FE model of the intact femur consisted of 56,039 elements and 84,269 nodes (*Figure 1*).

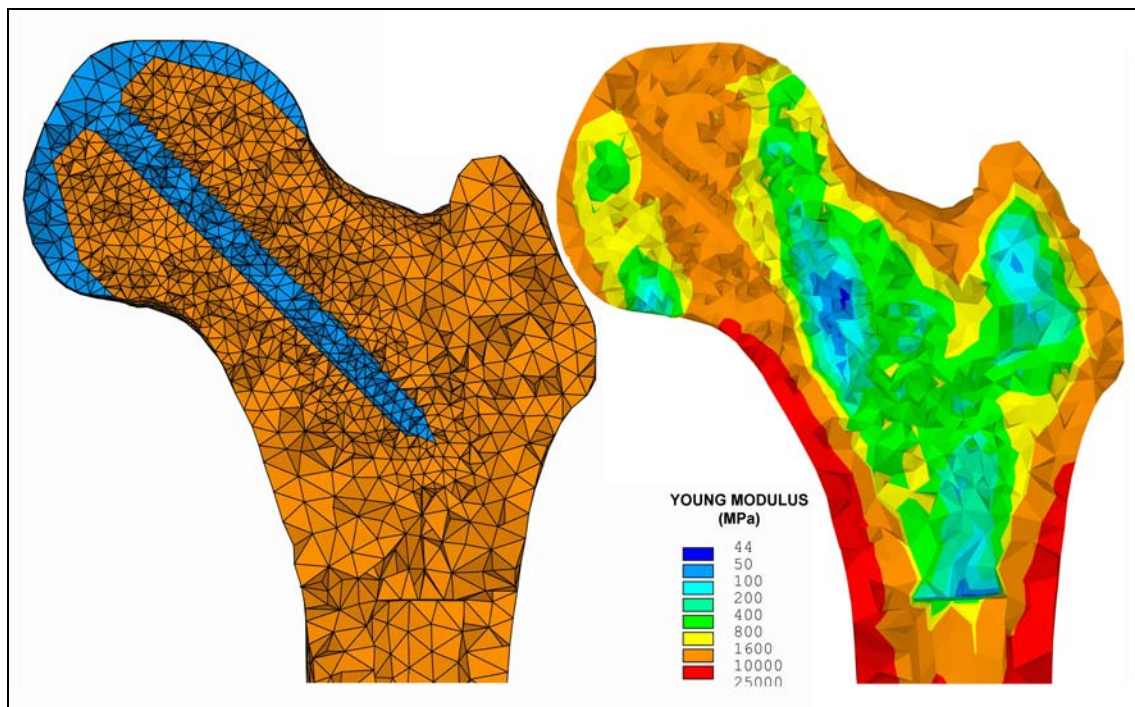


Figure 1 - A section of the tetrahedral mesh of the intact femur. On the left the used sub-modeling techniques, on the right the resulting map of the subject elastic properties

5.1.1.7 Loading conditions for numerical simulations

The femur was assumed fully constrained in the distal-most region. The proximal femur was loaded using physiological loading scenarios. Data contains a collection of hip reaction measure [13, 14] expressed in terms of body weight (BW) for slow walking, normal walking, fast walking, up stairs, down stairs, standing up, sitting down, standing and knee bending on four subjects. In addition, estimated muscle forces are available for the principal muscle groups during normal walking and up-stairs climbing.

Forces acting in the model were defined coherently with Heller's definition [15, 16]. The hip reaction force was assumed to pass through the hip joint centre, condition that is coherent with the assumption of a frictionless ball and socket joint. The force magnitude was scaled by the donor body weight (735 N).

Simulations of all tasks were run on both the intact and the implanted model and the most critical loading case for each risk of failure was identified (Table 3).

Failure risk	Critical motion task
Prosthesis failure	Upstairs climbing
Cement failure	Upstairs climbing
Femur neck fracture	Single leg stance
Prosthesis-cement fretting	Upstairs climbing
Excessive micro-movement	Upstairs climbing
Bone re-sorption	Level walking

Table 3 - Most critical motion task for any investigated failure risk

5.1.2 Results

5.1.2.1 Femoral neck fracture

Load-to-failure tests indicated that the intact femurs failed at 10.5 ± 2.6 BW, while the controlateral BHR implants failed at 9.5 ± 2.1 BW. This reduction of strength was not statistically significant (paired t-test, $p=0.2$) probably because of the low number of tested specimens.

5.1.2.2 Prosthesis fractures

The highest Von Mises stress in the prosthesis was 85 MPa predicted for stair climbing and located at mid-stem (Figure 2, right). Such value is well below both the yield stress (450 MPa) and the fatigue limit (200 MPa).

5.1.2.3 Aseptic loosening caused by cement damage

In the cement mantle the numerical model predicted a peak tensile stress of 3 MPa under the stair climbing load case located in the anterior region of the cement collar (Figure 2, left). Such value is well below both the cement strength (tensile strength: 27MPa; compressive strength: 83.9 MPa) [31] and the fatigue limit (11MPa) [39]. No cement regions showed a relevant compressive strain.

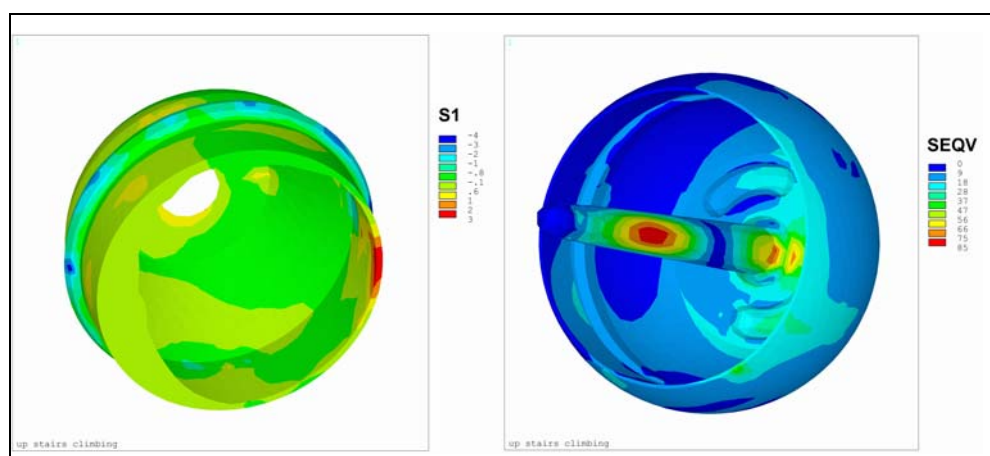


Figure 2 - On the left: principal tensile stress map on the cement predicted for the upstairs climbing. On the right: the equivalent Von Mises stress map on the prosthetic component predicted for the upstairs climbing

5.1.2.4 Aseptic loosening caused by fretting debris of the cement

The peak fretting micromotion at the cement-implant interface was predicted for stairs climbing (Figure 3, right). The peak contact pressure (10 MPa) was also predicted for the same loading case in a small region close to the border of the hollow surface under the dome. The highest micromotions coupled with a sticking status of the two contact surfaces were up to 10 microns in the medial most region of the contact surface. Thus, predicted values are well below the stick-slip limit [32].

5.1.2.5 Aseptic loosening caused by lack in bone-prosthesis in-growth

The peak bone-implant absolute micromotion (27 microns) was predicted for stairs climbing, at the medial stem location (

Figure 3, left). This value is well below the safe threshold of 150 microns.

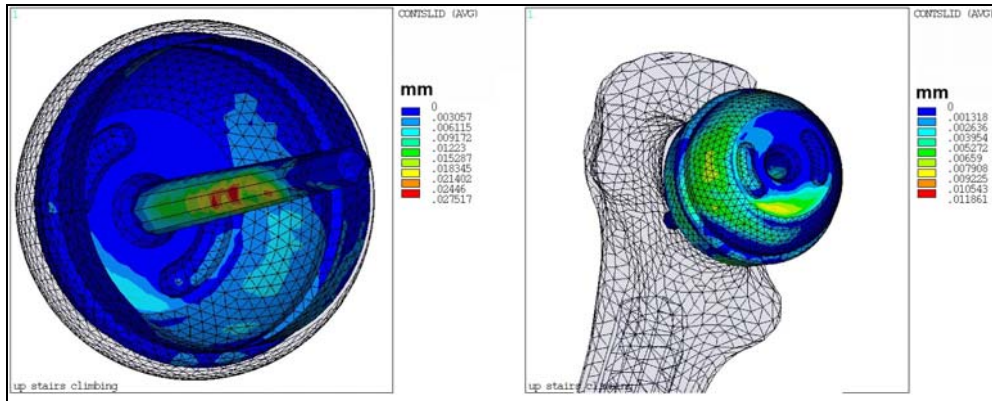


Figure 3 - On the left: bone-prosthesis micromotion predicted under the up stairs climbing load case On the right: bone-cement micromotion predicted under the up stairs climbing load case

5.1.2.6 Aseptic loosening caused by damage of cancellous bone

Results inside the femur neck volume (

Figure 4) showed the highest strain values close to the prosthesis stem for stairs climbing. Strain values remains always well below the plastic limit [30] with the exception of a very small region close to the lateral stem where both tensile and compressive strains exceeds the plastic limit. This region embraces the 0.02% of femoral epiphysis volume and it is interested by a mineral ash density lower than $0.04 \text{ g} \cdot \text{cm}^{-3}$.

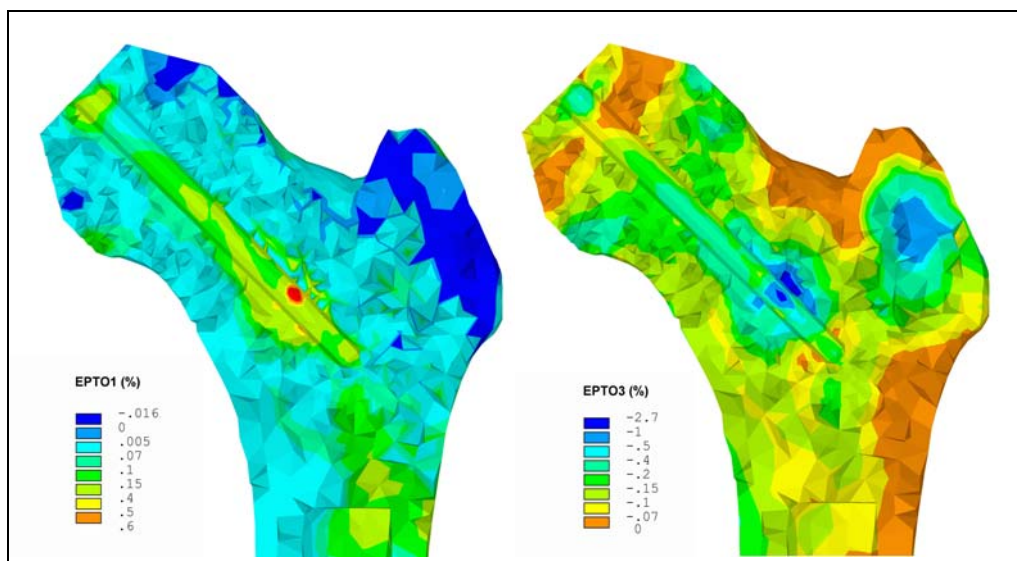


Figure 4 - On the left the principal tensile strain map and on the right, the principal compression strain map predicted under the up stairs climbing load case. Graph threshold were defined accordingly to Bayraktar [30] founding's on cancellous bone elastic properties.

5.1.2.7 Aseptic loosening caused by bone re-modelling

Changes in SED were considered in the proximal femur above the inferior margin of lesser trochanter. This region is interested by the strain field distortion produced by the implant. The studied implant produce a very small risk of positive bone remodelling (Figure 5) as only less than 0.02% of the volume exceed limit values. None of the elements shown negative activation signal.

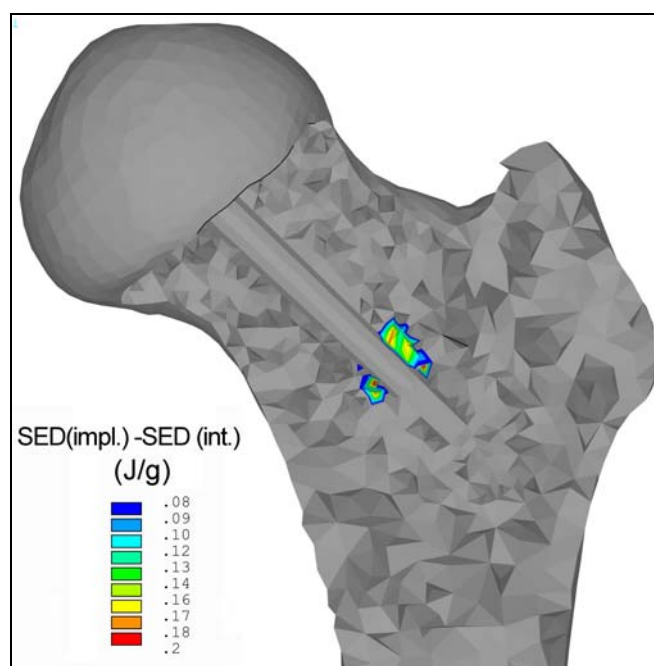


Figure 5 - Change in SED (SED of the implanted bone minus SED of the intact bone) for bone re-modelling. Grey regions are interested by an activation signal for which no re-modelling is expected, no regions are present showing risk of bone resorption while a very small area shows a small chance for positive bone re-modelling.

5.1.3 Discussion

Aim of the present study was to propose a method to address the bio-mechanical failure of resurfaced femurs by means of a combined numerical-experimental study. To this aim, experimental tests addressed the risk of neck fractures after resurfacing while simulations, through a validated FE model, addressed a variety of failure modes coherent with dysfunctional conditions observed in the clinics. The study investigated a representative design for a broad category of HRA devices, confirming its success on the market.

The protocol predicted a low risk of the implant failure for each studied scenario:

1. Femoral neck strength was not significantly influenced by resurfacing. Thus HRA surgeries are not expected to increase the risk of spontaneous fractures of the original intact femur.
2. Cement and prosthesis never exceeded the safe fatigue thresholds, thus cement fractures would unlikely occur.

3. The risk of aseptic loosening was very low for each investigated failure mode coherent with loosening, hence loosening is not expected.
4. Significant changes over time of present results are not expected as a significant re-sorption of the hosting bone would unlikely occur. SED changes were within the model accuracy and low enough for a good preservation of the femoral bone stock. The only exception was found in a very small region close to the lateral stem where both strain and SED exceeded its respective threshold limits. The local material properties revealed that it is an extremely weak region interested by a very low bone mineral density ($< 0.04 \text{ g cm}^{-3}$), thus likely a little bone vacancy.

To date no retrospective studies report long-term follow up for this kind of devices [1, 7]. Available data report short and mid-term results that are very promising and in a very good agreement with our findings.

Many authors [1, 2, 4, 7] clinically evaluate a large number of cases finding excellent outcomes. Other studies investigated specific aspects known to be key factors for successful implants. Stability were studied during a two years follow up finding the prosthesis always in a good stability with no evidence of migration or loosening [21, 49]. The risk of mid-term bone re-sorption was addressed by Kishida [17], highlighting that HRA better preserve the bone stock after surgery over traditional endomedullary stems.

The two major concerns for resurfacing implants (i.e. aseptic loosening and femoral neck fractures) have been numerically investigated by other authors.

Loosening has been considered due to only bone re-sorption on the majority of numerical studies [8, 10, 12, 20, 23]. They warned about loosening basing their conclusions either on stress shielding [12] or strain shielding [8, 10, 12, 20, 23].

Long [9] associated the risk of loosening both to cement fractures and bone re-sorption subsequent to strain shielding. Although, our predictions of the stress/strain field in bone are in agreement with his results we didn't rise any warning about remodelling. On the authors opinion the different criterion here used, proposed by Huiskes [35, 36], might be responsible of different conclusions.

Since the ability of current modelling techniques in predicting the ultimate load to failure in bones remains poor [51], in the present study the risk of neck fractures is addressed by destructive tests[42]. Results indicated a low incidence of the prosthesis implantation on the natural risk of fracture of the original intact femur, in agreement with what found by Marker [50] when the prosthesis was ideally positioned in the hosting femur.

A limitation of this study might be the different devices used for the numerical and the experimental study as they differ for small anti-rotational features under the dome. However this choice is common with other authors as the specific type of device implant is expected of minor importance [11, 22].

On the author opinion the major limitation of the present study is the analysis of a single femur of average size, normal bone stock and with an optimal implant positioning. Therefore results should be intended in general terms.

Further work should be done to study the effect of influencing co-factors such as surgical uncertainties, anatomical and physiological variability and a larger set of physiological loads. Although performed simulations represent a large set of daily activities, the analysis should include accidental task such as stumbling to understand the hip biomechanics in case of unexpected conditions. Nonetheless, the individual neuro-muscular control strategy that define the muscular pattern of contraction is far to be understood [52].

Another concerns might be raised on the low number of specimens for the destructive tests, which might result in an ineffective ability to discriminate significant differences between the strength of the intact and of the implanted femur.

To discriminate between critical and safe conditions it is necessary to compare predictions to critical values by a chosen criterion. Thus, both the accuracy of predictions and the validity of chosen criterions for predicting failure are key factors in predicting dysfunctional conditions. The model here used has a known accuracy and adopted criterions did not rise any concern of failure.

In conclusion, the method was able to identify the most critical activities in producing failure and to predict dysfunctional conditions in good agreement with current clinical outcomes. Although it present some limitation, the protocol is a good candidate for the pre-clinical validation and the design optimisation of new devices.

Further work is needed to understand the method ability to discriminate critical conditions and to extend the analysis to the entire variability of boundary conditions the implant might face during its service life.

5.2 Conclusions

The aim of the present study was to analyse the biomechanical behaviour of a resurfacing prosthesis by means of the protocol described in Chapter 4 so as to test the its ability in predicting known clinical outcomes.

The risk of failure was predicted on the base of the stress/strain field on the bone, the cement and the prosthesis and on the interaction mechanic at the prosthesis-bone and at the prosthesis-cement interface. The analysis was repeated for a large set of motion activities of daily living.

Results were able to identify, among others, the most critical activity for each type of investigated failure mode. The risk of failure was low, rising no concerns of failure for any of the studied scenarios.

The major limitation of this study is that the analysis was conducted for an ideal case (i.e. an average sized femur, normal bone stock and a bone-prosthesis ideal positioning). As surgery uncertainties [7, 19, 23, 53] and the inter-subject anatomical variability [54] are considered to affect the risk of failure, results here reported should be read in general terms.

Despite the cited limitation, present results encouraged the authors to analyse a new prosthesis prototype to test the ability of the proposed protocol to discriminate critical conditions. The next chapter reports the biomechanical analysis, the design optimisation and an extended pre-clinical validation process over a selected population of interest of a prototype of a new proximal epiphyseal replacement.

REFERENCES

1. McMinn, D. and J. Daniel, *History and modern concepts in surface replacement*. Proc Inst Mech Eng [H], 2006. **220**(2): p. 239-51.
2. Grigoris, P., et al., *Hip resurfacing arthroplasty: the evolution of contemporary designs*. Proc Inst Mech Eng [H], 2006. **220**(2): p. 95-105.
3. Amstutz, H.C., et al., *Metal-on-metal hybrid surface arthroplasty: two to six-year follow-up study*. J Bone Joint Surg Am, 2004. **86-A**(1): p. 28-39.
4. Back, D.L., et al., *Early results of primary Birmingham hip resurfacings. An independent prospective study of the first 230 hips*. J Bone Joint Surg Br, 2005. **87**(3): p. 324-9.
5. Beaulé, P.E., et al., *Metal-on-metal surface arthroplasty with a cemented femoral component: a 7-10 year follow-up study*. J Arthroplasty, 2004. **19**(8 Suppl 3): p. 17-22.
6. Little, C.P., et al., *Osteonecrosis in retrieved femoral heads after failed resurfacing arthroplasty of the hip*. J Bone Joint Surg Br, 2005. **87**(3): p. 320-3.
7. Mont, M.A., et al., *Hip resurfacing arthroplasty*. J Am Acad Orthop Surg, 2006. **14**(8): p. 454-63.
8. Gupta, S., A.M. New, and M. Taylor, *Bone remodelling inside a cemented resurfaced femoral head*. Clin Biomech (Bristol, Avon), 2006. **21**(6): p. 594-602.
9. Long, J.P. and D.L. Bartel, *Surgical variables affect the mechanics of a hip resurfacing system*. Clin Orthop Relat Res, 2006. **453**: p. 115-22.
10. Taylor, M., *Finite element analysis of the resurfaced femoral head*. Proc Inst Mech Eng [H], 2006. **220**(2): p. 289-97.
11. Udofia, I.J., A. Yew, and Z.M. Jin, *Contact mechanics analysis of metal-on-metal hip resurfacing prostheses*. Proc Inst Mech Eng [H], 2004. **218**(5): p. 293-305.
12. Watanabe, Y., et al., *Biomechanical study of the resurfacing hip arthroplasty: finite element analysis of the femoral component*. J Arthroplasty, 2000. **15**(4): p. 505-11.
13. Bergmann, G., *Hip 98 - Loading of the hip joint*. Vol. Compact Disk ISBN 3980784800. 2001: Free University of Berlin.
14. Bergmann, G., et al., *Hip contact forces and gait patterns from routine activities*. J Biomech, 2001. **34**(7): p. 859-71.
15. Heller, M.O., et al., *Musculo-skeletal loading conditions at the hip during walking and stair climbing*. J Biomech, 2001. **34**(7): p. 883-93.
16. Heller, M.O., et al., *Determination of muscle loading at the hip joint for use in pre-clinical testing*. J Biomech, 2005. **38**(5): p. 1155-63.
17. Kishida, Y., et al., *Preservation of the bone mineral density of the femur after surface replacement of the hip*. J Bone Joint Surg Br, 2004. **86**(2): p. 185-9.
18. Amstutz, H.C., P.A. Campbell, and M.J. Le Duff, *Fracture of the neck of the femur after surface arthroplasty of the hip*. J. Bone Jt. Surg. Am., 2004. **86**: p. 1874-1877.
19. Shimmin, A.J., J. Bare, and D.L. Back, *Complications associated with hip resurfacing arthroplasty*. Orthopaedic Clin. North America, 2005. **36**: p. 187-193.
20. Ong, K.L., et al., *Biomechanics of the Birmingham hip resurfacing arthroplasty*. J Bone Joint Surg Br, 2006. **88**(8): p. 1110-5.
21. Itayem, R., et al., *Stability of the Birmingham hip resurfacing arthroplasty at two years. A radiostereophotogrammetric analysis study*. J Bone Joint Surg Br, 2005. **87**(2): p. 158-62.

22. Morlock, M.M., et al., *Biomechanical, morphological, and histological analysis of early failures in hip resurfacing arthroplasty*. Proc Inst Mech Eng [H], 2006. **220**(2): p. 333-44.
23. Radcliffe, I.A. and M. Taylor, *Investigation into the effect of varus-valgus orientation on load transfer in the resurfaced femoral head: a multi-femur finite element analysis*. Clin Biomech (Bristol, Avon), 2007. **22**(7): p. 780-6.
24. Kelly, D.J. and P.J. Prendergast, *Mechano-regulation of stem cell differentiation and tissue regeneration in osteochondral defects*. J Biomech, 2005. **38**(7): p. 1413-22.
25. Cehreli, M., S. Sahin, and K. Akca, *Role of mechanical environment and implant design on bone tissue differentiation: current knowledge and future contexts*. J Dent, 2004. **32**(2): p. 123-32.
26. Duyck, J., et al., *The influence of micro-motion on the tissue differentiation around immediately loaded cylindrical turned titanium implants*. Arch Oral Biol, 2006. **51**(1): p. 1-9.
27. Brown, L., et al., *Reproduction of fretting wear at the stem-cement interface in total hip replacement*. Proc Inst Mech Eng [H], 2007. **221**(8): p. 963-71.
28. Taddei, F., et al., *A combined experimental and finite element study on load transfer and micromotions of a resurfacing hip prosthesis*. Journal of Biomechanical Engineering, Submitted.
29. Lattanzi, R., et al., *Hip-Op: an innovative software to plan total hip replacement surgery*. Med Inform Internet Med, 2002. **27**(2): p. 71-83.
30. Bayraktar, H.H., et al., *Comparison of the elastic and yield properties of human femoral trabecular and cortical bone tissue*. J Biomech, 2004. **37**(1): p. 27-35.
31. Lewis, G., *Properties of acrylic bone cement: state of the art review*. J Biomed Mater Res, 1997. **38**(2): p. 155-82.
32. Zhou, Z.R., V. Pellerin, and L. Vincent, *Fretting - Wear of aluminium and titanium alloys*, in *Titanium & aluminium*, P.A. Coulon, Editor. 1989, I.I.T.T. International. p. 145-153.
33. Viceconti, M., et al., *Numerical model to predict the long-term mechanical stability of cementless orthopaedic implants*. Med Biol Eng Comput, 2004. **42**(6): p. 747-53.
34. Viceconti, M., et al., *Effect of the initial implant fitting on the predicted secondary stability of a cementless stem*. Med Biol Eng Comput, 2004. **42**(2): p. 222-9.
35. Huiskes, R., et al., *Adaptive bone-remodeling theory applied to prosthetic-design analysis*. J Biomech., 1987. **20**(11-12): p. 1135-50.
36. Huiskes, R., H. Weinans, and B. van Rietbergen, *The relationship between stress shielding and bone resorption around total hip stems and the effects of flexible materials*. Clin Orthop Relat Res, 1992(274): p. 124-34.
37. Semlitsch, M. and H. Willert, *Properties of implant alloys for artificial hip joints*. Medical and Biological Engineering and Computing, 1980. **18**(4): p. 511-520.
38. Teoh, S.H., *Fatigue of biomaterials: a review*. International Journal of Fatigue, 2000. **22**(10): p. 825-837.
39. Krause, W., R.S. Mathis, and L.W. Grimes, *Fatigue properties of acrylic bone cement: S-N, P-N, and P-S-N data*. J Biomed Mater Res, 1988. **22**(3 Suppl): p. 221-44.
40. Vandamme, K., et al., *The effect of micro-motion on the tissue response around immediately loaded roughened titanium implants in the rabbit*. Eur J Oral Sci, 2007. **115**(1): p. 21-9.
41. Viceconti, M., et al., *Even a thin layer of soft tissue may compromise the primary stability of cementless hip stems*. Clin Biomech (Bristol, Avon), 2001. **16**(9): p. 765-75.

42. Cristofolini, L., et al., *In vitro replication of spontaneous fractures of the proximal human femur*. J Biomech, 2007. **40**(13): p. 2837-45.
43. Cristofolini, L., et al. *Biomechanical testing of the proximal femoral epiphysis: intact and implanted condition*. in *8th Biennial Conference on Engineering Systems Design and Analysis ASME-ESDA 2006*. 2006. Turin: ASME.
44. Taddei, F., et al., *Subject-specific finite element models of long bones: An in vitro evaluation of the overall accuracy*. J Biomech, 2005.
45. Taddei, F., et al., *The material mapping strategy influences the accuracy of CT-based finite element models of bones: an evaluation against experimental measurements*. Med Eng Phys, 2007. **29**(9): p. 973-9.
46. Giddings, V.L., et al., *A small punch test technique for characterizing the elastic modulus and fracture behavior of PMMA bone cement used in total joint replacement*. Biomaterials, 2001. **22**(13): p. 1875-81.
47. Mann, K.A., et al., *Mechanical characteristics of the stem-cement interface*. J Orthop Res., 1991. **9**(6): p. 798-808.
48. Nuno, N., R. Groppetti, and N. Senin, *Static coefficient of friction between stainless steel and PMMA used in cemented hip and knee implants*. Clin Biomech, 2006. **20**: p. 20.
49. Glyn-Jones, S., et al., *Roentgen stereophotogrammetric analysis of the Birmingham hip resurfacing arthroplasty*. J Bone Joint Surg Br., 2004. **86-B**(2): p. 172-176.
50. Marker, D.R., et al., *Femoral Neck Fractures After Metal-on-Metal Total Hip Resurfacing: A Prospective Cohort Study*. The Journal of Arthroplasty, 2007. **22**(7, Supplement 1): p. 66-71.
51. Schileo, E., et al., *Subject-specific finite element models implementing a maximum principal strain criterion are able to estimate failure risk and fracture location on human femurs tested in vitro*. J Biomech, 2008. **41**(2): p. 356-67.
52. Viceconti, M., et al., *Biomechanics Modeling of the Musculoskeletal Apparatus: Status and Key Issues*. Proceedings of the IEEE, 2006. **94**(4): p. 725-739.
53. Radcliffe, I.A. and M. Taylor, *Investigation into the affect of cementing techniques on load transfer in the resurfaced femoral head: a multi-femur finite element analysis*. Clin Biomech (Bristol, Avon), 2007. **22**(4): p. 422-30.
54. Viceconti, M., et al., *Extracting clinically relevant data from finite element simulations*. Clinical Biomechanics, 2005. **20**(5): p. 451-454.

Chapter 6

Design optimisation and pre-clinical validation of a new conceptual design of a resurfacing prosthesis²

In the previous chapter the method developed for the bio-mechanical analysis of the resurfaced femur has been found able to correctly predict, in general terms, clinical outcomes of a well established design. The next step, described in the present chapter, was to apply the method to a new conceptual design of a new resurfacing prosthesis to test further the ability of the method in predicting the biomechanics of the implanted femur.

To this aim the method was applied to the first prototype of the prosthesis and used to identify the critical regions where adverse conditions may exist and potentially propagate up to failure. Once the first prototype presented a sub-optimal biomechanical behaviour, a geometry optimisation loop was carried out modifying the prosthesis design and analysing the intermediate geometries by means of finite element (FE) models.

The resulting optimised design presented a very low risk of failure for all of the investigated failure mode, under a large series of conditions the prosthesis may face during its service life. This result was partially confirmed by destructive tests conducted in parallel by the experimental group of the LTM, which highlighted a significantly reduced risk of neck fractures on cadaver femurs implanted with the optimised prosthesis

Although a large series of different implants and boundary conditions are represented by its respective model, a complete pre-clinical validation study should include the entire range of probable situations over the whole population the prosthesis is indicated to.

² The prosthesis name and geometry and all results obtained during the study to which this chapter refers to are protected by a non-disclosure agreement between IOR and the Manufacturer. The results reported in this chapter have been intentionally altered not to publish confidential information but, at the same time, to allow a clear explanation of the work done.

An agreement on future publications has already been achieved between the two parts, so results will be shortly public. Current tentative titles are:

- Pre-clinical validation of a new hip resurfacing prosthesis. Part I: design revision and optimisation by means of a combined numerical-experimental procedure
- Pre-clinical validation of a new hip resurfacing prosthesis. Part II: evaluation of the clinical indication by means of a FE probabilistic study
- Combined influence of body weight, degree of osteoporosis and load intensity on the risk of spontaneous fracture in the femoral neck during daily activities: a probabilistic FE study

This was the aim of the next analysis which was statistically performed by simulating the variation of a number of factors depending on surgery uncertainties and on the individual anatomy and activity.

Results confirmed the low risk of failure of the optimised design emerged from the deterministic analysis, thus the prosthesis which recently started the clinical trials, should be considered safe for its intended function.

6.1 Preliminary finite element study of the first prosthesis prototype

The conceptual design of the first prototype of the prosthesis was carried out by the manufacturer and provided to LTM in the form of 3D models defining both the prosthesis geometry and the reaming preparation of the host femur. The initial analysis of the proposed design was aimed to:

1. Building a provisional finite element model (FEM) of the bone-implant system;
2. Solving possible meshing problems;
3. Providing a preliminary indication of the potential results that can be derived from this finite element model.
4. Assessing the effect of different adhesion at the stem bonding interface;

6.1.1 Materials and methods

6.1.1.1 CT Dataset

CT data used in present study have been already discussed by Taddei [1], most important aspects are briefly reported:

- Right femur from a 51-year-old male, weight 75 kg
- CT scan (HiSpeed, General Electric Co., USA) performed using physical parameters of clinical practice (tube current: 180mA, 120kVP)

6.1.1.2 The finite element model of the intact femur

An extensive description of the intact model is given in chapter 2. The reader should refer to that section for further details.

Creation of the FE model of the implanted femur

The model used in the present study was developed using the aforementioned procedure. After the creation of the NURBS model of the femur, this was imported into a CAD program (UG, Unigraphics Solutions, USA) together with the CAD model of the prosthesis and of the reaming tools which is used to create the cavity in the hosting bone where to seat the prosthesis. The relative position of the prosthesis and the femur was defined in agreement with the pose planned by the surgeon inside the Hip-Op[®].

The prosthetic model was de-featured in order to remove those small geometric features that would prevent an accurate finite element modelling. The cavity inside the femur, sufficient to host the nominal cement thickness, was generated by Boolean subtraction from the femur of the rasp geometry.

The femur was meshed with 30305 ten-node quadratic tetrahedral elements. A progressing refinement was used toward the interface with the cement, in order to accurately follow the expected stress gradient.

The cement layer was modelled with 3384 eight-node iso-parametric hexahedral elements in the interface region, and with 2198 ten-node quadratic tetrahedral elements in the distal cone, 132 pyramidal elements were used to connect the two sub-regions.

The prosthesis was meshed with 15397 ten-node quadratic tetrahedral elements in the stem region, connected to 6050 eight-node iso-parametric hexahedral elements in the head region. 2687 pyramidal elements and 1580 pentahedral elements connected the two sub-regions.

The bone was modelled as linear elastic, locally isotropic but non-homogeneous material, which produced a globally anisotropic model. The local mechanical properties of the bone tissue were derived from the CT data following the method described for the intact femur [1]. The resulting constitutive description includes 366 independent materials.

The prosthesis and the cement were modelled as linear elastic isotropic materials. The prosthesis was given the average material properties of a typical CoCr medical alloys ($E = 200$ GPa, Poisson = 0.3). The cement was given the material properties of Simplex P (Simple P, Stryker, USA) ($E = 2500$ MPa, Poisson = 0.3, [2]), a cement type largely used in resurfacing surgeries [3, 4].

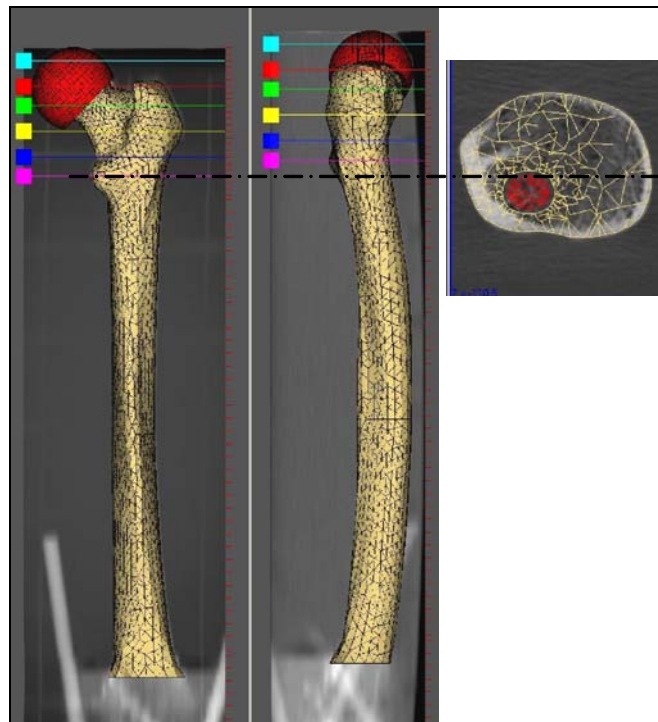


Figure 1 - visualisation of the femur mesh superimposed to the CT data set

Boundary conditions

Two loading conditions were modelled, mimicking the peak joint load instants during level walking (LW) and stair climbing (SC) [5]. The most important muscle groups acting in the proximal femur were modelled, according to previous studies [6].

Modelling of different conditions at the prosthesis-bone and prosthesis-cement interface

Two separate models were generated in order to simulate two extreme conditions.

In the first model, three contact interfaces were defined. Bone-cement interface was assumed fully bonded in all cases. Bone-prosthesis and cement-prosthesis were assumed in frictional unilateral contact, with coefficient of friction equal to 0.3[6, 7].

A second model was created where also the prosthesis interface was assumed fully bonded. Contact was modelled using zero-thickness face-to-face large-sliding contact elements that monitor the co-penetration at the Gauss points.

Solution

The final model has 343128 unconstrained degrees of freedom. The model was non-linear because of the contact condition, which was formulated using an Augmented Lagrangian approach. The non-linearity was solved using a Newton-Raphson solver, which monitored the convergence on the quadratic norm of the residual force vector. Convergence tolerance was set to 0,5% of the L2-norm of the force vector. The single iteration within the Newton-Raphson scheme was solved using a Pre-Conditioned Conjugate-Gradient Solver with a convergence tolerance set to 1.0E-07.

Verification of the numerical accuracy of the model

Verification aim to establish the numerical accuracy of the results obtained with a finite element model. In the present study we can identify two potential sources of numerical errors: errors due to the discretisation of the domain, and errors due to the penetration recovery at the contact interfaces.

The quality of the mesh was assessed using the post-hoc error indicator proposed by Zienkiewicz and Zhu [8] under the stair climbing loading condition, which was the one producing the stronger stress gradients. For the mesh of the prosthesis, the average error was 8% and the E90 (90th percentile of the error distribution) maximum error was 23%. For the cement mesh the average error was 13%, and the E90 maximum error was 28%.

For the femur, the problem was more complex since this error estimator cannot be applied to non-homogeneous materials. When the model was solved assigning to the bone elements a homogeneous elastic modulus of 7000 MPa, the average error was 26% and the E90 maximum error 34%.

An analogous post-hoc indicator, based on the strain energy error yielded an E90 maximum error of 5% for the prosthesis, 8% for the cement, and 12% for the femur.

The co-penetration error, due to the imperfect solution of the contact was used as an indicator of the numerical accuracy of the contact results. In both loading conditions the model reported a co-

penetration of less than 2 microns over most of the interface, with only a peak of 5 microns (level walking) and 8 microns (stair climbing) in the area where the joint reaction was applied.

Validation of the model

In this preliminary study a direct validation of the finite element model of the implanted femur against experimental measurements was not required. On the basis of previous studies we can claim a typical average accuracy in the order of 10-20% with respect to in vitro measurements [9].

6.1.2 Results

Prosthesis

The predicted levels of stress induced in the prosthesis by the two loading conditions here considered are moderate. Under the load case associated to the peak joint load during level walking the peak principal tensile stress is 80 MPa, while the Von Mises stress reaches the 100 MPa. The peaks of stress were located in the medial and lateral aspects of the stem. The stress distribution was uniform, indicating a proper design of this region. Under the loading condition mimicking the peak joint load during stair climbing the two peak stresses were 90 MPa and 120 MPa, respectively.

The prosthetic interface was quite stable. The model predicts a peak inducible tangential micromotion of only 70 microns during level walking and of 90 microns during stair climbing.

The peak inducible normal micromotion at the prosthesis interface (detachment) was much larger, topping 500 microns in both loading cases. However, this very high value is associated to a border element, and thus it is not significant. Most of the implant interface detach for less than 30 microns. Notable exceptions were two longitudinal bands in the lateral aspect of the stem, where the detachment reaches 250 microns. This pattern was not compatible with a rigid motion at the interface and thus can be explained only with a complex stress pattern in that region. If the model was run with only the joint force applied, this contact pattern did not change substantially. Thus, it can be excluded that this contact pattern is due to an artefact related to the application of the muscle forces.

Cement

The cement mantle is subject to significant stresses. The peak principal tensile stress is 70 MPa simulated during level walking and 80 MPa during stair climbing. Both peaks are located at the distal end of the cement mantle. This stress condition in the cement mantle is confirmed by the contact pressure at the interface, which reaches its maximum value, 60 MPa, at the distal tip of the stem.

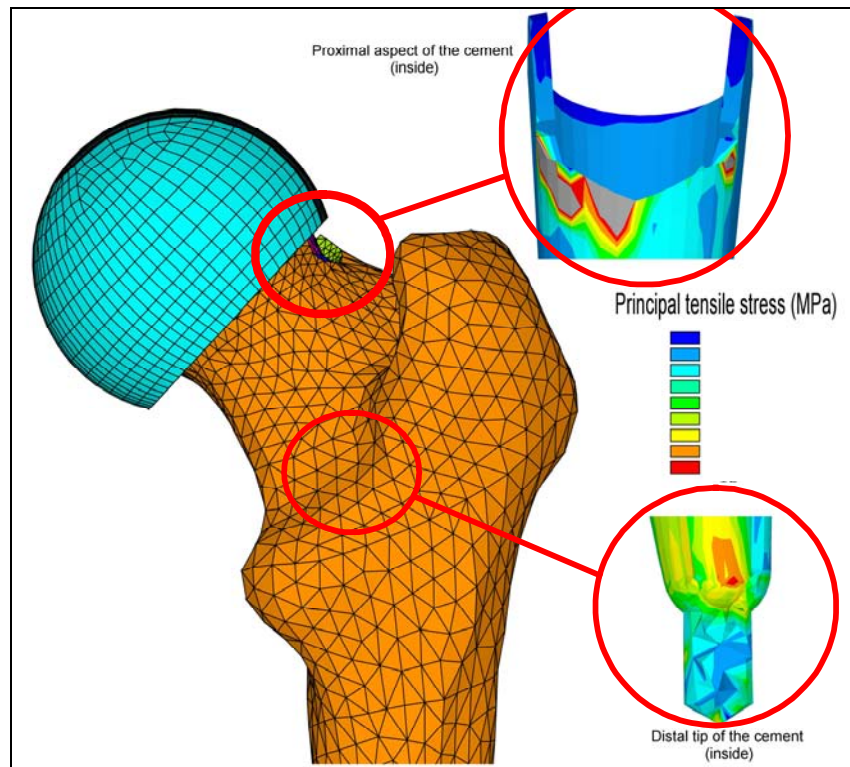


Figure 2 – Regions at high risk of fracture on the bone cement

Host bone

The stresses in the bone were monitored in a region of interest (epiphysis and the metaphysis of the femur) with the exclusion of two small lateral regions where the concentrated application on the muscle forces produces artefacts.

The stresses in the superior aspect of the femoral neck were always lower than 30 MPa. The risk of fracture, computed using an already validated procedure[10], was calculated on the basis of the density value derivable from the CT dataset. The ultimate stress value, for each element of the mesh, was defined taking into account the different behaviour of bone to tension and compression stresses. Simulations of the stair climbing loading condition highlighted a risk of failure lower than 60%.

The levels of hydrostatic stress in the portion of bone encapsulated by the prosthesis was below 10 MPa everywhere. Also the contact pressure on the bone was always in the order of one MPa.

Bonded vs. Frictional contact model

When the interface between the prosthesis and the cement was also assumed bonded, the stress pattern in the cement did not change substantially, with one notable exception. Under the stair climbing loading condition the peak principal tensile stress reaches the 500 MPa in a small region near the superior border of the cement mantle. The peak contact pressure at the bonded interface is 250 MPa. This value is positive, indicating interface traction. Similar values are predicted for the level walking condition. *Table 1* reports the main nodal stress values predicted by the two models in the position where the frictional contact model predicts the peak value for that result.

Normal walking load case		Frictional contact	Bonded contact
Cement	Principal tension stress[MPa]	40	30
	Principal compression stress [MPa]	-20	0
Contact	Contact pressure [MPa]	40	10
Up stairs load case		Frictional contact	Bonded contact
Cement	Principal tension stress[MPa]	40	37
	Principal compression stress [MPa]	-25	-10
Contact	Contact pressure [MPa]	60	20

Table 1 – Comparison of peak stress values predicted by the frictional contact and the bonded contact model

6.1.3 Discussion

The results are commented in the frame of the most common failure scenarios reported for joint replacements.

Prosthesis fracture

Due to the minimal stress levels the event of a prosthesis fracture unlikely occur.

Cement fracture

The cement presents a tensile strength in the range of 10-50 MPa, and a fatigue limit at one million cycles of 14 MPa [2]. Due to the high peak tensile principal stress (>50 MPa) predicted there are very high chances that the cement mantle will fracture within the first million of loading cycles. Locations of peak tensile stresses are at the connection of the mantle with the tip and at the superior rim. Thus, it is possible that the distal bottom of the cement will detach from the rest of the mantle, and that a crack propagates from the superior rim downward through the cement mantle. It is unclear how failure would progress once the cement starts fracturing. It may be possible that after some damage, the stresses redistribute and the scenario do not evolve into a complete fragmentation.

Bone fracture

Standing on the indications obtained from the finite element model, it seems that the presence of the prostheses mildly reduce the strength of the host bone. However, for a normal healthy bone like the one here considered, this reduction does not produce any failure scenario under physiological loading conditions. From these results however, it is difficult to say what may be the condition when osteopenic bones are involved.

Interfacial tissue differentiation due to excessive micromotion

This failure scenario, typical of cementless devices, could eventually appear here in the subcapital plateau, where the cement thickness is nearly zero. However, the level of inducible

tangential micromotion predicted by the model does not raise any concern in this sense. In all loading conditions the peak micromotion was always below those 100-150 microns, which is the threshold for fibrous differentiation [11, 12].

Bone resorption due to debris produced by metal-cement fretting

The production of fretting debris is governed by a combination of large contact pressures and large tangential micro-movements. For what concerns the risk of fretting behaviour, monitored by the stem-cement relative displacement, the calculated micromotion never exceeded the critical value[13]. Thus, the production of PMMA debris would unlikely happen.

6.2 Sensitivity of the risk of failure to some factors of influence

The bio-mechanics of the implanted femur depends on a variety of bio-mechanical parameters which characterise any specific implantation and potentially affect the resulting risk of implant failure. The first bio-mechanical analysis of the proximal femur over a large set of operative conditions is described in this paragraph. The analysis explored:

- The influence of different surface finishes of the stem
- Different penetration depth of the cement in the bone layer surrounding the prosthesis stem
- Different levels of bone mineralization so as to simulate the structural effect of the osteoporosis.

To this aim a significant number of FE models were generated by varying each bio-mechanical parameter of interest.

Results highlighted that the main concerns of failure raised by the first study are consistent also through a large number of operative conditions here reported, thus revision of the prosthesis geometry should be considered.

6.2.1 Roughness of the stem surface

Manufacturing a new product is an activity that requires a number of choices which might have some implications on the final performances. One of these choices involve defining the surface roughness of the device surfaces.

The effect of the friction coefficient at the two counter-faced surfaces on the stability of the implant prosthesis micromovement was not clear. The aim of this study is to verify if the stem surface roughness significantly affects the prosthesis micro-movements and the cement stresses.

6.2.1.1 Modelling data

The femur, the size of the prosthesis and its positioning were the same and discussed with more detail in paragraph 1.1. Following lines explain only the new aspects of the present study.

Loading condition

The set of boundary conditions simulated in paragraph 6.1 was completed by the simulation of a third activity. This new added load (single leg stance, SLS) was found to be significant in producing neck fractures, reasonably coherent with spontaneous fractures observed *in-vivo* [14]. This scenario is discussed with more details in Chapter 4.

Contact conditions

To verify the sensitivity of the predicted micro-movements to stem surface roughness two new models were generated with null friction coefficient, simulating a perfectly polished surface, and with friction coefficient 0.6, simulating a pretty rough matte surface.

6.2.1.2 Results

Bone-cement relative micromotion

The most critical activity for this failure mode was SLS. The inducible elastic tangential micromotion (*Table 2*), is significantly higher for the frictionless stem which reaches a value (50 microns) close to the safe threshold for cement fretting (50 microns) [13].

	$\mu = 0$	$\mu = 0.6$
Max Sliding (μm)	50	25

Table 2 – Maximal sliding distance (microns). μ = friction coefficient.

Cement stresses

The peak principal tensile and compressive stresses induced in the cement mantle under a stair-climbing loading condition, which is the most critical for the cement, are reported in the table below (*Table 3*). The peak tensile stress is slightly influenced by the variation of the friction coefficient, on the contrary the tensile stress, located at tip stem, is slightly higher for the frictionless stem.

	$\mu = 0$	$\mu = 0.6$
Principal tensile stress (MPa)	10	10
Principal compressive stress (MPa)	-20	-10

Table 3 – Principal cement stresses (MPa). FC = friction coefficient.

6.2.2 Interdigitation

Aim of this study was to investigate the effect on the implant biomechanics of two different level of interdigitation.

6.2.2.1 Methods

The range of thickness of the interdigitated bone layer was assumed to range between zero and three millimetres, with localised peaks of 7-8 mm as estimated by an experienced surgeon. We selected the surface that in the model separates the cement from the bone, and created a new surface by offsetting the first by a given amount. We created two surfaces, one offset by 2 mm, and the second offset by 4 mm. We assumed the two layers of elements are representative of the

interdigitation layer for a mild and strong penetration of the cement. From the CT images of the proximal femur, the separating contour between the cortical and the cancellous bone was visually identified. The average density (0.55 gr/cm^3) of the separating contour was defined as the density threshold to distinguish between cortical and cancellous bone regions. From the interdigitated layers we excluded all elements with a mineral density above 0.55 gr/cm^3 , as we assumed that the cements can penetrate only in the cancellous bone.

At this stage it was of interest the estimation of the sensitivity of the FE results to the variation of the elastic support of the peri-prosthetic bone thus the effect of the interdigitation was roughly modelled (see paragraph 6.8 for a more sophisticated model of the elastic effect of interdigitation). The elasticity modulus of the interdigitated layer was increased assuming that penetrated layers reached the average module of elasticity of the pure cement.

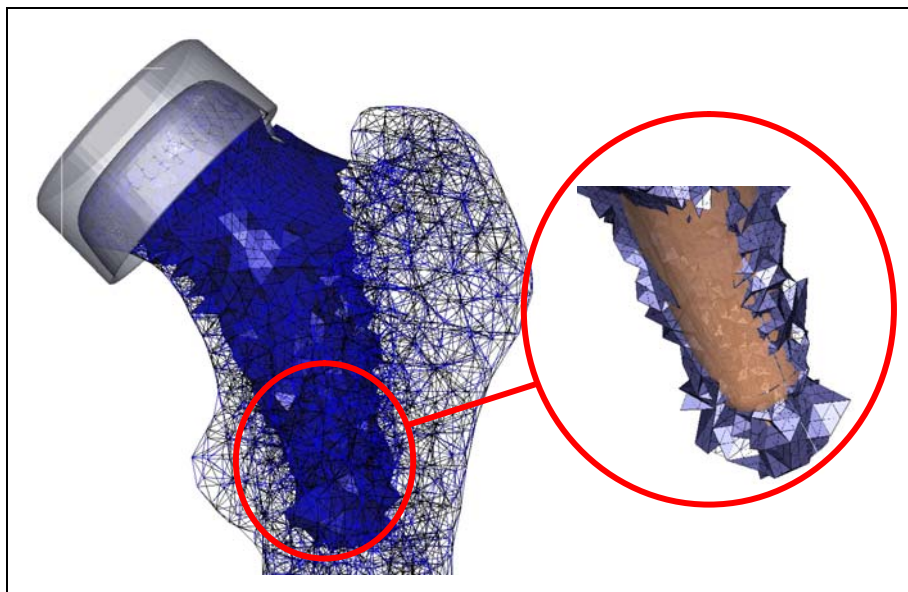


Figure 3 - Interdigitation layer. Left: region of the bone assumed to be filled with cement; Right: interdigitation elements emerge from the original cement-bone interface

6.2.2.2 Results

The presence of interdigitation reduced substantially the stresses in the cement mantle. The peak stresses in the cement mantle at the distal tip and at the supero-lateral aspect of the stem remain above the fatigue limit for the PMMA (8-10 MPa, [2]). Under stair climbing loads the peak tensile principal stress was 20 MPa in the apex region and 250 MPa in the superior-lateral region.

6.2.3 Osteoporosis

In the previous study we predicted the risk of fracture in the bone tissue during stair climbing and level walking. These results were referred to the degree of mineralization of the cadaver femur we used to generate the FE model, which was considered non-pathological. Aim of the present study was to verify how the risk of fracture map changes if the host bone is affected by a

mid or a severe osteopenia. To this aim a reduction of the bone mineral content was applied to the cortical and the trabecular bone generating two additional models: one representing a femur affected by a severe osteoporosis and the second representing a mid way between the severe osteoporosis and the normality.

Simulations highlighted a significant increase of the risk of bone fractures as the osteoporosis level increase, particularly on the implanted femur. These results support, once again, the need of reviewing the prosthesis geometry.

6.2.3.1 Methods

The main problem was to define how the tissue density changes during the osteoporosis as function of the initial tissue density, or better of the histological type of bone tissue (cortical, cancellous, etc.). In similar studies other authors assumed that the cancellous bone resorb twice as quickly as the cortical bone[15]. This observation is confirmed by an experimental study where the ratio between the mineral density at the age of 20 years and at the age of 80 years is 20% for the cortical bone, and 50% for the cancellous bone[16].

The CT data do not provide information on the histological type of the bone tissue. Thus, we have to discriminate cortical and cancellous bone only on the basis of the tissue mineral density. Three independent operators estimated the density value that separates the cancellous bone from the cortical bone. The average value 0.55 gr/cm^3 was assumed as the threshold to distinguish between the two tissues types.

We created two osteoporosis models, one reducing the mineral density of the cortical bone elements by 10% and of the cancellous bone elements by 20%; the second by reducing the cortical bone of 20% and the cancellous bone of 40%. Simulations were run for level walking (LW) and stair climbing (SC). The risk of fracture were computed as the ratio between the predicted bone strain and the ultimate strain to fracture of 0.7%[17].

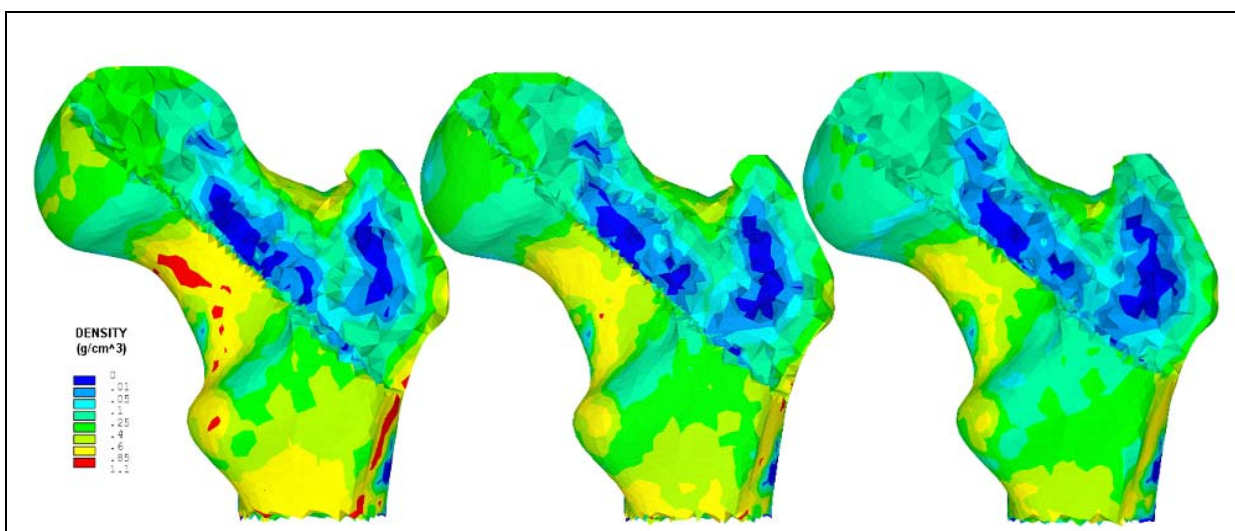


Figure 4 - Mineral density distribution (g/cm^3) in the normal model (left), in the 10-20% model (centre) and in the 20-40% model (right).

6.2.3.2 Results

The maximum risk for femoral neck fractures computed for each model and activity is reported in Table 4. The normal femur has a risk of fracture always below 50%, predicting a fracture scenario only for sever impacts. The 10-20% femur has a risk of fracture of 80%, so no spontaneous fractures are expected, but there is a risk of fracture for simple side falls. The 20-40% femur has high chances to develop spontaneous fractures of the femoral neck during daily activities.

Mineralization	Model	RF ave		RF peak		Vol RF>1 [mm ³]	
		Level walking	Stair climbing	Level walking	Stair climbing	Level walking	Stair climbing
NORMAL	Intact	25%	20%	57%	66%	0	0
	Implanted	18%	20%	200%	200%	5	5
OSTEOPOROSIS 10-20	Intact	30%	30%	100%	100%	0	0
	Implanted	20%	22%	150%	200%	5	5
OSTEOPOROSIS 20-40	Intact	40%	50%	150%	150%	100	180
	Implanted	30%	45%	200%	300%	100	300

Table 4 - Average (RF Ave) and peak (RF peak) risk of fracture in the femoral neck region. The table also reports the volume of bone tissue in the femoral neck region that in each case has a risk of fracture greater than 100%.

6.2.4 Discussion

Roughness

The aim was to investigate the effect of different surface roughness on relevant parameter for the prosthesis stability. Results shown that a rough surface finish produces a significant reduction of both micromovement and cement stresses over polished surfaces. Hence, rough surfaces at the bone-prosthesis and cement-prosthesis bonding interface are preferable.

Interdigitation

The aim was to investigate the effect of different interdigitation thickness to the implant stability. The module of elasticity of the cancellous bone in that region is lower than that of the cement; thus we are making a very optimistic assumption. Even so, the cement interdigitation thickness do not allows a significant reduction of cement stresses, thus a revision of the prosthesis design should be considered.

Osteoporosis

The aim was to investigate the effect of different levels of the bone mineralization on the risk of neck fractures. When the predictions of the various models are compared, a figure of sense emerges. In the normal bones the presence of the prosthesis stem does not substantially alter the risk of fracture of the intact femur. During level walking the average risk is reduced, while in stair climbing is unchanged. The prosthesis created a small notch in the superior-lateral aspect of the femoral neck, and in that region the risk of fracture goes quite high. However, it is difficult to

predict the real risk associated to the stress raiser as only a very small volume of bone was interested by excessive stresses. The severe osteoporosis (osteoporosis 20-40) model yields mixed results. The average risk is always reduced. The volume of bone tissue with risk higher than 100% decreased under level walking and increases under stair climbing.

6.3 Results of experimental tests on the first prototype

The experimental group of LTM carried out disruptive tests on a first group of cadaver femurs. The scope of this work was to assess the failure load and failure mechanism of the proximal femur implanted with the first prototype.

A total of 7 pairs of fresh frozen cadaver human femurs obtained through the International Institute for the Advancement of Medicine.

Statistics on the failure load, normalized in terms of the average strength of the intact femur, are reported in the

Figure 5. The femur implanted with the first prosthesis prototype resulted, in average, 20% weaker than the intact contralateral one.

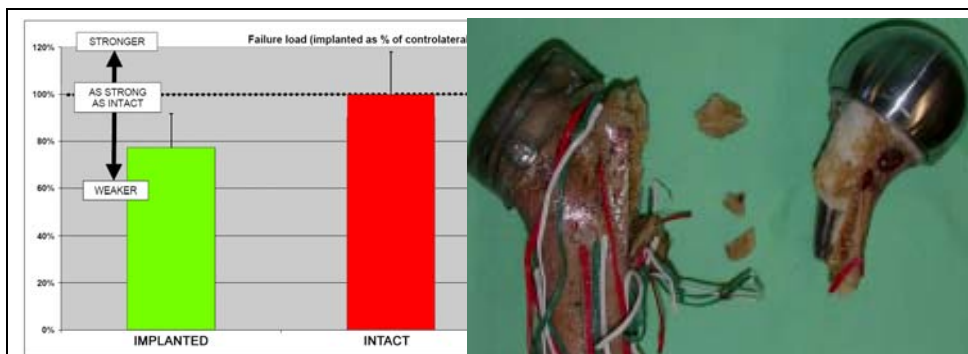


Figure 5- Failure loads: On the left, the average load to failure between specimens. On the right, an image of a fractured specimen.

Failure of the implanted femur initiated consistently from the notch on the lateral side of the neck, caused by implantation. The FE study resulted in excellent agreement with present results.

6.4 First step of design revision: refinement of the first prototype geometry

In order to reduce the stress levels in the cement mantle, resulted excessively high in previous simulations, the prosthesis shape was modified. The aim of this study was to investigate the biomechanical behaviour of the first prototype after the first revision of the geometry.

6.4.1 Materials and methods

Material details, modelling techniques, model verification and validation and simulations details were similar to what described in paragraph 6.1. The new model was generated modifying the procedure described above in the following aspects:

1. The stem was reduced in the medio-lateral thickness, preserving the medial curvature.

2. The rasp geometry was modified in order to guarantee a minimum thickness of cement of the mantle even when no interdigitation occurs. Lastly, the length of the rasp was increased so as to guarantee a thickness of the cement mantle also at the distal tip of the stem.
3. The presence of the interdigitation layer was considered a variable, and we investigated the model with and without it. The biomechanical properties of the interdigitated layer were defined in agreement with the previous study.
4. The mesh of the intact femur was modified so as to present the mesh of the stem as a sub-structure. In other words, on both models the elements that mapped bone tissue were identical in terms of numbering and geometry. This allowed an element-wise calculation of the stress shielding.
5. The resulting constitutive description include 366 independent materials. The final model had 362543 unconstrained degrees of freedom.
6. The modified intact bone model yielded results substantially identical to the previous one, which was fully validated.

6.4.2 Results

Stem stresses

Even with this significant reduction in size the stresses in the stem was significantly below the fatigue limit of the alloy used to manufacture it. We can thus exclude any risk of fracture of the metallic stem.

Bone-cement relative micromotion

The new design was significantly more stable than the previous one, with a reduction of the peak inducible tangential micromotion of 30 microns against the 100 microns of the previous design. Also the detachment was always below 50 microns. Thus, we can exclude any risk of fretting-related failure scenarios.

Cement stresses

The peak tensile stress in the cement mantle of the new design was significantly lower than in the previous design. Also the huge stress peaks in the supero-lateral aspect were now absent. On the contrary, the peak Von Mises stresses in the distal tip remains quite high even though in a very small region. Another interesting result is that if the interdigitation is removed, the stresses in the cement were decreased. This seems to suggest that the cement mantle design is now optimal.

Risk of bone fracture

The optimised design solved the stress concentration problem in the supero-lateral aspect. The principal tensile strains in the femoral neck are now below those predicted for the intact femur under similar conditions. Thus, we can exclude any failure scenario related to the spontaneous fracture of the femoral neck under the action of physiological loads.

Stress shielding

Also the stress shielding produced by the new stem design was reduced with respect to the previous model. The principal compressive stress map predicted after the geometry revision was more similar to the one predicted for the intact femur than what predicted for the first prototype of the prosthesis. The significant stress shielding that the first prototype was producing in the medial aspect of the femoral neck is drastically improved. The histogram of frequency of the changes of the strain energy density, which is commonly considered as the biomechanical stimulus for bone remodelling [18], shows that in the original prosthesis design a significant number of elements were exposed to changes if SED (Strain energy density) larger than 0.008 J/gr. This produce a significant skewness in the histogram, which was almost absent in the histogram of the new design. With the new design less than 1% of bone volume of the reamed ephyphiseal femur was affected by changes in the SED field exceeding the activation threshold.

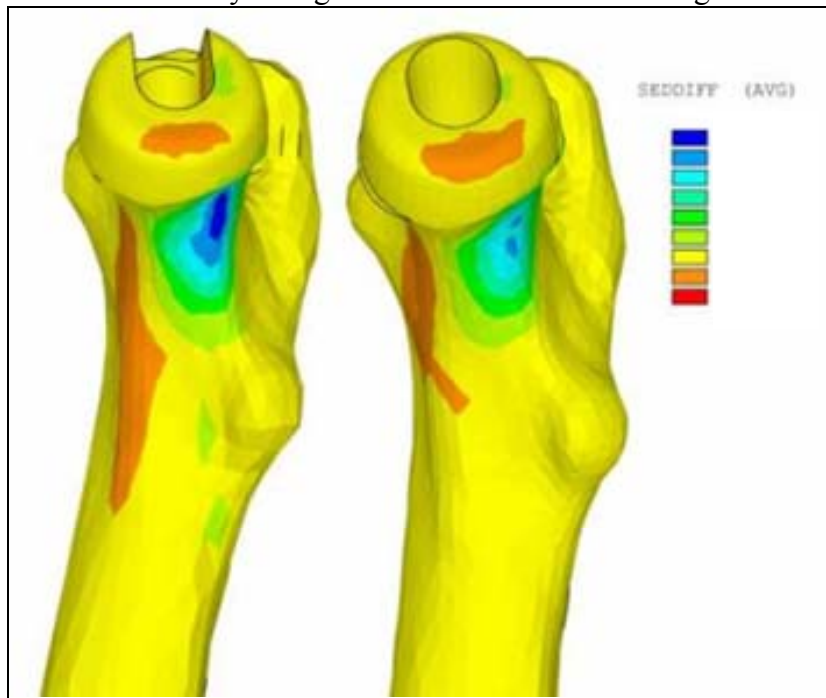


Figure 6 - Change in the strain energy density due to the presence of the prosthesis stem in the old design (left) and in the new design (right)

6.4.3 Discussion

The results for the revised design were discussed in the frame of the most common failure scenarios reported for joint replacements.

Prosthesis fracture

On the basis of the present results the risk of fatigue fracture of the prosthesis stem is negligible.

Cement fracture

On the basis of the present results the risk of fatigue fracture of the cement mantle is negligible. However, the fatigue fracture of the cement cannot be completely excluded as the peak stress remains high even if in a very small region. As the volume interested by high stresses is very low

it is not possible to discriminate between two different possible scenarios. On one hand, it is not possible to exclude a damage accumulation leading to fracture and in the other hand it is not possible to exclude that, after a local plastic deformation of the implant would reach a stable state.

Production of PMMA fretting debris

On the basis of the present results the risk associated to the production of debris due to the stem-cement relative micromotion under load is negligible.

Bone fracture

On the basis of the present results the risk of spontaneous fracture of the femoral neck in non-osteoporotic patients is negligible. However, a very low level of bone mineralization seems to significantly increase the risk of neck fractures. This aspect might be studied by a parametric FEM analysis so as to evaluate how this risk changes for mildly and severely osteoporotic patients.

Risk of adverse bone remodelling

In this analysis we evaluated the so-called stress shielding, the changes in the strain energy field in the bone tissue due to the insertion of the stem [18]. In general the stress shielding was moderate; the revised design achieved also the objectives of minimal stress shielding requested in the design specifications. It is, however, unclear whether this limited region of stress shielding should be a source of concern.

6.5 Sensitivity of the risk of failure to influencing co-factors

In this paragraph the sensitivity study of the first prototype after the first revision of the geometry is described. Different operative conditions were studied by simulating the surgical uncertainties, the maximum and the minimum implant size and different surface finish of the stem.

6.5.1 Surgical errors: prosthesis mispositioning

The uncertainties with which the prosthesis is inserted in the hosting femur are variables that potentially affect the implant success or failure. It is necessary to understand if and to what extent the desired bio-mechanical behaviour of the implant is influenced by a sub-optimal positioning of the prosthesis. This would provide interesting information on the effectiveness of the current prosthesis geometry and on the accuracy needed for implants of good quality.

Aim of this study is to quantify the effects of implanting the prosthesis with slight position/orientation mismatches, on the stress levels in the cement mantle and the periprosthetic bone. The study should conclude with a recommendation to the degree of accuracy and repeatability that the prosthesis size range and surgical instruments should attain for safe implantation.

6.5.1.1 Material and methods

The description of data used for the generation of the FE model has been extensively discussed in paragraph 6.1 as well as modelling procedures. In the following lines modelling aspects and methods adopted for simulating the prosthesis misalignment and misplacement, of interest in present study, are described.

Four additional models were generated to simulate the prosthesis malpositioning during surgery. An estimate of realistic extreme errors in prosthesis position was provided by an experienced surgeon. The new models were obtained by translating the prosthesis 3 mm superiorly, laterally, inferiorly, and medially, with respect to the ideal position (paragraph 6.4).

Other two models were added to simulate angular misalignment in varus and valgus direction. The prosthesis was rotated with respect to the head centre of 2° in the valgus direction and 10° in the varus direction. The resulting positions were obtained in the HipOp[®] software [19].

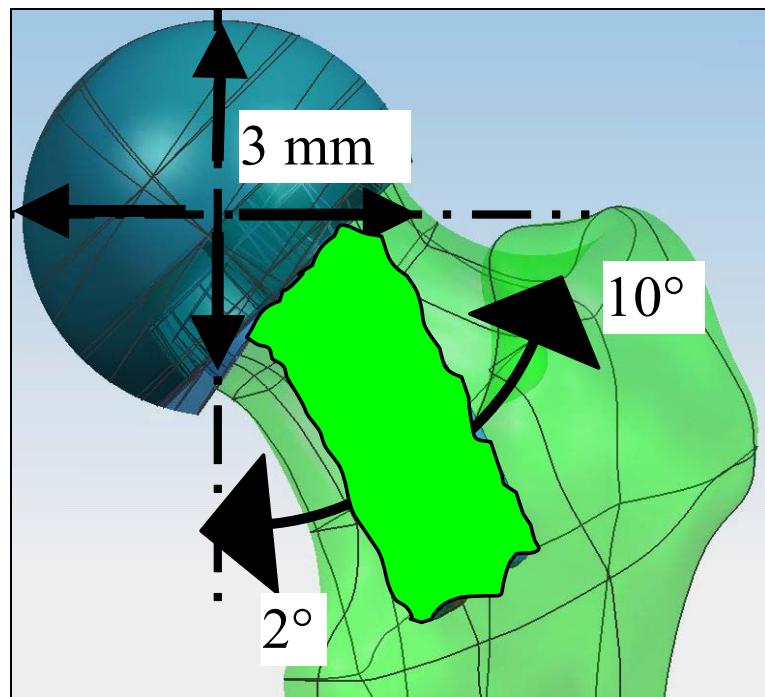


Figure 7 – Scheme of the simulated misalignment (10° in the varus and 2° in the valgus direction) and mislocation (3mm in the medial, lateral, cranial and caudal direction) of the stem

6.5.1.2 Results

Stem mispositioning

The main results are summarised in *Table 5*. The inducible micromotion was mildly sensitive to the stem position. The peak micromotion changes between 25 and 50 microns, with the notable exception of the superior stem under single leg stance where the peak micromotion is 100 microns.

		positions				
		ideal position	superior	lateral	inferior	medial
SL	Slid_max [μm]	25	100	30	50	50
	$\sigma_{1\text{cem}}$ [MPa]	5	5	5	6	9
	$\sigma_{1\text{neck}}$ [MPa]	10	5	7	7	10
SC	Slid_max [μm]	35	50	20	40	35
	$\sigma_{1\text{cem}}$ [MPa]	5	5	10	10	10
	$\sigma_{1\text{neck}}$ [MPa]	10	10	10	10	10

Table 5 - peak inducible micromotion (*Slid_max*) and peak tensile stress in the cement ($\sigma_{1\text{cem}}$) and in the femoral neck ($\sigma_{1\text{neck}}$) under the action of Single Leg Stance loading (SLS) and stair climbing loading (US) for the five positions of the stem.

The average peak tensile stress in the cement over the five positions was 6 MPa under single leg stance and 8 MPa under stair climbing loading. The largest stress is 10 MPa, found in the model with the stem translated medially under stair climbing.

The peak tensile stress in the femoral neck for the translated models is always equal or inferior to that predicted for the ideal position, suggesting that the ideal position produces the least stress shielding. No stress concentrations was found in any position.

Stem misalignment

In all examined prosthesis positions, the highest stresses were found in the stem and it was significantly below the fatigue limit of the alloy used to its manufacturing. We can thus exclude any risk of fracture of the metallic stem. The highest stresses were calculated for the 2° valgus position and decrease as the prosthesis is rotated in the varus direction.

In all cases the prosthesis was stable with a peak inducible tangential micromotion always lower than 40 microns. Thus, we can exclude any risk of fretting-related failure scenarios.

For all the models, the peak contact pressure is found near the tip of the prostheses for the upstairs climbing loading scenario. The maximum value is reached in 2° valgus condition (30 MPa), higher than in the other two positions, for which the peak is around 10 MPa. This increase is probably due to the slight cortical penetration achieved with the 2° valgus position.

The peak stresses in cement increase as the prosthesis is rotated towards the valgus direction (Table 6). The principal tensile stress is however always lower than the fatigue limit of the cement (14 MPa).

	10° varus	Optimal pos.	2° valgus
Principal tensile stress	3	10	15
Principal compressive stress	-15	-20	-30

Table 6 - Principal cement stresses (MPa)

The position and the magnitude of the peak tensile strain region in the femoral neck are comparable in all three cases and are below those predicted for the intact femur under similar conditions. Thus, failure scenario related to the spontaneous fracture of the femoral neck is not expected.

No relevant stress shielding is registered for all different positions, as the bone volume exceeding the activation threshold for bone remodelling never exceeded the 4% in volume of the femoral epiphysis. The maximum value is predicted for the 2° valgus position, in the medio-posterior aspect of the femoral neck. The stress-shielded bone volume reduces as the prosthesis is moved in the varus direction.

6.5.2 Anatomical variability: femur size

The aim of present study was to verify that no failure scenario is significantly affected by the implant size. To this aim the simulation of the biomechanical behaviour of the implant, under the SLS, LW and US loading case, was repeated on two additional models, representing the two extremes of the patients' anatomy from the IOR database. We retrieved two CT scan that present a normal anatomy and bone stock. The smallest femur (biomechanical length: 370 mm) represented the lower extreme and the biggest one (biomechanical length: 480mm) represented the upper extreme for femur sizes. These two femurs were used to create two additional FE models so as to simulate the smallest and the biggest implant.

6.5.2.1 Material and methods

The description of data used for the generation of the average size FE model has been extensively discussed in paragraph 6.1 as well as modelling procedures. The other two models were generated following the same procedures, thus in the following lines are described materials and modelling aspects that distinguish the new models from the one already generated.

CT dataset

Among the CT dataset of patients collected in-vivo for clinical purposes available in the IOR database, the two dataset representing the biggest and the smallest femur were selected for the present study. Details of the two individuals and of CT data (Patient A and patient C) are reported in *Table 7* together with data of the femur used for the previous study (Patient B):

	Biggest femur (Patient A)	Medium femur (Patient B)	Smallest femur (Patient C)
Patient age	66 y.o.	51 y.o.	53 y.o.
Patient weight	88 kg	75 kg	58 kg
Body mass index	24.4	24.8	24.8
Biomechanical length	480 mm	412 mm	370 mm
Helical scan protocol (HipOp [®])	200mA 120 kVP	180mA 120 kVP	190mA 120 kVP
Pixel size	0.74 mm	0.46 mm	0.74 mm

Table 7 - Individual data and CT scans parameter of interest for the two selected individual in this study (Patient A and C) and the individual of the previous study (Patient B). The biomechanical length is calculated as the least distance in the frontal plane between the intercondylar fossa and the trochanteric fossa.

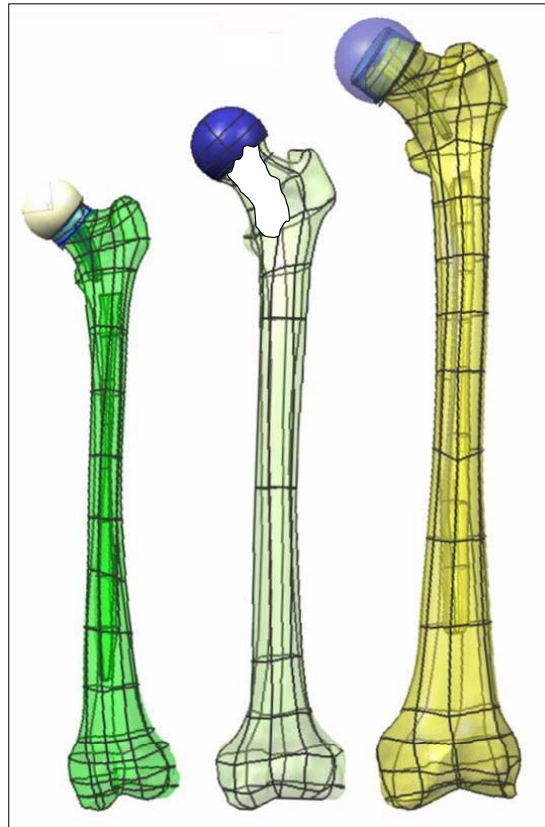


Figure 8 – Snapshot of CAD models of the three femurs spanning the range of sizes within the IOR database (from the left: patient A, B and C)

Finite element models

Differently from what reported in paragraph 6.4 the prosthesis component and the cement mantle were meshed using the same algorithm adopted for the femoral component resulting in a 10-noded all-tetrahedral mesh. The refinement of the prosthesis and cement meshes was high enough to guarantee the same model accuracy obtained with the previously adopted hexahedral modelling strategy.

All results were collected together with the ones obtained in the previous study, where medium size prosthesis was implanted in a medium-sized femur.

6.5.2.2 Results

The results are discussed in the frame of the most common failure scenarios reported for joint replacements.

Stem stresses

In all examined sizes, the highest stresses are registered in the stem significantly below the fatigue limit of the alloy used to manufacture it. We can thus exclude any risk of fracture of the metallic stem.

Bone-cement relative micromotion

No significant differences are found between the three models. In all cases the prosthesis was stable with a peak inducible tangential micromotion always lower than 20 microns. Thus, we can exclude any risk of fretting-related failure scenarios.

Bone-cement contact pressure

The peak contact pressure was located near the stem tip for all models and it lowers as the stem size increases. The maximum value is found for the patient A which represent the smallest implant.

Cement stresses

The peak principal tensile and compressive stresses induced in the cement mantle under a stair-climbing loading condition, which is the most critical for the cement, are reported in the table below. As a reference, the same results obtained in the previous work (paragraph 6.4) are reported as well. The peak stresses increase as the prosthetic sizes is reduced, reaching the maximum values for the smallest size (*Table 8*). The principal tensile stress is comparable to the fatigue limit of the material (14 MPa) [2].

	Patient A	Patient B	Patient C
Principal tensile stress	15	10	5
Principal compressive stress	-30	-15	-5

Table 8 - Principal cement stresses (MPa)

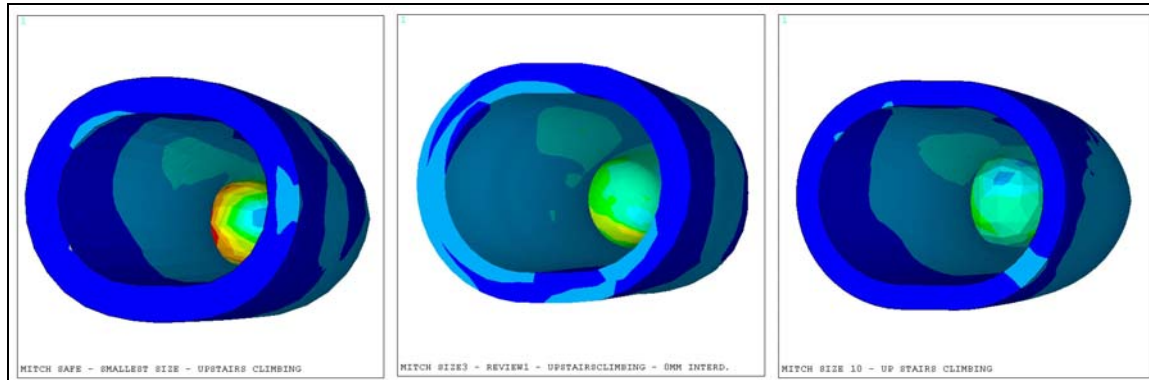


Figure 9 - Principal tensile stress in the cement mantle induced by a US load

Risk of bone fracture

The position and the magnitude of the peak tensile strain region are comparable in all three cases and are below those predicted for the intact femur under similar conditions. Thus, we can exclude any failure scenario related to the spontaneous fracture of the femoral neck under the action of physiological loads.

Stress Shielding

The estimation of the stress-shielding effect was performed as described in paragraph 6.4. No relevant stress shielding is registered for all femurs. In the femur used in the previous study (centre) a slightly higher, but still moderate, stress shielding was predicted with respect to the new femurs. In that case the 2% of the proximal epiphysis volume was interested by a stress

shielding higher than the activation threshold for adverse bone remodelling reported in the literature [18].

6.5.3 Roughness of the stem surface

At the bone-prosthesis interface a rough surface would play in favour of a more effective prosthesis osteointegration while at the cement-prosthesis interface a polished surface would reduce the risk of excessive debris of the cement [20].

The scope of this study was to verify if and to what extent the investigated failure scenarios were affected by different surface roughness of the optimised design. To this aim the whole FE investigation was repeated on an additional model, simulating the proper friction conditions for the different surface finishing of the stem and the part under the donut of the prosthesis.

6.5.3.1 Materials and methods

The new model generated for this study was based on the model described in paragraph 6.4.

The different surface roughness was taken into consideration by varying the friction coefficient at the contact surfaces between the prosthesis-cement and the prosthesis-bone (**Errore. L'origine riferimento non è stata trovata.**). Friction coefficients were related [3] to the nominal roughness indicators provided by the Manufacturer. A friction coefficient of 0.3 was adopted to simulate the polished distal part of the stem while a friction coefficient of 0.6 was used to simulate the presence of a rough surface ($R_a = 1.5\text{-}1.7$ microns) at the prosthesis-bone interface.

6.5.3.2 Results

Results were collected together with the results obtained from the optimized model (paragraph 6.4), which simulated a contact surface entirely polished, for comparison.

Prosthesis stresses

For both models, the highest stresses were found in the stem for the upstairs climbing loading scenario. No relevant differences were found between the two different surface finishing. The maximum stress was, in both cases, significantly below the fatigue limit of the alloy used to manufacture the prosthesis. We can thus exclude any risk of fracture of the metallic stem.

Bone-cement relative micromotion

In both cases the prosthesis was in good stability with a peak inducible tangential micromotion always lower than 50 microns. The stem micromotions are slightly reduced for each of the considered loading scenario in the dual surface finishing model. Thus, we can exclude any risk of fretting-related failure scenarios since the micromotion absolute value is very small and no high contact pressures were detected in the regions where the highest micromotions were present.

Bone-cement contact pressure

The peak contact pressure is found for both models near the tip of the stem in the upstairs climbing loading scenario. The distribution and maximum values of the contact pressure do not differ between the two surface finish conditions simulated. The peak values are quite localised and does not raise any particular concern.

Cement stresses

The peak principal tensile and compressive stresses in the cement mantle are found for both models under a stair-climbing loading condition, which confirms to be the most critical for the cement and reported in the table below. The peak stresses slightly decrease in the model where a dual surface finishing is simulated (*Table 9*). The principal tensile stress remains always lower than the fatigue limit of the material [2] (14 MPa).

	Uniform surface finish (paragraph 6.4)	Rough and polished (present study)
Principal tensile stress	5	5
Principal compressive stress	-10	-10

Table 9 - Principal stress in the cement mantle (MPa)

Risk of bone fracture

The peak tensile strain is found for both the friction conditions on the supero-lateral neck surface, when a single stance (standing) load case is imposed. No significant differences were found in the position and magnitude of the peak tensile strain region in the two models. Thus, we can exclude any failure scenario related to the spontaneous fracture of the femoral neck under the action of physiological loads.

Stress Shielding

No relevant stress shielding is registered for the two models, irrespectively of the friction condition simulated. The volume subjected to a stress shielding higher than the activation threshold for adverse bone remodelling, as reported in the literature [18], never exceeds the 1% of the proximal epiphysis bone volume either when a uniform surface finishing or a blasted and polished surface are simulated.

6.5.4 Discussion*Variation of results to different positioning of the prosthesis*

The relative micro-movements at the cement-prosthesis and bone-prosthesis interface were below the safety limits for all positions. A particular combination of stem in the superior position and single leg stance load produces a higher micromotion in the dome region, but still the magnitude of the relative displacements was not a source of major concern.

The cement stress was mildly sensitive to the stem positioning; medial stems are the most critical and thus this position should be avoided if possible, so as to achieve ideal biomechanical conditions.

The risk of femoral neck fracture was totally insensitive to the stem position, which confirms the lack of significant notching with the new stem design.

The angular orientation in the frontal plane of the prosthesis does not produce an high risk of failure of the implant. However there is a clear trend of worsening in all failure indicators when the prosthesis is moved in the valgus direction, in particular for the cement stresses.

Thus the current design the current design do not present any particular concern for failure, although clinical recommendations should include to avoid an excessively superior or excessively medial position.

Variation of results to different femur sizes

The implant size does not significantly affect the prosthesis micro-movements, which are always below the safety limits for all stem sizes and do not raise particular concerns. Similarly, the risk of femoral neck fracture seems to be insensitive to the implant size as do stress shielding.

The major concern regards the stresses induced in the cement mantle that seem to present a high sensitivity to the implant size. The peak stress in the cement mantle shows a monotonic increasing behaviour with the reduction of the stem size: small stems are more critical. To our opinion this is a consequence of a stress concentration due to the small curvature radius of the stem tip in the smallest prosthesis size. To solve this problem a second review of the prosthesis shape should be done.

Variation of results to different roughness of the surface finish

The inclusion in the model of two different friction coefficients, to simulate the presence of a rough blasted surface under the prosthesis donut and of a more finely polished surface in the rest of the stem, does not significantly affect any of the investigated failure scenario.

6.6 Second step of design revision: geometry optimisation of small sizes

The smallest size of the prosthesis was found to produce high stresses at the distal tip of the stem requiring a second revision of the geometry. The aim of present study is to verify if the optimised geometry bio-mechanically guarantees a low risk of failure as the bigger sizes of the prosthesis do. To this aim, the entire modelling process was repeated for the smallest femur, simulating the implantation of the smallest prosthesis after the second design revision.

6.6.1 Materials and methods

The stem geometry was revised modifying the lateral curvature and the radius at the tip stem. The rasp shape was consequently modified so as to guarantee a minimal thickness (3mm) of the cement mantle around the tip stem.

Data used for the generation of the FE model of the femur are described in paragraph 6.5.2.1 (Patient A) and modelling procedures are described in paragraph 6.1.1, refer to that section for a more exhaustive description.

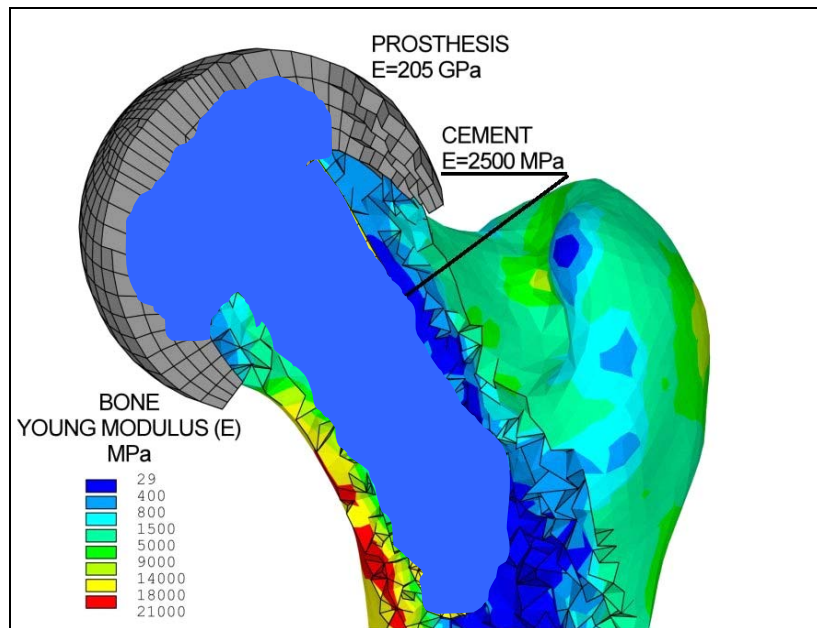


Figure 10 - A section of the finite element model of the implanted femur. The non-homogeneous distribution of the Young modulus in bone is shown.

6.6.2 Results

Stem stresses

The highest stresses are still registered in the stem and are not influenced significantly by the design revision. The Von Mises stresses in up-stair climbing loading condition, which is the most critical for the stem.

Bone-cement relative micromotion

The inducible elastic tangential micromotion was found under stair climbing loading condition. In all cases the prosthesis was in good a stability with a peak inducible tangential micromotion always lower than 50 microns.

Bone-cement contact pressure

The peak contact pressure is still located near the stem tip but the maximum value was significantly reduced to 15 MPa.

Cement stresses

The peak principal tensile and compressive stresses induced in the cement mantle under a stair-climbing loading condition, which is the most critical for the cement, are reported in the table below. As a reference the same results obtained in the previous work are reported as well. The peak tensile stress is notably lower in the new design and well below the fatigue limit [2]. Also the peak compressive stress is lower than what observed for the old prosthesis shape (Table 10).

	Small size Old shape	Small size New shape
Principal tensile stress	15	10
Principal compressive stress	25	15

Table 10 - Principal cement stresses (Mpa)

Risk of bone fracture

Principal tensile strains in the neck region of the implanted femur due to the most critical loading, single leg stance, among those observed under physiological conditions. The position and the magnitude of the peak tensile strain region are comparable for both prosthesis designs.

Stress Shielding

The change in the strain energy density due to the presence of the prosthesis is shown (old shape on the left, new shape on the right). The new design produce a higher risk of bone remodelling slightly overtaking the activation threshold, the 1% of the proximal epiphysis volume was interested by a stress shielding higher than the activation threshold for adverse bone remodelling reported in the literature.

6.6.3 Discussion

The new design of the prosthesis seems to definitely reduce the risk of cement fatigue fracture since both the principal tensile and compressive stresses are lowered far below the fatigue limit of the material. The contact pressure between the implant and the cement is reduced as well. On the contrary, the design revision did not significantly affect the micro-movements, which remained below the safety limits, the risk of femoral neck fracture and neither the stress shielding. The new smallest size of the prosthesis lowers the stresses in the cement mantle to a safe level.

6.7 Results of experimental tests on the optimised device

The experimental group of LTM carried out disruptive tests on a second group of cadaver femurs. The scope of this work was to assess the failure load and failure mechanism of the proximal femur implanted with the optimised design.

A total of 7 pairs of fresh frozen cadaver human femurs obtained through the International Institute for the Advancement of Medicine.

Statistics on the failure load, normalized in terms of the donor body weight, are reported in the **Errore. L'origine riferimento non è stata trovata.** The implanted femur resulted, in average, 15% stronger than the intact controlateral one.

Results indicate that, after revision the notching effect previously observed is dramatically reduced. Failure load is $115\% \pm 34\%$ that of the controlateral intact (the implant strengthens the femur by 15%). Failure in most specimens initiated on the lateral side of the neck, under the edge

of the prosthetic component, and propagated vertical along the neck, passing close to the lesser trochanter.

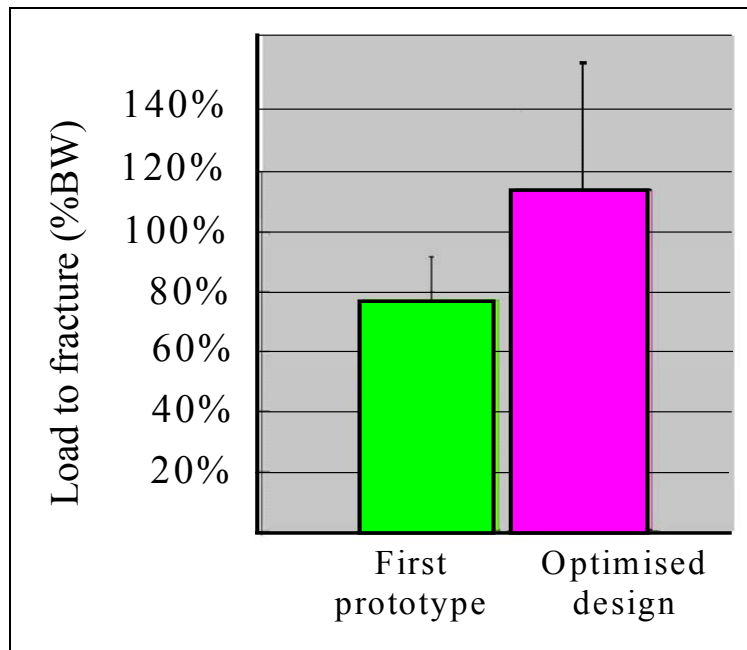


Figure 11 – On the left: Comparison of the load to fracture measured on the first prototype and the optimised prosthesis, values are given as percent of the donor bodyweight. On the right: the FE mesh of the first prototype (left section) and of the optimised prosthesis (right section).

6.8 Extended pre-clinical validation of the finalized design on a simulated population

Previous paragraphs described the optimisation process of the prosthesis geometry, conducted with the support of a significant number of simulations to represent different specific operative conditions of the implant. Results were very promising as they did not raise any concern of failure for any of the investigated failure scenario. Although simulations were representative of various conditions the implant might face during its service life, a complete pre-clinical validation process should take into consideration the variability of the entire population to which the prosthesis is indicated to.

The scope of this study was to define what is the extended indication that can be reasonably recommend for the device. This aim was pursued on a statistical basis, using the Monte Carlo method to perform a sensitivity analysis to certain clinical parameters on FE models.

Input variables included patient-related and surgery-related factors as well as factors related to the activity type and level of the patient. The output was the estimated distribution of the risk of failure over the entire population.

The study allowed identified critical combinations of the input variables, considering their mutual interaction, which lead to high risks of failure. Last, the sensitivity analysis underlined the more relevant variables in producing a high risk of failure.

Although the statistical analysis on the implanted femur confirmed the quality of the optimised design for all investigated failure mode, a few percent (< 5%) of cases (characterised by a critical

combination of osteoporosis, body weight and level activity) showed a high risk of neck fractures.

A second analysis compared the risk of fracture of the implanted femur and of the same femur in the non-operated conditions. Results underlined that the prosthesis do not alter the risk of fracture with respect to the original femur. Conversely, results seem to indicate a moderate strengthening of the implanted femur even if this statement cannot be supported by statistical power.

6.8.1 Materials and methods

The FE model was based on the CT data described in paragraph 6.1 as well as modelling procedures, while the prosthesis geometry used to simulate the implantation was the final optimised geometry. In the following lines the definition of the probabilistic study which has been approached by using the Monte Carlo method is described.

6.8.1.1 Analysis of the implanted femur

A number of parameters that define the finite element model of the implanted femur (input variables) were assumed to be statistically variable. For each parameter a probability distribution was defined, on the basis of clinical or experimental results, and also considering the design target (Table 11).

Variable	Distribution type	Loading case	Mean value	Standard deviation	Min Value	Max value
Bodyweight (kg)	Truncated Gaussian	All	73.7	14.4	44.8	116.7
Osteoporosis level (T-score)	Uniform	All	//	//	-5.0	0.0
Interdigitation degree	Uniform	All	//	//	0	1
Load intensity factor	Truncated Gaussian	Standing	1.29	0.29	1	1.89
		Walking	1.07	0.11	0.90	1.33
		Climbing	1.15	0.14	0.90	1.48

Table 11 - Summary of the input parameters distribution implemented in the probabilistic models

Three input variables were defined to account for the patient's bodyweight, the bone tissue material properties, and the degree of bone-cement interdigitation.

Patient bodyweight

To determine the probability distribution of patient bodyweight the Register of Orthopaedic Prosthetic Implants (RIPO, <https://ripo.cineca.it>) database was used. It was first observed that, in hip patients, the patient weight has no correlation with the size of the prosthesis implanted. Patient bodyweight data were found to fit a Gaussian curve with mean value 722 N (73.6 kg force) and standard deviation 141 N. The input variable was therefore made vary as a Gaussian curve, truncated at the lowest and highest values found in the sample, i.e. 440 N (45kg force) and 1145 N (117kg force).

Bone tissue material properties (osteoporosis)

Bone material properties were varied on the basis of the bone density distribution, in terms of mineral content, to simulate various degrees of osteoporosis. The modelling strategy was based on the established definition of osteoporosis (AJM, 1991 Osteoporosis Consensus Development Conference), in terms of T-score obtained from a DEXA exam (number of standard deviations from the average DEXA density for a young population).

This raises the first problem on how to relate the definition of osteoporosis which is based on a 2D information (DEXA), to a 3D density distribution as provided by CT data. A preliminary analysis was carried out to compare DEXA data with the volume density obtained with DataManager [21] software. Volume densities on selected CT-scan trabecular bone regions (femoral head and neck) and DEXA densities in the neck region (Mod. Eclipse, Norland Co., USA) were compared on a cohort of 20 femurs. Results showed a very high correlation ($R^2 > 0.9$) in the range from normal to severely osteoporotic (T-score between +0.5 and -4.5) between the two measures which made it possible to define the scaling parameters to simulate a range of densitometric conditions, from extremely osteoporotic (T-score = -5) to normal (T-score = 0, i.e. density of the reference young population), in the FE modelled femur.

A differential rate of osteoporosis for cancellous and cortical bone was applied, according to the hypothesis of bone resorption depending on available free-surface and to in-vivo observed patterns. Since this study aims at defining the “extension of the indication”, the probability distribution of this input variable was assumed to be uniform, therefore considering an equal chance of the prosthesis being implanted on a young, high-density bone or on a severely osteoporotic bone [22, 23] (paragraph 6.2.3).

Bone-cement interdigitation

Interdigitation was deemed possible on a continuous irregular layer surrounding the cement layer with an average thickness of 4mm, as indicated by the surgeons.

Cement interdigitation was assumed to act only as a reinforcement, through an increase in elastic modulus, and only on the trabecular tissue, where a significant fraction of open porosity is present [22].

The degree of bone-cement interdigitation was hypothesised to be a function of local tissue density, which is known, and flow conditions, like cement viscosity, insertion pressure, etc., which are largely variable and unknown. Therefore, a cortical/trabecular density threshold was defined on the CT dataset and a void fraction parameter was computed for each element representing trabecular tissue.

The cement was assumed to fill the existing porosity, to the extent given by a statistical parameter varying from 0 (no penetration) to 1 (cement filling all pores), accounting for the flow conditions. The cement reinforcement was then computed with the mixture rule, according to the relative volume fractions of bone and cement. Given on an element basis the bone elastic modulus (E_{bone}), the corresponding void fraction parameter (θ), the cement elastic modulus (E_{cement}) and the filling parameter (α), for each element it can be written:

$E_{\text{interdigitated}} = E_{\text{bone}} + \theta * \alpha * E_{\text{cement}}$

Since the flow condition determining the filling parameter (α) are largely unpredictable, and the study aims at verifying the robustness of the design towards an extended indication, the statistical parameter was given a uniform statistical distribution.

A statistically determined variation of the applied load for each motor task was defined as an additional input variable.

Inclusion of a load intensity variation

An extensive literature review was performed to identify the more appropriate way to include the fundamental factor of load variability in the probabilistic framework. As a result, modelling the intra- and inter-subject neuromotor variability in the execution of a task was found to be a more meaningful and reliably referenced target with respect to modelling the variation in the patient level of activity [5, 24]. In fact, while there is literature evidence that the ground reaction forces measured during a certain motor task are actually scalable with the task intensity (from slow chair raising (0.5 BW) through walking (1-1.4 BW) to running and downhill running (up to 3BW)) [5, 25, 26], this scaling cannot be translated to the forces acting at the hip, since the force equilibrium at the hip joint heavily involves muscles action. Hence the subject-specific movement and contraction strategy (i.e. the neuro-motor control strategy) would play a fundamental role in defining the implant boundary conditions.

The only available data on joint reaction measurements and muscles forces simulation at the hip are those by Bergmann [5], where a limited number of motor tasks and patients were investigated.

Given these indications, the load intensity parameter was statistically varied to replicate the overall (inter- and intra-subject) variability reported for the performance of each of the three basic motor tasks so far investigated: walking, up-stair climbing, and single leg stance. The intensity parameter was given a truncated Gaussian distribution, with mean, standard deviation, maximum and minimum values determined for each of the three tasks.

Stem misalignment

The whole statistical FE investigation was repeated on two additional models, to include the sensitivity of prosthesis mechanical behaviour to the varus/valgus positioning uncertainty, as performed on the standard deterministic model described in paragraph 6.5.

Output parameters

Output parameters have been defined to represent risk indicators each corresponding to a clinical failure scenario, according to what previously reported [27]:

- peak von Mises stem stress to monitor the risk of stem fracture;
- peak tensile cement stress (and peak compressive stress) to monitor the risk of stem-cement loosening);
- peak principal strain in a selected region encompassing the whole femoral neck to monitor the risk of femoral neck fracture. This indicator, though differing from those reported in the

Contract 2nd Amendment (peak tensile and von Mises bone stress), was chosen in agreement with the Customer, since recent research advances [28] have shown that failure is better described by strain parameters;

- peak stem-cement abrasive micromotion (in conjunction with contact pressure and peak cement compressive stress) to monitor the risk of abrasive fretting;
- Peak contact pressure between the stem/cement complex and bone to monitor the risk of ischemic necrosis.

6.8.1.2 Comparative analysis of the implanted and the intact femur

The comparative analysis was run to evaluate the effect of the prosthesis implantation on the biomechanical behaviour of the hosting bone by simulating a paired analysis on the intact and on the implanted femur. To this aim, for each sample point, generated by the MonteCarlo method, the same condition was simulated on the intact and on the implanted femur so as to allow a direct comparison of the same biomechanical parameter predicted on the intact and on the implanted femur.

The description of data used for the generation of the FE model has been extensively discussed in paragraph 6.1 as well as modelling procedures. Refer to that section for an extensive description of materials and methods used for generating the FE model.

In the following lines is described the definition of the probabilistic study which has been approached using a Monte Carlo method.

The patient bodyweight, the bone tissue material properties and the load intensity (input variables) were assumed to be statistically variable. For each parameter a probability distribution was defined, on the basis of clinical or experimental results (Table 29).

Variable	Distribution type	Loading case	Mean	Standard deviation	Minimum Value	Maximum value
			value			
Bodyweight (kg)	Truncated Gaussian	All	73.7	14.4	44.8	116.7
Osteoporosis level (T-score)	Uniform	All	//	//	-5	0
Load intensity factor	Truncated Gaussian	Standing	1.29	0.29	1	1.89
		Walking	1.07	0.11	0.9	1.33
		Climbing	1.15	0.14	0.9	1.48

Table 12 - Summary of the input parameters distribution implemented in the probabilistic model of the intact femur

The only output parameter defined was the peak principal strain in a selected region encompassing the whole femoral neck, to monitor the risk of femoral neck fracture.

6.8.2 Results

The probabilistic Monte Carlo analysis applied a Latin Hypercube Sampling method and consisted of 150 runs for each loading condition. The distribution of the input parameters satisfactorily replicated the assumed probability distributions, and spanned the whole range of

input values, tails included. The trends of the average values of each output parameter were consistently steadied for the number of runs performed.

Results are presented so as to underline the probability that a certain outcome is observed, and the sensitivity that each input variable has on each output variable.

6.8.2.1 Analysis of the implanted femur

The statistical influence of the input variables (cement interdigitation level, bodyweight, osteoporosis level, varus/valgus misalignment and load intensity factor) on the output variable (peak von Mises stem stress, peak tensile cement stress, peak principal strain in the femoral neck, peak stem-cement abrasive micromotion and peak contact pressure) was conducted. For completeness additional results are reported in Appendix C.

Results showed small changes of the location of the peak value for each output variable underlining a low sensitivity to the variation of the input parameters. The comprehensive mean (or median in case data followed a non-normal distribution) and maximum values for each output parameter are shown in Table 13.

Biomechanical parameter (output variable)	Mean Value	Max value	Limit value
Stem Von Mises stress (MPa)	80	170	200
Cement principal tensile stress (MPa)	5	10	14
Cement principal compressive stress (MPa)	-10	-25	-40
Bone maximum principal strain (ϵ)	0.0022*	0.01	0.0073 (tensile) 0.0104 (compressive)
Maximum stem micromotion (μm)	30*	50	50 (fretting)**

*median value

Table 13 - Comparison of mean and maximum values with limit values. The median values are reported for bone maximum principal strain and maximum stem micromotion since their distribution did not follow a Gaussian curve (One Sample Kolmogorov-Smirnov Test, $p < 0.05$)

The upper tail of bone principal strains and stem micromotions exceeded the safe threshold for a low number of cases (< 5%). In

Figure 12 are shown the frequency distribution histograms where the 150 peak values simulated, for both the bone principal strains and the stem micromotions, are collected and grouped in 10 categories. The diagram reports on the x-axis the value of the biomechanical parameter and on the y-axis the probability that a value occur within the corresponding category of the biomechanical parameter. The safe limit for the two cited parameters is visualised by a red line.

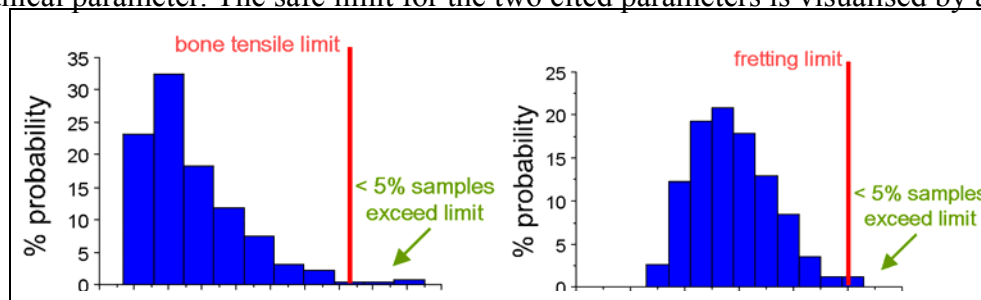


Figure 12 - The histograms of output parameters found to exceed the safe threshold. Relative frequency for bone max principal strain (left) and stem micromotion (right)

The input parameter arrays yielding critical values are reported in Table 14. The subset of conditions at risk of failure are characterised by the co-presence of high bodyweight, severe osteoporosis, and balance impairment or other neuromotor disorders causing high muscle contractions in case an asymmetric loading condition is sustained.

Critical values exceeded	Load Intensity factor	Body weight (Kg)	OP (T-score)	Interdigitation
Bone strain, Micromotion	1.83	88	-4.6	High
Bone strain, Micromotion	1.48	104	-4.5	Normal
Bone strain	1.59	101	-4.3	High
Bone strain, Micromotion	1.45	90	-4.8	Normal
Bone strain, Micromotion	1.62	82	-4.6	Scarce
Bone strain, Micromotion	1.71	92	-3.8	Scarce

Table 14 - Detailed description of the input parameter samples yielding critical values

The sensitivity analysis (the so-called pie-plots are reported in Appendix C) highlights that the patient's bodyweight influences all output parameters in all loading conditions, its relative influence is similar among different loading cases, and accounts on average for a 40% of each output parameter variation, with a stronger influence on maximum compressive stress and contact pressure.

The load intensity variation influences all output parameters in all loading condition, with the exception of the maximum bone strain during walking. However, level walking is the least challenging motor task and with the least variation among those simulated. The relative influence of load intensity on output parameter variation is high (about 40% on average) when single leg stance is considered and moderately low (less than 20%) for walking.

The level of osteoporosis significantly influences the variation of most output parameter. The only exception was the cement compressive stress during single leg stance. Osteoporosis level seems to play a minor role in determining cement compressive stress also in the other loading cases, while its relative influence is higher (around 30%) for the other parameters and predominant for bone maximum principal strain in the neck region.

The degree of interdigitation showed an overall low influence on the output parameters variation: it shows significant a correlation only when walking was simulated.

The varus/valgus misalignment did not raise any concern for failure although a generally higher risk was found for stems 2° rotated in the valgus direction (Table 15).

Biomechanical parameter (output variable)	Median value			
	10° varus	Optimal position	2° valgus	Limit value
Stem Von Mises stress (MPa)	70	80	90	200
Cement σ_1 (MPa)	2	5	5	14
Cement σ_3 (MPa)	-5	-10	-15	-40
Bone ε_1 (ε)	0.002	0.002	0.002	0.0073 (tensile) 0.0104 (compr.)
Maximum stem micromotion (μm)	30	30	30	50 (fretting)**

Table 15 - Comparison of median values for the three models with a different stem alignment with respect to the femoral neck axis (10° varus, optimal position, 2° valgus).

6.8.2.2 Comparative analysis of the implanted and the intact femur

The statistical influence of the input variables (bodyweight, osteoporosis level and load intensity factor) on the variation of the risk of neck fractures after implantation was conducted, for simplicity to the reader results are here resumed, when needed the Appendix C reports additional details.

A typical contour of the bone maximum principal strain is reported in the following *Figure 13*.

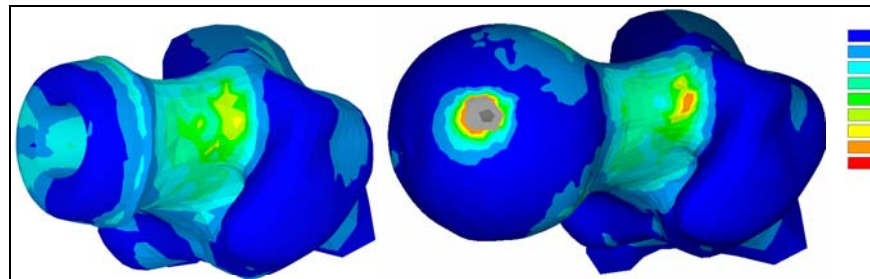


Figure 13 - Typical contours of the bone maximum principal strain in the intact (right) and implanted (left) conditions under a single stance loading, shown to qualitatively describe the parameter patterns and the locations of the maximum values.

Results on bone strains revealed a general tendency for higher risk of neck fractures of the intact (*Table 16*) with respect to the implanted femur. However, this difference was not significant (paired T-test, $p = 0.05$).

Biomechanical parameter (output variable)	Load-case	Mean % change	Maximum % change
Bone maximum principal strain (ϵ)	Single stance	15%	20%
	Level walking	20%	30%
	Upstairs climbing	5%	10%

Table 16 - Percentage differences on the bone maximum principal strain between the intact and the implanted model. Differences are reported for mean and maximum values over the 150 simulated sampling points. Positive percentages indicate higher values for the intact model.

Histograms (*Figure 14*) show that a group of individuals smaller than the 5% of the entire population exceeded the bone strains safe threshold for both the intact and the implanted femur.

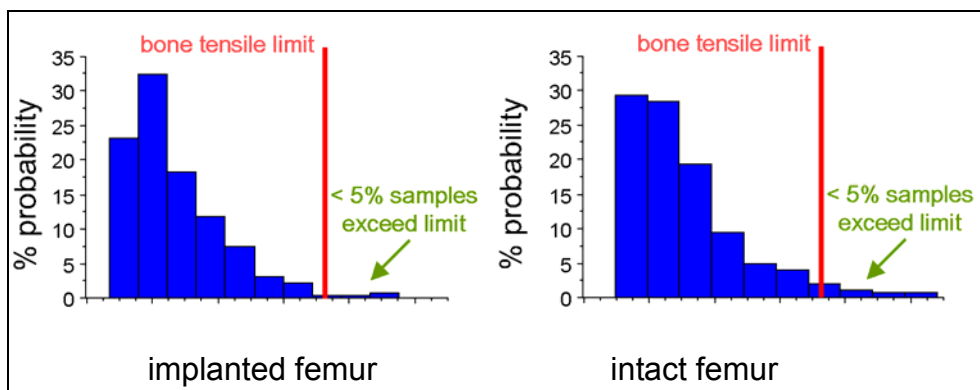


Figure 14 - The histogram of peak maximum principal strain probability for the implanted (left) and the intact femur (right)

The subset of sampling points, which were found to exceed the safe limit, was characterised by severe patient conditions (i.e. co-presence of severe osteoporosis, high bodyweight, and high load intensity factor (Appendix C).

The sensitivity study (Figure 15) highlighted that the contribution to the variation of the output parameter was nearly 50% due to loading conditions (body weight and level of activity) and for the resting part to the osteoporosis level

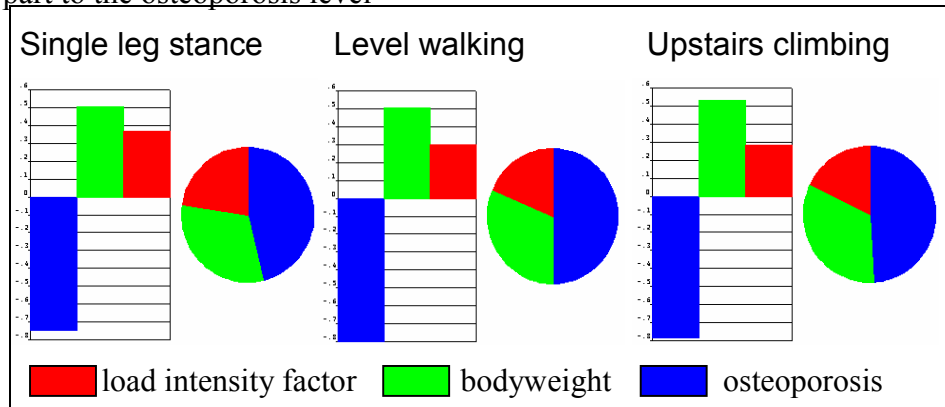


Figure 15 - Linear correlation sensitivities shown as pie-plot and histogram for each loading condition. The significance and relative importance of the input variable variation is identified.

6.8.3 Discussion

Previous deterministic studies investigated the biomechanical behaviour of the prosthesis, implanted in the optimal position in one single average femur, and subjected to loading tasks of average intensity, was analysed by means of deterministic FE models with respect to the simulation of six failure scenarios (stem fatigue failure, cement tensile and compressive fatigue failure, bone failure, cement fretting, fibrotic tissue differentiation at the bone-prosthesis interface). In those average conditions, it showed a safe biomechanical behaviour.

The risk associated to each failure scenario over a simulated population was investigated in the present study by means of a probabilistic FE framework, including the variability of some key-factors that may determine the prosthesis successful outcome.

Variables explored were: the inter-subject variability of bodyweight, OP level, the inter- and intra-subject variability of load intensity, stem misalignment and the variation of the cement interdigitation level achieved in the surgical procedure.

The results showed that in the vast majority of simulated conditions the failure indicators maintained a value significantly lower than the relative critical values. In particular, the prosthesis design did not reach critical values for any of the simulated conditions with respect to four of the investigated scenarios (stem fatigue failure, cement tensile and compressive fatigue failure and lack in bone in-growth). For the two remaining failure scenarios (fretting abrasion and femoral neck fracture) the critical values were exceeded in a small set of cases (<5%).

For what concerns the risk of cement fretting, monitored by the stem-cement relative displacement, the calculated micromotion exceeded only for a very limited extent the critical

value for less than 5% of cases (maximum value: 53 microns, critical value: 50 microns). It must be noted that even in the few cases where the stick-slip limit is exceeded the amplitude of the slip will be minimal. Thus we can translate this result in negligible risk of having massive abrasions, and a small risk (<5%) of having limited abrasion patches, which do not likely have any clinically relevant implication.

For what concerns the risk of bone failure, the critical value was reached in a limited number of samples, around 4% of the total. They were all found for a single stance loading condition with the critical concurrent presence of high OP level, high body weight and a high load intensity factor.

The presence of a high bone failure risk only in the single leg stance loading condition can be explained because a single leg stance loading induces the highest bone tensile strains in the neck [14], among the physiologically activities considered relevant for the biomechanical behaviour of the proximal femur (Chapter 5).

For what regards the comparative analysis of the biomechanical behaviour of the hosting bone when intact or implanted, the probabilistic evaluation of the fracture risk of femoral neck femur yielded comparable results: all failures were predicted for a single stance loading condition with the critical concurrent presence of high OP level, high body weight and a high load intensity factor. No statistical differences were found for the maximum bone strain distribution in the intact and implanted conditions when analysing the samples exceeding 75% of the bone failure limit. This seems to indicate that the 4% bone failure risk reported for the simulated loading and patient conditions in the implanted condition is statistically equivalent to failure risk calculated for the intact bone.

The few results we have from *in-vitro* paired tests suggest that the fracture load remains unchanged when the stem is implanted. A clinical incidence of femoral neck fracture comparable to that predicted in our simulated population is observed for osteoporosis female patients with T-score < -3.5 and aged over 75 [29].

A slightly higher number of failure cases were reported for the same simulated population when the intact femur was simulated. This may suggest that the presence of the implant slightly reduces the risk of fracture of the femoral neck, in accordance with the experimental results. However, the difference was not statistically significant. Hence, on the basis of the presented results it can only be concluded that the presence of the implant definitely does not worsen the femoral neck strength.

Observing the sensitivity plots (*Figure 15*) we shall notice that the load intensity factor had a high influence on the risk of spontaneous fractures of the femoral neck. Among all parameters (osteoporosis, bodyweight, load intensity factor), the load intensity factor is the most difficult to define since it cannot be directly related with the patient's level of activity. Moreover the base data used in its definition were the few measurements of the hip force available in the literature, for a small number of patients and a limited number of tasks of motion. Thus, while for the bone quality and the body weight we represent here a realistic population, for the overloading we can

only state that the range of values here considered is physiologically possible, but with no guarantees on the probability.

6.9 Conclusions

The aim of the present study was to analyse the bio-mechanics of a proximal femur implanted with the first prototype of a new epiphyseal replacement, to identify the origin of possible complications after surgery, to optimise the initial geometry and to test the performances of the optimised design when implanted on a population of interest.

The analysis was conducted on the first prototype by using the protocol developed (chapter 4), based on a procedure for generating finite element models of skeletal segments developed in the past years at LTM [30, 31].

Numerical simulations were able to identify the origin of possible complications at each step of the optimisation loop and to quantify the bio-mechanical benefit after each cycle of design optimisation. The optimised design showed a low-risk risk of failure for all of the investigated failure scenario under a large set of physiologically relevant conditions. These results were partially confirmed by the experimental group of the LTM as only the influence of the prosthesis implantation on the risk of spontaneous fractures of the femoral neck was measured. Destructive test highlighting a high increase of the neck strength on cadaver femurs when implanted with the optimised design over cadaver femurs implanted with the first prototype.

Once the bio-mechanical performance of the optimised design was satisfactorily, the pre-clinical validation analysis was extended over a simulated population by means of a statistical analysis of the risk of failure. The results were all in a good agreement with what emerged from the deterministic studies confirming a low risk of failure of the prosthesis to all investigated failure modes. For what concern the risk of femoral neck fractures, it can be stated that the prosthesis implantation should not be attributed of an increased risk with respect to the intact controlateral femur. Conversely, both numerical simulations and destructive tests seem to suggest that the prosthesis implantation strengthen (+15% in average on the ultimate load to failure) the intact femoral neck. However, this statement is not supported by statistical power.

The statistical analysis provided some critical combinations of the input parameters (i.e. related to the individual anatomy, activity and the surgery accuracy) which were found critical. These scenarios might constitute a contra-indication during the patient selection phase before surgery.

The most important limitation of the present study is about loading conditions at the proximal femur, as it is underlined in the paragraph above. In fact, the full understanding of the contribute to the joint equilibrium during motion of muscle forces and joint reactions is still an open question for researchers. The loading schemes simulated in the present study can be considered relevant but not exhaustive. Nevertheless, to the full understanding of the implant bio-mechanics, more activities of daily living should be considered, taking into account accidental tasks, such as stumbling, and the whole range of loadings depending on the variability of the studied activity, of the individual anatomy and on the individual neuro-motor control strategy.

Since experimental techniques to non-invasively measure in-vivo muscle forces are not yet available, the only feasible method to study the bio-mechanical interaction between the skeleton, muscles and tendons is through muscle-skeletal models. To this aim a new research activity was started by a literature review on muscle-skeletal models of the lower limb which is the topic of the next chapter.

In conclusion, the proposed protocol was able to achieve all goals ahead of the work, so as the prosthesis stem recently started the clinical trials.

REFERENCES

1. Taddei, F., et al., *Subject-specific finite element models of long bones: An in vitro evaluation of the overall accuracy*. J Biomech, 2006. **39**(13): p. 2457-67.
2. Lewis, G., *Properties of acrylic bone cement: state of the art review*. J Biomed Mater Res, 1997. **38**(2): p. 155-82.
3. Nuno, N., R. Groppetti, and N. Senin, *Static coefficient of friction between stainless steel and PMMA used in cemented hip and knee implants*. Clin Biomech (Bristol, Avon), 2006. **21**(9): p. 956-62.
4. Viceconti, M., et al., *Large-sliding contact elements accurately predict levels of bone-implant micromotion relevant to osseointegration*. J Biomech, 2000. **33**(12): p. 1611-8.
5. Bergmann, G., et al., *Hip contact forces and gait patterns from routine activities*. J Biomech, 2001. **34**(7): p. 859-71.
6. Heller, M.O., et al., *Musculo-skeletal loading conditions at the hip during walking and stair climbing*. J Biomech, 2001. **34**(7): p. 883-93.
7. Rancourt, D., et al., *Friction properties of the interface between porous-surfaced metals and tibial cancellous bone*. J Biomed Mater Res, 1990. **24**(11): p. 1503-19.
8. Zienkiewicz, O.C. and Z. J. Z., *A Simple Error Estimator and Adaptive Procedure for Practical Engineering Analysis*. International Journal for Numerical Methods in Engineering, 1987. **24**: p. 337-357.
9. Martelli, S., et al. *Accuracy Of Subject-Specific Finite Element Models Of Long Bones From Ct Data: An In-Vitro Study*. in ICCB. 2005.
10. Taddei, F., et al., *Mechanical strength of a femoral reconstruction in paediatric oncology: a finite element study*. Proc Inst Mech Eng [H], 2003. **217**(2): p. 111-9.
11. Viceconti, M., et al., *Effect of the initial implant fitting on the predicted secondary stability of a cementless stem*. Med Biol Eng Comput, 2004. **42**(2): p. 222-9.
12. Viceconti, M., et al., *Numerical model to predict the long-term mechanical stability of cementless orthopaedic implants*. Med Biol Eng Comput, 2004. **42**(6): p. 747-53.
13. Zhou, Z.R., V. Pellerin, and L. Vincent, *Titanium & aluminium*. 1989, P.A.: Coulon.
14. Cristofolini, L., et al., *In vitro replication of spontaneous fractures of the proximal human femur*. J Biomech, 2007. **40**(13): p. 2837-45.

15. Polikeit, A., L.P. Nolte, and S.J. Ferguson, *Simulated influence of osteoporosis and disc degeneration on the load transfer in a lumbar functional spinal unit*. J Biomech, 2004. **37**(7): p. 1061-9.
16. Horikoshi, T., et al., *Peripheral quantitative computed tomography of the femoral neck in 60 Japanese women*. Calcif Tissue Int, 1999. **65**(6): p. 447-53.
17. Bayraktar, H.H., et al., *Comparison of the elastic and yield properties of human femoral trabecular and cortical bone tissue*. J Biomech, 2004. **37**(1): p. 27-35.
18. Huiskes, R., et al., *Adaptive bone-remodeling theory applied to prosthetic-design analysis*. J Biomech, 1987. **20**(11-12): p. 1135-50.
19. Lattanzi, R., et al., *Hip-Op: an innovative software to plan total hip replacement surgery*. Med Inform Internet Med, 2002. **27**(2): p. 71-83.
20. Cehreli, M., S. Sahin, and K. Akca, *Role of mechanical environment and implant design on bone tissue differentiation: current knowledge and future contexts*. J Dent, 2004. **32**(2): p. 123-32.
21. Viceconti, M., et al., *The multimod application framework: a rapid application development tool for computer aided medicine*. Comput Methods Programs Biomed, 2007. **85**(2): p. 138-51.
22. Rey, R.M., Jr., et al., *A study of intrusion characteristics of low viscosity cement Simplex-P and Palacos cements in a bovine cancellous bone model*. Clin Orthop Relat Res, 1987(215): p. 272-8.
23. Frei, H., et al., *Cement flow during impaction allografting: a finite element analysis*. Journal of Biomechanics, 2006. **39**(3): p. 493-502.
24. Bergmann, G., F. Graichen, and A. Rohlmann, *Hip joint loading during walking and running, measured in two patients*. J Biomech, 1993. **26**(8): p. 969-90.
25. Gottschall, J.S. and R. Kram, *Ground reaction forces during downhill and uphill running*. J Biomech, 2005. **38**(3): p. 445-52.
26. Nilsson, J. and A. Thorstensson, *Ground reaction forces at different speeds of human walking and running*. Acta Physiol Scand, 1989. **136**(2): p. 217-27.
27. Martelli, S., et al., *An explorative finite element study of a new conservative proximal epiphyseal replacement*. Journal of Biomechanics, 2006. **39**(Suppl. 1): p. 125.
28. Nalla, R.K., J.H. Kinney, and R.O. Ritchie, *Mechanistic fracture criteria for the failure of human cortical bone*. Nat Mater, 2003. **2**(3): p. 164-8.
29. Cummings, S.R., D. Bates, and D.M. Black, *Clinical use of bone densitometry: scientific review*. Jama, 2002. **288**(15): p. 1889-97.
30. Taddei, F., A. Pancanti, and M. Viceconti, *An improved method for the automatic mapping of computed tomography numbers onto finite element models*. Med Eng Phys, 2004. **26**(1): p. 61-9.
31. Viceconti, M. and F. Taddei, *Automatic generation of finite element meshes from computed tomography data*. Crit Rev Biomed Eng, 2003. **31**(1-2): p. 27-72.

Chapter 7

Modelling the musculoskeletal system for predicting *in-vivo* muscle forces: the new challenge

The analysis of the femoral biomechanics (Chapter 6) highlighted that either the loading intensity or the loading scheme, even physiological, significantly influence the risk of femoral neck fractures, both in case of implanted and intact femur.

Unfortunately the current knowledge on the physiological forces acting on the skeletal system does not allow a complete description of the full range of conditions the implant may undergo during its operating life. In fact, the direct measurement of joint reactions is possible only on few patients which have been implanted with an instrumented prosthesis [1]. Conversely the direct measurement of muscular forces during motion is not currently feasible as, up to now, no techniques are known for non-invasively register the muscular forces on living individuals. To the authors knowledge, the only information on muscles activity during the execution of an assigned task of motion are obtainable through elettromiographic exams (EMG) [2], the measurement of the tension on few tendons [3] or indirectly through the measurement of the oxygen consumption [4]. None of these techniques allows a full and quantitative evaluation of the contribute that each muscle gives to the motion.

Another method to estimate the muscle forces during motion is through modelling the musculoskeletal system. Current modelling techniques compute the instantaneous pattern of muscles activation assuming that the human nervous system selects a certain contractile pattern from the infinite set available, in order to minimize a chosen cost function [5, 6]. Although there is a general accord on which type of functions best produce realistic results, the real strategies adopted by the neuro-motor control system during motion are far to be understood. Thus the cost function do not have any theoretical support, and neuro-motor control strategy are probably non unique through the individuals and the types of motion. Moreover the impossibility to compare the predicted values with reliable measurements of the complete set of forces exerted by the muscular system, strongly limit the reliability of models predictions.

Therefore, the published boundary conditions at the hip representing activities of daily living on few individuals, simulated during this research study can be considered significant but probably cannot be considered exhaustive.

On the author opinion, developing statistical musculoskeletal models to predict the entire set of muscle activation patterns coherent with a selected task of motion should allow a better understanding of the hip biomechanics. To this aim it is necessary to develop musculoskeletal models that, instead of constraining the solution to a selected cost function, are able to identify the entire space of solutions, coherent with the studied motion. Once available, the many possible activation pattern can be used as a statistical input during the biomechanical analysis of the proximal femur.

The focus of the last part of this research activity was therefore moved to modelling the musculoskeletal system. It was immediately clear that, due to the high complexity of the human body, the description of biomechanical competences of the musculoskeletal system require the knowledge of a huge number of parameters. Hence, to provide the entire set of data needed for the generation of musculoskeletal models it is necessary to fuse data, coming from different sources, with a complex and a multidisciplinary approach. To this aim, the data fusion of medical data is considered a powerful tool in collecting the entire set of information.

In the frame of the LHDL project (www.livinghuman.org), an experienced team of pathologist is collecting data by digitising the cadaver anatomy on two specimens through dissection. Another team is developing a software (LHPBuilder, www.biomedtown.org) which is a virtual environment for the integration of collected data. The final goal of the project is to provide to the scientific community a common repository to share data, and a tool to fuse them, so as to facilitated the research activity in biomechanics.

The current state of the art on biomechanical modelling of the musculoskeletal system is presented in the present chapter together with current challenges the LTM is dealing with. The work started in parallel with the analysis reported in the previous chapter, and it is continued as the principal activity of the last year of Ph.D. The work done in modelling the musculoskeletal system. After a four month training on musculoskeletal models of the upper limb (see Appendix D) at the Bio-mechanical Laboratory of the Delft Technique University the activity started at IOR was to develop methods to generate musculoskeletal models of the lower limb from medical images. The work started on the base of a large amount of clinical data from a IOR patient. The paragraph 7.2 describe the first application of the method under development, which allowed the biomechanical analysis of both femurs during walking by simulating the individual motion as well as the individual bony structure.

7.1 Biomechanical modelling of the musculoskeletal apparatus: status and key issuesⁱ

Although biomechanics is a relatively young discipline, the research activity over these 30 years has been intense. However, the impact of biomechanics today is not yet as great as one may have expected. One of the main factors limiting the application of biomechanics results is that, to answer most practical questions, a global model is required.

ⁱ Viceconti M., Testi D., Taddei F., Martelli S., Clapworthy G.J., Van Sint Jan S., “Biomechanics modelling of the musculoskeletal apparatus: status and key issues” Proceedings of the IEEE, 94(4) , 2006, p: 725-739

We provide an example for clarification. A patient has a skeletal defect—say, in the femoral shaft—which weakens the femur. The orthopaedic surgeon would like to know if this means that the patient is risking a femoral fracture in his normal daily life. To provide an accurate answer, we need to measure how the patient performs the movements that are known to impart the greatest stress on the femur. Then, we have to create a subject-specific model of the lower body (body level) in order to predict the muscle and joint forces that the patient must exert to perform the given movement (Figure 1).

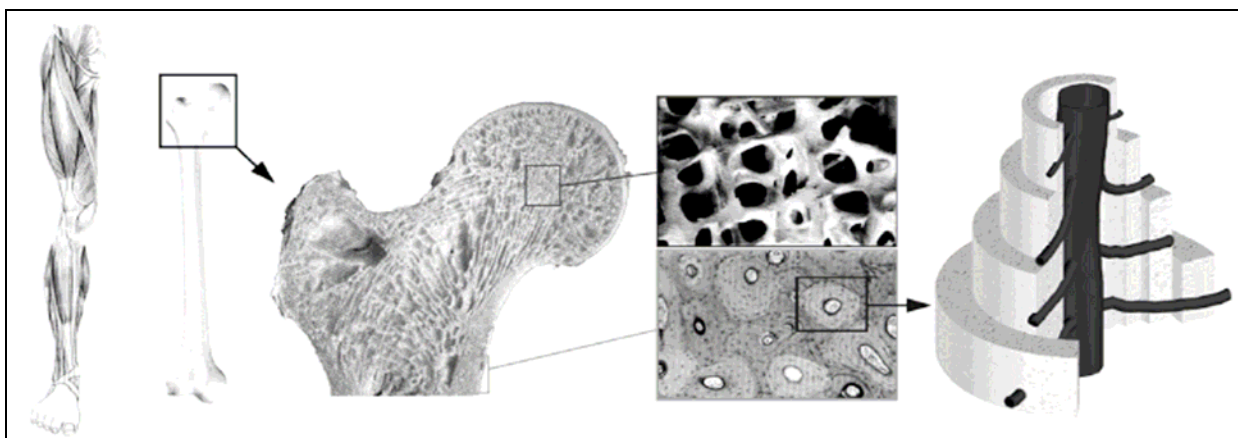


Figure 1 - Biomechanical models should span multiple dimensional scales.

Once we know these forces, and the velocities and accelerations of each bone with respect to the others, we can create a model of the femur (organ level) and compute the stresses and strains at the continuum level, e.g., by assuming that physical quantities, such as energy and momentum, can be handled spatially in the infinitesimal limit. In some regions of the femur, the bone is very porous, so the assumption of a continuum is only partially valid. If we need a more accurate prediction, we need to make a local model, which explicitly represents the tissue morphology in the region of peak stress (tissue level). Finally, from this model, we can derive the true mechanical stress that the tissue experiences during that movement and, hence, knowing the strength of the bone tissue, we can estimate the risk of fracture.

This poses two problems. The first is that we need multiple models that are coupled, with each modelling the phenomenon at a different dimensional scale. In mechanobiological problems, such as bone remodelling (the process in which bone is reabsorbed and new bone formed at the same site), the researcher must go down to the cell level, in order to model the mechanical interaction between the tissue and the cells [7]. Each model relies on different assumptions and requires different numerical methods: in the body model, the bones can be assumed infinitely rigid, and the problem can be modelled using ordinary differential equations; at the organ level, we can make a continuum assumption and model the bone with partial differential equations solved using the finite- element method; at the tissue level, the topological complexity is usually too high, and we need special discretization methods and, consequently, custom solvers different tools, different methods, different skills. Furthermore, all of these models are, in principle, coupled, and should thus be solved simultaneously.

The second problem is that, to create and fully identify all of these subject-specific models, we need a large amount of information on the patient's body. As we shall see, some of these data

can be measured non-invasively, while others can be estimated from diagnostic imaging. But this still leaves some for which the only possible form of measurement is invasive. When this is not possible, or ethically unacceptable, we would generally resort to average data, relying on the assumption that, for the specific parameter, our patient is not greatly different from the rest of the population. This assumes the existence of a large volume of normative data collected invasively, and the ability of our models to cope with an input parameter that is given as a distribution rather than as a single value.

The aim of this review paper is to report on the current state of the art in creating in silico humans that are able to predict the biomechanics of the human body at all scales of interest. The focus will be on the musculoskeletal apparatus, although much of what is written is valid also for the biomechanical modelling of other apparatuses. The review is organized in three sections. In the first section, we briefly summarize the state of the art of computational biomechanics at body, organ, tissue, and cell levels. The second section summarizes recent achievements in the area of multiscale models. The final section deals with the challenges to be faced before we can realize a true living human model. These challenges will be overcome by addressing major problems in numerical analysis, computer graphics, data management, etc., the complexity of which suggests that the Living Human Project will remain a fertile subject for multidisciplinary projects for some considerable time to come.

7.1.1 Biomechanical modelling of the body

7.1.1.2 Modelling strategies

The mesh word biomechanics, introduced into Medline in 1968, yields 453.788 records. Adding the word body reduces them to 19 041. It can thus be seen that the biomechanics of the human body has been a very vital research area in the recent past, and it is certain that it will continue to be the subject of much investigation for the foreseeable future. The ability to predict how the whole body will move and how it will exchange forces with the environment is of great importance in fields such as sport sciences, ergonomics, safety, as well as in clinical sciences. A comprehensive literature review on the computer modelling and simulation of human movement was published in 2001 [8].

Many computational models that have been developed for the whole body have had a very narrow focus, and have thus tended to be highly simplified [8, 9]. In contrast, in relation to the creation of an in silico human, we shall focus only on those modelling approaches that have a broader scope.

The biomechanics of the whole body is usually investigated by representing the human body as a multielement mechanism, in which the bones are the elements of the chain, the articulations between bones are the joints of the mechanism, and the muscles are the actuators that, by contracting, accelerate the elements of the mechanism (*Figure 2*).

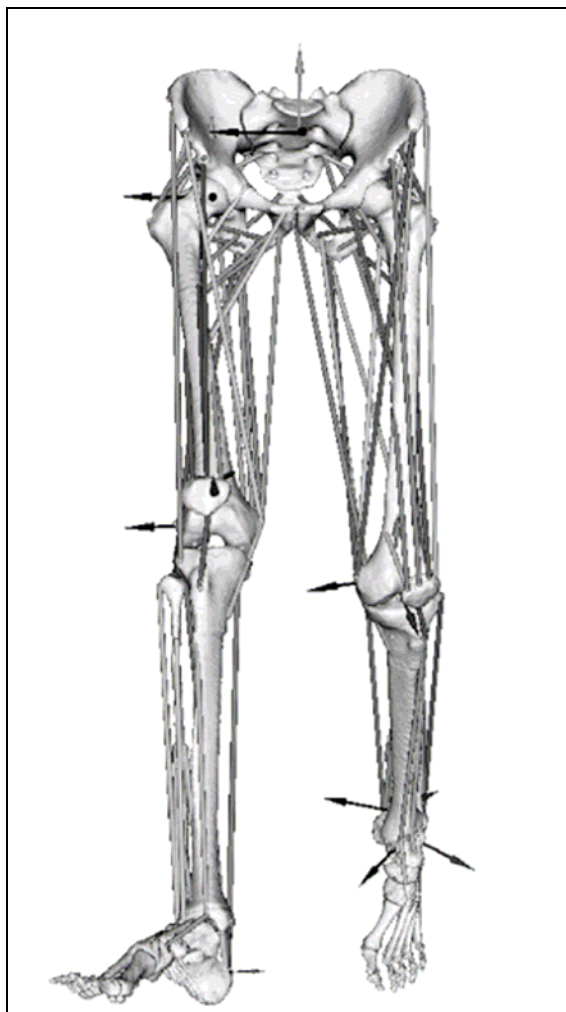


Figure 2 - Example of a whole-body musculoskeletal model (data from visible human man)

By contracting the muscle in a proper temporal sequence, we can generate a wide range of movements or create forces to be exerted on external objects.

To model the body as a multielement mechanism, it is usually assumed that the bones are infinitely rigid [10, 11], that the body articulations can be assumed to be ideal joints, [12, 13], and that each major bundle of the skeletal myotendinous units can be represented with a linear actuator oriented as the conjunction between the centroid of the area of insertion and the centroid of the area of origin (line of action) [14].

Even with these major simplifications, there are many nontrivial problems to be solved. For some muscles, the assumption of a straight line of action is unacceptable, and muscles with complex pennation angles (the orientation of the muscle fibres) are difficult to decompose into subbundles having most fibres oriented in a dominant direction. One possible approach in such cases is to use multiple actuators to model a single bundle, placed in series or in parallel [15].

During movement, the line of action of each muscle changes, and many muscles wrap around other anatomical structures. Thus, the configuration of the lines of action must be recomputed for each instant, and when the muscle wraps, a single line of action must be replaced with two serial

lines of action [16]. An alternative approach is to consider curvilinear lines of action, but this subsequently complicates all the actuator calculations [17].

Further, some authors have suggested that factors we currently neglect are, in reality, of some importance, for example, the biomechanical role of the skin or the fasciae (soft tissue sheets connecting bones and muscles) [18] or the transverse interactions between muscle bundles [19].

7.1.1.3 Possible uses of Whole-Body Models

Once a computer model of the musculoskeletal dynamics is available, it can be employed in two different ways. In the first of these, it is assumed that the body motion and the instantaneous ground reactions are known, and the model is used to solve the inverse dynamics problem, determining the joint forces and moments that can produce the observed motion. For slow motions, we can assume an instantaneous static equilibrium and neglect the inertia while, for rapid movements, it is necessary to solve a fully multibody inverse dynamics problem formulated as a set of ordinary differential equations.

These generalized force vectors acting at the joints are, in part, resisted by the joints themselves and, in part, balanced by the forces expressed by the muscles. Here we face the so-called myoskeletal indeterminacy problem [12, 20]. It is possible to achieve the same equilibrium condition with very different contractile patterns obviously, these will translate into different muscular forces being exerted at a given instant of the motion. Even if electromyography measurements are available, at the current state of the art they provide information only on which muscles are contracting at any instant, not on how strongly they are contracting. Attempts to predict the muscle force directly from the EMG signal are producing contradictory results [21]. The most common approach used to solve this problem, pioneered by Seireg and Arvikar in 1973 [22], is to presume that our motor control selects a certain contractile pattern from the infinite set available, in order to minimize some factor the risk of damaging the muscle, the oxygen consumption, or other similar variables [5, 6].

The alternative use of musculoskeletal models acts in the reverse direction. By implementing models of the motor control strategies that selectively activate the muscle actuators, the resulting motion is computed using forward dynamics. Here the greatest challenge relates to the definition of a proper goal for the motor task a cost function that must be minimized in order to find the contractile pattern, and hence the movement, that is desired. Interesting suggestions have been proposed for holding the posture [23, 24], rising from a sitting position [25], walking [26], pedaling [27], etc. The less constrained the motor task is, the more difficult it is to define the cost function, and the more computationally demanding the solution of the optimization problem becomes [13].

7.1.1.4 Model identification

The identification of these very complex models (i.e., the definition of the geometries, of the material properties, of the boundary conditions, etc.) is not trivial. It is recognized that the most significant challenges facing the modelling community today is finding new ways to more accurately describe the structure of the musculoskeletal system [8]. An accurate definition of the

functional anatomy of the body, at the level of detail required for modern whole-body biomechanical models, is an open challenge. However, an even more severe challenge is the development of methods that would allow us to create such functional anatomy models for each subject/patient.

The skeletal anatomy for a specific subject can be accurately defined from computed tomography (CT) data [28]. However, the associated radiation dose the subject receives must be ethically justified. MRI data are also used to reconstruct the geometry of the bones, but it is unclear what accuracy one can expect in this case.

The muscle geometry can be well extracted from MRI data [29, 30], while attempting the same process on CT data appears quite challenging. A recent method involving reference to a generic atlas partially solves this problem [31].

The instantaneous moment arms of each muscle can be computed once we can account somehow in the model for the wrapping of the muscles around the bones [32]. A number of other anatomical measurements, extremely important for biomechanical modelling, such as muscle-fibres and tendon rest length or muscle-fibbers pennation angles, can currently be obtained only via dissection, and are thus not available in subject-specific studies.

The shape of major ligaments, as well as the thickness of the articular cartilages, can be estimated using MRI data [33], but an accurate reconstruction of the articular surface geometry can be obtained only invasively on cadavers or on patients during operations [34].

Last, but not least, the body mass distribution is required to model inertia. The mass is usually lumped by decomposing the body into segments (head, forearms, arms, trunk, thighs, shanks, and feet) and applying the weight force vector at the centre of gravity of each body segment. The volume of the various body segments can be measured in a specific subject using laser scanning [35] or, more commonly, derived from tabulated values these provide the average inertial data of each segment for a certain study population [36].

In addition to these measurements, which are required by all models, inverse dynamics models also require, as input, an accurate measurement of the joint angles and of the ground reaction forces. However, even the most popular method, infrared stereo-photogrammetric tracking of passive skin markers, tends to be only moderately accurate [37]. Likewise, forward dynamics models also require all the parameters needed to identify the excitation-contraction coupling models [38, 39].

From this review, it is evident that, at present, it is impossible to measure, non-invasively, all of the parameters required to identify a whole-body biomechanical model for a specific subject. Thus, it is essential to create large public repositories of functional anatomy data, which can be used to generate population-averaged data to complement the few subject-specific data available [40, 41].

Even the ideal whole-body model would not be able to answer questions on how the forces act on the single organs that form the body. For this purpose, it is necessary to develop models of the single organs at a smaller dimensional scale.

7.1.2 Biomechanical modelling of organs

7.1.2.1 Modelling strategies

When our body performs a motor task, or is acted on by external forces (such as during a fall or an automobile accident), all of the various organs forming the musculoskeletal apparatus are subjected to significant loads. Under the action of such loads, these organs are displaced or deformed, and may even face damage if the load is excessive. Thus, it is of great interest to know the displacements, the stresses and the strains that applied loads induce in each organ.

Detailed reviews of biomechanical modelling are available for particular organs including muscles [42, 43], ligaments [44], and cartilage [45, 46], for bone mesh generation [47] and for orthopaedic biomechanics in general [48, 49]. At this scale, all organs are normally assumed to be continuous solids, in the sense of classical solid mechanics [50].

7.1.2.2 Whole bones

Bones are hard solids and their geometry can be accurately determined on dissected specimens with contact methods [51]. It is also possible to define subject-specific bone geometry by using medical imaging data.

The boundary conditions (forces acting on the bone) can be derived from whole-body models. However, as the complexity of setting up a whole-body model only to compute the joint and muscle forces acting on the femur is overwhelming, many authors use boundary conditions reported in the literature [1, 14, 16, 52], even though these forces were computed on an anatomy different from that being modelled.

Another issue is posed by the modelling of the tendon insertion. Muscle forces are transferred to bones via tendons, which are inserted into the bone over a finite area of variable size. However, since whole-body models represent muscles by lines of action, most authors model the muscle forces acting on the bones as being concentrated at the insertion centroid [53, 54]. Recent studies have criticized this simplification, suggesting that it may be a significant source of error [55].

A similar problem applies to joint forces, which are either predicted with models [52] or measured in vivo [56], but always provided as concentrated forces. The actual pressure distributions at the joint surfaces can be measured only in cadaver preparations, where the loads are externally imposed [57, 58], although recent research for the prediction of such distributions using models [59], or in vivo measurements [60, 61] is promising.

However, the most challenging aspect remains the definition of the constitutive equation. In cadaver specimens, it is possible to separate the various histological types of bone (cortical and cancellous). The mechanical behaviour of cortical bone has been investigated under disparate loading conditions [62, 63], while the constitutive equations of cancellous bone are still the subject of debate, in particular those relating to post-elastic behaviour [64, 65] and the failure criteria [66, 67].

The complexity increases drastically for subject-specific models. Currently the only information on the tissue that we can derive from medical imaging is the tissue density, which can be derived

from properly calibrated CT data [68]. Thus, current subject-specific models assume bone to be a non-homogeneous, but isotropic, tissue, deriving the mechanical properties of bone, i.e., Young's modulus and strength, from the CT measured density [69, 70]. However, the anisotropy information (which depends upon the local morphology) can be determined only invasively either with traditional two-dimensional (2-D) histomorphometry or micro CT on bone biopsies [71, 72]. Some recent studies have attempted to determine the trabecular structure using high-resolution MRI [73]; this approach could be applied *in vivo*, but the accuracy obtainable is still a matter of study [74]. Other *in vivo* methods use dual X-ray absorptiometry technique [75].

Biomechanics models of bone are usually formulated as linear elastic problems, solved with static finite-element analysis (FEA) [76-78]. Nonlinear models, always solved with FEA, are employed when the investigator is seeking to model the post-elastic behaviour or when the forces applied produce large displacements [79]. Special pre-processing codes are used to map the inhomogeneous tissue properties derived from CT data (Figure 3) on to the finite-element model [80].



Figure 3 - Example of a subject-specific finite-element model of a complex biological reconstruction performed on a paediatric oncology patient. Left: finite element mesh. Centre: CT-based mapping of tissue elastic properties. Right: prediction of principal tensile stresses (MPa) induced in the reconstruction at peak load instant of level walking.

7.1.2.3 Myotendinous units

Whole-organ models of muscle tendon complexes are relatively rare in the literature. The geometry of each muscle can be derived from MRI [81] or, for dissected specimens, from laser scanning [35]. The problem is that this geometry is never in an undeformed state. Because of the

low modulus of elasticity of soft tissues, dissected muscles deform under their own weight; in MRI taken from living subjects, the muscles appear always to be more or less contracted.

The boundary conditions are relatively simple to define if we assume that each muscle is an isolated solid [82]. In reality, however, during contraction, each muscle will actually press against other muscles and bones to the authors' knowledge, this condition has not yet been successfully modelled.

The constitutive equation of the passive muscle is viscoelastic, as it is for most soft tissues [83]. For slow movements, the viscous contribution is neglected and hyperelastic models are used for the constitutive equation [84]. For more rapid movements, the combination of viscous forces and large deformations makes the models extremely nonlinear, and it is necessary to adopt explicit integration schemes to solve them [85]. Some elegant theoretical formulations have been proposed to model a self-contracting elastic solid [86] but their numerical implementation appears challenging. Thus, in general, more heuristic approaches are preferred, such as those based on composite materials [87].

7.1.2.4 Ligaments and cartilages

Ligaments are usually represented by condensed parameter models, rather than by continuum solid models. Many ligaments are slender and can be modelled using nonlinear springs [44, 88]. Bundles of parallel springs are used to model the progressive recruitment of the ligament fibres during loading [89]. Continuum models are rare [90], but most of what was written above about the modelling of the passive behaviour of muscles is valid also for these models. A notable exception is the periodontal ligament, whose biomechanical behaviour is fundamental for the stability of human teeth, and which has thus attracted considerable attention in dental biomechanics [91, 92].

The numerical modelling of the mechanical behaviour of human cartilage would require a review article for itself. The numerical modelling of the complex fluid-structure interaction due to the proteoglycans requires some of the most sophisticated models yet proposed in computational biomechanics. A classical approach [93, 94] employs a poro-elastic constitutive equation originally proposed by Biot [95]. In this formulation, it is assumed that the presence of the fluid is represented implicitly, with a mixed displacement-pressure formulation. An interesting review, which highlights the multiscale nature of articular cartilages, can be found in Mow [45].

7.1.2.5 Joint models

A separate category of models contains those that aim to simulate the biomechanics of whole joints. In these models the multibody dynamics problem and the finite-element problem have to be solved simultaneously.

A typical example is the human knee. This is an articulation that is only lightly constrained by the bone geometry (diarthrodial joint), so its dynamics is heavily dependent upon the deformation of the soft tissues (ligaments, cartilages, menisci, muscles, and tendons) that form it.

An interesting approach (Figure 4), developed as part of the SimBio project,ⁱⁱ and is to use explicit finite-element modelling to solve the dynamics of the deformable bodies directly [96 189].

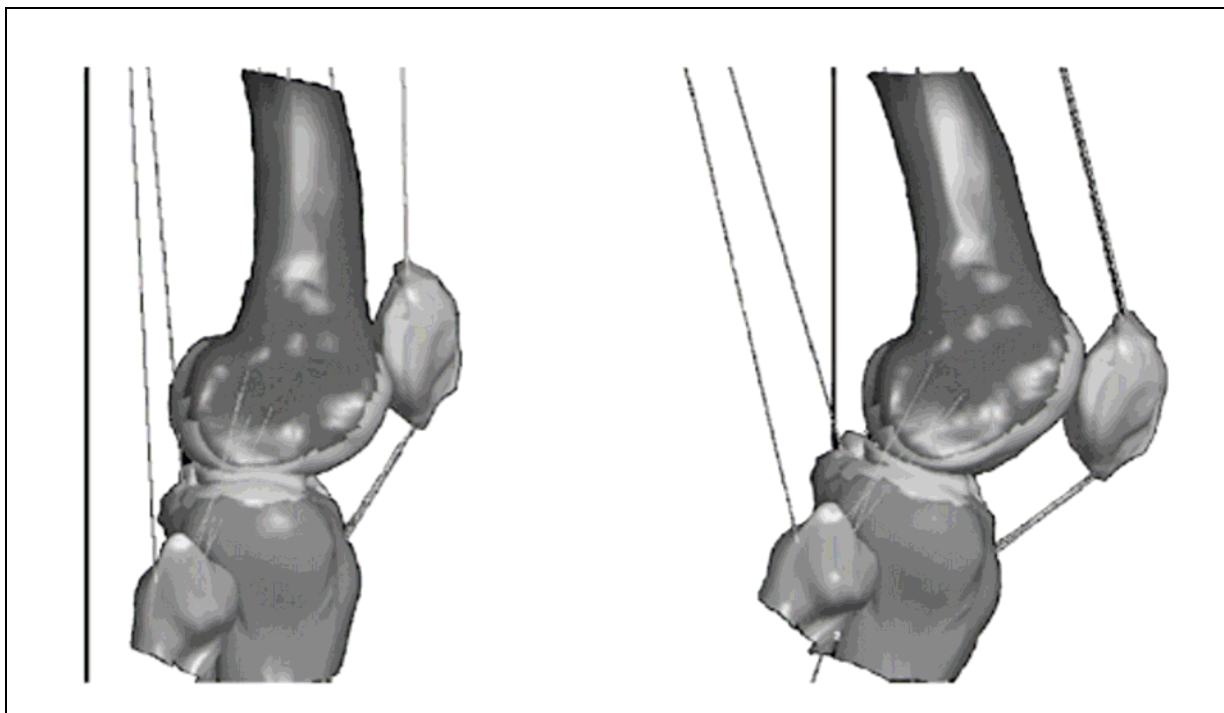


Figure 4 - Explicit finite-element model of the knee joint developed as part of the SimBio project (image courtesy of the SimBio consortium).

A similar model, published more recently, investigated the biomechanics of the implanted knee [97]. The modelling involved in these methods contains a considerable level of complexity and it should be mentioned that, to the authors' knowledge, none of them has yet been extensively validated.

A similar approach is used to investigate the risk of dislocation in prosthetic hips [98] and in the normal function of the jaw joint [99]. Another knee model, recently published [100], will be discussed in the multiscale modelling section.

Combining in vitro six-degrees-of-freedom model of the lower limb with in vivo gait motion analysis opens up new perspectives for more accurate analysis of muscle and ligament behaviour [101]. In vivo modelling from medical imaging and joint kinematics [102] is also possible when using accurate definitions for palpation of landmarks used for registration [103].

7.1.3 Biomechanical modelling of tissues

When the assumption of a continuum is unacceptably inaccurate, or when it is necessary to consider the microscopic mechanisms underlying macroscopic behaviour, it is necessary to incorporate computer models of tissue biomechanics. Extensive reviews are available on the

ⁱⁱ Available: <http://www.simbio.de/>

modelling of visco-elastic fluids [85], bone tissue [104], cartilaginous tissue [46], etc. The modelling strategies used in tissue biomechanics cannot be easily summarized as very different modelling approaches have been employed, depending upon the circumstances. One aspect that appears very important at this scale is the adaptive behaviour of tissues, which is usually regulated by complex mechanobiological processes.

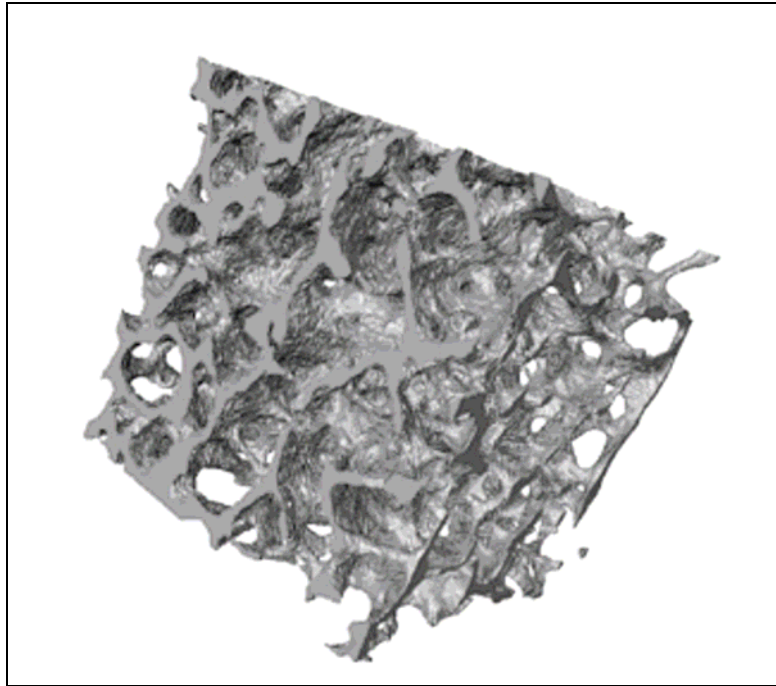


Figure 5 - Surface rendering of the microCT data relating to a sample of cancellous bone taken from the femoral neck region of a total hip replacement patient.

7.1.3.1 Some examples of tissue biomechanics modelling

The biomechanical models of cortical bone tissue are usually based on simple continuum mechanics models, which provide good predictions of the biomechanics behaviour of this dense mineralized tissue [105]. In contrast, cancellous bone is usually modelled with finite-element models that represent the intricate microstructure of this tissue [106], high-resolution microCT scanners provide the data necessary to create these complex models [107]. A direct conversion of CT image voxels into the finite elements of a Cartesian mesh avoids the complexity of generating an unstructured mesh for a geometry that possesses such intricacy (Figure 5) [106], although this does produce models made of millions of elements, which require special algorithms to be solved efficiently [108]. At a smaller scale, there are studies that analyze the role of the collagen fabric in the stiffness properties of a single bone lamella [109].

Finite-element models have also been used to investigate the length of sarcomeres within muscle fibres [110] or the bulk biomechanical behaviour of isolated muscles [59, 84]. The role of the collagen fabric has also been investigated in cartilage tissue [111].

7.1.3.2 Models of tissue adaptation

Probably the most investigated instance of tissue adaptation is bone remodelling, which has a copious literature for a slightly dated review see [48]. The same author has also provided an

interesting commentary arguing against the hypothesis that bone remodelling is an optimization process in the strict sense [112]. Adaptation of cancellous bone at the tissue level has been represented by some authors as a surface remodelling process [113]. Another interesting perspective is that of considering the damage accumulating in the tissue as the driving factor for bone remodelling; this was first proposed at the continuum level [114], but has, more recently, been explored also at the tissue level [115]. The fluid flow within the osteocytarian processes is also suspected of having a role in this [116].

7.1.4 Multiscale and probabilistic models

In biomechanics, the term multiscale model can suggest very different things. For example, we may use the term to indicate models of complex anatomical structures such as the spine, where the biomechanics is defined by the interaction of bony vertebral bodies, intervertebral discs, muscle and ligaments inserting on the spine, etc. However, here we shall use the term to indicate models that span multiple dimensional scales.

Most human tissues are organized in a hierarchical fashion. One effect is that most biomechanical properties depend upon features that are present at multiple dimensional scales; in many such cases, it is not easy to condense these properties into synthetic parameters. In the literature, we can identify two main strategies: approaches based on homogenization, and a few pioneering studies that use multiple coupled models, each describing a single dimensional scale.

Homogenized models have frequently been proposed to model the multiscale nature of cortical bone tissue. Cortical bone is formed by osteons, which are formed by lamellae, which are formed by organized strands of mineralized collagene [117]. If we can describe the topology at one scale in a periodic way, we can derive, using a process called homogenization, the structural properties that the continuum would exhibit at the upper dimensional scale, and correlate these properties [118]. The most recent work to use this approach reached a high level of sophistication [119]. A numerical optimization approach, called homogenization-based topology optimization is used to design bone tissue regeneration scaffolds with given biomechanical properties [120].

The multiple coupled methods include a recent approach to investigating the biomechanics of human hair [121]. Molecular dynamics is used to estimate the uncoiling force of filament proteins; these results are used in a statistical mechanics code to predict the relationship between yield stress and temperature. The composite structure of hair at the nanometer scale is addressed using a particle-based model for a macrofibril. Mesoscale particles representing coiled coils of keratin proteins were assembled into filaments and embedded in a matrix of soft particles cross-linked to a network. The macro fibril was extended in a non-equilibrium computer simulation, while monitoring the tensile force.

Only recently have these approaches started to be used in musculoskeletal biomechanics. A very elegant patella-tracking model, developed by Hunter's group [100], uses an explicit finite-element model of the knee, but describes the stress and strains of the tissues with reference to microstructurally based material coordinate systems. This is useful when describing a constitutive law that refers to microstructural directions, and adding active contractile forces to the fibres direction component (Figure 6).

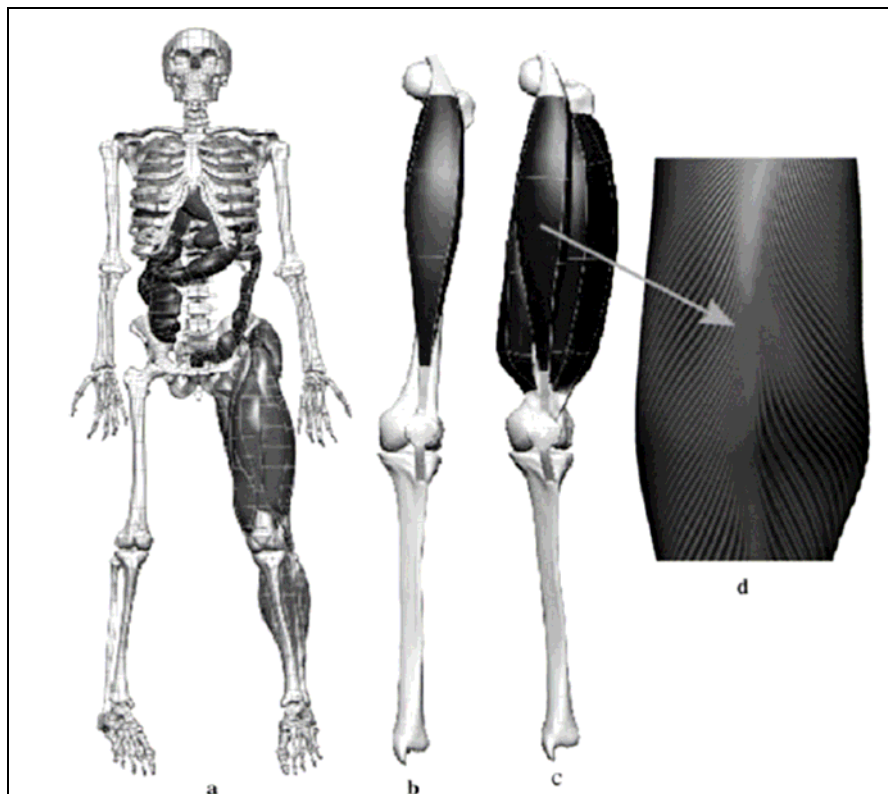


Figure 6 - Musculoskeletal model for the study of the patella motion described in [100]. *a* Geometry from the model database. *b* Single rectus femoris. *c* Multiple quadriceps subsets with *d* fitted bipennate fibre field for rectus femoris (reprinted from [100]).

The authors also propose an interesting mapping strategy for the mechanical properties of the tissues derived from the imaging data. The image lattice is superimposed on, but disjoint from, the finite-element mesh, and the numerical integration is performed on both grids. Most models average the tissue properties derived from imaging data at the node-element level (see Section III-B).

The need to investigate multiple dimensional scales with computationally efficient models is also addressed with original numerical approaches [122], while probabilistic models are frequently used to account for intersubject variability [123]. Typical statistical variables are muscle co-activation in modelling specific trunk motion tasks [124], tissue properties in modelling spine mobility [125], microcrack density in modelling the global damage accumulation in bone tissue [126], or microfiber recruitment in modelling the tensile properties of connective tissue [127].

One aspect that has not been addressed so far is that of the relationship between tissues and cells. This is another argument of great range and complexity that is difficult to summarize in a few sentences. As an example, the interested reader may consider the mechanobiology of bone remodelling. Important models that try to capture the competitive interaction between the different cellular populations that participate in the tissue adaptation process have been proposed, e.g., [128]. Most specific studies try to understand the form of mechanosensory mechanism that is embedded in bone cells [129]. A major problem of all of these studies is the lack of quantitative information of bone cells and their mechanochemical processes, and the difficulty of developing controlled experiments to validate the predictive models.

While multiscale and probabilistic modelling are currently posing major challenges, in perspective they should replace, in most cases, the aforementioned single-scale models. If I want predict the risk of fracture of a certain bone under a certain condition, first I need to know the muscle, joint, and inertial forces acting on that bone in that condition (and this requires me to solve the whole-body model); second, I need to know the stress concentration that the bone tissue microstructure may produce at various locations of that bone (and this requires me to solve tissue-level models).

In most cases, it is difficult to know in a deterministic way the essential parameters that identify my multiscale models; for many, the only thing I know is the range of value they assume in a certain population. Thus, another long-term goal will be the combination of multiscale and statistical models.

While desirable, these scenarios are currently far beyond the capabilities of all research labs worldwide. The only way to tackle them is through coordinated efforts and large-scale international research projects, such as those described in the following section.

7.1.5 The living human project: current challenges

7.1.5.1 Community building and data repositories

The anatomical collections currently available (the most famous of which is probably the Visible Human Projectⁱⁱⁱ) do not account extensively for multisubject, gender, sex, age, and pathology associated variations. Such is the variation in human anatomy that we cannot extrapolate comfortably from a single sample. Likewise, the collections totally lack any functional information.

In 2002, the Biomechanics European Laboratory (BEL), a virtual community of biomechanics researchers, distilled a wide-ranging preparatory discussion among the 4500 researchers on the BIOMCH-L mailing list, into a set of statements identifying hot topics and fundamental issues in computational biomechanics. These formed the focus of a subsequent conference the BioNet Event attended by more than 100 delegates from the most prestigious European research institutions. The outcome of that conference was the launch of the Living Human Project (LHP)^{iv} in late 2002.

This project aims to develop a worldwide, distributed repository of anatomo-functional data and an associated set of simulation algorithms, fully integrated into a seamless simulation environment and directly accessible by any researcher in the world. Its ultimate objective is to build an *in silico* model of the human musculoskeletal apparatus and this is being pursued with three parallel activities:

- The collection of data describing the anatomical, functional, and biomechanical properties of molecules, tissues, and organs relevant to the musculoskeletal apparatus, from multiple subjects that will be sufficiently numerous potentially to represent statistically the whole of humanity;

ⁱⁱⁱ Available: http://www.nlm.nih.gov/research/visible/visible_human.html

^{iv} Available: <http://www.tecno.ior.it/VRLAB/LHP/index.html>.

- the development of an application framework to support the easy and rapid deployment of software applications aimed at solving the specific problems associated with multimodal visualization, data fusion, and data exchange;
- The development of numerical models that are able to predict the biomechanical behaviour of the musculoskeletal apparatus, from the whole body down to the molecular level.

These visionary objectives pose a number of technical challenges in the domain of applied computer science that are briefly summarized below. They also pose a number of logistic and organizational issues. One of particular importance is to identify the most effective business model under which to run data and model repositories.

The BEL repository^v is currently based on a free-access concept, in which the user is forced to accept a licence agreement that prevents him from using the data for profit and from redistributing them; it also obliges him to acknowledge the source and its author in any publication or presentation. However, it is not clear that these rules are always respected and, in any case, their enforcement is not really practicable. Alternative models are being discussed, including a give get model in which only those who post data can download data. Of course, the more complex the business model becomes, the more expensive it will be to create and operate such repositories; this poses the parallel issue of the long-term sustainability of these initiatives, which are currently based entirely on the efforts of volunteers.

7.1.5.2 Data fusion and data processing

In-silico human models will have to combine enormous amounts of data describing the human body from many different perspectives and at disparate dimensional scales. Furthermore, in order to be of any clinical use, these models will have to account for intersubject variability and will possibly be required to merge population-averaged data with those few data available for a specific subject, in order to personalize the simulations. This poses a number of problems related to data fusion, spatial and temporal registration, data processing, etc.

Our group has recently released a software framework called the Multimodal Application Framework^{vi} (MAF), which allows the rapid development of applications for computer-aided medicine. The framework, which is distributed under a BSD-like open source license, approved by the Open Source Initiative (OSI),⁶ and incorporates a distributed ownership model, is also an ideal environment in which to accumulate all of the algorithms that may be necessary for the data fusion and data modelling needs of in silico human projects.

MAF incorporates some of the best open source software toolkits available: VTK for visualization,^{vii} ITK for registration and segmentation of biomedical data,^{viii} V-collide for collision detection in dynamic simulations,^{ix} etc. Thus, MAF is primarily a sort of distribution (in

^v Available: http://www.tecno.ior.it/VRLAB/researchers/repository/BEL_repository.html.

^{vi} Available: <http://sirio.cineca.it/B3C/MAF/>.

^{vii} Available: <http://www.vtk.org>

^{viii} Available: <http://www.itk.org>.

^{ix} Available: http://www.cs.unc.edu/~geom/V_COLLIDE/.

the Linux sense) a collection of useful tools wrapped into a coherent development environment. On top of these powerful tools, the consortium that developed MAF through a three-year international research project funded by the European Commission has added a number of very powerful capabilities. The current version of MAF includes methods for the registration of points, surfaces and volumes; it can fuse and visualize data from any digital medical imaging device, including 4-D datasets such as cine-MRI; it can fuse and visualize data from motion capture, finite-element analysis, multibody dynamics simulations, and special biomedical signals such as electromyography. All of these data can be imported, registered with each other in space and time, and processed using a number of algorithms such as filtering, decimation, re-sampling, segmentation, etc. In the latest release, to be made available shortly, we shall also include a linear elastic finite-element analysis solver, fully integrated into the framework. MAF applications can provide an integrated interface to very complex data collections (Fig. 7).

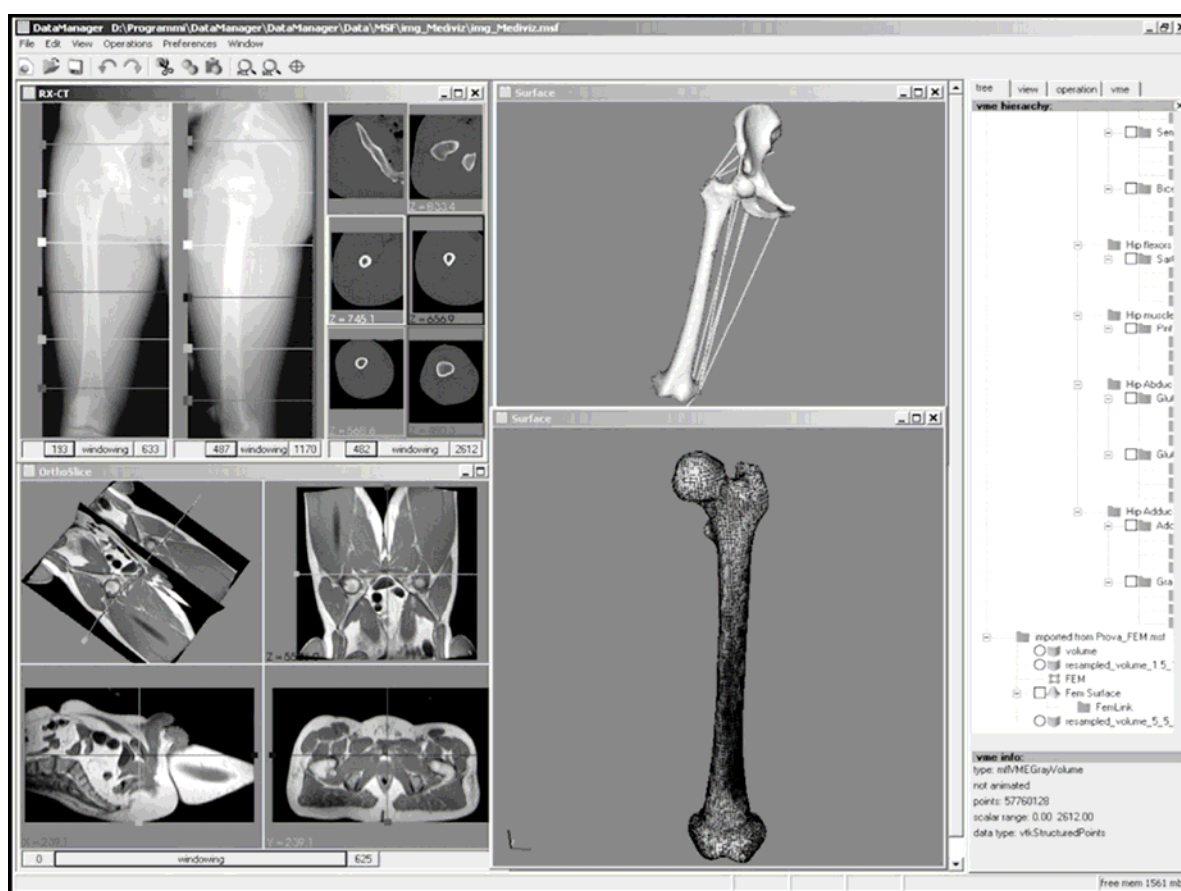


Figure 7 - A typical interface of a MAF application with different types of data and representations.

7.1.5.3 A framework for numerical modelling

What the MAF is currently missing is a framework for simulation. The development of a serious simulation environment, such as a general-purpose finite-element analysis package similar to Ansys (Ansys Inc., Canonsburg, PA) or Abaqus (Abaqus Inc., Providence, RI), may require hundreds of person-years of development. Thus, it is likely that all such products are, or will become, commercial.

Unfortunately, very little work has been done to ensure interoperability between them. On the contrary, most of the commercial packages tend to discourage the use of multiple products by using arcane and undocumented storage formats, very peculiar modelling approaches that cannot be easily translated into another product, etc. Last, but not least, all of these products mainly target the important industrial markets such as the automotive or aerospace sectors, and it is thus unlikely that features that are useful only to bioengineering problems will be implemented.

This is an open problem, which does not admit an easy solution. One may consider the development of a front-end environment, which would provide a unifying interface to all of these disparate codes. An example of this is ModeFrontier,^x a product for multiobjective optimization that acts as a front-end for many commercial products such as Catia, Nastran, Marc, Abaqus, CFX, Tascflow, Star-CD, Fidap, Fluent, Adams, Magma, Lagrange, HissD, Straus, Matlab, Femlab, and CAD-Mould.

Another approach is to develop an integration framework, such as the MAF. This approach has been pursued by the Open Cascade open source project,^{xi} which aims to provide components for three-dimensional (3-D) surface and solid modelling, or the JSIM project^{xii} which is a simulation framework for signal modelling. To the authors' knowledge, no similar initiative has been started for a framework relating to solid and fluid mechanics. Probably the closest approximation is the GiPSi project, an open source/open architecture framework for developing organ-level surgical simulations.^{xiii}

7.1.5.4 Information and scientific visualization

Advances in medical technology continue to provide data with increasing resolution, while new forms of data also emerge to supplement those that currently exist. The result is that clinicians and researchers are faced with ever-expanding data sets that they need to consider to resolve the problems they are investigating.

Grid technology [130] provides one solution in terms of access to data and the computational power needed to process it. Developing a comprehensive software framework, as described above, will also help by providing a unified environment within which all the necessary operations can be combined. However, there still remain issues in ensuring that generic information can be adapted accurately to a specific individual and that information at different levels of detail can be merged appropriately.

Using medical data in computer-based visualization of the human form has been taking place for many years, and in that time, many spectacular images containing considerable detail have been produced. However, the most striking images have generally been created from specific, highly detailed data sets, such as those of the Visible Human project. There remain many challenges in producing visual information containing the required detail related to a specific individual,

^x Available: <http://www.esteco.it/Products/modeFrontier/>

^{xi} Available: <http://www.opencascade.org>

^{xii} Available: <http://nsr.bioeng.washington.edu>

^{xiii} Available: <http://gipsi.case.edu/>

particularly if the imaging modalities used have been constrained by cost implications for example, if the use of MRI imaging is not justified for the condition being investigated, or if the region on which imaging is performed is highly localized.

In such circumstances, mapping data from a detailed generic atlas on to the available, rather limited, data from the specific individual may provide improved insights. The implementation of this mapping depends greatly upon the quality of the subject data and the difficulty associated with identifying corresponding points in the two anatomies. A large volume of work on registration has been undertaken over many years [131, 132] but there remain many problems, particularly related to the mapping of soft tissue. One approach in a case in which there exist no landmarks within the soft tissue is reported in [31].

Recent developments in 3-D texture mapping may also allow an enrichment of the visual information available. Developing large texture patterns from small samples in 2-D has seen intensive publication of research papers over the last few years, [133] and these techniques are now being extended to 3-D, [134]. The early methods in this area are still rather slow because of heavy computational demands but it is expected that, by shifting much of the calculation to the GPU, improved performance can be rapidly achieved. Two obvious examples in which this approach would be useful are in demonstrating muscle fibre orientation and the trabecular structure of spongy bone. In both cases, the availability of a measure of high-level parametric control would be essential so that generic texture maps could be adapted to the specific individual using knowledge acquired by the medical professional from the individual's profile.

The use of 3-D texture may also provide a bridge between data captured at different scales. The models used in visualization are often, of necessity, highly complex because of the complexity of the structures they seek to represent. Representing a microlevel model as a texture within the macrolevel model may provide a way of making available, when visualizing at the macro level, information on the most significant features of the micro model, without expanding the macro model to an impractical level of complexity.

However it is finally achieved, ensuring that visual representations derived from calculations at one level of detail remain consistent with those derived from calculations at the levels of detail above and below will be one of the foremost challenges to be faced when visualizing the *in silico* human.

7.1.5.5 The road ahead

The idea of a technological infrastructure for Physiome- related research is slowly becoming established within our community. The American National Institute of Health, as part of its NIH Roadmap for Medical Research Grants, has recently supported the SimBios project.^{xiv} The fundamental aims of Simbios is to develop a Simulation Tool Kit (SimTK), which will enable biomedical scientists to develop and share accurate models and simulations of biological structures, from atoms to organisms.

^{xiv} Available: <http://simbios.stanford.edu/index.html>

Meanwhile, the European Commission has recently published the first draft of a white paper produced by a group of experts after a recent meeting in Barcelona, Spain, entitled “Toward the Virtual Physiological Human: Multilevel Modelling and Simulation of the Human Anatomy and Physiology”^{xv}. The promoters intend the Virtual Physiological Human (VPH) to be an organized collection of computational frameworks and ICT-based tools for the multilevel modelling and simulation of the human anatomy and physiology. Once sufficiently developed, the VPH will provide an essential technological infrastructure to the Physiome Project, to pathology-specific initiatives in translational research, and to vertical solutions for the biomedical industry. As part of this endeavour, the STEP16 coordination action will organize a focused discussion to define a detailed European research roadmap for the development of the VPH technology. STEP^{xvi} will commence in January 2006 and run for 15 months; its activities will include a major conference concentrating on all aspects of the VPH and related matters, in late 2006.

Further, the European Commission has committed to support a three-year research project entitled LHDL: The Living Human Digital Library, 17^{xvii} which aims to realize a significant part of the infrastructure described above. This project, while mainly focused of the development of the technological infrastructure, will also include a significant data-collection campaign, which should provide the first extensive collection of data and models of the musculoskeletal apparatus from the proteins to the whole body.

7.1.6 Discussion

In this paper, we have made a survey of the state of the art in that part of computational biomechanics research that is aiming to create an in silico model of the human musculoskeletal apparatus. We have also indicated what we consider some major technological challenges that need to be solved in order to achieve this ambitious objective.

It is evident that some of these challenges exceed the potential currently available within computational biomechanics, worldwide. To tackle them effectively, it will be necessary not only to coordinate all of the efforts involved in a coherent way, but also to increase the level of resources deployed in this endeavour. For this, we should seek to generate an increased level of awareness of the concept of the in silico human, so that strategic initiatives like the Physiome Project and derived activities such as the Living Human Project receive a similar amount of attention to that accorded in the recent past to the Genome project. We shall have to convince large federal funding agencies such as the American NIH or the European Commission that providing a special funding allocation for these initiatives will be worthwhile.

Thus, it is essential that we, as a community, communicate to society as a whole how strategic this research objective is, and how dramatic its impact will be once we achieve it. Further, we must emphasize that the benefits will accrue not only at the research level, but will also cascade down to the man in the street in terms of improved health care based on personalized models.

^{xv} Available: http://europa.eu.int/information_society/activities/

^{xvi} Available: <http://www.europphysiome.org>.

^{xvii} Available: <http://www.europphysiome.org/>.

Without such a movement, it is difficult to see how the critical mass necessary to provide the coherent approach demanded by the problem can be created in a suitable timescale to take full advantage of the possibilities afforded by recent technological advances.

7.2 Subject-specific musculoskeletal models from medical images^{xviii}

Limb-salvage surgery has been increasingly adopted in the treatment of primary bone sarcomas, but still the optimal reconstruction is debated. The finite element (FE) method is a powerful tool to investigate the mechanical behaviour of bone segments. The methods recently developed to generate subject-specific FE models of bones from Computed Tomography (CT) data are reliable; relevant validation studies having confirmed that these can be used in a clinical context, and their predictions are accurate.

Aim of the present work is to present a subject-specific FE study to analyse the evolution of the mechanical strength of a complex distal femoral reconstruction during the first three years of follow-up.

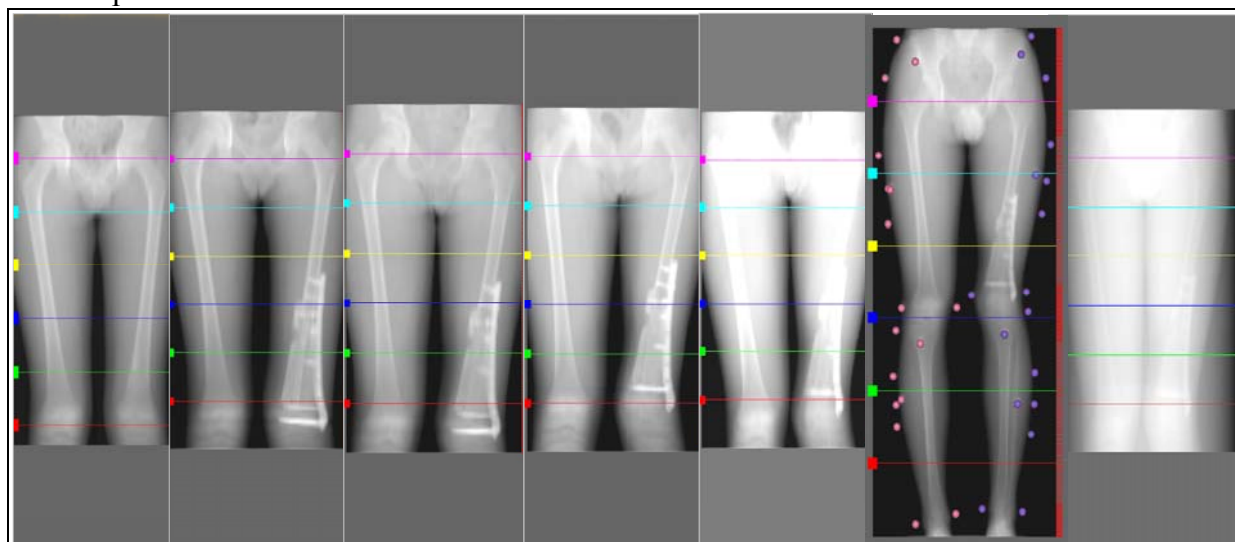


Figure 8 - The available CT exams. From left to right: pre-op, post-op, 7, 13, 29, 36, 44 moths of follow-up. In the sixth CT exams the markers for the gait analysis are visible.

7.2.1 Material and Methods

In 2001 a 10 years-old boy underwent a distal femoral reconstruction for a primary bone sarcoma, by means of a massive bone allograft in conjunction with a vascularised fibula autograft. During the first three years of follow-up the patient was CT scanned at nearly regular time intervals. One pre-operative and six post-operative CT exams were available. At the time of the sixth exam, the patient underwent also gait analysis at the Movement Analysis Laboratory. An innovative protocol [135] was used, applying skin reflective markers prior to CT scanning, to allow for the spatial registration of patient's kinematics to the skeletal model.

^{xviii} F. Taddei, S. Martelli, L. Montanari, V. Greco, A. Leardini, M. Manfrini, M. Viceconti. "Changes in the mechanical strength of a reconstructed femur during follow-up: a subject-specific finite element study". WCB 2006, July 29th - August 4th, Munich, Germany

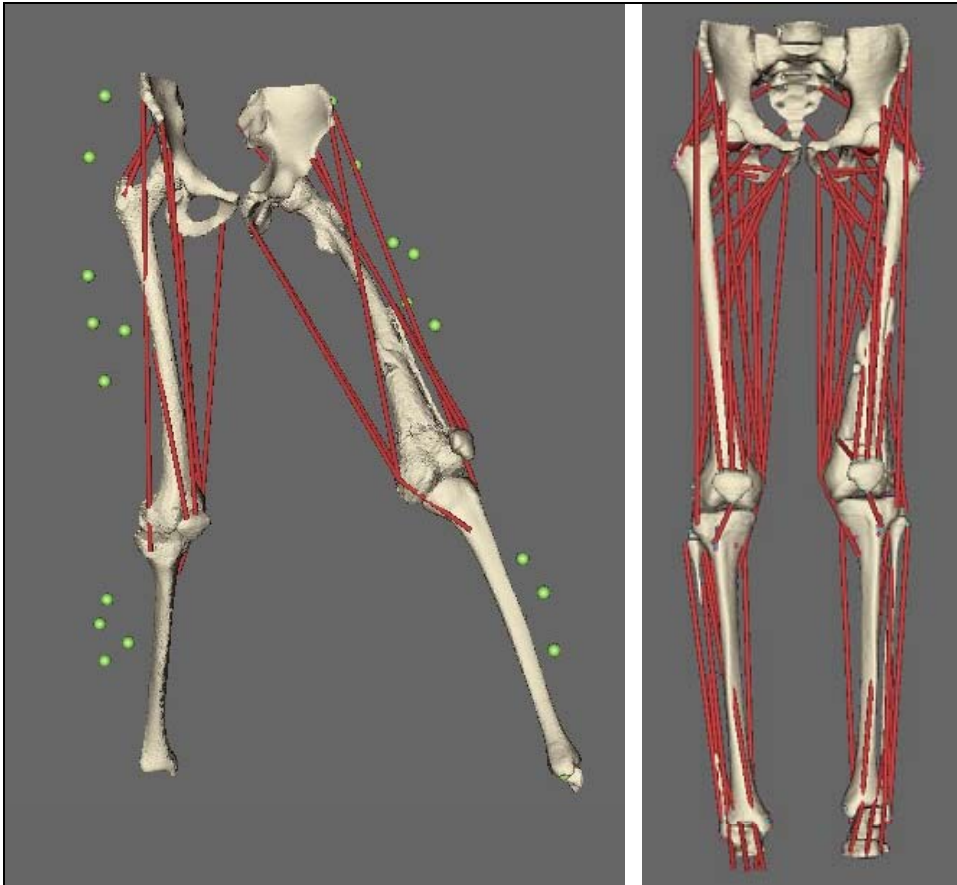


Figure 9 - The complete MS model of the patient (right) and the patient's specific registration with the gait analysis data with the DataManager© (left)

A complete subject-specific muscle-skeletal (MS) model of the patient's lower limbs was built integrating CT with kinematics data using the DataManager[©]. Muscles were represented with linear segments starting from the muscles' origin to their insertion. Muscles with broad origin or insertion areas were represented with more than one segment.

FE models of the operated femur and of the intact contralateral one, at each control exam, were built from the CT data by using a validated procedure [136]. The muscles' forces acting on the femurs, at the instant of maximum hip joint reaction, were estimated and used as boundary conditions for the FE models scaled to take into account the changes in the patient's weight.

A Risk of Fracture (RF) was defined on the basis of the maximum principle tensile stress [137]:

$$RF = \epsilon_1 / \epsilon_{yield} \quad (\epsilon_{yield} = 1.02\% \text{ [138]})$$

The evolution of the femoral strength was then put into relation with the changes in the bone density and morphology occurred over the follow-up.

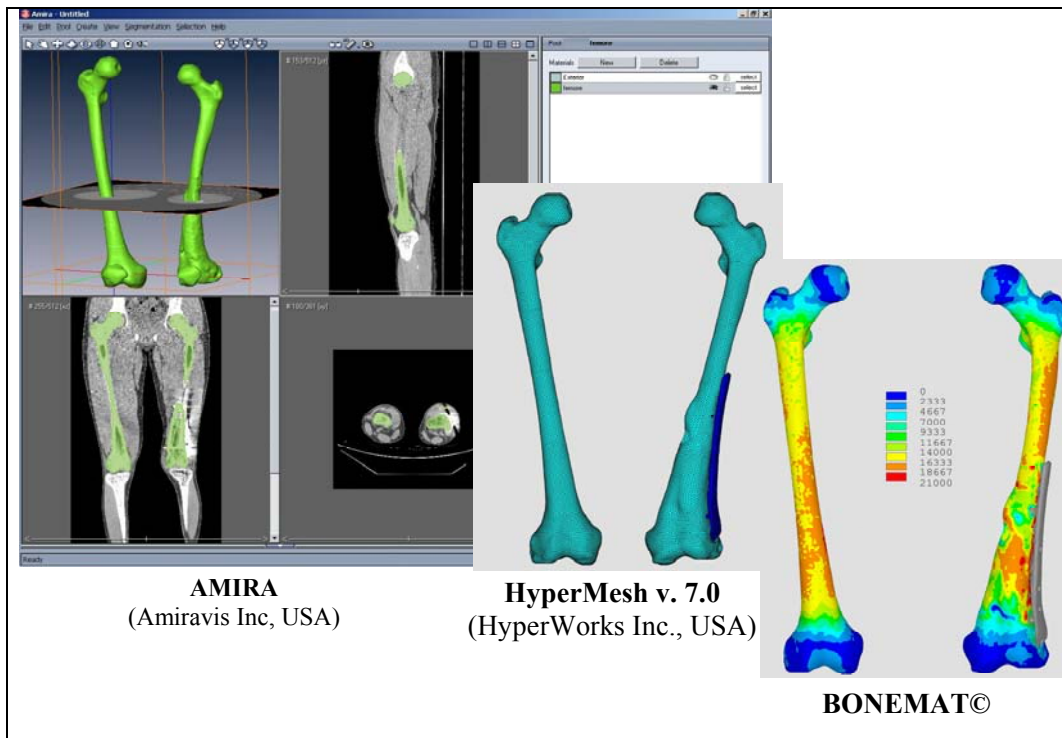


Figure 10 - The mesh generation procedure

7.2.2 Results and Discussion

The left femur showed a different mechanical behaviour with respect to the intact contralateral one, due to the altered morphological and mechanical conditions, and to the presence of the metal synthesis. This difference is made evident in the structural displacement (Figure 11) and in the stresses and strain distribution.

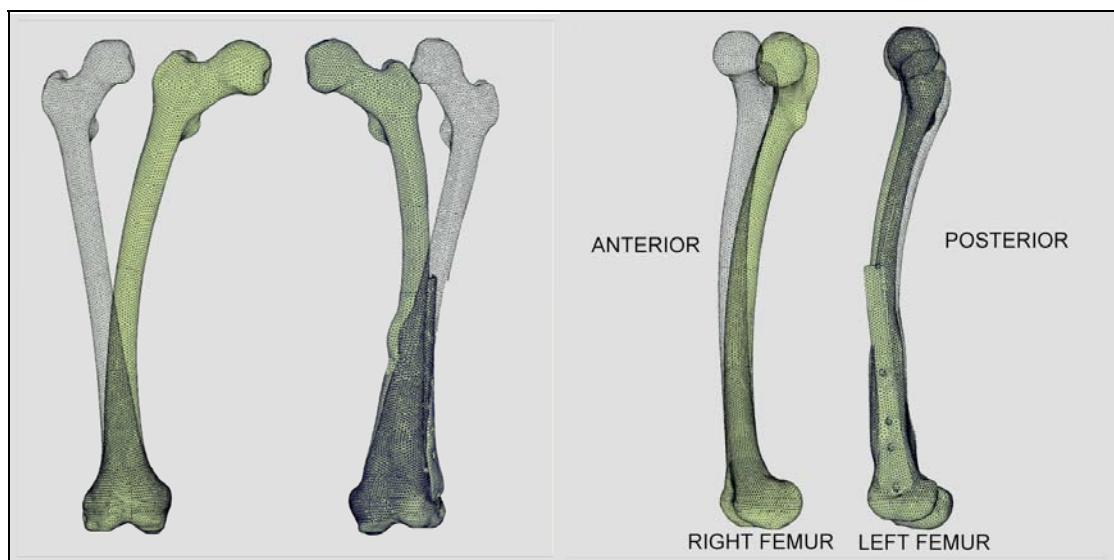


Figure 11 - The displacement of the two femurs intentionally exaggerated to increase readability

The RF in the intact right femur (Figure 12) showed the same pattern in all control exams, remaining always lower than 0.5, despite the changes in the femoral dimensions and load intensity.

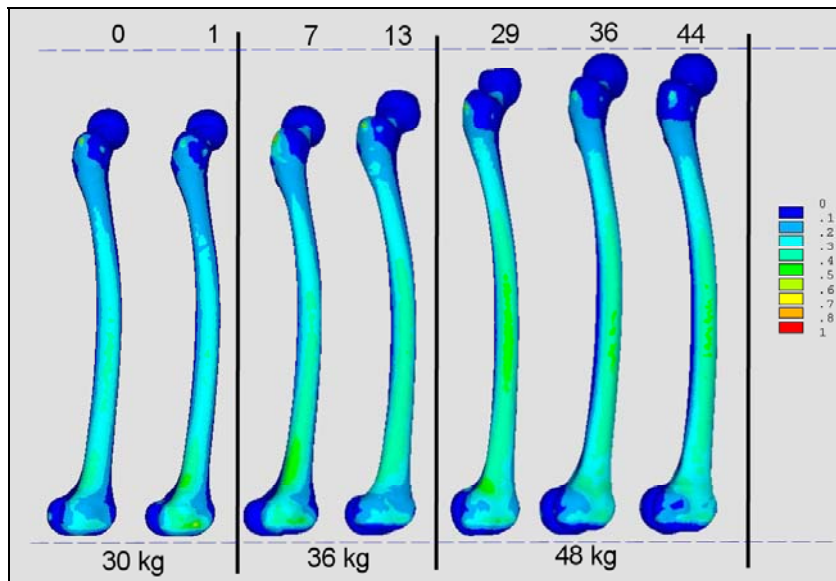


Figure 12 - The RF in the right femur in the follow-up

The RF in the proximal part of the left femur was very similar to the contralateral one in the pre-op and immediately post-op controls, but showed an evident increase in the first year of follow-up. These high RF, that is however always less than unity, seemed to lower in the following months. In the last control exam, the RF in the proximal part of the left femur appeared still reduced, although still higher than in the intact femur, showing that the mechanical strength is not yet fully recovered. A very similar pattern was found for the femoral neck mineral density, measured on the same CT exams (Figure 13). This suggests that the demineralization of the patient's bone, due to the protracted load protection during the first year of follow-up, resulted in an increase in the bone RF. Once the load was increasingly restored, and consequently the bone density increased, the reconstructed bone tended to recover its full mechanical competency.

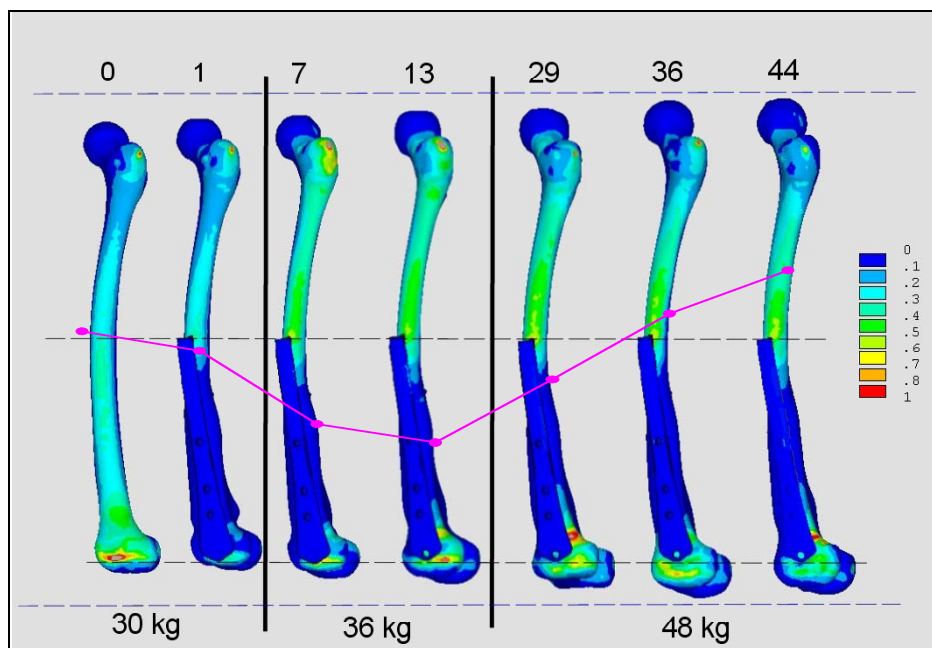


Figure 13 - The RF in the left femur in the follow-up. The pink line represents the femoral neck density in the same period.

The only concern may be relative to the metal plate where, in the regions of the unused screw holes, a stress concentration leads to stresses comparable to the fatigue limit of the material. This is consistent with the clinical evidence that reported fatigue plates fracture initiated in those locations (Figure 14).

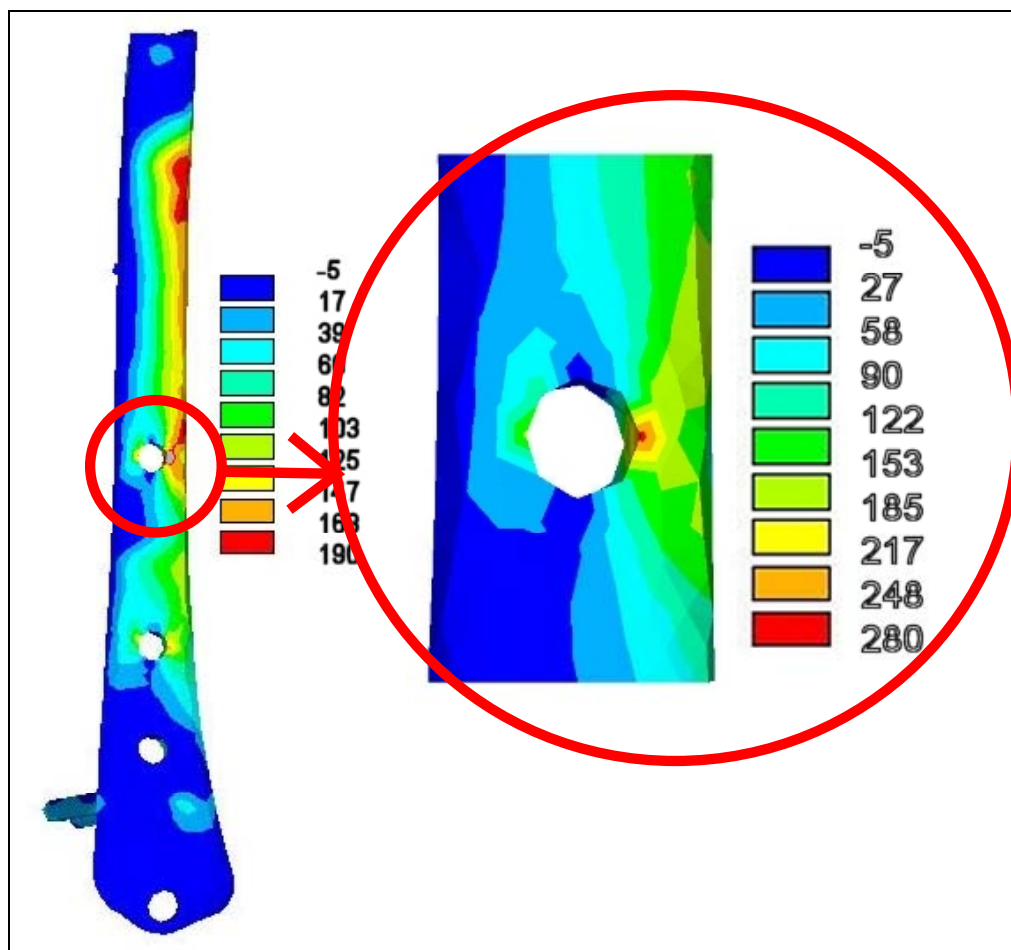


Figure 14 - The Von Mises stress (MPa) in the metal plate.

The major limit of the presented work is relative to the lack of direct validation of the predicted muscles' forces acting on the bone segments during motion, which is still a major challenge of the biomechanical research. However, the applied method proved to be a powerful tool to investigate the mechanical strength evolution of such complex structures and could be used in the future in more extended studies to optimise the rehabilitation therapy and the surgical technique.

7.3 Conclusions

The literature review presented in this chapter summarise the current state of the art in modelling the musculoskeletal system of the human body, with particular attention to the lower limb. The high complexity of this apparatus emerge from the large number of data that should be integrated in the model to completely describe the muscle contribute to the body movements.

Moreover, the variability of the biomechanical environments through the entire population complicates further the biomechanical studies of orthopaedic devices. In fact, to study the

prosthesis biomechanics it is necessary to study all possible operating conditions the prosthesis may face by analysing a representative group of musculoskeletal systems during the execution of a representative set of task of motions.

To collect such an enormous amount of data the most appropriate technique is probably the data fusion of medical data collected through different sources. To this purpose the software (LHPBuilder) developed into the frame of the LHDL project is a good tool for the integration of subject-specific information fulfilling needs for the subsequent development of adequate models.

This would provide effective tools to study the prosthesis biomechanics and in general to answer the open questions on the human skeletal biomechanics. For example, the paragraph 7.2 reports an application of the method to a patient which underwent a massive skeletal reconstruction of the distal femur. Conclusions of such simulations may end up with indication to pre-clinically optimise the reconstruction so as to achieve a more stable fixation and, post-operatively to optimise the rehabilitation therapy. This was the direction the research moved in the last years.

REFERENCES

1. Bergmann, G., et al., *Hip contact forces and gait patterns from routine activities*. J Biomech, 2001. **34**(7): p. 859-71.
2. Leardini, A., et al., *Advanced multimodal visualisation of clinical gait and fluoroscopy analyses in the assessment of total knee replacement*. Comput Methods Programs Biomed, 2005. **79**(3): p. 227-40.
3. Finni, T., P.V. Komi, and J. Lukkariniemi, *Achilles tendon loading during walking: application of a novel optic fiber technique*. Eur J Appl Physiol Occup Physiol, 1998. **77**(3): p. 289-91.
4. Praagman, M., et al., *Muscle oxygen consumption, determined by NIRS, in relation to external force and EMG*. J Biomech, 2003. **36**(7): p. 905-12.
5. Anderson, F.C. and M.G. Pandy, *Static and dynamic optimization solutions for gait are practically equivalent*. J Biomech, 2001. **34**(2): p. 153-61.
6. Pandy, M.G., F.C. Anderson, and D.G. Hull, *A parameter optimization approach for the optimal control of large-scale musculoskeletal systems*. J Biomech Eng, 1992. **114**(4): p. 450-60.
7. Huiskes, R., et al., *Effects of mechanical forces on maintenance and adaptation of form in trabecular bone*. Nature, 2000. **405**: p. 704-6.
8. Pandy, M.G., *Computer modeling and simulation of human movement*. Annu Rev Biomed Eng, 2001. **3**: p. 245-73.
9. Glitsch, U. and W. Baumann, *The three-dimensional determination of internal loads in the lower extremity*. J Biomech, 1997. **30**(11-12): p. 1123-31.
10. Huston, R.L. and C.E. Passerello, *On the dynamics of a human body model*. J Biomech, 1971. **4**(5): p. 369-78.
11. Spagele, T., A. Kistner, and A. Gollhofer, *Modelling, simulation and optimisation of a human vertical jump*. J Biomech, 1999. **32**(5): p. 521-30.

12. Anderson, F.C. and M.G. Pandy, *Individual muscle contributions to support in normal walking*. Gait Posture, 2003. **17**(2): p. 159-69.
13. Crowninshield, R.D. and R.A. Brand, *A physiologically based criterion of muscle force prediction in locomotion*. J Biomech, 1981. **14**(11): p. 793-801.
14. Brand, R.A., et al., *A model of lower extremity muscular anatomy*. J Biomech Eng, 1982. **104**(4): p. 304-10.
15. Delp, S.L., et al., *An interactive graphics-based model of the lower extremity to study orthopaedic surgical procedures*. IEEE Trans Biomed Eng, 1990. **37**(8): p. 757-67.
16. Duda, G.N., E. Schneider, and E.Y. Chao, *Internal forces and moments in the femur during walking*. J Biomech, 1997. **30**(9): p. 933-41.
17. Garner, B.A. and M.G. Pandy, *The Obstacle-Set Method for Representing Muscle Paths in Musculoskeletal Models*. Comput Methods Biomech Biomed Engin, 2000. **3**(1): p. 1-30.
18. Yucesoy, C.A., et al., *Effects of inter- and extramuscular myofascial force transmission on adjacent synergistic muscles: assessment by experiments and finite-element modeling*. J Biomech, 2003. **36**(12): p. 1797-811.
19. Teran, J., et al., *Creating and simulating skeletal muscle from the visible human data set*. IEEE Trans Vis Comput Graph, 2005. **11**(3): p. 317-28.
20. Pandy, M.G., *Simple and complex models for studying muscle function in walking*. Philos Trans R Soc Lond B Biol Sci, 2003. **358**(1437): p. 1501-9.
21. Potvin, J.R. and S.H. Brown, *Less is more: high pass filtering, to remove up to 99% of the surface EMG signal power, improves EMG-based biceps brachii muscle force estimates*. J Electromyogr Kinesiol, 2004. **14**(3): p. 389-99.
22. Seireg, A. and R.J. Arvikar, *A mathematical model for evaluation of forces in lower extremities of the musculo-skeletal system*. J Biomech, 1973. **6**(3): p. 313-26.
23. Kuo, A.D. and F.E. Zajac, *A biomechanical analysis of muscle strength as a limiting factor in standing posture*. J Biomech, 1993. **26 Suppl 1**: p. 137-50.
24. Kuo, A.D. and F.E. Zajac, *Human standing posture: multi-joint movement strategies based on biomechanical constraints*. Prog Brain Res, 1993. **97**: p. 349-58.
25. Pandy, M.G., B.A. Garner, and F.C. Anderson, *Optimal control of non-ballistic muscular movements: a constraint-based performance criterion for rising from a chair*. J Biomech Eng, 1995. **117**(1): p. 15-26.
26. Neptune, R.R., F.E. Zajac, and S.A. Kautz, *Muscle force redistributes segmental power for body progression during walking*. Gait Posture, 2004. **19**(2): p. 194-205.
27. Raasch, C.C., et al., *Muscle coordination of maximum-speed pedaling*. J Biomech, 1997. **30**(6): p. 595-602.
28. Garner, B.A. and M.G. Pandy, *Musculoskeletal model of the upper limb based on the visible human male dataset*. Comput Methods Biomech Biomed Engin, 2001. **4**(2): p. 93-126.
29. Arnold, A.S., S.S. Blemker, and S.L. Delp, *Evaluation of a deformable musculoskeletal model for estimating muscle-tendon lengths during crouch gait*. Ann Biomed Eng, 2001. **29**(3): p. 263-74.

30. Cheung, J.T., M. Zhang, and K.N. An, *Effects of plantar fascia stiffness on the biomechanical responses of the ankle-foot complex*. Clin Biomech (Bristol, Avon), 2004. **19**(8): p. 839-46.
31. Krokos, M., et al. *Patient-Specific Muscle Models for Surgical Planning*. in *MediViz 05*. 2005. London: IEEE Computer Society Press.
32. Arnold, A.S., et al., *Accuracy of muscle moment arms estimated from MRI-based musculoskeletal models of the lower extremity*. Comput Aided Surg, 2000. **5**(2): p. 108-19.
33. Beneke, R., J. Neuerburg, and K. Bohndorf, *Muscle cross-section measurement by magnetic resonance imaging*. Eur J Appl Physiol Occup Physiol, 1991. **63**(6): p. 424-9.
34. van Ruijven, L.J., et al., *The accuracy of joint surface models constructed from data obtained with an electromagnetic tracking device*. J Biomech, 2000. **33**(8): p. 1023-8.
35. Tikuisis, P., P. Meunier, and C.E. Jubenville, *Human body surface area: measurement and prediction using three dimensional body scans*. Eur J Appl Physiol, 2001. **85**(3-4): p. 264-71.
36. de Leva, P., *Adjustments to Zatsiorsky-Seluyanov's segment inertia parameters*. J Biomech, 1996. **29**(9): p. 1223-30.
37. Stagni, R., et al., *Quantification of soft tissue artefact in motion analysis by combining 3D fluoroscopy and stereophotogrammetry: a study on two subjects*. Clin Biomech (Bristol, Avon), 2005. **20**(3): p. 320-9.
38. Pandy, M.G., et al., *An optimal control model for maximum-height human jumping*. J Biomech, 1990. **23**(12): p. 1185-98.
39. Thelen, D.G., F.C. Anderson, and S.L. Delp, *Generating dynamic simulations of movement using computed muscle control*. J Biomech, 2003. **36**(3): p. 321-8.
40. -, *The VAKHUM project: Virtual animation of the kinematics of the human*. 2005.
41. Van Sint Jan, S., et al., *High resolution magnetic resonance imaging application in anatomy: the extensor digitorum muscle insertion on the first phalanx*. Magma, 1997. **5**(1): p. 21-7.
42. Zajac, F.E., *Muscle and tendon: properties, models, scaling, and application to biomechanics and motor control*. Crit Rev Biomed Eng, 1989. **17**(4): p. 359-411.
43. Huijing, P.A., *Muscular force transmission necessitates a multilevel integrative approach to the analysis of function of skeletal muscle*. Exerc Sport Sci Rev, 2003. **31**(4): p. 167-75.
44. Weiss, J.A. and J.C. Gardiner, *Computational modeling of ligament mechanics*. Crit Rev Biomed Eng, 2001. **29**(3): p. 303-71.
45. Mow, V.C., A. Ratcliffe, and A.R. Poole, *Cartilage and diarthrodial joints as paradigms for hierarchical materials and structures*. Biomaterials, 1992. **13**(2): p. 67-97.
46. Guilak, F., et al., *The deformation behavior and mechanical properties of chondrocytes in articular cartilage*. Osteoarthritis Cartilage, 1999. **7**(1): p. 59-70.
47. Viceconti, M. and F. Taddei, *Automatic generation of finite element meshes from computed tomography data*. Crit Rev Biomed Eng, 2003. **31**(1-2): p. 27-72.

48. Huiskes, R. and S.J. Hollister, *From structure to process, from organ to cell: recent developments of FE-analysis in orthopaedic biomechanics*. J Biomech Eng, 1993. **115**(4B): p. 520-7.
49. Huiskes, R. and E.Y. Chao, *A survey of finite element analysis in orthopedic biomechanics: the first decade*. J Biomech, 1983. **16**(6): p. 385-409.
50. Fung, Y.C. and P. Tong, *Classical and computational solid mechanics*. Advanced Series in Engineering Science. Vol. 1. 2001, Portland, OR: World Scientific Publishing Company.
51. Zoghi, M., et al., *A three-dimensional morphometrical study of the distal human femur*. Proc Inst Mech Eng [H], 1992. **206**(3): p. 147-57.
52. Heller, M.O., et al., *Musculo-skeletal loading conditions at the hip during walking and stair climbing*. J Biomech, 2001. **34**(7): p. 883-93.
53. Taylor, M.E., et al., *Stress and strain distribution within the intact femur: compression or bending?* Med Eng Phys, 1996. **18**(2): p. 122-31.
54. Duda, G.N., et al., *Influence of muscle forces on femoral strain distribution*. J Biomech, 1998. **31**(9): p. 841-6.
55. Polgar, K., et al., *Strain distribution within the human femur due to physiological and simplified loading: finite element analysis using the muscle standardized femur model*. Proc Inst Mech Eng [H], 2003. **217**(3): p. 173-89.
56. Bergmann, G., et al., *Hip joint forces during load carrying*. Clin Orthop, 1997(335): p. 190-201.
57. Conzen, A. and F. Eckstein, *Quantitative determination of articular pressure in the human shoulder joint*. J Shoulder Elbow Surg, 2000. **9**(3): p. 196-204.
58. Bruns, J., M. Volkmer, and S. Luessenhop, *Pressure distribution in the knee joint. Influence of flexion with and without ligament dissection*. Arch Orthop Trauma Surg, 1994. **113**(4): p. 204-9.
59. Yoshida, H., et al., *Three-dimensional dynamic hip contact area and pressure distribution during activities of daily living*. J Biomech, 2006. **39**(11): p. 1996-2004.
60. Anderson, I.A., et al., *A novel method for measuring medial compartment pressures within the knee joint in-vivo*. J Biomech, 2003. **36**(9): p. 1391-5.
61. Morrell, K.C., et al., *Corroboration of in vivo cartilage pressures with implications for synovial joint tribology and osteoarthritis causation*. Proc Natl Acad Sci U S A, 2005. **102**(41): p. 14819-24.
62. Lotz, J.C., T.N. Gerhart, and W.C. Hayes, *Mechanical properties of metaphyseal bone in the proximal femur*. J Biomech, 1991. **24**(5): p. 317-29.
63. Snyder, S.M. and E. Schneider, *Estimation of mechanical properties of cortical bone by computed tomography*. J Orthop Res, 1991. **9**(3): p. 422-31.
64. Ford, C.M., T.M. Keaveny, and W.C. Hayes, *The effect of impact direction on the structural capacity of the proximal femur during falls*. J Bone Miner Res, 1996. **11**(3): p. 377-83.
65. Keyak, J.H., et al., *Postfailure compressive behavior of tibial trabecular bone in three anatomic directions*. J Biomed Mater Res, 1996. **31**(3): p. 373-8.

66. Morgan, E.F., H.H. Bayraktar, and T.M. Keaveny, *Trabecular bone modulus-density relationships depend on anatomic site*. J Biomech, 2003. **36**(7): p. 897-904.
67. Morgan, E.F. and T.M. Keaveny, *Dependence of yield strain of human trabecular bone on anatomic site*. J Biomech, 2001. **34**(5): p. 569-77.
68. Kalender, W.A., *A phantom for standardization and quality control in spinal bone mineral measurements by QCT and DXA: Design considerations and specifications*. Medical Physics, 1992. **19**(3): p. 583-586.
69. Keller, T.S., *Predicting the compressive mechanical behavior of bone*. J Biomech, 1994. **27**(9): p. 1159-68.
70. Carter, D.R. and W.C. Hayes, *The compressive behavior of bone as a two-phase porous structure*. J Bone Joint Surg Am, 1977. **59**(7): p. 954-62.
71. Issever, A.S., et al., *A micro-computed tomography study of the trabecular bone structure in the femoral head*. J Musculoskelet Neuronal Interact, 2003. **3**(2): p. 176-84.
72. Muller, R., et al., *Morphometric analysis of human bone biopsies: a quantitative structural comparison of histological sections and micro-computed tomography*. Bone, 1998. **23**(1): p. 59-66.
73. Newitt, D.C., et al., *In vivo assessment of architecture and micro-finite element analysis derived indices of mechanical properties of trabecular bone in the radius*. Osteoporos Int, 2002. **13**(1): p. 6-17.
74. Sell, C.A., et al., *Quantification of Trabecular Bone Structure Using Magnetic Resonance Imaging at 3 Tesla-Calibration Studies Using Microcomputed Tomography as a Standard of Reference*. Calcif Tissue Int, 2005. **5**: p. 5.
75. Lindsey, C., et al., *Association of physical performance measures with bone mineral density in postmenopausal women*. Arch Phys Med Rehabil, 2005. **86**(6): p. 1102-7.
76. Cattaneo, P.M., M. Dalstra, and L.H. Frich, *A three-dimensional finite element model from computed tomography data: a semi-automated method*. Proceedings of the Institution of Mechanical Engineers. Part H, Journal of engineering in medicine., 2001. **215**(2): p. 203-13.
77. Taddei, F., et al., *Mechanical strength of a femoral reconstruction in paediatric oncology: a finite element study*. Proceedings of the Institution of Mechanical Engineers. Part H, Journal of engineering in medicine., 2003. **217**(2): p. 111-9.
78. Viceconti, M., et al., *Automatic generation of accurate subject-specific bone finite element models to be used in clinical studies*. J Biomech, 2004. **37**(10): p. 1597-605.
79. Zhang, G., *Avoiding the material nonlinearity in an external fixation device*. Clin Biomech (Bristol, Avon), 2004. **19**(7): p. 746-50.
80. Taddei, F., A. Pancanti, and M. Viceconti, *An improved method for the automatic mapping of computed tomography numbers onto finite element models*. Med Eng Phys, 2004. **26**(1): p. 61-9.
81. Reid, J.G., L.A. Livingston, and D.J. Pearsall, *The geometry of the psoas muscle as determined by magnetic resonance imaging*. Arch Phys Med Rehabil, 1994. **75**(6): p. 703-8.

82. Martins, J.A.C., et al., *A numerical model of passive and active behaviour of skeletal muscles*. Computer Methods in applied mechanics and engineering, 1998. **151**: p. 419-433.
83. Hutter, R., K.U. Schmitt, and P. Niederer, *Mechanical modeling of soft biological tissues for application in virtual reality based laparoscopy simulators*. Technol Health Care, 2000. **8**(1): p. 15-24.
84. Johansson, T., P. Meier, and R. Blickhan, *A finite-element model for the mechanical analysis of skeletal muscles*. J Theor Biol, 2000. **206**(1): p. 131-49.
85. Keunings, R., *Finite element methods for integral viscoelastic fluids*, in *Rheology review 2003*, D.M.B.a.K. Walters, Editor. 2003, British Society of Rheology. p. 167-195.
86. Oomens, C.W., et al., *Can loaded interface characteristics influence strain distributions in muscle adjacent to bony prominences?* Comput Methods Biomech Biomed Engin, 2003. **6**(3): p. 171-80.
87. Yucesoy, C.A., et al., *Three-dimensional finite element modeling of skeletal muscle using a two-domain approach: linked fiber-matrix mesh model*. J Biomech, 2002. **35**(9): p. 1253-62.
88. Li, G., et al., *A validated three-dimensional computational model of a human knee joint*. J Biomech Eng, 1999. **121**(6): p. 657-62.
89. Mommersteeg, T.J., et al., *A global verification study of a quasi-static knee model with multi-bundle ligaments*. J Biomech, 1996. **29**(12): p. 1659-64.
90. Johnson, G.A., et al., *A single integral finite strain viscoelastic model of ligaments and tendons*. J Biomech Eng, 1996. **118**(2): p. 221-6.
91. Limbert, G., et al., *A transversely isotropic hyperelastic constitutive model of the PDL. Analytical and computational aspects*. Comput Methods Biomech Biomed Engin, 2003. **6**(5-6): p. 337-45.
92. McGuinness, N.J., et al., *A stress analysis of the periodontal ligament under various orthodontic loadings*. Eur J Orthod, 1991. **13**(3): p. 231-42.
93. Cheung, J.T., M. Zhang, and D.H. Chow, *Biomechanical responses of the intervertebral joints to static and vibrational loading: a finite element study*. Clin Biomech (Bristol, Avon), 2003. **18**(9): p. 790-9.
94. Lee, K.K. and E.C. Teo, *Poroelastic analysis of lumbar spinal stability in combined compression and anterior shear*. J Spinal Disord Tech, 2004. **17**(5): p. 429-38.
95. Biot, M.A., *Theory of propagation of elastic waves in a fluid-saturated porous solid, I. low-frequency range*. Journal of the Acoustical Society of America, 1956. **28**: p. 168-78.
96. Penrose, J.M., et al., *Development of an accurate three-dimensional finite element knee model*. Comput Methods Biomech Biomed Engin, 2002. **5**(4): p. 291-300.
97. Halloran, J.P., A.J. Petrella, and P.J. Rullkoetter, *Explicit finite element modeling of total knee replacement mechanics*. J Biomech, 2005. **38**(2): p. 323-31.
98. Nadzadi, M.E., et al., *Kinematics, kinetics, and finite element analysis of commonplace maneuvers at risk for total hip dislocation*. J Biomech, 2003. **36**(4): p. 577-91.
99. Koolstra, J.H. and T.M. van Eijden, *Combined finite-element and rigid-body analysis of human jaw joint dynamics*. J Biomech, 2005. **38**(12): p. 2431-9.

100. Fernandez, J.W. and P.J. Hunter, *An anatomically based patient-specific finite element model of patella articulation: towards a diagnostic tool*. Biomech Model Mechanobiol, 2005. **4**(1): p. 20-38.
101. Sholukha, V., et al., *Double-step registration of in vivo stereophotogrammetry with both in vitro 6-DOFs electrogoniometry and CT medical imaging*. J Biomech, 2006. **39**(11): p. 2087-95.
102. Van Sint Jan, S., et al., *In vivo registration of both electrogoniometry and medical imaging: development and application on the ankle joint complex*. IEEE Trans Biomed Eng, 2006. **53**(4): p. 759-62.
103. Van Sint Jan, S. and U. Della Croce, *Identifying the location of human skeletal landmarks: why standardized definitions are necessary--a proposal*. Clin Biomech (Bristol, Avon), 2005. **20**(6): p. 659-60.
104. van Rietbergen, B., *Micro-FE analyses of bone: state of the art*. Adv Exp Med Biol, 2001. **496**: p. 21-30.
105. Huiskes, R., *On the modelling of long bones in structural analyses*. J Biomech, 1982. **15**(1): p. 65-9.
106. van Rietbergen, B., et al., *A new method to determine trabecular bone elastic properties and loading using micromechanical finite-element models*. J Biomech, 1995. **28**(1): p. 69-81.
107. Feldkamp, L.A., et al., *The direct examination of three-dimensional bone architecture in vitro by computed tomography*. J Bone Miner Res, 1989. **4**(1): p. 3-11.
108. Hollister, S.J., J.M. Brennan, and N. Kikuchi, *A homogenization sampling procedure for calculating trabecular bone effective stiffness and tissue level stress*. J Biomech, 1994. **27**(4): p. 433-44.
109. Jasiuk, I. and M. Ostoja-Starzewski, *Modeling of bone at a single lamella level*. Biomech Model Mechanobiol, 2004. **3**(2): p. 67-74.
110. Maas, H., et al., *The relative position of EDL muscle affects the length of sarcomeres within muscle fibers: experimental results and finite-element modeling*. J Biomech Eng, 2003. **125**(5): p. 745-53.
111. Wilson, W., et al., *Stresses in the local collagen network of articular cartilage: a poroviscoelastic fibril-reinforced finite element study*. J Biomech, 2004. **37**(3): p. 357-66.
112. Huiskes, R., *If bone is the answer, then what is the question?* J Anat, 2000. **197 (Pt 2)**: p. 145-56.
113. Tsubota, K. and T. Adachi, *Changes in the fabric and compliance tensors of cancellous bone due to trabecular surface remodeling, predicted by a digital image-based model*. Comput Methods Biomech Biomed Engin, 2004. **7**(4): p. 187-92.
114. Viceconti, M. and A. Seireg, *A generalized procedure for predicting bone mass regulation by mechanical strain*. Calcif Tissue Int, 1990. **47**(5): p. 296-301.
115. Taylor, D. and A. Tilmans, *Stress intensity variations in bone microcracks during the repair process*. J Theor Biol, 2004. **229**(2): p. 169-77.
116. Han, Y., et al., *Mechanotransduction and strain amplification in osteocyte cell processes*. Proc Natl Acad Sci U S A, 2004. **101**(47): p. 16689-94.

117. Gray, H., *Anatomy of the Human Body*. 1918, Philadelphia: Lea & Febiger.
118. Crolet, J.M., B. Aoubiza, and A. Meunier, *Compact bone: numerical simulation of mechanical characteristics*. J Biomech, 1993. **26**(6): p. 677-87.
119. Hellmich, C., F.J. Ulm, and L. Dormieux, *Can the diverse elastic properties of trabecular and cortical bone be attributed to only a few tissue-independent phase properties and their interactions? Arguments from a multiscale approach*. Biomech Model Mechanobiol, 2004. **2**(4): p. 219-38. Epub 2004 Mar 31.
120. Lin, C.Y., N. Kikuchi, and S.J. Hollister, *A novel method for biomaterial scaffold internal architecture design to match bone elastic properties with desired porosity*. J Biomech, 2004. **37**(5): p. 623-36.
121. Akkermans, R.L. and P.B. Warren, *Multiscale modelling of human hair*. Philos Transact A Math Phys Eng Sci, 2004. **362**(1821): p. 1783-93.
122. Agoram, B. and V.H. Barocas, *Coupled macroscopic and microscopic scale modeling of fibrillar tissues and tissue equivalents*. J Biomech Eng, 2001. **123**(4): p. 362-9.
123. Viceconti, M., et al., *Primary stability of an anatomical cementless hip stem: a statistical analysis*. J biomech, 2005. **in press**.
124. Mirka, G.A. and W.S. Marras, *A stochastic model of trunk muscle coactivation during trunk bending*. Spine, 1993. **18**(11): p. 1396-409.
125. Espino, D.M., et al., *Stochastic finite element analysis of biological systems: comparison of a simple intervertebral disc model with experimental results*. Comput Methods Biomech Biomed Engin, 2003. **6**(4): p. 243-8.
126. Guo, X.E., et al., *Finite element modeling of damage accumulation in trabecular bone under cyclic loading*. J Biomech, 1994. **27**(2): p. 145-55.
127. Hurschler, C., P.P. Provenzano, and R. Vanderby, Jr., *Application of a probabilistic microstructural model to determine reference length and toe-to-linear region transition in fibrous connective tissue*. J Biomech Eng, 2003. **125**(3): p. 415-22.
128. Ruimerman, R., et al., *A theoretical framework for strain-related trabecular bone maintenance and adaptation*. J Biomech, 2005. **38**(4): p. 931-41.
129. McGarry, J.G., et al., *A comparison of strain and fluid shear stress in stimulating bone cell responses--a computational and experimental study*. Faseb J, 2005. **19**(3): p. 482-4.
130. Authors, V., ed. *Special Issue on Grid Computing*. Proceedings of the IEEE, ed. M. Parashar. Vol. 93(3). 2005.
131. Couteau, B., Y. Payan, and S. Lavallee, *The mesh-matching algorithm: an automatic 3D mesh generator for finite element structures*. J Biomech, 2000. **33**(8): p. 1005-9.
132. Castellano Smith, A., et al. *Constructing Patient Specific Models for Correcting Intraoperative Brain Deformation*. in *Medical Image Computing and Computer-Assisted Intervention (MICCAI 2001)*. 2001. Utrecht, NL,: Springer Verlag.
133. Turk, G. *Texture Synthesis on Surfaces*. in *SIGGRAPH 2001*. 2001.
134. Dong, F. and G.J. Clapworthy, *Volumetric Texture Synthesis for Non-Photorealistic Volume Rendering of Medical Data*. Visual Computer, 2005. **in press**.
135. Leardini, A., et al., *A new software tool for 3D motion analyses of the musculo-skeletal system*. Clin Biomech (Bristol, Avon), 2006. **21**(8): p. 870-9.

136. Taddei, F., et al., *Subject-specific finite element models of long bones: An in vitro evaluation of the overall accuracy*. J Biomech, 2006. **39**(13): p. 2457-67.
137. Taylor, D., *Fracture mechanics: How does bone break?* Nat Mater, 2003. **2**(3): p. 133-4.
138. Currey, J.D., *Tensile yield in compact bone is determined by strain, post-yield behaviour by mineral content*. J Biomech, 2004. **37**(4): p. 549-56.

Conclusions

The aim of this research thesis was to develop musculoskeletal models for the pre-clinical validation and the design optimisation of hip resurfacing devices. This would facilitate the objective ahead of designers to produce performing orthopaedic devices which guarantee a low-failure rate when implanted in population of interest. To this aim, a method to analyse the various type of failure scenario the prosthesis may face during its operating life was developed and tested on two different type of prosthesis. The main problems faced during the work consisted in:

- Defining the accuracy of model predictions
- Defining the sensitivity of modelling techniques to the uncertainties on modelling parameters
- Defining the protocol for the biomechanical analysis of hip resurfacing prosthesis
- Testing the protocol in predicting known clinical outcomes for a successful design of prosthesis
- Optimising the geometry of a first prototype of a potentially new device
- Pre-clinically validating the optimised design of the new device

To shoulder the listed challenges, a protocol to analyse the risk of failure associated with the biomechanical behaviour of the implanted femur was developed by matching clinical evidences with engineering techniques in predicting failure.

During the first part of the work two finite element models, one of an intact femur and the other of the same femur implanted with a resurfacing device, were validated comparing the models prediction to the experimental measurements provided by the experimental group of LTM (Chapter 2). The intrinsic accuracy of prediction on bone stresses (RMSE < 10%) was found, on both models, of the same order of magnitude of other published works. This result is aligned to the current state of the art for finite element models of long bones from medical images. The accuracy of prediction of the bone-prosthesis micromovement was found within a micron, which is also an excellent result if compared with the current literature.

The sensitivity of models prediction to uncertainties on modelling parameter was found also below 10% (Chapter 3). This result together with the intrinsic accuracy fully characterise the adopted methodology confirming its validity to study the resurfaced femur biomechanics.

The complete protocol for the analysis of resurfaced femurs included the simulation of the prosthesis biomechanics to investigate most of the relevant failure modes and the experimental evaluation of the strength of the femoral neck. Models were a valid support for the identification

of the experimental set-up. Simulations indicate the correct loading scheme to produce femoral fractures coherent with spontaneous fractures of the femoral neck observed in the clinics (Chapter 4).

Once the method for the biomechanical analysis of resurfaced femurs was completely identified, its first application was carried out analysing a successful design on the market to study the method ability in predicting known clinical outcomes. The analysis resulted in a very good agreement with published retrospective studies for this class of devices (Chapter 5) and encouraged its further application to a first prototype of a new prosthesis.

The design of the first prototype was analysed and the geometry of the prosthesis was optimised producing a final design with a very low risk of failure associated to all investigated failure modes. The following pre-clinical validation statistically confirmed the minimal risk of the optimised design over the entire range of surgery uncertainties, individual anatomies and on a significant range of patient activities. A parallel experimental study (conducted by the experimental group of LTM) confirmed the quality of the optimised design and indirectly, of the original conceptual design.

In summary, the developed protocol was able to accurately predict known clinical outcomes when applied to a well established device. When applied to a new prosthesis, models were able to correctly predict the prosthesis biomechanics, to support the design optimisation phase and to provide important information on critical combinations of influencing cofactors in relation to the patient characteristics. The performances of the optimised design showed a significant improvement with respect to the first prototype. Also when compared to current competitors on the market, the optimised design showed very good results so the new prosthesis recently started the clinical trials.

For what regards the applicability to different type of implants and to different anatomical districts, the presented approach does have a relevant generality that would allow the extension of the protocol to a large set of orthopaedic scenarios with minor changes. Hence, a failure mode analysis criterion can be considered a suitable tool in developing new orthopaedic devices.

Nevertheless this study has some limitations. Although significant, the boundary conditions used in the presented studies were derived from the few data available in the literature, which are hardly representative of the entire variability of boundary conditions the implant might face over the patients population. This limitation is to be attributed to the complexity of *in-vivo* measurements of the joint reaction (e.g. by using instrumented prosthesis on operated subjects), the impossibility of current techniques to measure *in-vivo* muscle forces and to the consequent impossibility to fully validate the modelling techniques. It is still a major challenge for researchers.

This moved the object of the study to the modelling of the musculoskeletal system of the lower limb. The work started with a literature review (Chapter 7) and, after a four month training on modelling musculoskeletal systems at the Delft Technical University, the ongoing activity is to develop subject-specific musculoskeletal models from medical images (Appendix D).

The limitations of the study highlight the steps to be taken for the further development of more predictive protocols:

- Even if very promising, the method should be applied to other implants to confirm its expected advantages.
- The analysis of the implant biomechanics during a more extensive set of activities should be added. Accidental motion tasks, such as side fall, should be included to study the implant response to severe and undesired events.
- The musculoskeletal modelling activity should be completed so as to simulate the entire range of the physiological loading conditions at the hip depending on the individual anatomy, the physiology and the neuro-motor control strategy potentially adopted by the central nervous system.

These will be the subjects of the next future research.

Acknowledgments

The presented work was entirely carried out at Laboratorio di Tecnologia Medica (LTM) of Istituti Ortopedici Rizzoli (IOR). The work was conducted with the support of Ing. Marco Viceconti and Ing. Fulvia Taddei ahead of the computational group of LTM and with the supervision of Prof. Luca Cristofolini. The application of the method to a new prototype of prosthesis was possible thanks to the base idea and the financial support of the Manufacturer. The author would like to thank Prof. Angelo Cappello for his constructive comments on the musculoskeletal modelling activity.

BIBLIOGRAPHY

Publications on international journals

1. Taddei, F., Martelli, F., Reggiani, B., Cristofolini, L., Viceconti, M., "Subject-specific finite element modelling of human bones: sensitivity to geometry and material uncertainties", *J Biomech*, 2006. 39(13): pp. 2457-67
2. Marco Viceconti, Debora Testi, Fulvia Taddei, Saulo Martelli, Gordon Clapworthy. "Biomechanics modeling: status and key issues". The proceedings of IEEE, Special issue on: The physiome: in-silico living human, April 2006. 94(4): pp. 725-739
3. Fulvia Taddei, Saulo Martelli, Barbara Reggiani, Luca Cristofolini and Marco Viceconti., "Finite element modelling of bones from CT data: sensitivity to geometry and material uncertainties", *IEEE Trans on Biomed Eng.* 2006 Nov;53(11): pp. 2194-200
4. Luca Cristofolini, Mateusz Juszczuk, Saulo Martelli, Fulvia Taddei, Marco Viceconti "In vitro replication of spontaneous fractures of the proximal human femur". *J Biomech*, 2007. 40(13): pp. 2837-45
5. M. Juszczuk, E. Schileo, S. Martelli, L. Cristofolini, M. Viceconti, "A method to improve experimental validation of Finite Element models of long bones", *Strain*, In Press.
6. Saulo Martelli, Luca Cristofolini, Fulvia Taddei, Marco Viceconti. "Combined numerical-experimental pre-clinical validation of epiphyseal prostheses: validation of a protocol based on an established design", to be submitted in March 2004 to *Journal of Biomechanics* for publication considerations.
7. S. Martelli, F. Taddei, L. Cristofolini, E. Schileo, R. Field, N. Rushton, M. Viceconti, "Pre-clinical validation of a new hip resurfacing prosthesis: design revision and optimisation by means of a combined numerical-experimental procedure". to be submitted to *Journal of Biomechanics* for publication considerations.

International Congresses

1. F. Taddei, B. Reggiani, S. Martelli, B. Bordini, M. Viceconti, "Finite element modelling of human bones from ct data: a sensitivity study on the influence of geometry and material uncertainties", 1st International Congress On Computational Bioengineering, 24th-27th September, 2003, Saragoza, Spain.
2. S. Martelli, F. Taddei, E. Varini, L. Cristofolini, H.S. Gill, M. Viceconti, and A.Toni., "Accuracy of subject-specific finite element models of long bones from CT data: an in-vitro study". 2nd International Congress On Computational Bioengineering, Lisbon(Portugal), September 14th-16th, 2005.

3. F. Taddei, L. Montanari, V. Greco, S. Martelli, A. Leardini, M. Viceconti, and M. Manfrini., “Risk of fracture of a reconstructed femur during walking: data-fusion and subject-specific finite element modelling”, 2nd International Congress On Computational Bioengineering, Lisbon(Portugal), September 14th-16th, 2005.
4. F. Taddei, Greco V, Montanari L, Martelli S, Viceconti M, Astolfi L, Leardini A, Mercuri M and Manfrini M. “New aspects in computer-assisted planning and monitoring of complex skeletal reconstructions”. European MusculoSkeletal Oncology Society. Trieste(Italy), May 25th-27th, 2005.
5. Viceconti M., Montanari L., Taddei F., Martelli S., Manfrini M., Toni A. “Combining subject-specific and collection data to create predictive models to be used in the clinical practice”. European Orthopaedic Research Society, Bologna(Italy), June 7th-9th, 2006.
6. Taddei F., Martelli S., Montanari L., Greco V., Leardini A., Viceconti M., Manfrini M. “Mechanical strength evolution of a reconstructed femur during follow-up”. European Orthopaedic Research Society, Bologna(Italy), June 7th-9th, 2006.
7. Montanari L., Taddei F., Martelli S., Leardini A., Manfrini M, Viceconti M. “Subject-specific muscle-skeletal models of the lower limbs for the prediction of muscle forces during gait”. European Orthopaedic Research Society, Bologna(Italy), June 7th-9th, 2006.
8. F. Taddei, S. Martelli, L. Montanari, V. Greco, A. Leardini , M. Manfrini , M. Viceconti. “Changes in the mechanical strength of a reconstructed femur durino follow-up: a subject-specific finite element study”. 5th World Congress of Biomechanics 2006, Munich (Germany), July 29th-August 4th, 2006.
9. L. Montanari, F. Taddei, S. Martelli, A. Leardini, M. Manfrini, M. Viceconti “Muscle forces acting on the skeleton durino gait: data fusion and subject-specific muscle-skeletal modelling”. 5th World Congress of Biomechanics 2006, Munich (Germany), July 29th-August 4th, 2006.
10. Martelli S., Moindreau M., Rushton N., Field R., Viceconti M. .“Pre-clinical validation of a new conservative THR femoral component”. 5th World Congress of Biomechanics 2006, Munich (Germany), July 29th-August 4th, 2006.
11. Martelli S., Moindreau M., Rushton N., Field R., Viceconti M., “An explorative finite element study of a new conservative proximal epiphyseal replacement”. 5th World Congress of Biomechanics 2006, Munich (Germany), July 29th-August 4th, 2006.
12. L. Cristofolini, F. Pallini, E. Schileo, M. Juszczuk, E. Varini, S. Martelli, F. Taddei., “Biomechanical testing of the proximal femoral ephiphysis: intact and implanted conditions”. 8th Biennial Conference on Engineering Systems Design and Analysis ASME-ESDA, Turin (Italy), July 4th-7th, 2006.
13. S. Martelli, H.E.J. Veeger, Van der Helm, “Scaling of shoulder musculoskeletal model to individual subject data” XXI congress of the International Society of Biomech., Taipei(Taiwan), July 1st-5th, 2007.

14. S. Martelli, F. Taddei, E. Varini, F. Pallini, M. Viceconti. “Modellazione del comportamento meccanico strutturale delle ossa lunghe”. Forum in Bone and Mineral Research, Torino (Italy), June 3th-14th, 2006.
15. S. Martelli, F. Taddei, L. Cristofolini, and M. Viceconti. “Preclinical validation of epiphyseal prostheses”. IMechE Engineers and Surgeons: Joined at the Hip Conference, London (UK), April 19th-21st, 2007.
16. S. Martelli, F. Taddei, M. Viceconti, “Modelli numerici per la validazione preclinica di impianti ortopedici”, Forum in Bone and Mineral Research, Viareggio(Italy), January 23rd-24th, 2007.
17. S. Martelli, H.E.J. Veeger, Van der Helm, “Scaling of shoulder musculoskeletal model do not lead to significant improvement”. 7th meeting of the International Shoulder Group, Bologna(Italy), July 10th – 13th, 2008

Appendix A

A method to improve experimental validation of Finite Element models of long bonesⁱⁱ

The validation of finite element (FE) models of intact and implanted long bones using experimentally derived data is a fundamental step to ensure model accuracy and reliability in predicting mechanical stress and risk of failure [1], especially given the complexity of geometry and materials involved [2-8]. Given the clinical implications, validation is a fundamental step when FE models are used to investigate failure scenarios or optimize implantable devices [9]. Validation can be achieved by means of dedicated in vitro experiments and purpose-designed transducers to enhance comparisons of the numerical results with the experimental measurements [9]. To quantitatively validate an FE model of a long bone (e.g. a femur), reliable data, especially concerning boundary conditions, need to be transferred from the experimental field to the computational model [10, 11]. Thus, it is necessary to design an experiment in which precise boundary conditions can be determined and transferred to the model, and also so that allows for the identical loading of the physical specimen and the FE model.

One of the most critical factors determining the output, such as the strain/stress distribution or the failure risk, of an FE model of a long bone is the position of the applied force relative to the bone. For instance, when the hip joint force is applied to the femoral head in-vitro [2, 9, 12-15], it is not possible a priori to determine accurately the position of the resultant force, mainly due to the large deformation of the bone surface in the area where the load is distributed and due to the structural behaviour of the femur under load. Additionally, it is not possible to predict a priori the trajectory of the applied force while the bone specimen is deflecting due to the material deformation as load is applied. It has been experimentally shown [16, 17] that an error of only a few millimeters in positioning the hip joint force onto the femur can result in extremely high errors in the estimated stress. This can compromise the reliability of failure risk predictions. Thus, accurate identification of the load position is a major issue when investigating the biomechanics of long bones, such as femurs, using FE models.

ⁱⁱ Mateusz Juszczak, Enrico Schileo, Saulo Martelli, Luca Cristofolini and Marco Viceconti. "A method to improve experimental validation of Finite Element models of long bones", Accepted by Strain, In Press

To the authors' best knowledge, no studies have tracked the actual position of the applied joint force during mechanical tests of long bones, such as femurs, and none have incorporated such information into FE models designed to replicate the same bone. In some FE studies the load position has been identified based on a physical specimen, based on the ideal force position (i.e. independently of the local and global bone deformation) [5, 10, 15]. In other cases no information has been provided on the location and the distribution of the applied load that were used to replicate the experimental loads on the FE models (e.g. Ota et. al., 1999 [2]).

One such means of measuring the position of an applied force is a transducer such as those designed for indirectly measuring the application point of an applied force in milling machines [16]. Such transducers are normally load cells, designed to measure forces or bending moments. The actual position of a given force can be calculated using load cells to measure the applied force and the bending moment that the force generates.

To locate the precise position of the force applied to the femoral head, the bending moment applied to a femur has been measured using strain gauges directly attached to the femur diaphysis [18]. However, determining the position of the applied force with such an arrangement depends on the pre-identification of the centre of the diaphysis, which cannot be achieved without a means to calculate the neutral axis of complex geometries, because of the irregular shape of bones.

In our research, we adapted the concept of load cells in order to measure the position of the force applied to the bone specimen in in vitro biomechanical tests in order to validate FE models of the same bone specimen. In the research reported here, we:

- 1) Developed a force-position transducer (FP-transducer) to be incorporated into the in vitro setup for mechanical testing of long bones, in order to determine the precise position of the force and to incorporate this positional information into the corresponding FE model. We built a strain gauge-based load cell to measure the bending moment generated by the position of the load applied to the bone in order to determine the precise coordinates of the applied load in relation to the bone specimen.
- 2) Determined the intrinsic accuracy of the FP-transducer– that is, we determined the accuracy of the FP-transducer independently of its use in any mechanical testing.
- 3) Determined the performance and overall accuracy the FP-transducer when incorporated in a typical mechanical test of long bones.

Materials and methods

Overview of the Validation Test Setup

To develop and test the FP-transducer, we used an experimental setup used for investigating the strength of intact and operated proximal femur [10, 17, 19]. As shown in Fig. 1, the setup consisted of the load cell forming the base of the testing machine, with the FP-transducer mounted on top of the load cell. The FP-transducer tracked the horizontal position of the force

applied to the bone specimen by measuring the bending moments about two perpendicular axes. The bone specimen was mounted on top of the FP-transducer using interchangeable wedges that held and tilted the bone at the prescribed angles. This layout allowed the coordinates of the applied force (ΔA and ΔB in Fig. 1) to be measured by the FP-transducer with respect to a known reference system. In this setup, the bone was fully constrained distally, while a vertical load was applied proximally by the actuator of the testing machine, through a system of low-friction cross-rails that eliminated any horizontal force component.

Design of the FP-transducer

In the study reported here, the FP-transducer was designed and optimized in order for it to be suitable for the geometry and the loads of human femurs. However, a transducer based on this concept can be tuned to test other long bones, such as the tibia or the humerus.

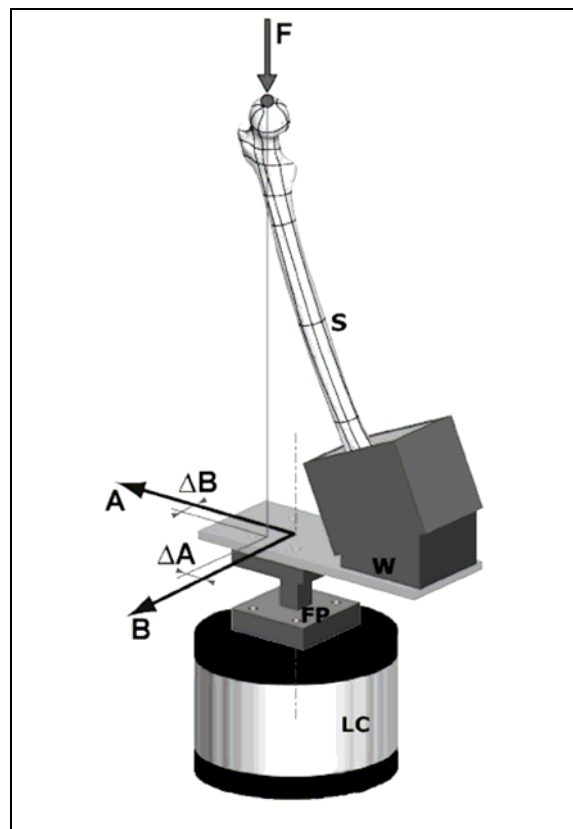


Figure 1 - Schematic of the loading setup for the biomechanical testing of long bones (a femur in this instance) in different anatomical positions. The bone specimen (S: a femur, in this instance) is mounted on top of interchangeable wedges (W) that are attached to the transducer and allow tilting the specimen at prescribed angles (24° in the coronal plane with respect to the vertical axis in this instance). The FP-transducer (FP) measuring the force position is mounted below the specimen. Its reference axes (A and B) are indicated, as well as the coordinates (ΔA and ΔB) of the applied load F relative to the transducer reference. The entire system is mounted on top of the load cell (LC) of the testing machine, which is measuring the load (F) applied by the actuator of the testing machine.

The FP-transducer measures the bending moment in two orthogonal directions generated by a load applied to the bone specimen. The load cell of the testing machine measures the force value

(Fig. 1). Thus, the coordinates of the applied load (i.e., the lever arms) can be easily obtained if the transfer function of the FP-transducer is known.

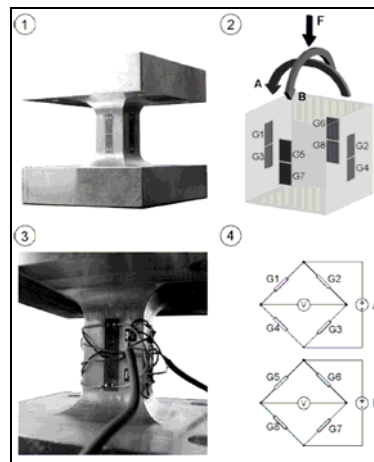


Figure 2 - The FP-transducer in construction: (1) Instrumented FP-transducer core, with two strain gauges mounted one adjacent to the other on each side of the sensing beam. (2) Schematic of the strain gauge (G1 to G8) positions on the transducer core; also indicated is the applied force F and the two directions (A and B) of the measured bending moments. (3) Photo of the wired strain gauges. (4) a schematic of the wiring of the strain gauges showing the grids connected to the two Wheatstone bridges. Two full Wheatstone bridges were built so as to measure the bending moments A and B separately, while eliminating the effect of the axial load F (which was measured by the load cell of the testing machine, see Fig. 1 and 4).

As shown in Fig. 2, the FP-transducer consisted of two plates and a connecting beam, which was the sensing element for bending measurement. The connecting beam, which was the transducer core, had a square section. The transducer core was sufficiently bulky to guarantee small bending when loaded (less than 0.2° with the maximum load) and prevent buckling. Such geometry allowed easy manufacturing of the transducer core, easy strain gauge application, and simple tension-compression measurements in both perpendicular directions.

The dimensions of the transducer were chosen based on the anatomical variability and different loading directions of the femur specimen. The testing protocol adopted by these authors [10, 19] involved positioning the femur at different prescribed angles to cover the range of physiological loads during daily motor tasks [20, 21]. In order to reduce the range of bending moments to be measured by the FP-transducer, the interchangeable wedges above the FP-transducer were designed to keep the load application point close to the axis of the FP-transducer. A simulation including the prescribed loading angles [10, 19] and three anatomical parameters (diaphyseal length, neck anteversion, and neck length) confirmed that the load application point always fell within 55mm from the axis of the FP-transducer. Based on previous experience [10, 17, 19], the maximum load to be applied to the femur in a non-destructive test was estimated to be 2500 N. Thus, the maximum resultant moment during testing could be estimated (less than 140 Nm).

In order to obtain accurate measurements, it was essential that the transducer core provided large, linear and repeatable strain to be measured. The FP-transducer was machined out of a single block of Al2011-T6 aluminum alloy (UNS-A92011). This alloy was chosen because it has high elastic range, low Young's modulus, and ease of manufacture. The cross section of the instrumented beam measured $24 \times 24 \text{ mm}^2$, to ensure that maximum stress during use was 60 MPa (4.5 times lower than the yield stress of the selected alloy, which was 270 MPa).

Eight strain gauges (1-LY41- 6/350, HBM, Darmstadt, Germany) were bonded on the connecting beam with cyanacrylate adhesive (Z70, HBM). They were placed two on each face of the beam: each pair was centered longitudinally (Fig. 2). The strain gauges were aligned parallel to the connecting beam, so that they measured strain (induced by bending) along the beam axis. The strain gauges were connected in groups of four to form two Wheatstone bridges (Fig. 2). A full Wheatstone bridge configuration was used for each direction of bending to amplify the output signal of the FP-transducer (bending strain was amplified four-fold, while the axial component was eliminated). Thus, the FP-transducer provided two independent measurements (Bridges A and B) related to bending in two orthogonal directions. In order to reduce thermal drift and maximize signal, a bridge excitation of 5 V was chosen based on the strain gauge size. The Wheatstone bridges were wired around the beam to ensure the shortest possible bridge arms. Because testing of real bones often necessarily involves wet test environment, the instrumented transducer core, was covered with two layers of polyurethane (PU-120, HBM) for insulation and a layer of silicone rubber (SG-250, HBM) for mechanical protection. An external copper shell over the FP-transducer core was provided to shield the FP-transducer from electrical noise.

Transfer of FP-transducer readouts to an FE model

Details of the procedure for transferring experimentally measured coordinates of the applied force to the FE model are reported elsewhere [19]. Briefly, once the load trajectory was obtained in the experimental field for the physical bone specimen, a spatial registration (such as the one described in [10]) was applied, to identify the spatial transformation that registers the FE model of the bone with respect to the physical bone specimen. A digitizer (Micro Scribe 3DX, Immersion Corporation, USA) was used to measure coordinates in the experimental area and an iterative-closest-point algorithm was used to register the FE model surface. Finally, the load trajectory could be replicated on the FE model once it was measured by means of the FP-transducer with respect to the physical test specimen.

Electrical testing of the FP-transducer

Electrical tests were performed to assess the quality of the signal provided by the FPtransducer, to ensure that baseline noise would not compromise signal quality. Signal high-frequency noise and long-term drift were checked at different sampling rates (1 to 5000 Hz) and on different time intervals (up to 12 hours of monitoring), with a high-speed scanner (System6000, Vishay, Malvern, USA), when the transducer was unloaded.

Calibration of the FP-transducer and assessment of its accuracy

We devised a calibration procedure to measure the intrinsic precision of the FP-transducer in calculating the position of the applied load. Known calibration loads were applied at a set of known positions on the FP-transducer to determine the parameters of the transfer functions. A

hydraulic uniaxial testing machine (Instron-8502, Instron, Norwood, USA) was used. A jig was designed to control the position and direction of the force applied during calibration. Twenty-five holes were grid-wise machined (five in five lines, each 20 mm from each other) on an aluminum calibration plate, which was mounted on top of the FP-transducer, collinearly with the main bending axes (Fig. 3). The calibration loads were applied by means of a 6 mm steel ball placed in each hole. Low-friction cross-rails were used to ensure a frictionless transmission of the calibration loads.

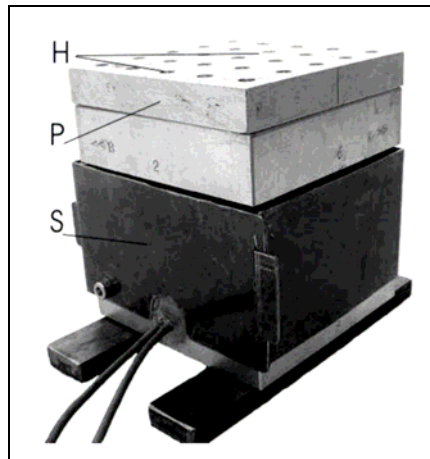


Figure 3 - The fully assembled FP-transducer (including the external shielding (S)) is visible, with the loading plate used for calibration mounted on the top face (P). Twenty-five holes were grid-wise machined on the calibration plate to accurately locate the calibration force by means of a steel ball (H).

The maximum calibration load was calculated based on the maximum allowed bending moment of the FP-transducer (maximum bending: 140 Nm). Each calibration point was tested three times using a sequence of loading steps: 400 N, 800 N, and 1200 N.

Automatic data-processing procedures were custom-written in MatLab (MatLab 6.1, MathWorks, Natick, MA, US). The readouts from the two Wheatstone bridges of the FPtransducer (the bending moment in two directions A and B, Fig. 2) were normalized by dividing them by the corresponding load value (measured by the load cell of the testing machine). A “black-box” approach [22] was used to define the correlation between collected readouts of the FP-transducer and known positions of the applied calibration loads. First-order equations, both with and without interaction between the two Wheatstone bridges, were tested, using least squares fitting.

Measurement precision (repeatability) was computed as the standard deviation among repeated estimates of the coordinates of the applied load when the load was applied in the same position. The accuracy (closeness to target value) of the FP-transducer was estimated based on the difference between the actual coordinates of the applied load, and the ones calculated based on the calibrated FP-transducer. The average error and the Root Mean Squared Error (RMSE) were used as indicators of the accuracy.

Assessment of the performance of the FP-transducer in a real testing setup

To assess the behaviour and the applicability of the FP-transducer to measure the position of the force applied to a long bone, a real testing setup was simulated where the FP-transducer was included. To test the transducer in a controlled arrangement, a simplified setup was implemented. To ensure repeatable and predictable deformation of the bone in this trial, a dummy bone model was built. As in the present application the FP-transducer was optimized for testing a femur specimen, a dummy femur was used. This femur was made of a steel T-profile 50 cm long and was welded to a flat plate at a 70° inclination (Fig. 4), replicating a typical testing setup for a femur [10, 17, 19]. The dummy specimen was fixed to the top of the FP-transducer and mounted on the testing machine. A spherical bearing on top of the dummy femur (simulating the femoral head) and low-friction crossrails (to avoid transmission of horizontal force components) were used to ensure a frictionless load transfer. The load was applied in 50 N steps, up to 700 N. Readouts from the transducer were collected and converted to position coordinates. To independently validate the force position estimated by the FP-transducer, the actual horizontal deflection of the dummy femur head was measured in two directions by means of two dial gauges (precision: 0.01mm, Fig. 4; 2046EB-08, Mitutoyo, Kawasaki, Japan). Five load repetitions were performed. The entire testing setup was dismantled and reassembled for each test repetition.

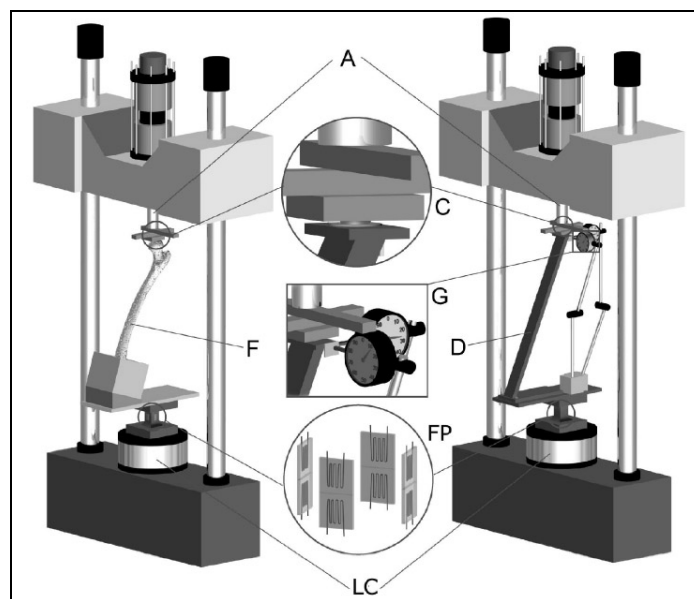


Figure 4 - Testing setup for a long bone, including the FP-transducer: setup for testing a real femur (left); simplified setup for validating the force-position transducer using a dummy femur (right). The actuator of the testing machine (A) applies the load from top, through a system of cross-rails (C), which eliminate the horizontal force components. The femur (F) and the dummy specimen (D) are mounted in the same respective position and inclination. The FP-transducer (FP) is mounted just below the fixture to hold the specimen at prescribed angles. The load cell of the testing machine (LC) measures the applied vertical force. In addition, two dial-gauges (G) measure the deflection of the dummy femur in the two measuring directions to validate the readout from the force-position transducer.

Results

Electrical testing

In the preliminary electrical tests, signal noise (including long-term drift and high frequency noise) was within +/-0.30 microstrain. This corresponds to an error of 0.05 mm on the estimated force position when a typical load of 1000N was applied. Thus, the error caused by electrical noise was almost two orders of magnitude lower than any other source of error (see below), and was negligible with respect to the measurement range (+/- 55 mm).

Calibration

The first-order equations including the interaction between the two Wheatstone bridges (corresponding to the two directions of bending A and B, Fig. 2), yielded the most accurate results (Table 1):

1. The errors of the estimated force position were similar in both directions.
2. The measurement repeatability when the calibration load was applied to the same assigned position was better than 0.2 mm as a resultant (Table 1, first row).
3. The accuracy of the FP-transducer, expressed as a vector distance between the estimated and the actual position of the applied calibration load, was 0.42 mm (vector sum of the RMSE; Table 1, last row).

	A DIRECTION	B DIRECTION	RESULTANT VECTOR
PRECISION (mm) (variation btw 3 replicates)	STD: 0.15	STD: 0.14	STD: 0.20
ACCURACY (mm) (difference btw measured value and assigned calibration load position)	Average: 0.31 RMSE: 0.35	Average: 0.19 RMSE: 0.24	Average: 0.36 RMSE: 0.42

Table 1 – Calibration of the FP-transducer. Errors are reported for both measurement directions (A and B); the last column reports the resultant error computed as vector sum of the errors in the two directions. The first row reports the measurement precision (repeatability) on the same assigned position of the calibration load, computed as standard deviation among measurement repetitions. The last row reports the accuracy (closeness to target value) of the FP-transducer as the difference between the actual coordinates of the applied load, and the coordinates provided by the FP-transducer. The average error and the Root Mean Squared Error (RMSE) are reported.

Performance of the FP-transducer in a real testing setup

In the preliminary application with the dummy femur, a maximum horizontal deflection of 25 mm was measured by the dial gauges, which is comparable to the deflection found with a real femur when similar loads are applied [19]. A comparison between the horizontal deflection measured by the dial gauges and the deflection estimated from the FPtransducer provided an indication of the overall error when the FP-transducer was applied to long bone testing:

1. The deflection measured by the dial gauges and the deflection measured by the FP-transducer correlated well as load was increased ($R^2 = 0.99$)
2. The RMSE in the force position was 0.85 mm in each direction (1.2 mm was the vector sum).

Thus, it can be assumed that, when the FP-transducer is used, the position of the force applied to a long bone can be measured with an accuracy of better than 1.2 mm. Therefore, the proposed method allows reporting the position of the applied force onto an FE model with an accuracy of 1.2 mm. This accuracy compares extremely well with the average element length in a state-of-the-art FE mesh (2-5 mm [10]). Preliminary FE analyses showed that an accuracy of 2.0 mm on the position of the applied force is needed to obtain the calculated peak stress with an accuracy of better than 5% in [19]. The FP-transducer allows meeting such requirement.

Limitations

One limitation is that the FP-transducer not only measures the bending moments generated by the horizontal position of the applied vertical force, but it is also affected by the bending moment generated by horizontal forces (if present) that are generally “multiplied” by a large lever arm (the bone length). Although the proposed setup in principle features only a vertical load, the horizontal deflection of the bone under load, combined with friction, generates a passive horizontal force component.

For instance, to obtain an overall accuracy of 2 mm when a femur 50 cm long is loaded with a force of 700N, the horizontal force component (caused by friction) should not exceed 3N. This can be obtained only if the vertical force is applied with a low-friction system (coefficient of friction ≤ 0.004) that ensures extremely low frictional forces. Thus, care should be taken in evaluating each possible source of friction, such as worn or badly mounted cross-rails. Users should also be aware that the longer the vertical lever arm, the bigger the effect of friction, as the lever arm acts as a multiplier of the horizontal force component.

A second limitation of this study is that the FP-transducer was tested only when the resultant hip joint force was simulated. While this is definitely a relevant simulation for several applications concerning the proximal femur [10, 13, 14, 23], there are instances where also muscle forces need to be simulated [24, 25]. It must be pointed out that the FPtransducer operating principle is such that it can measure the position of any resultant force. Therefore, if the in vitro setup is modified to include simulation of selected muscle forces, the FP-transducer would still be capable of measuring the actual position of the resultant force.

Comparison with previous similar works

Comparisons of the present results with the literature are difficult as there have been no other studies published, that quantify the accuracy of estimates of the load application point in FE models. The effect of such uncertainty the FE model output has also never been addressed

before. The error affecting the estimated position of the applied load in previous cross-validation experiments where the FP-transducer was not present was more than 10 mm [19], due to uncertainty and variability in identifying the contact area under load. This error may seriously affect the stress predicted by an FE model [17, 26].

Discussion

The aim of the research reported here was to provide a method to improve validation of FE models of long bones.

We designed a transducer that was incorporated into a standard testing setup for long bones, so as to measure the bending moments. The FP-transducer successfully estimated the position of the force applied to the proximal extremity of the femur. The intrinsic accuracy of the FP-transducer was 0.42 mm when tested alone, and better than 1.2 mm when incorporated in a setup for testing a femur.

The overall accuracy achieved in the present application (1.2 mm) was one order of magnitude better than previously reported and was less than half the characteristic element dimension commonly found in a converged FE mesh of a femur [10, 27]. Moreover, the proposed method was able to account for the trajectory of the applied load throughout the load application. This possibility is extremely important when replicating destructive tests with FE models, as bone deflections of the order of several millimeters are observed [10, 17, 19]. Thus, the accuracy of FE analyses of long bones may be improved with a better definition of boundary conditions (the actual position of the applied load).

REFERENCES

1. Roache, P.J., *Verification and Validation in Computational Science and Engineering*, ed. Hermosa. 1998, Albuquerque.
2. Ota, T., I. Yamamoto, and R. Morita, *Fracture simulation of the femoral bone using the finite-element method: how a fracture initiates and proceeds*. J Bone Miner Metab, 1999. **17**(2): p. 108-12.
3. Les, C.M., et al., *Development and validation of a series of three-dimensional finite element models of the equine metacarpus*. J Biomech, 1997. **30**(7): p. 737-42.
4. Lengsfeld, M., et al., *Comparison of geometry-based and CT voxel-based finite element modelling and experimental validation*. Med Eng Phys, 1998. **20**(7): p. 515-22.
5. Keyak, J.H., et al., *Prediction of femoral fracture load using automated finite element modeling*. J Biomech, 1998. **31**(2): p. 125-33.
6. Keyak, J.H., et al., *Validation of an automated method of three-dimensional finite element modelling of bone*. J Biomed Eng, 1993. **15**(6): p. 505-9.
7. Gupta, S., et al., *Development and experimental validation of a three-dimensional finite element model of the human scapula*. Proc Inst Mech Eng [H], 2004. **218**(2): p. 127-42.
8. Couteau, B., et al., *Finite element analysis of the mechanical behavior of a scapula implanted with a glenoid prosthesis*. Clin Biomech (Bristol, Avon), 2001. **16**(7): p. 566-75.
9. Viceconti, M., et al., *Extracting clinically relevant data from finite element simulations*. Clin Biomech (Bristol, Avon), 2005. **20**(5): p. 451-
10. Taddei, F., et al., *Subject-specific finite element models of long bones: An in vitro evaluation of the overall accuracy*. J Biomech, 2006. **39**(13): p. 2457-67.
11. Keyak, J.H., H.B. Skinner, and J.A. Fleming, *Effect of force direction on femoral fracture load for two types of loading conditions*. J Orthop Res, 2001. **19**(4): p. 539-44.
12. Keyak, J.H., et al., *Predicting the strength of femoral shafts with and without metastatic lesions*. Clin Orthop Relat Res, 2005. **439**: p. 161-70.
13. Cristofolini, L., et al., *In vitro replication of spontaneous fractures of the proximal human femur*. J Biomech, 2007. **40**(13): p. 2837-45.
14. Cristofolini, L., A. Cappello, and A. Toni, *Experimental errors in the application of photoelastic coatings on human femurs with uncemented hip stems*. Strain, 1994. **30**(3): p. 95-103.
15. Cody, D.D., et al., *Femoral strength is better predicted by finite element models than QCT and DXA*. J Biomech, 1999. **32**(10): p. 1013-20.
16. Saglam, H. and A. Unuvar, *Three-component, strain gage based milling dynamometer design and manufacturi*. Journal of Integrated Design and Process Science, 2001. **5**: p. 95-109.
17. Cristofolini, L. and M. Viceconti, *Towards the standardization of in vitro load transfer investigations of hip prostheses*. Journal of Strain Analysis for Engineering Design, 1999. **34**(1): p. 1-15.
18. Villa, T., R. Pietrabissa, and V. Quaglioni. *Testing procedure for biomechanical evaluation for nailed femur*. in *Proc. Proceedings of the 12th Conference of the European Society of Biomechanics*. 2000. Dublin.
19. Cristofolini, L., et al. *Biomechanical testing of the proximal femoral epiphysis: intact and implanted condition*. in *Proc*. 2006. Torino.

20. Bergmann, G., F. Graichen, and A. Rohlmann, *Hip joint loading during walking and running, measured in two patients*. J Biomech, 1993. **26**(8): p. 969-90.
21. Bergmann, G., et al., *Hip contact forces and gait patterns from routine activities*. J Biomech, 2001. **34**(7): p. 859-71.
22. Draper, N.R. and H. Smith, *Applied Regression Analysis*. 1966, John Wiley & Sons: New York.
23. Cristofolini, L., et al., *Preclinical assessment of the long-term endurance of cemented hip stems. Part 1: effect of daily activities--a comparison of two load histories*. Proc Inst Mech Eng [H], 2007. **221**(6): p. 569-84.
24. Colgan, D., et al., *A review of joint and muscle load simulation relevant to in-vitro stress analysis of the hip*. Strain, 1994. **30**: p. 47-61.
25. Britton, J.R., C.G. Lyons, and P.J. Prendergast, *Measurement of the relative motion between an implant and bone under cyclic loading*. Strain, 2004. **40**: p. 193-202.
26. Cristofolini, L. and M. Viceconti, *In vitro stress shielding measurements can be affected by large errors*. J Arthroplasty, 1999. **14**(2): p. 215-9.
27. Taddei, F., et al., *Mechanical strength of a femoral reconstruction in paediatric oncology: a finite element study*. Proc Inst Mech Eng [H], 2003. **217**(2): p. 111-9.

Appendix B

In vitro replication of spontaneous fractures of the proximal human femurⁱⁱⁱ

Spontaneous fractures of the hip can be defined as those fractures deriving from physiological or sudden loading, but not from a traumatic event (they may eventually result in secondary trauma, but they are not caused by trauma) [1, 2]. They most frequently occur in elderly (osteoporotic) subjects. Yang [3] developed two in vitro simulations (later replicated numerically by Gomez-Benito [4]) to determine the biomechanical background for spontaneous hip fractures. They suggested that abnormal muscle contraction of the rotator muscles could induce hip fracture. In addition, bone fractures may occur as a consequence of excessive cyclic loading [1, 2]. However, cyclic fractures typically occur because of excessive load/activity, and usually do not involve the proximal femur. As the focus of this paper is on fractures of the proximal femur occurring in elderly subjects, cyclic fractures will not be considered hereafter. There are mainly two reasons to investigate the biomechanics of spontaneous fractures of the proximal femoral metaphysis:

- (1) A significant fraction (though not the majority) of fractures of the untreated hip in the elderly are not associated with a primary traumatic event [1]. While the actual estimate of such fraction is difficult (elderly patients are often unable to report whether they fell before or after the fracture), it must account for 10-60% of the hip fractures [5-8] suggested that buckling of the thin cortical shell could be one failure-initiating event if the underlying trabeculae are weakened by osteoporosis.
- (2) With the recent return to resurfacing prostheses, concerns exist about risk of neck fractures due to physiological loading [9-12]. This event is clinically undesirable. It also has serious legal implications (especially in the case of spontaneous fractures).

In most cases, patients cannot recall what motor task was performed at the time of fracture, or report having been stumbling or tripping on an obstacle [5, 7]. In the first case the motor task is unknown, but even in the second case the direction of the applied loads is hard to determine. Therefore, there is no clear indication as to which is the relevant loading mode when

ⁱⁱⁱ Luca Cristofolini, Mateusz Juszczak, Saulo Martelli, Fulvia Taddei, Marco Viceconti. “*In-vitro* replication of spontaneous fractures of the proximal human femur”. *J Biomech.*,40,2007, p:2837–45

spontaneous fractures occur. Additionally, the type of fracture that will develop and the required load cannot be easily predicted a priori [13].

Traumatic femoral fractures due to impact on the greater trochanter as a consequence of sideways fall have been extensively investigated in vitro [6, 14-16]. Traumatic and spontaneous fractures exhibit different cracking modes and regions [1, 14, 17-20].

Several numerical and in vitro studies have been carried out attempting to simulate spontaneous fractures. However, there is no consensus concerning the relevant loading scenario to be simulated. The direction of the force applied on the femoral head ranges between 0° [16, 21-23], 11° [24], 20° [15, 18, 25], 24° [26], and 25° [27, 28] in the frontal plane, or even perpendicular to the shaft [29]. In other cases (e.g. Alho [30]; [31]; Patel and Murphy[32]) the loading direction is not specified (with limitations discussed elsewhere[33]). This lack of agreement concerning the loading scenario undermines comparison between tests, as the direction of the load severely affects the stress distribution [34-36], hence failure. Keyak et al. [19, 20] addressed the issue of the loading direction and tried to assess the relevance of the muscle force on simulated failure [37]. Their conclusions were that it should not be necessary to simulate the muscles, and single-leg stance (resultant force at 10° in the frontal plane) and stair-climbing (30° in the sagittal plane) are the most relevant loading conditions. However, their indications cannot be considered conclusive, as they never tested experimentally the single-leg stance loading condition they identified (in all experiments they applied a resultant force at 20° in the frontal plane [15, 19, 20, 37]). In addition in the cited work [19, 20], they did not provide any indications on the femoral region subjected to the highest stress-strain levels in the one-leg stance configuration, thus providing no numerical evidence that this configuration may result in clinically relevant neck fractures. Therefore, there is a need for more extensive work based on state-of-the-art FE models, to confirm which is the most relevant loading scenario for replicating in vitro spontaneous neck fractures.

The goals of this work were to:

- develop a rationale and identify the most relevant loading scenario to recreate in vitro spontaneous hip fractures;
- develop the simplest possible testing protocol so as to increase repeatability and reproducibility (including assessment of the need to apply the muscle forces in the in vitro setup);
- validate such protocol by testing a sample of human femurs, and assessing the fractures recreated in vitro, in comparison with those observed in the clinical practice.

Materials and methods

Identification of the most critical loading scenario: FE simulations

A highly detailed finite element (FE) model of a human femur, which was previously validated against experimental measurements [38, 39] was used to complement this study. A relevant

donor for the FE study was selected (male, died 51 of intracerebral hemorrhage, free of musculoskeletal disease, smoker, osteoporotic, 175 cm tall, weighing 75 kg). The FE model included a dedicated material mapping strategy to assign suitable material properties to each element [38, 39]. It was used to perform a preliminary sensitivity analysis to address the following two questions:

- (1) Does the application of the muscle forces (below the intertrochanteric region) affect the strain distribution in the head-neck region, or is it sufficient to apply the joint load with the right direction and intensity? This question was addressed by simulating inclusion and exclusion of the muscle forces, when the same resultant joint force was simulated under simulated single-leg stance during gait [40].
- (2) Which is the direction of the hip joint resultant force that can cause the highest risk of failure in the head-neck region with respect to the diaphyseal one, to obtain clinically relevant failure scenario for the proximal femur. In fact, a preliminary study indicated that when unsuitable scenarios are applied, diaphyseal fractures might occur before the head-neck region fails. Once the first question was answered, the second one was addressed by exploring the five most frequent loading scenarios (level walking, stair climbing and descending, one-leg stance, standing up), as reported in [40].

The model consisted of 76,026 10-node tetrahedral elements. The inhomogeneous material properties were derived from the calibrated computed tomography (CT) dataset of the same femur [41] and resulted in 381 different materials. More details are reported in Taddei et al. [38, 39].

Experimental setup, measurements and recording

The in vitro set-up was designed based on previous experience with nondestructive testing of the proximal [34, 35, 42, 43].

The femur specimens were prepared with a set of reference axes to allow for reproducible alignment throughout the test, following a validated protocol [35, 44]. The femurs were stored at -25°C when not in use. During the test, they were wrapped in clothes soaked with physiological solution and tested at a room temperature of $27\text{-}30^{\circ}\text{C}$.

The femoral condyles were potted in a steel box with dental cement meeting the ISO 5833 requirements. The femur was mounted on top of the load cell of the testing machine with the diaphysis at an angle of 81° in the frontal plane (as defined by the sensitivity analysis performed with the FE, Section 3.1). Load was applied to the femora head through a system of rails to avoid transmission of horizontal force components (Fig. 1). A copy of each femoral head was prepared with dental cement (covering $1/5$ head diameter) to allow uniform load transfer from the actuator to the head. Muscle forces were not simulated, as the FE models indicated this is not necessary in this application (Section 3.1).

Load was applied at a constant displacement rate of 2 mm/s, which resulted in the femurs failing within 0.5-2 s. Load and displacement were recorded by the testing machine (8502, Instron, Canton, MA, USA) at 1000 Hz.

During the destructive test, the event was filmed by means of a high-speed camera (FastCam-X1024PCI, Photron, UK) at 3000-9000 frames/s (actual frame rate depended on the size of the field of vision cropped for each specimen). The camera pointed at the superior-lateral part of the neck. Two mirrors were used to film at the same time the anterior-medial and posterior-medial portions of the neck.

Assessment of the test protocol

The test protocol above was applied to 10 cadaveric human femurs (Table 1) to confirm if clinically relevant failure modes and fracture load could be obtained. Specimens were chosen from relatively aged donors so as to represent the target population. Suitable fresh-frozen bone specimens were obtained through IIAM (Jessup, PA, USA). They were DEXAscanned (Excel-Plus, Norland, USA) and CT-scanned (HiSpeed, General Electric, USA) to document bone quality and lack of abnormality or defects. Anatomical dimensions (head diameter and biomechanical length) were measured (Table 1, Ruff and Hayes, 1983 [35, 44]).

Results

Most critical loading scenario: FE simulations

In the FE model, the inclusion/exclusion of the abductor muscles affected the strain distribution in the superior aspect of the head-neck region (Fig. 2). However, this effect was quite moderate. Moreover, higher peak tensile strains were found when the muscles were not simulated. Therefore, exclusion of the muscles tends to slightly overestimate the risk of fracture (when the same joint resultant force is applied).

The FE models indicated that, among the directions recorded by Bergmann [40], the loading scenario that generates the highest risk of failure of the neck region is the one-leg stance configuration, when the force lies in the frontal plane at 81° from the diaphysis (Fig. 3). In fact, while other scenarios have a larger stress below the trochanteric region or in the diaphysis, this is the condition with the highest risk in the neck (i.e. one-leg stance is the loading scenario that, if incrementally scaled, may lead to a fracture in the head-neck region first).

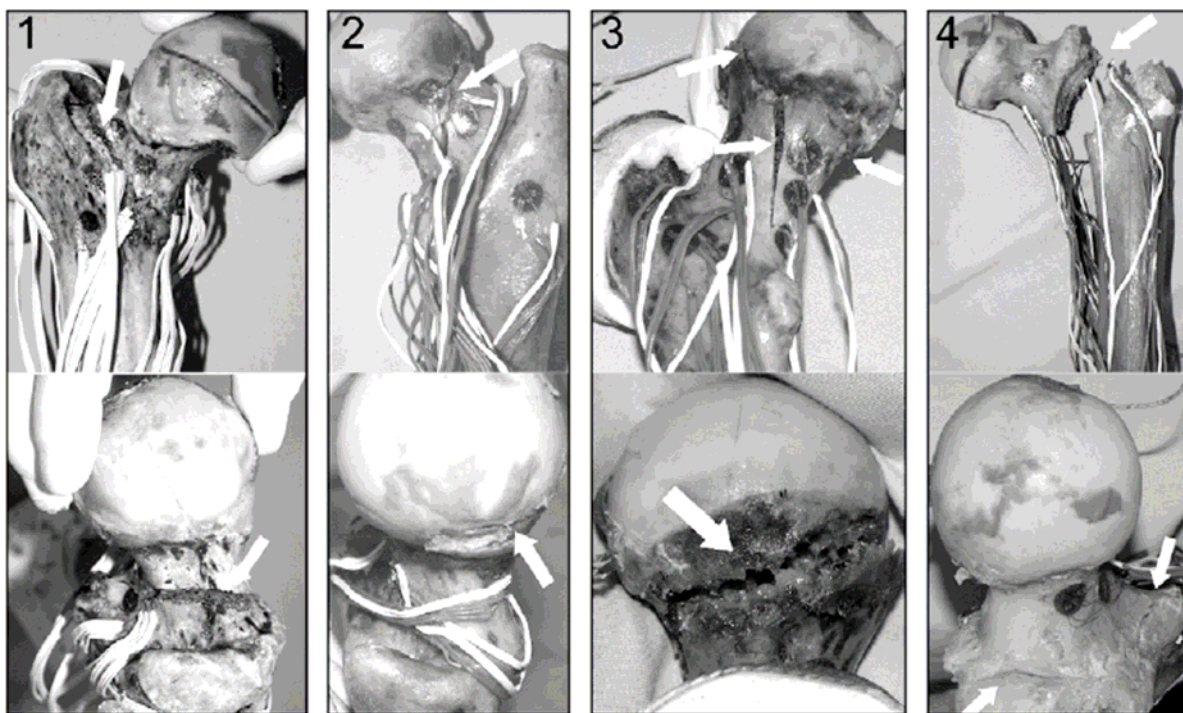


Figure 5 - Typical fractures found in the in vitro fractured specimens (highlighted by the white pointers). (1) Base-of-the-neck fracture, close to the greater trochanter (top: frontal view; bottom: detail from the lateral-superior side of the neck). (2) Cervical fracture, showing two crack initiation sites laterally, which indicate uniform fracture risk area (top: posterior view on top; bottom: detail from the lateral-superior side of the neck). (3) Cervical fracture, propagating parallel to the neck, and including a secondary subcapital crack on the medial side (top: posterior view; bottom: lateral view of the head).

Results from 10 bone specimens

The test protocol was successfully applied to all specimens, with fractures occurring in the head-neck region (i.e. the region where spontaneous fractures are most likely to occur). In vitro fractures varied from specimen to specimen, and ranged from cervical to inter-trochanteric (Fig. 4). Most of the fractures (80%, Table 1) initiated from the most proximal portion of the neck.

Load-displacement curves were highly linear ($R^2 > 0.99$) for most of the loading ramp. Linearity decreased only in the last few hundred Newton, prior to sudden failure. The failure load was 9344 ± 3140 N, corresponding to 10.9 ± 3.0 body weight (BW) (Table 1). The error affecting the measured failure load was of 2.6% (This includes the intrinsic uncertainty of the testing machine ($< 0.5\%$), as well as the errors caused by the transient occurring upon failure). High-speed movie were successfully obtained for all specimens. They allowed observing the exact time when fracture initiated, and how it propagated across the bone (Fig. 5). A sample movie is available from the Journal website.

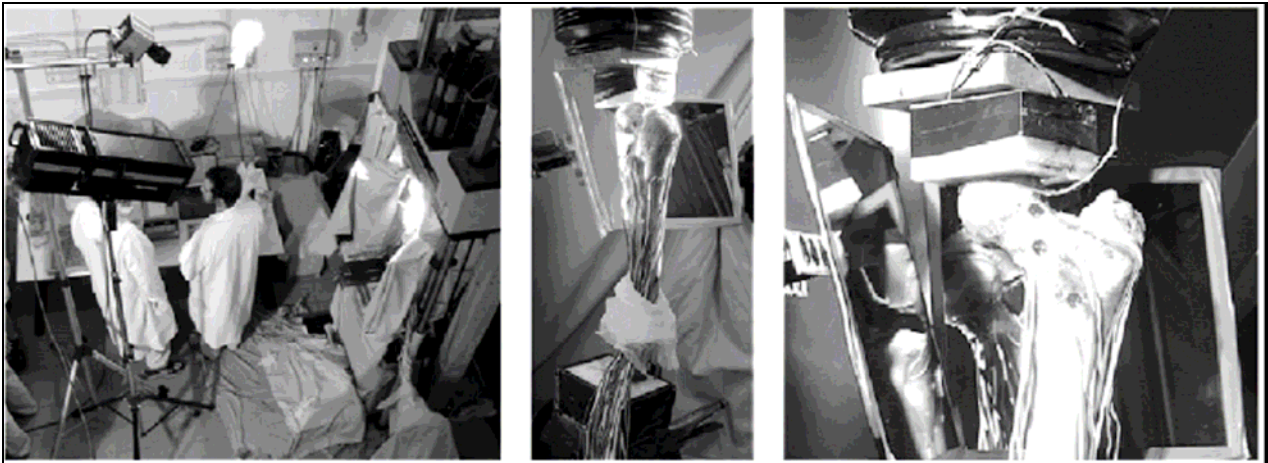


Figure 6 - Experimental setup used to fracture the proximal femurs in vitro. Left: overview of the testing setup where the high-speed camera is visible on the left (directly facing the superior-lateral part of the femur), together with the light source; the bone specimen is under the testing machine on the right. Centre: Intact femur mounted on the material testing machine with the diaphysis at 81° from vertical; the cross-rails to eliminate horizontal force components are visible on the top; the two mirrors are visible near the femur (they were oriented so as to reflect the anterior-medial and posterior-medial sides of the femur). Right: detail of the proximal femur, with the mirrors and the copy of the femoral head for applying the load to the femur. The strain gauges bonded on the bone surface were part of a separate study.

Table
Details of the 12 femur specimens investigated

Donor's details				Femur's data					Failure load		Failure mode		
Sex	Age at death	Donor height (cm)	Donor weight (kg)	SIDE	DEXA% young reference	DEXA% age matched	Average head diameter (mm)	Biomech. length (mm)	N	x BW	Anatomical location	AO Müller	Pauwels
Male	67	173	82	Left	75.9%	90.0%	49.7	415	11370	14.13	Intracapsular: base neck	31B	III
Male	72	173	100	Right	82.5%	100.1%	46.6	414	11170	11.39	Intracapsular: transcervical (+ subcapital) ⁽¹⁾	31B (+ 31C)	III (+ II)
Male	70	175	90	Left	66.2%	79.6%	47.7	443	11770	13.33	Transcervical extracapsular ⁽²⁾	31B (+ 31A)	III
Male	51	175	164	Left	91.0%	99.4%	53.5	463	16040	9.97	Extracapsular: base neck	31B	II
Female	83	157	48	Left	60.9%	77.8%	46.8	421	7931	16.84	Intracapsular: transcervical ⁽³⁾	31B	III
Male	80	178	88	Right	62.2%	76.4%	52.0	437	7093	8.22	Intracapsular: transcervical ⁽⁴⁾	31B	III
Male	67	175	88	Right	59.1%	70.0%	52.0	423	7427	8.60	Intracapsular: transcervical ⁽⁴⁾	31B	III
Male	71	178	91	Right	76.2%	92.0%	53.3	443	7921	8.87	Intracapsular: transcervical (near base neck)	31B	II
Male	82	175	78	Left	47.9%	58.9%	49.4	432	6401	8.37	Intracapsular: transcervical	31B	III
Male	73	175	73	Left	47.7%	58.2%	46.9	433	6319	8.82	Intracapsular: transcervical (near base neck)	31B	III

In the first four columns, details of the donor are listed. Bone quality is reported in the 6th and 7th column (bone density as % of the young reference population, and of the age-matched population computed based on the Norland DEXA scanner reference population). Biomechanical dimensions (Ruff and Hayes, 1983) are reported in the 8th and 9th columns. Failure load in Newton and as a fraction of the donor's body weight is reported. The failure mode is reported in the last three columns: based on anatomical location (Rockwood et al., 1991); AO Muller Classification (31-A = extracapsular trochanteric; 31-B = intracapsular neck; 31-C = intracapsular head) (Ruedi and Murphy, 2001); Pauwels' classification based on fracture direction (I = fracture nearly perpendicular to femoral diaphysis; II = nearly perpendicular to neck axis; III = nearly parallel to femoral diaphysis) (Pauwels, 1935).

Note(1): Failed due to transcervical fracture, but subcapital fracture initiated in parallel;

Note(2): Started from lateral cartilage edge, propagated below lesser trochanter;

Note(3): Started from lateral cartilage edge, bifurcated and propagated along cartilage edge;

Note(4): Started from lateral cartilage edge, propagated along the neck (above lesser trochanter).

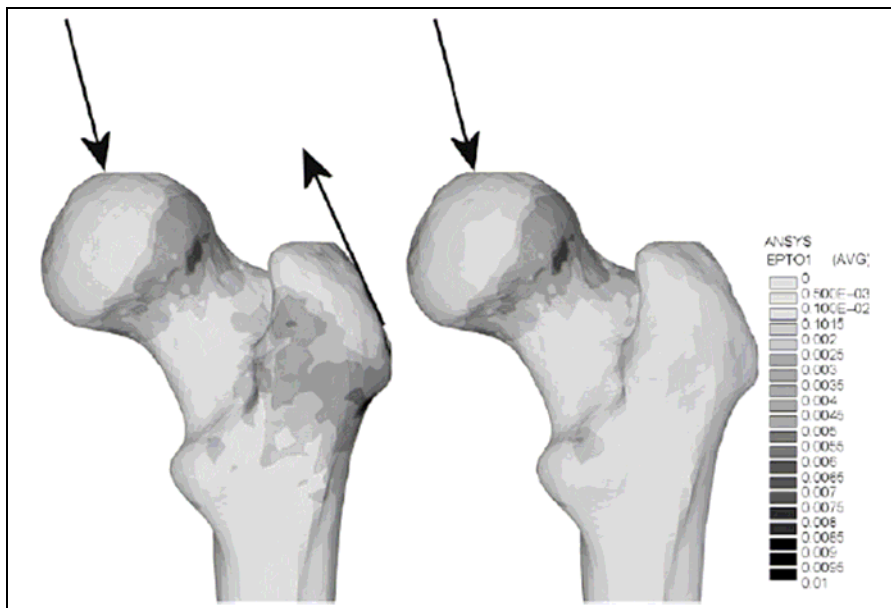


Figure 7 - Principal tensile strain in the proximal femur when the abductor muscles are simulated (left) and when these muscles are not simulated, while the same resultant force is applied to the femoral head (right). The plots show that minimal strain alterations are induced in the head-neck region by the inclusion/exclusion of the abducting muscles.

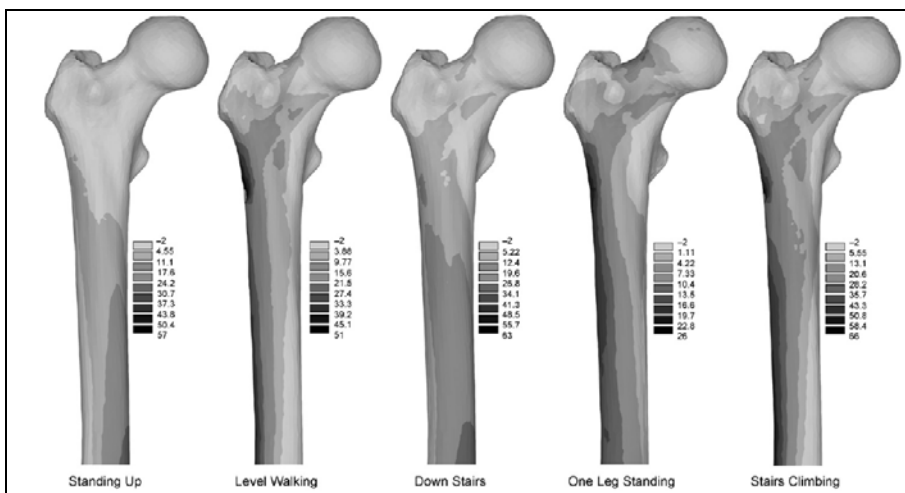


Figure 8 - Principal tensile stress distribution as predicted by finite element analysis for five different loading scenarios. Different scales are used for the five loading scenarios, to allow comparison between the head-neck and diaphyseal region within the same case. These plots were explored to determine for which loading scenario the stress in the head-neck region is higher, in comparison with the diaphysis (i.e. proximal fractures are more likely than diaphyseal ones).

Discussion

Spontaneous fractures of the hip are caused by occasional overloads during daily activities, and are associated with hip resurfacing implants [1, 2]. They are associated with poor bone quality due to age and osteoporosis. In fact, a decrease of bone tissue toughness is associated with age [45].

Despite some preliminary study [19, 20, 37], there is no strong indication concerning the most relevant loading scenario for replicating spontaneous neck fractures in vitro. The final scope of

this paper was to design a knowledge-based test setup to simulate in vitro spontaneous fractures of the proximal femur. The three original goals were successfully met:

- Based on a validated FE model, the most critical loading scenario (among the possible motor tasks that a subject typically performs when spontaneous fractures occur) was identified, which should be simulated in vitro.
- Based on past experience and on the current FE simulations, the simplest possible testing protocol was designed and implemented. It was demonstrated that it is not necessary to simulate the action of the muscles to investigate fractures in the head-neck region. This enables simplification and better reproducibility both of experimental simulations and of in vitro test setups.
- Application of the protocol to 10 femur specimens confirmed its feasibility and reproducibility. Clinically relevant fractures were obtained in vitro in all specimens, with failure loads which were compatible with occasional overloads [40].

The loading scenario identified as most critical here is compatible with numerical studies [19, 20], and is quite similar to the one used by Link et al. [24] (11° in the frontal plane). Also, this study indicated that it is not necessary to simulate the muscle forces to create a suitable stress state in the head-neck region in accordance with previously published works [27, 37].

It must be stressed that the scope of this study was to recreate in vitro the conditions for spontaneous fractures of the proximal caused by a single sudden loading event (typically in elderly subjects), as opposed to fatigue fractures, which are caused by cyclic loading (usually associated with active subjects, and involving other regions than the proximal femur [1, 2]. Consistently with most of similar works, the authors recommend simulation of a single-loading ramp, as this seems to best represent the occasional overloading leading to non-traumatic fractures) [2, 5, 7, 8]. Others [16, 21, 22] have chosen to apply loading cycles of increasing magnitude.

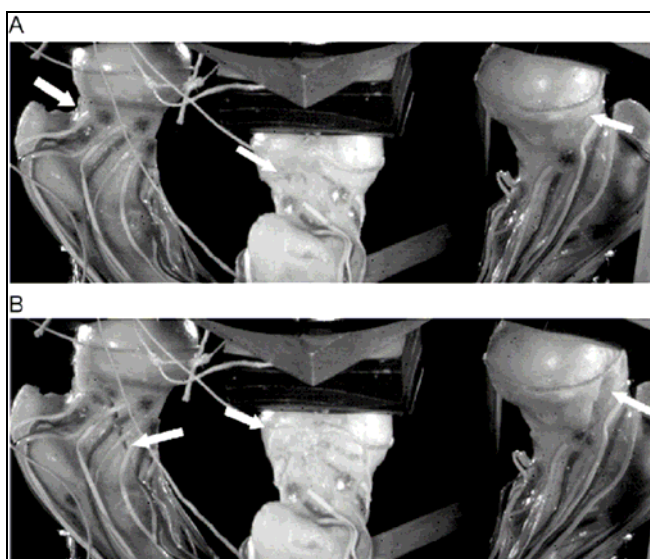


Figure 9 - Frames obtained from a high-speed movie during a fracture test on a right femur. The image in the centre of each picture is a direct view of the femoral neck from superior-lateral; the ones on the left and right

(postero-medial and antero-medial views of the neck respectively) are reflected images obtained from the two mirrors placed next to the femur and suitably oriented (Fig. 1). Picture A shows the instant when the crack starts opening on the lateral part of the neck (indicated by the white pointer). Picture B (2.8 ms after Picture A) shows a later stage of propagation. Strain gauges can be seen, that were not part of this study. Also, strings are visible that were glued to several points of the head and neck (they were slack, and bonded to unloaded regions): they were used to prevent excessive spreading of bone fragment upon fracture. The pictures have low resolution (1 pixel $\frac{1}{4}$ approximately 0.2mm on the physical specimen) because they were acquired by the high-speed camera; view is clearer when the movie provided in the Supplementary material is watched.

The most common fracture initiation site was the subcapital region (80% of the specimens). This is the most common type of spontaneous fractures [1]. Indeed, a similar fraction of subcapital fractures was obtained in vitro by others (69%, Cody et al. [27] and 94%, Keyak et al. [19, 20]).

The failure loads found here (9344 ± 3140 N) are comparable with the values reported in the literature: Ota et al. [31] reported a failure load of 8400N (loading direction not specified); Link et al. [24] reported a failure load of 8890 ± 3770 N (simulated stance); Duchemin et al. [46] reported a failure load of 9032 ± 3412 N (11° in the frontal plane); Smith et al. [26] reported a range of 4937-16148 N; Cody et al. [27] reported a value of 9920 ± 3219 N (25° in the frontal plane). Such values are found in occasional overloading events such as stumbling or miss-stepping [40], which are a suspected cause of spontaneous fractures [1].

The variability of the failure load expressed in N in this study (coefficient of variation, CoV = 34%) is comparable to the values reported in the literature: Lochmuller et al. [16, 21] reported CoV = 27-39%; Duchemin et al. [21] CoV = 38%; Eckstein et al. [14] and Link et al. [24] CoV = 42% (both values are referred to a sample with a wider age range); Cody et al. [27] CoV = 32%. In fact, a comparison on paired femurs [14] indicated that the lower bound for repeatability is 15%.

It must be noticed that variability was reduced when the failure load was expressed in terms of fraction of the donor's BW, rather than in N: the coefficient of variation decreased from 33.6% to 27.5%. This supports the idea of reporting bone strength as a fraction of BW rather than in absolute terms, and is in agreement with the findings of Lochmuller et al. [16].

It is worth remarking that the strength of the femur measured under this loading scenario is a potential predictor of neck strength when the femur is subjected to a lateral impact [18, 21, 46].

There are some limitations of this work that should be discussed. First, the sample size investigated was relatively small. However, the scope of the experimental tests was not to measure the average strength of the femur on a given population, but to provide a validation to the methodology. Moreover, as no in vivo recording is available for such traumatic events, the FE simulation relied on scaled muscle forces based on stance conditions ([40], similarly to Keyak et al. [37]). The test protocol developed and validated herein can thus be applied to investigate spontaneous fractures of the natural femur. It could also be extended to address neck fractures in the presence of epiphyseal prostheses.

REFERENCES

1. Cotton, D.W., et al., *Are hip fractures caused by falling and breaking or breaking and falling? Photoelastic stress analysis*. Forensic Sci Int, 1994. **65**(2): p. 105-12.
2. Jeffery, C.C., *Spontaneous fractures of the femoral neck*. Orthop Clin North Am, 1974. **5**(4): p. 713-27.
3. Yang, K.H., et al., *The relationship between loading conditions and fracture patterns of the proximal femur*. J Biomech Eng, 1996. **118**(4): p. 575-8.
4. Gomez-Benito, M.J., J.M. Garcia-Aznar, and M. Doblare, *Finite element prediction of proximal femoral fracture patterns under different loads*. J Biomech Eng, 2005. **127**(1): p. 9-14.
5. Grisso, J.A., et al., *Risk factors for falls as a cause of hip fracture in women. The Northeast Hip Fracture Study Group*. N Engl J Med, 1991. **324**(19): p. 1326-31.
6. Mayhew, P.M., et al., *Relation between age, femoral neck cortical stability, and hip fracture risk*. Lancet, 2005. **366**(9480): p. 129-35.
7. Michelson, J.D., et al., *Epidemiology of hip fractures among the elderly. Risk factors for fracture type*. Clin Orthop Relat Res, 1995(311): p. 129-35.
8. Muckle, D.S., *Iatrogenic factors in femoral neck fractures*. Injury, 1976. **8**(2): p. 98-101.
9. Amstutz, H.C., P.A. Campbell, and M.J. Le Duff, *Fracture of the neck of the femur after surface arthroplasty of the hip*. J Bone Joint Surg Am, 2004. **86-A**(9): p. 1874-7.
10. Shimmin, A.J. and D. Back, *Femoral neck fractures following Birmingham hip resurfacing: a national review of 50 cases*. J Bone Joint Surg Br, 2005. **87**(4): p. 463-4.
11. Shimmin, A.J., J. Bare, and D.L. Back, *Complications associated with hip resurfacing arthroplasty*. Orthop Clin North Am, 2005. **36**(2): p. 187-93, ix.
12. Siebel, T., S. Maubach, and M.M. Morlock, *Lessons learned from early clinical experience and results of 300 ASR hip resurfacing implantations*. Proc Inst Mech Eng [H], 2006. **220**(2): p. 345-53.
13. Jarvinen, T.L., et al., *Revival of bone strength: the bottom line*. J Bone Miner Res, 2005. **20**(5): p. 717-20.
14. Eckstein, F., et al., *Reproducibility and side differences of mechanical tests for determining the structural strength of the proximal femur*. J Bone Miner Res, 2004. **19**(3): p. 379-85.
15. Keyak, J.H., et al., *Prediction of femoral fracture load using automated finite element modeling*. Journal of Biomechanics, 1998. **31**(2): p. 125-33.
16. Lochmuller, E.M., et al., *Correlation of femoral and lumbar DXA and calcaneal ultrasound, measured in situ with intact soft tissues, with the in vitro failure loads of the proximal femur*. Osteoporos Int, 1998. **8**(6): p. 591-8.
17. Backman, S., *The proximal end of the femur: investigations with special reference to the etiology of femoral neck fractures; anatomical studies; roentgen projections; theoretical stress calculations; experimental production of fractures*. Acta Radiol Suppl, 1957(146): p. 1-166.
18. Keyak, J.H., *Relationships between femoral fracture loads for two load configurations*. J Biomech, 2000. **33**(4): p. 499-502.

19. Keyak, J.H., et al., *Prediction of fracture location in the proximal femur using finite element models*. Med Eng Phys, 2001. **23**(9): p. 657-64.
20. Keyak, J.H., H.B. Skinner, and J.A. Fleming, *Effect of force direction on femoral fracture load for two types of loading conditions*. J Orthop Res, 2001. **19**(4): p. 539-44.
21. Lochmuller, E.M., et al., *Mechanical strength of the proximal femur as predicted from geometric and densitometric bone properties at the lower limb versus the distal radius*. Bone, 2002. **30**(1): p. 207-16.
22. Lochmuller, E.M., et al., *In situ femoral dual-energy X-ray absorptiometry related to ash weight, bone size and density, and its relationship with mechanical failure loads of the proximal femur*. Osteoporos Int, 2000. **11**(4): p. 361-7.
23. Lotz, J.C., E.J. Cheal, and W.C. Hayes, *Fracture prediction for the proximal femur using finite element models: Part I--Linear analysis*. Journal of biomechanical engineering, 1991. **113**(4): p. 353-60.
24. Link, T.M., et al., *Structure analysis of high resolution magnetic resonance imaging of the proximal femur: in vitro correlation with biomechanical strength and BMD*. Calcif Tissue Int, 2003. **72**(2): p. 156-65.
25. Lang, T.F., et al., *Volumetric quantitative computed tomography of the proximal femur: precision and relation to bone strength*. Bone, 1997. **21**(1): p. 101-8.
26. Smith, M.D., et al., *Proximal femoral bone density and its correlation to fracture load and hip-screw penetration load*. Clin Orthop Relat Res, 1992(283): p. 244-51.
27. Cody, D.D., et al., *Femoral strength is better predicted by finite element models than QCT and DXA*. J Biomech, 1999. **32**(10): p. 1013-20.
28. Delaere, O., A. Dhem, and R. Bourgois, *Cancellous bone and mechanical strength of the femoral neck*. Arch Orthop Trauma Surg, 1989. **108**(2): p. 72-5.
29. Dalen, N., L.G. Hellstrom, and B. Jacobson, *Bone mineral content and mechanical strength of the femoral neck*. Acta Orthop Scand, 1976. **47**(5): p. 503-8.
30. Alho, A., T. Husby, and A. Hoiseth, *Bone mineral content and mechanical strength. An ex vivo study on human femora at autopsy*. Clin Orthop Relat Res, 1988. **227**: p. 292-7.
31. Ota, T., I. Yamamoto, and R. Morita, *Fracture simulation of the femoral bone using the finite-element method: how a fracture initiates and proceeds*. J Bone Miner Metab, 1999. **17**(2): p. 108-12.
32. Patel, S.H. and K.P. Murphy, *Fractures of the proximal femur: correlates of radiological evidence of osteoporosis*. Skeletal Radiol, 2006. **35**(4): p. 202-11.
33. Cristofolini, L. and M. Viceconti, *Comments on "Stair climbing is more critical than walking in pre-clinical assessment of primary stability in cementless THA in vitro" by Jean-Pierre Kassi, Markus O. Heller, Ulrich Stoeckle, Carsten Perka, Georg N. Duda, Published on J. Biomechanics 2005; 38: 1143-1154*. J Biomech, 2006. **39**(16): p. 3085-7; author reply 3087-40.
34. Cristofolini, L., *A critical analysis of stress shielding evaluation of hip prostheses*. Crit Rev Biomed Eng, 1997. **25**(4-5): p. 409-83.
35. Cristofolini, L. and M. Viceconti, *Towards the standardization of in-vitro load transfer investigations of hip prostheses*. J. Strain Anal. Eng. Des., 1999. **34**: p. 1-15.

36. Voide, R., G.H. Van Lenthe, and R. Muller. *Femoral neck stiffness critically depends on loading direction*. in *Fifth World Congress of Biomechanics Book of Abstracts*. 2006. Munich
37. Keyak, J.H., et al., *Predicting proximal femoral strength using structural engineering models*. Clin Orthop Relat Res, 2005(437): p. 219-28.
38. Taddei, F., et al., *Subject-specific finite element models of long bones: An in vitro evaluation of the overall accuracy*. J Biomech, 2006. **39**(13): p. 2457-67.
39. Taddei, F., et al., *The material mapping strategy influences the accuracy of CT-based finite element models of bones: an evaluation against experimental measurements*. Med Eng Phys, 2007. **29**(9): p. 973-9.
40. Bergmann, G., et al., *Hip contact forces and gait patterns from routine activities*. J Biomech, 2001. **34**(7): p. 859-71.
41. Taddei, F., A. Pancanti, and M. Viceconti, *An improved method for the automatic mapping of computed tomography numbers onto finite element models*. Medical engineering & physics, 2004. **26**(1): p. 61-9.
42. Cristofolini, L., et al., *Comparative in vitro study on the long term performance of cemented hip stems: validation of a protocol to discriminate between "good" and "bad" designs*. J Biomech, 2003. **36**(11): p. 1603-15.
43. Cristofolini, L., et al., *Influence of thigh muscles on the axial strains in a proximal femur during early stance in gait*. J Biomech, 1995. **28**(5): p. 617-24.
44. Ruff, C.B. and W.C. Hayes, *Cross-sectional geometry of Pecos Pueblo femora and tibiae--a biomechanical investigation: I. Method and general patterns of variation*. Am J Phys Anthropol, 1983. **60**(3): p. 359-81.
45. Wang, X. and S. Puram, *The toughness of cortical bone and its relationship with age*. Ann Biomed Eng, 2004. **32**(1): p. 123-35.
46. Duchemin, L., et al. *Femoral fracture load and failure energy in two load configurations: an in vitro study*. in *EORS, 16th Annual meeting, Bologna*. 2006.

Appendix C

Additional result plots for Chapter 6

Statistical analysis of the implanted femur, result plots

Variable	Distribution	Load case	Mean	St. Dev.	Min	Max
Bodyweight (N)	Truncated Gaussian	All	722	141	440	1145
Osteoporosis level (T-score)	Uniform	All	//	//	(-5.0)	(0.0)
Interdigitation degree	Uniform	All	//	//	0	1
Load intensity factor	Truncated Gaussian	Standing	1.29	0.29	1	1.89
		Walking	1.07	0.11	0.90	1.33
		Climbing	1.15	0.14	0.90	1.48

Table 2 - Summary of the input parameters distribution

First analysis of the implanted femur: sensitivity to the bodyweight, the osteoporosis, and the interdigitation level

Biomechanical parameter (output variable)	Load-case	Mean	St. Dev.	Minimum	Maximum
Stem Von Mises stress (MPa)	Single stance	66.2	14.5	36.4	118.6
	Level walking	73.2	16.2	40.0	132.0
	Upstairs climbing	72.7	16.4	39.5	132.4
Cement principal tensile stress (MPa)	Single stance	3.9	1.1	1.9	7.9
	Level walking	4.1	1.1	2.0	8.0
	Upstairs climbing	4.3	1.1	2.1	8.2
Cement principal compressive stress (MPa)	Single stance	-10.2	1.9	-16.7	-6.1
	Level walking	-8.9	1.7	-15.1	-5.3
	Upstairs climbing	-9.4	1.8	-16.0	-5.6
Bone maximum principal strain (ϵ)	Single stance	0.0030	0.0010	0.0014	0.0065
	Level walking	0.0015	0.0006	0.0007	0.0037
	Upstairs climbing	0.0019	0.0007	0.0009	0.0046
Maximum stem micromotion (mm)	Single stance	0.023	0.006	0.012	0.042
	Level walking	0.026	0.007	0.013	0.049
	Upstairs climbing	0.023	0.006	0.012	0.042
Maximum contact pressure (MPa)	Single stance	11.9	2.3	7.1	22.6
	Level walking	10.6	2.3	6.1	21.3
	Upstairs climbing	11.1	2.4	6.5	22.7

Table 3 - Descriptive statistics for the output parameters

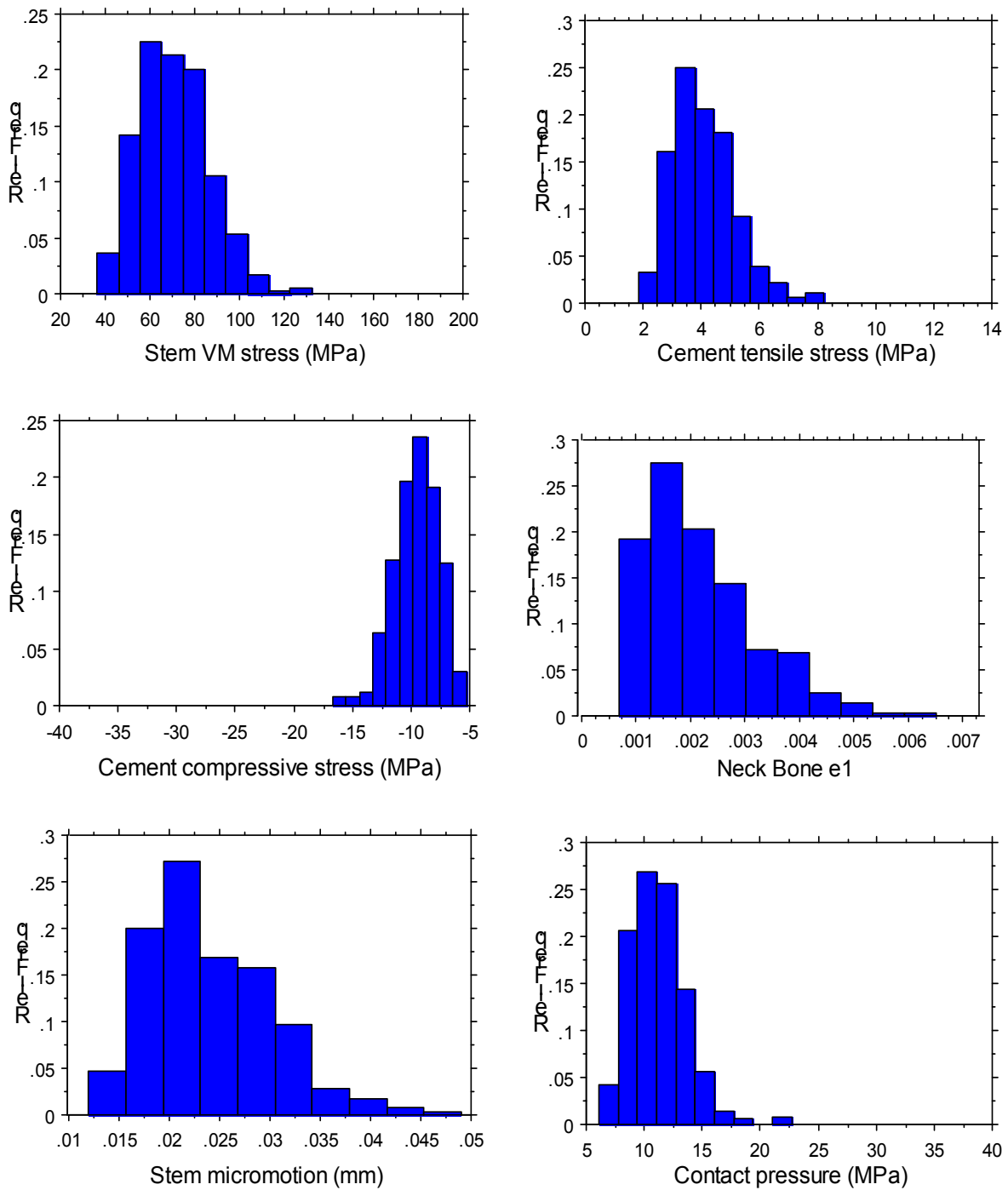


Figure 10 - The histograms of output parameters relative frequency

MATRIX OF CORRELATION COEFFICIENTS (INPUT vs. OUTPUT)	<i>Load-case</i>	Bodyweight	OP level	Interdigitation degree
Stem Von Mises stress	Single stance	0.816	-0.51	NS
	Level walking	0.811	-0.516	NS
	Upstairs climbing	0.802	-0.529	NS
Cement principal tensile stress	Single stance	0.721	-0.567	-0.358
	Level walking	0.734	-0.569	-0.326
	Upstairs climbing	0.764	-0.535	-0.316
Cement principal compressive stress	Single stance	-0.942	0.259	NS
	Level walking	-0.931	0.284	NS
	Upstairs climbing	-0.929	0.285	NS
Bone maximum principal strain	Single stance	0.546	-0.775	NS
	Level walking	0.472	-0.791	NS
	Upstairs climbing	0.47	-0.796	NS
Maximum stem micromotion	Single stance	0.687	-0.649	-0.273
	Level walking	0.674	-0.66	-0.263
	Upstairs climbing	0.688	-0.649	-0.241
Maximum contact pressure	Single stance	0.907	-0.305	NS
	Level walking	0.87	-0.364	NS
	Upstairs climbing	0.87	-0.357	NS

Table 4 - The coefficient matrix for the correlation of input and output parameter. NS indicates a non significant correlation (Linear Pearson test, significance level 0.05)



Figure 11 - Linear correlation sensitivities shown as pie-plot and histogram for each of the output parameters. The significance and relative importance of the input variable variation is identified in red for bodyweight, in green for osteoporosis level, in blue for interdigitation degree.

Second analysis of the implanted femur: the sensitivity to variation of the applied load for each motor task is added

Biomechanical parameter (output variable)	Load-case	Mean	St. Dev.	Minimum	Maximum
Stem Von Mises stress (MPa)	Single stance	90.5	25.8	48.7	173.6
	Level walking	79.2	18.3	40.0	125.0
	Upstairs climbing	83.9	19.2	44.1	134.1
Cement principal tensile stress (MPa)	Single stance	5.6	1.9	2.5	11.5
	Level walking	4.5	1.3	2.0	8.3
	Upstairs climbing	5.0	1.3	2.5	8.3
Cement principal compressive stress (MPa)	Single stance	-13.9	3.7	-25.3	-7.7
	Level walking	-9.6	2.0	-15.1	-5.3
	Upstairs climbing	-10.9	2.3	-18.3	-6.2
Bone maximum principal strain (ϵ)	Single stance	0.0041	0.0015	0.0019	0.0095
	Level walking	0.0017	0.0006	0.0007	0.0035
	Upstairs climbing	0.0022	0.0008	0.0010	0.0048
Maximum stem micromotion (mm)	Single stance	0.031	0.008	0.016	0.053
	Level walking	0.028	0.007	0.013	0.045
	Upstairs climbing	0.026	0.006	0.014	0.042
Maximum contact pressure (MPa)	Single stance	22.7	10.7	9.1	57.8
	Level walking	14.8	5.9	6.2	31.2
	Upstairs climbing	12.9	3.1	7.2	22.7

Table 5 - Descriptive statistics for the output parameters

Biomechanical parameter (output variable)	Load-case	Mean % change	Maximum % change
Stem Von Mises stress (MPa)	Single stance	37%	46%
	Level walking	8%	5%
	Upstairs climbing	15%	1%
Cement principal tensile stress (MPa)	Single stance	44%	46%
	Level walking	9%	3%
	Upstairs climbing	17%	1%
Cement principal compressive stress (MPa)	Single stance	36%	52%
	Level walking	8%	0%
	Upstairs climbing	15%	14%
Bone maximum principal strain (ϵ)	Single stance	36%	45%
	Level walking	8%	-7%
	Upstairs climbing	14%	4%
Maximum stem micromotion (mm)	Single stance	32%	27%
	Level walking	8%	-7%
	Upstairs climbing	14%	-2%
Maximum contact pressure (MPa)	Single stance	91%	156%
	Level walking	40%	46%
	Upstairs climbing	17%	0%

Table 6 - Percentage differences between base and intensity model. Positive percentages indicate higher values for the intensity model.

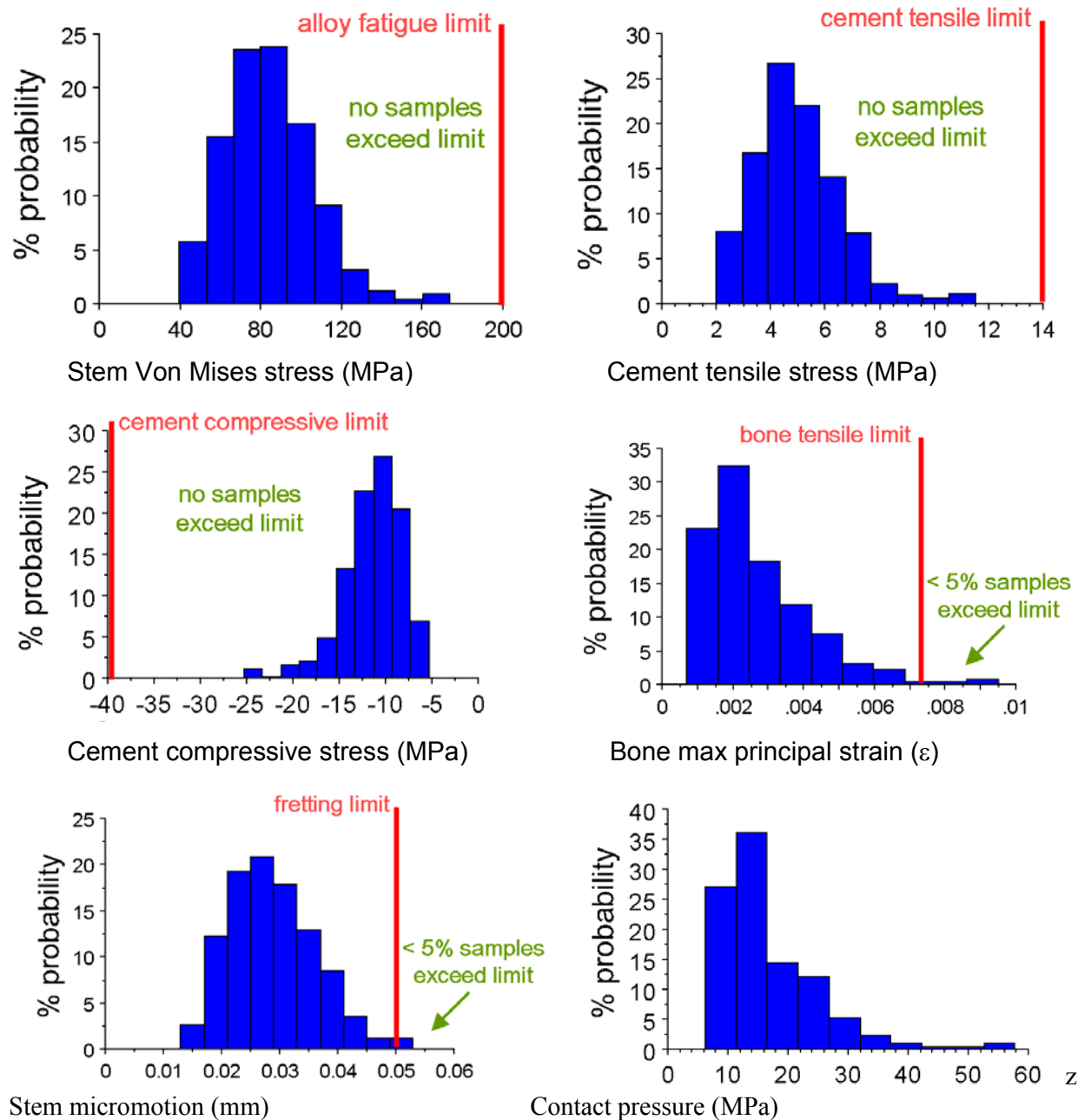


Figure 12 - The histograms of output parameters relative frequency

MATRIX OF CORRELATION COEFFICIENTS (INPUT vs. OUTPUT)	<i>Load-case</i>	Load intensity	Body weight	OP level	Interdigit. degree
Stem Von Mises stress	Single stance	0.645	0.707	-0.351	NS
	Level walking	0.25	0.758	-0.575	-0.231
	Upstairs climbing	0.408	0.683	-0.429	NS
Cement principal tensile stress	Single stance	0.614	0.651	-0.408	NS
	Level walking	0.233	0.715	-0.593	-0.4
	Upstairs climbing	0.397	0.65	-0.436	NS
Cement principal compressive stress	Single stance	-0.686	-0.773	NS	NS
	Level walking	-0.29	-0.841	0.368	0.247
	Upstairs climbing	-0.455	-0.785	0.185	NS
Bone maximum principal strain	Single stance	0.511	0.519	-0.638	NS
	Level walking	NS	0.473	-0.832	NS
	Upstairs climbing	0.222	0.363	-0.764	NS
Maximum stem micromotion	Single stance	0.597	0.641	-0.483	NS
	Level walking	0.209	0.67	-0.689	-0.326
	Upstairs climbing	0.351	0.579	-0.571	NS
Maximum contact pressure	Single stance	0.617	0.671	-0.395	NS
	Level walking	0.236	0.685	-0.627	-0.259
	Upstairs climbing	0.404	0.719	-0.31	NS

Table 7 - The coefficient matrix for the correlation of input and output parameter. NS indicates a non significant correlation (Linear Pearson test, significance level 0.05)

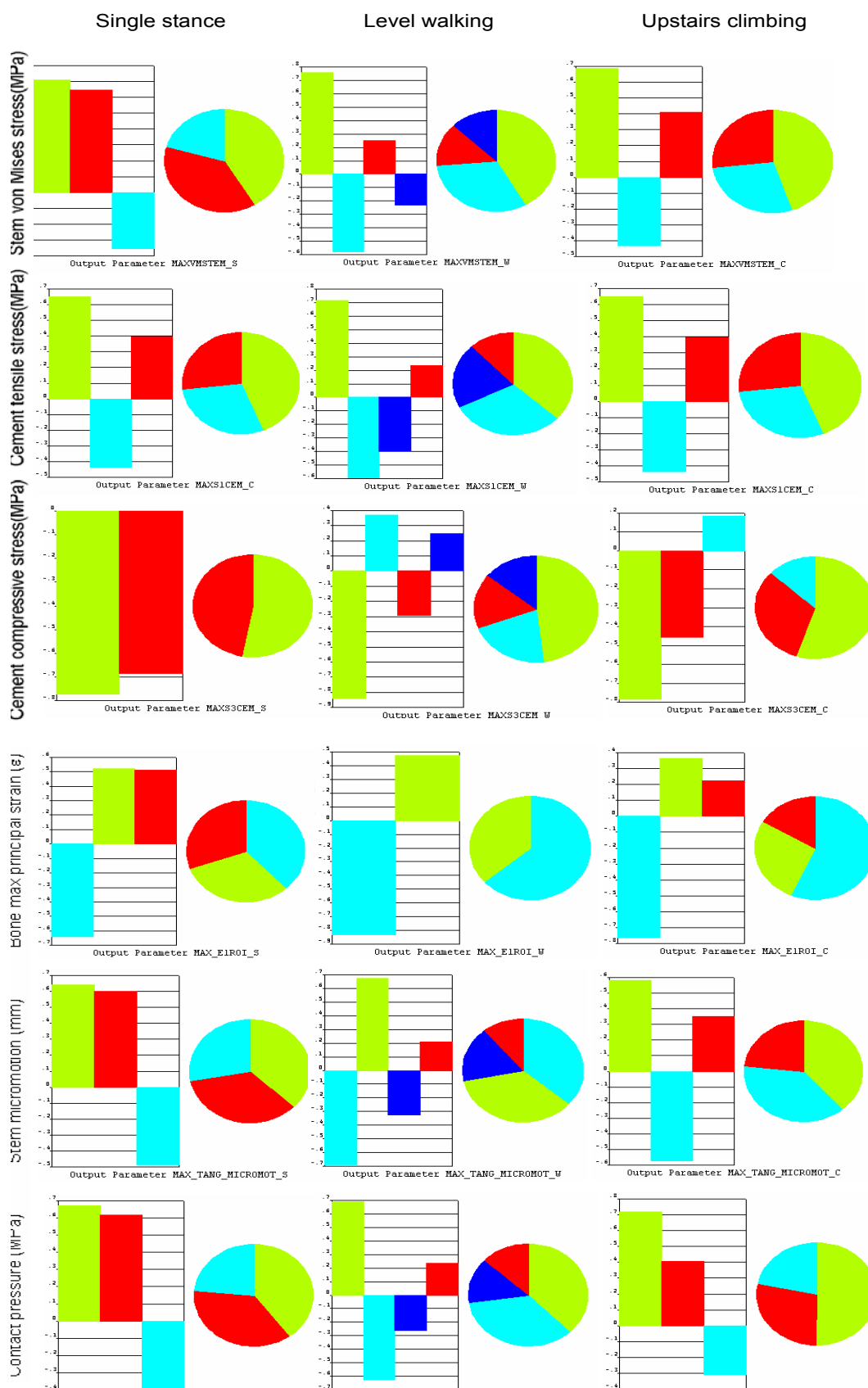


Figure 13 - Linear correlation sensitivities shown as pie-plot and histogram for each of the output parameters. The significance and relative importance of the input variable variation is identified in red for load intensity, in green for bodyweight, in light blue for osteoporosis level, in blue for interdigitation degree.

Analysis of the stem misalignment

Biomech. Par. (output)	Load case	Mean		St. Dev.		Minimum		Maximum	
		Varus	valgus	varus	valgus	varus	valgus	varus	valgus
Stem Von Mises stress (MPa)	SS	79.5	96.9	22.3	25.3	38.6	46.7	168	172.3
	LW	67.1	82.8	15.9	20.1	34.5	49	112.3	146.3
	US	73.6	90.2	17.6	22.6	38.4	45.7	136.9	143.8
Cement Max σ_1 (MPa)	SS	3.3	5.7	0.9	1.9	1.5	2.4	6.8	12
	LW	2.7	4.7	0.8	1.3	1.2	2.6	4.6	8.9
	US	3.1	5	0.9	1.4	1.5	2.3	6.3	8.4
Cement Max σ_3 (MPa)	SS	-6.6	-16.3	1.7	4	-13.6	-26.4	-3.5	-8.6
	LW	-5.7	-12.3	1.1	2.7	-8.7	-20.3	-3.2	-7.7
	US	-6	-13.4	1.3	3.1	-11	-21.1	-3.5	-7.2
Bone Max ϵ_1	SS	0.0041	0.004	0.002	0.0013	0.002	0.0016	0.009	0.0087
	LW	0.0014	0.0017	4E-04	0.0006	6E-04	0.0008	0.003	0.0035
	US	0.0018	0.0022	5E-04	0.0008	8E-04	0.0009	0.004	0.0045
Max. stem micromotion (mm)	SS	0.023	0.031	0.007	0.008	0.01	0.015	0.045	0.054
	LW	0.034	0.025	0.009	0.006	0.016	0.015	0.056	0.041
	US	0.032	0.027	0.009	0.006	0.015	0.013	0.063	0.041
Max. contact pressure (MPa)	SS	7.5	27.4	2.4	11.8	3.5	9.9	19.2	63.3
	LW	7	19.2	2.4	7.8	3.2	9	15.5	45.6
	US	6.8	16	1.6	4.4	4	8.3	14.4	28.8

Table 8 - Descriptive statistics for the output parameters in each loading

Biomech. Par. (output)	Load case	Mean % change		Maximum % change	
		varus	valgus	varus	valgus
Stem Von Mises stress (MPa)	SS	-12%	7%	-3%	-1%
	LW	-15%	5%	-10%	17%
	US	-12%	8%	2%	7%
Cement Max σ_1 (MPa)	SS	-41%	2%	-41%	5%
	LW	-39%	3%	-45%	7%
	US	-38%	1%	-24%	1%
Cement Max σ_3 (MPa)	SS	-52%	17%	-46%	4%
	LW	-41%	28%	-42%	35%
	US	-45%	23%	-40%	15%
Bone Max ϵ_1	SS	-1%	-3%	-8%	-9%
	LW	-17%	-2%	-27%	1%
	US	-17%	2%	-22%	-6%
Max. stem micromotion (mm)	SS	-26%	2%	-15%	2%
	LW	22%	-10%	24%	-8%
	US	22%	4%	49%	-4%
Max. contact pressure (MPa)	SS	-67%	21%	-67%	10%
	LW	-53%	30%	-50%	46%
	US	-48%	24%	-37%	27%

Table 9 - Percentage variations with respect to optimal position model, reported for mean and maximum values. Positive percentages indicate higher values with respect to the ideal case.

Appendix D

Musculoskeletal models for predicting skeletal loadings

Scaling of a shoulder musculoskeletal model does not lead to significant improvement^{iv}

To optimise the use of musculoskeletal models for clinical practice, individualized models are a prerequisite. This would allow for a more exact estimation of muscle contributions to a specific motion task and would enable researchers and clinicians to distinguish between general and subject-specific effects of anthropometry on the performance in a particular task. An individualized model will help quantify muscle actions in-vivo.

To date, only limited data sets are available for the construction of anatomically accurate models. These data sets are either based on cadaver data, or on quantification using imaging techniques (MRI). Both methods have their pro's and cons, but the general conclusion is that neither methods can produce 'complete' sets of individualized data and that optimisation of models using scaling principles is still the most feasible procedure. It is, however, unknown what scaling procedures will produce valid results. The current study applied different scaling techniques to fit an extensive musculoskeletal shoulder model onto the anatomy of 30 volunteers. Valid scaling techniques should lead to an improvement in the fit between the averaged (modified) model and averaged original individual trajectories

Material and methods

A detailed musculoskeletal shoulder model [1] created for the inverse dynamic simulation of the human shoulder district was scaled to the anatomy of 30 volunteers. Any bone segment is defined by a local coordinate system calculated from the palpated bony landmark [2] plus a rigidly connected node cloud that include muscle and ligament attachment sites, joint centre locations and palpated landmarks.

For each volunteer the full set of bony landmarks according ISB standards was recorded plus a set of 40 thorax locations along the ribs, the sternum and the spine. Scaling was based upon the geometrical relationship between bony landmarks of both the model and individual.

Three different methods were implemented to register the musculoskeletal model onto individual anatomy: uniform scaling method, intrasegmental uniform scaling and intrasegmental non-uniform scaling method.

^{iv} Extracted from:

1. S. Martelli, H.E.J. Veeger, Van der Helm, "Scaling of shoulder musculoskeletal model to individual subject data" International Society of Biomech., Taipei, Taiwan, July 1-5, 2007
2. S. Martelli, H.E.J. Veeger, Van der Helm, "Scaling of a shoulder musculoskeletal model does not lead to significant improvement" International Shoulder Group, Bologna, Italy, July 10-13, 2008

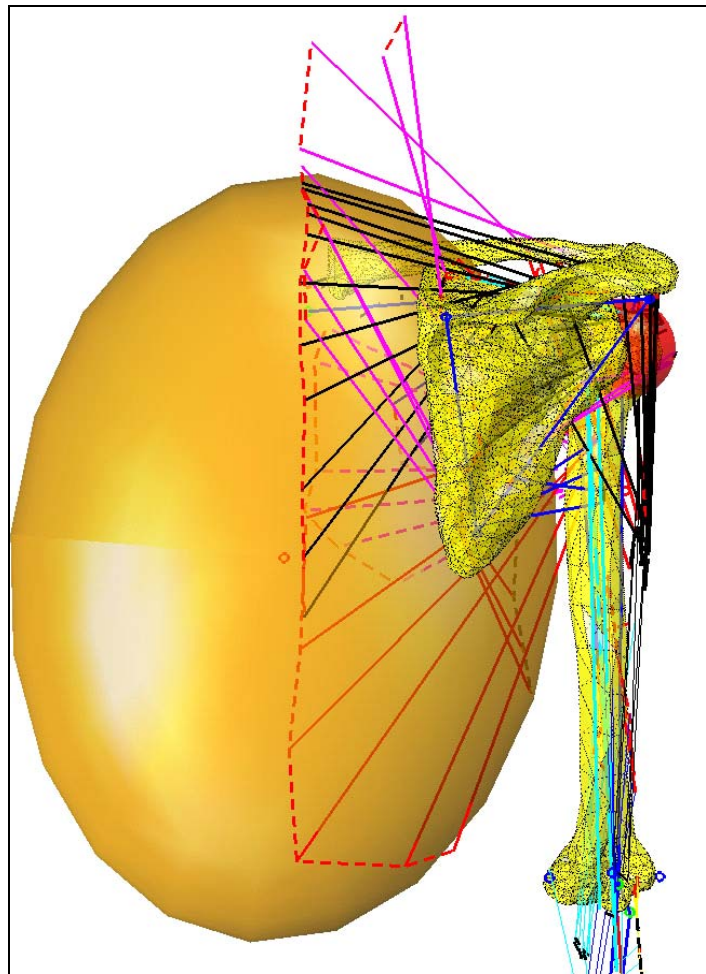


Figure 14 – Bones of the shoulder superimposed to the musculoskeletal model

Uniform scaling

The whole model was scaled by one size measure, i.e. arm length. The arm length was defined as the sum distance angulus acromialis (AA)-lateral epicondyle (EL) plus lateral epicondyle-radial styloid.

Inertial parameters and mass parameters were scaled by the second power and the third power of the scaling factor respectively.

Intrasegmental uniform scaling

Every segment node cloud was scaled using a single scaling factor based on a representative segment dimension for that segment. The shape of the thorax was approximated by an ellipsoid thus the thorax scaling factor was defined as the ratio of the vertical axes of the thorax surface between the subject and the model. The distance between the recorded landmarks and the surface was up to 2cm. The clavicle, humerus and forearm scaling factors were based on the segment

length defined as a joint-to-joint distance. Last, the scapula scaling factor was calculated based on the distance between the angulus acromialis (AA) and the trigonum scapulae (TS).

Intrasegmental non uniform scaling

The thorax scaling matrix was defined as the ratio between the thorax ellipsoid axes for each direction. Clavicle, humerus and forearm scaling matrix were defined using a longitudinal and a transversal scaling factor. The scapula scaling matrix was based on the edge length of the bounding box parallel to the local coordinate system of the scapula.

Results

The INUS models showed a compromised ability in following individual kinematics so comparisons were performed between cad, US and IUS models.

The closed chain mechanism of the shoulder girdle did not allow models to follow the entire group of individual kinematics. Simulations of the complete task of anteflexion was possible only for 3 out of 30 subjects, simulations of abduction was possible for 26 out of 30 subjects.

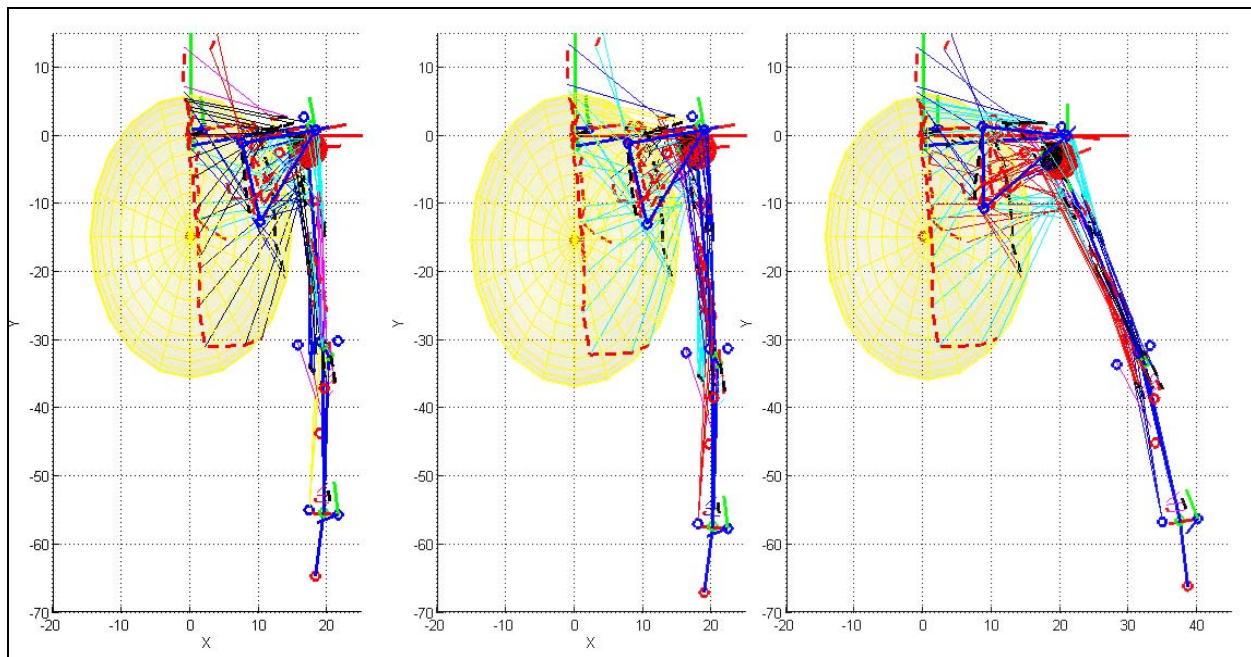


Figure 15 – From the left, the original musculoskeletal model, the original model uniformly scaled (US) on a specific individual and the original model scaled on the same individual by the IUS method.

Low correlations ($R^2 < 0.32$) were found between errors on joint centre trajectory and size (arm length).

Comparison of simulated and measured kinematics was as follow:

1. Errors on joint angles were not reduced by any scaling method, either in the mean value or dispersion.
2. IUS scaled models produced better trajectory of the gleno-humeral (gh) joint, reducing the mean position error (-33%) and dispersion (-23%).
3. US scaled models produced better trajectory of the elbow (el) and the wrist (wr) joint, reducing the mean position error up to 24% and dispersion (-40%)

Trajectory errors on joint centre (cm)						
	Wrist		Elbow		Gleno-Humeral	
	mean	dev. st.	mean	dev. st.	mean	dev. st.
cad	5.3	2.7	4.1	2.5	2.0	1.2
us	4.0 (-24%)	1.6 (-40%)	3.3 (-20%)	1.6 (-33%)	1.8 (-10%)	1.0 (-15%)
ius	4.4 (-16%)	2.3 (-13%)	4.1 (+1%)	1.9 (-24%)	1.4 (-33%)	0.9 (-23%)

Table 10 - Mean and standard deviation of errors in arm joint centre position trough simulated subjects and motions. In bracket the percent variation from what predicted by the original model.

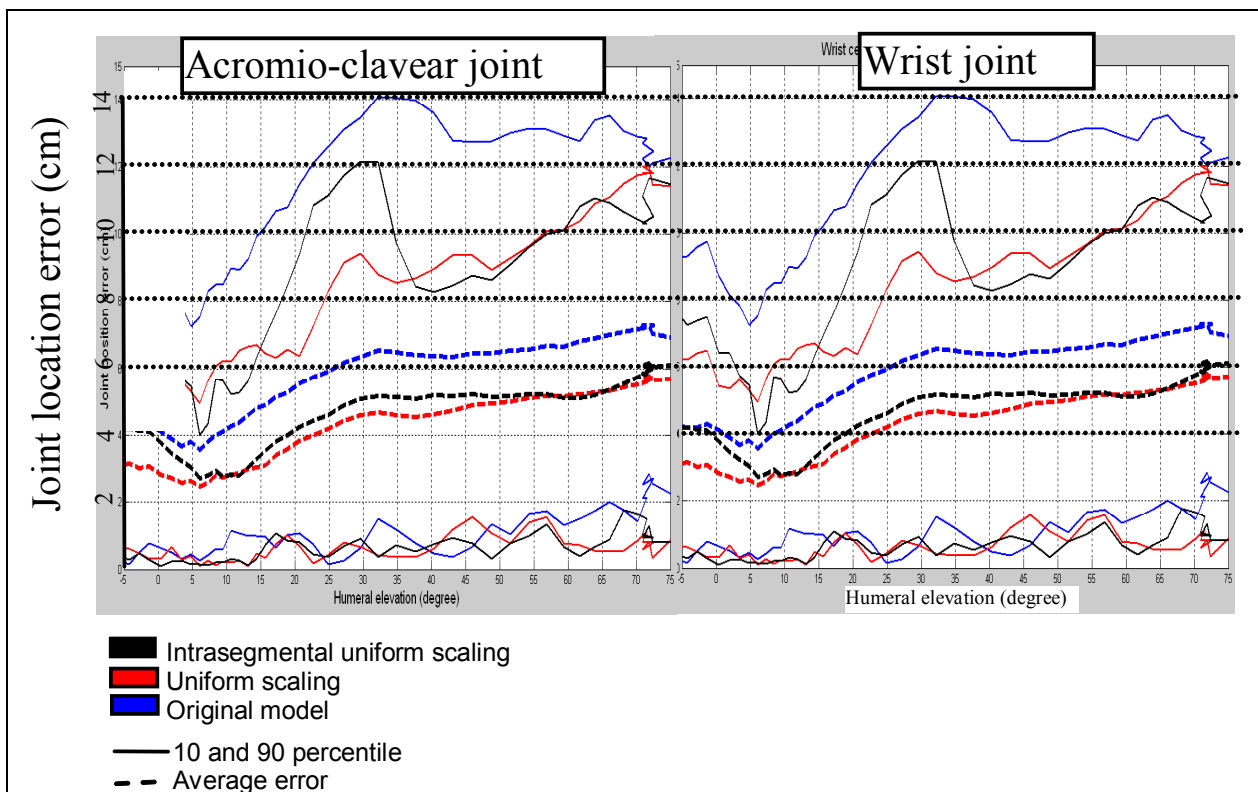


Figure 16 – General trends of the location of the joint centers during abduction. Distal joints (on the right the trend of the error of the wrist, which is the more distal joint) show a significant dependence of the mean error and of the dispersion error by the current configuration of the system. The position error of the centre location of proximal joint (on the left the trend of the error on the prediction of the acromio-clavear joint location) is not dependent by the current configuration of the system.

The variability on estimated muscle forces was high. Variations on the force exerted by principal muscle groups was found to exceed 40% and of the same order of magnitude of the uncertainty introduced by trajectory errors. Thus, to correctly distinguish the contribution on the individual performances of the individual anthropometry appears to be relevant to precisely simulate both

the individual action and anatomy. Timing of muscle forces predicted by the cad and the US model was changed by IUS models.

Discussion and conclusions

The presented methods allowed the simple generation of subject specific musculoskeletal models for clinical purposes.

Scaling based on anatomical measures demonstrated to reduce the average kinematics error of the original model and its dispersion. US models better predicted distal joints (el and wr) trajectory while IUS models better predicted trajectory of proximal joints and angles with respect predictions of the original model. INUS models showed a compromised ability to follow individual kinematics.

Nevertheless scaling the model on a single subject did not improve the model ability to follow individual kinematics while malpositioning of joint centres may strongly affect joint net moments and predictions of muscle forces.

Changes in size were able to explain only a minor part the muscle force variability. The uncertainty amplitude is big enough to overshadow the anthropometry effect on the performance.

This would be a limit for the clinical application of the method, so further work is needed for better predict the individual kinematics. To the authors' opinion, either anatomical or functional parameters should be considered in more advanced registering techniques.

REFERENCES

1. van der Helm, F.C., *A finite element musculoskeletal model of the shoulder mechanism*. J Biomech, 1994. 27(5): p. 551-69.
2. Wu, G., et al., *ISB recommendation on definitions of joint coordinate systems of various joints for the reporting of human joint motion--Part II: shoulder, elbow, wrist and hand*. J Biomech, 2005. 38(5): p. 981-992.